MICROCOPY RESOLUTION TEST CHART
NATIONAL BUREAU OF STANDARDS-1963-A
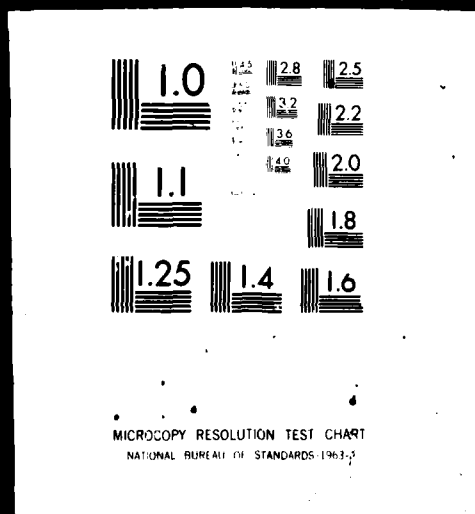
LEVEL III

A08 3972

(3)

CENTRIFUGAL MODELLING OF SOIL STRUCTURES
PART III

<u>THE STABILITY OF RIVER BANKS</u>

<u>AND FLOOD EMBANKMENTS</u>

Final Technical Report

by

Christopher John Padfield

October 1978

ADA084049

DTIC
SELECTED
MAY 9 1980
C

EUROPEAN RESEARCH OFFICE

United States Army

London   England

GRANT NUMBER DA-ERO - 76-G-040

A. N. Schofield

Approved for Public Release; distribution unlimited

411742

80   5   8   0?

REPORT DOCUMENTATION PAGE	READ INSTRUCTIONS BEFORE COMPLETING FORM

1. REPORT NUMBER	2. GOVT ACCESSION NO.	3. RECIPIENT'S CATALOG NUMBER
	AD-A084 049	

4. TITLE (and Subtitle)	5. TYPE OF REPORT & PERIOD COVERED
Centrifugal Modelling of Soil Structures, Part III. The Stability of River Banks and Flood Embankments	Final Technical 6 May 76 – 5 May 79
	6. PERFORMING ORG. REPORT NUMBER

7. AUTHOR(s)	8. CONTRACT OR GRANT NUMBER(s)
Christopher John Padfield Andrew N. Schofield	DAERO-76-G-040

9. PERFORMING ORGANIZATION NAME AND ADDRESS	10. PROGRAM ELEMENT, PROJECT, TASK AREA & WORK UNIT NUMBERS
Department of Civil Engineering Cambridge University Cambridge, United Kingdom	ITI61102BH57 01

11. CONTROLLING OFFICE NAME AND ADDRESS	12. REPORT DATE
U. S. Army Research & Standardization Box 65 FPO NY 09510	October 1978
	NUMBER OF PAGES
	183

14. MONITORING AGENCY NAME & ADDRESS(if different from Controlling Office)	15. SECURITY CLASS. (of this report)
USAE Waterways Experiment Station P. O. Box 631 Vicksburg, MS 39180	Unclassified
	15a. DECLASSIFICATION/DOWNGRADING SCHEDULE

16. DISTRIBUTION STATEMENT (of this Report)

Distribution unlimited

17. DISTRIBUTION STATEMENT (of the abstract entered in Block 20, if different from Report)

18. SUPPLEMENTARY NOTES

19. KEY WORDS (Continue on reverse side if necessary and identify by block number)

Bank stability, centrifugal modelling, bank failure, soil mechanics, scale models, embankment failures, river banks, liquifaction, flowslides

20. ABSTRACT (Continue on reverse side if necessary and identify by block number)

Instabilities may develop in river banks at times of flood and threaten to re-establish the natural regime of rivers. The two problems of instability which were selected for this study both involve the interaction of two layers of soil. In each case the river bank instability make take alternative forms depending on the relative geometry of the soil layers involved. The modes of failure which are observed in the field may be understood in terms of the mechanism by which the two layers interact with one another during failure. The instability that affects Thames River flood embankments occurs when they are subjected to flood

THE STABILITY OF RIVER BANKS

AND FLOOD EMBANKMENTS

by

Christopher John Padfield

A Dissertation submitted for the

Degree of Doctor of Philosophy

at Cambridge University

A centrifugal model study of the influence
of the interaction of two deforming layers in the
analysis of two river bank stability problems

Darwin College   October 1978

SUMMARY

This dissertation concerns two real problems of instability on the banks of major rivers. The two rivers, the Thames and the Mississippi, are both extensively canalised. Instabilities may develop in the river banks at times of flood and threaten to re-establish the natural regime of the rivers with a concomitant risk to life and installations behind the flood defences. The two problems of instability were selected for this study both for their practical importance, and for their illustration of a theme: the interaction of two layers of soil. In each case the river bank instability may take alternative forms depending on the relative geometry of the soil layers involved. The objective of the investigation was to show that the modes of failure which are observed in the field may be understood in terms of the mechanisms by which the two layers interact with one another during failure.

The instability that affects the Thames flood embankments occurs when they are subjected to flood water levels combined with high uplift pressures in a permeable layer which underlies the marsh upon which they are built. The most extreme loading occurs when a storm flood surge coincides with high spring tides. The investigation reported in Part I of this dissertation was designed to discover the nature of the failures which result from different extreme combinations of self weight and uplift loading on such an embankment.

The experimental technique used throughout the investigation was that of centrifugal modelling using the large new Geotechnical Centrifuge at Cambridge. A series of 1/50 scale model embankments was constructed and tested to failure on the centrifuge. Each model was brought into equilibrium at 50 gravities and then subjected to a planned sequence of rapid perturbations of loading. Both self weight of the embankment and

uplift pressure in the foundation were varied. The load combinations were determined which caused failure of the embankments. The geometry of the embankment was kept constant in all tests, but the depth of the underlying marsh was varied. By selecting suitable parameters the failure load combinations are shown to plot on an interaction diagram, the shape of which depends on the relative depth of the embankment and the marsh upon which it is built. The shape of the failure surface which developed was observed to depend on the nature of the loading which causes the collapse.

The experimental investigation is supported by a simple analytical derivation of the shape of the interaction diagram. The analysis uses material properties relevant to the centrifuge models but is, in principle, applicable to the prototype embankments along the Thames. A preliminary analysis is also presented that accounts for the dependance of the form of failure surface on the nature of the loading.

The instability that affects the Mississippi river banks is caused by intense erosion of the channel bed at times of high river discharge. Where the bank is composed of fine grained 'point bar' deposits of a certain type, flowslides sometimes develop which rapidly destroy large portions of the river bank, as shown in the frontispiece. The normal explanation for the ability of a sand layer to generate a flowslide has been that the sand which is assumed to be initially loose, liquefies and flows away. It is shown in this dissertation that a 'flowslide' scar may develop in a sand layer which is initially dense and that the feature that governs whether a particular failure will or will not become a flowslide, is the ability of the sand to flow unimpeded from the scar, and not its ability to liquefy. An analysis is developed which, with several unresearched assumptions, predicts the final geometry of a failure by this mechanism.

On the Mississippi the agency which is able, in certain circumstances, to impede the flow of sand, is the cohesive overburden. The interaction of the two layers was researched experimentally using a series of centrifuged

models. The influence of geometry on the mechanisms of deformation was investigated by varying the relative thickness of the two layers. It was found that two alternative mechanisms of deformation of the clay overburden can result from the creation of an erosion crater in the sand layer. These distinct mechanisms correspond to the two types of failure observed along the Mississippi: shear type and flow type failure, and they are governed simply by the relative thickness of the overburden and sand layers. This geometrical relationship is justified analytically in terms of the ability of the overburden to arch across the crater.

PREFACE

I was fortunate during my three years at Cambridge to have been supervised by Professor A. N. Schofield, for whose leadership, stimulation and guidance I am extremely grateful. It has been a privilege to be a member of the Soil Mechanics Group, and I am grateful for its friendly and dynamic atmosphere. I have benefited from discussions with Dr. R. G. James and am deeply endebted to many other people for assistance in specific areas of my work:

Messrs R. E. Ward, J. Doherty, W. Gwizdala, A. Balodis, C. Hodson and Mrs. V. Johnson for very substantial technical backup in centrifuge model preparation.

Mr. C. Collison and Mr. S. Boniface who built, service and run the Cambridge centrifuge, for an excellent working partnership.

Mr. R. Julian and Mr. W. Gillman and the staff of the Department Workshops for their patience and craftsmanship.

Mrs. S. Venn and Miss J. Stroud who typed the manuscript.

I certify that, except where specific reference is made in the text to the work of others, the contents of this dissertation are original and have not been submitted to any other university.

C. J. Padfield

October, 1978.

TABLE OF CONTENTS

(vii)

PART II

LIST OF SYMBOLS USED

A	Zone A sand thickness in point bar deposit
A, a	Velocity of flow of a viscous layer of liquefied sand
a	Radius of crater in trapdoor tests
A, $\bar{B}$	Pore pressure parameters
b	Width
C	Concentration of grains
c_H, c_u	Undrained shear strength
C_v	Coefficient of consolidation
D	Diameter
D, d	Height of retrogressing face in a flowslide
E	Young's modulus
e	Voids ratio
F	Gravitational self weight loading parameter
F_s	Safety factor
G	Shear modulus
g	Earth's gravitational acceleration
H	Drainage path length
	Head of uplift above marsh surface
	Horizontal load
H, h	Thickness of viscous layer
h	Thickness of clay plate
i	Hydraulic gradient
K_o	Coefficient of lateral earth pressure
k	Permeability
	q intercept of 'Hvorslev line'
M	Thickness of marsh layer
m_{vc}	Coefficient of volume compressibility
N	Over-consolidation ratio
n	Multiplier for gravitational loading (ng)

n	exponent
O	Overburden thickness in point bar deposit
P	A force
	A particle or element
p'	Effective spherical pressure
p'_u	Undrained critical state pressure
p'_x	Critical state pressure on yield curve
Q	Volume discharge
q	Axial deviator stress
q_u	Undrained critical state value of q
q_x	Critical state value of q on yield curve
R	Radius of slip circle
R_F	Frictional resistance
S	Slope of river bed
	Lateral force
s, t	Stresses in plane strain
T_v	Time factor in consolidation
t	Time
U	Uplift loading parameter
u	Pore pressure
	Water pressure
V	Vertical load
	Velocity of rise of surface of resedimentation of a liquified sand layer
v	Specific volume
v_x	Critical state value of v on yield curve
v'	Volumetric strain
W	Body weight
W_d	Fall velocity of a dispersion of grains
W_o	Free fall velocity of a single grain

w	Water content
x y z	Cartesian co-ordinate axes
X	Distance travelled by uppermost layer of grains - liquefied sand layer
Z	Velocity of a retrogression of the steep face in a flowslide in dense sand
α, β	Characteristics (Sokolovsky)
α, β	Angles
γ	Saturated bulk density
γ'	Submerged bulk density (By mass)
γ_w	Density of water
η	Ratio of stresses q/p'
η	Special parameter (Sokolovsky)
κ'	Special parameter (Sokolovsky)
κ	Gradient of swelling line
λ	Gradient of compression line
μ	Viscosity
ν'	Poissons ratio in terms of effective stress
ξ	Special parameter (Sokolovsky)
ρ	Angle of friction
σ	Total stress
σ'	Effective stress
τ	Shear stress
ϕ	$\begin{cases} \text{Potential function} \\ \text{Angle of friction} \end{cases}$
Γ	Ordinate of critical state line
M	Critical state frictional constant
Σ	Major principal stress (Sokolovsky)

CHAPTER 1

INTRODUCTION

1.1 Outline of the Dissertation

A common feature of many low-lying alluvial plains is that there are lengths of river bank where a cohesive alluvial layer is underlain by sands or gravels. Embankments founded on these layers afford flood protection to the low-lying plain. In this dissertation it is suggested that the interaction during failure of the alluvial and sand layers or of the alluvium and the embankment, is fundamental to an understanding of the stability of the river bank and embankments at such sites.

It is argued that the stability of a river bank where an alluvial layer overlies sands and gravels depends on the thickness of this alluvial layer relative to the thickness of the layer with which it interacts.

Two real problems were studied which relate to different aspects of river bank instability, one on the tidal Thames and the other on the lower Mississippi. In both cases the embankments which defend the low-lying alluvial plain against high flood waters are built on cohesive alluvium underlain by granular material. On the Mississippi certain types of failure occur which have usually been understood with reference to a classical study of liquefaction by Casagrande, 1936. A new understanding is presented in this dissertation. On the Thames a dangerous type of failure, reported by Marsland, 1961, occurs by the interaction of the embankment itself with the uplifted alluvial layer. This type of failure is also the subject of a new analysis.

The aim throughout this dissertation has been to seek to discover possible mechanisms which might characterise the phenomena involved in the two real river bank stability problems and to scrutinise these hypothetical mechanisms with a variety of experimental and analytical techniques.

In both of these investigations small-scale soil models have been subjected to a high gravitational acceleration on a geotechnical centrifuge to search experimentally for mechanisms which may occur at prototype scale along the two major rivers. No attempt has been made to predict directly the behaviour of the prototype. The analyses presented relate to the model tests and use the material properties of the models.

The experimental technique used for the two investigations was that of centrifugal modelling. The Geotechnical Centrifuge at the Cambridge University Engineering Department was new at the outset of this project and had neither peripheral equipment nor services. Further, there were no containers designed to use with the machine, nor experimental expertise available for its exploitation. A theme which runs throughout the dissertation is that the experiments conducted for this research not only required development in themselves, but required at the same time development of the Cambridge centrifugal facility. As a result of these limitations, techniques were chosen which, though not sophisticated, were possible in the circum-stances. Attention was also given to the development of equipment, methods, and expertise in experimentation which would be directly applicable by later research workers on the machine, since a considerable saving in time is effected if existing apparatus can be modified. The account takes the form at certain points of a critique of centrifugal model testing.

The dissertation is essentially divided into two parts which deal individually with the two real stability problems mentioned above. Both problems are introduced in this chapter where the common theme is the interaction of two layers to generate mechanisms. The details of the mechanisms depend on the geometry of the layers involved. Independent conclusions are drawn for the two problems and finally general conclusions are presented.
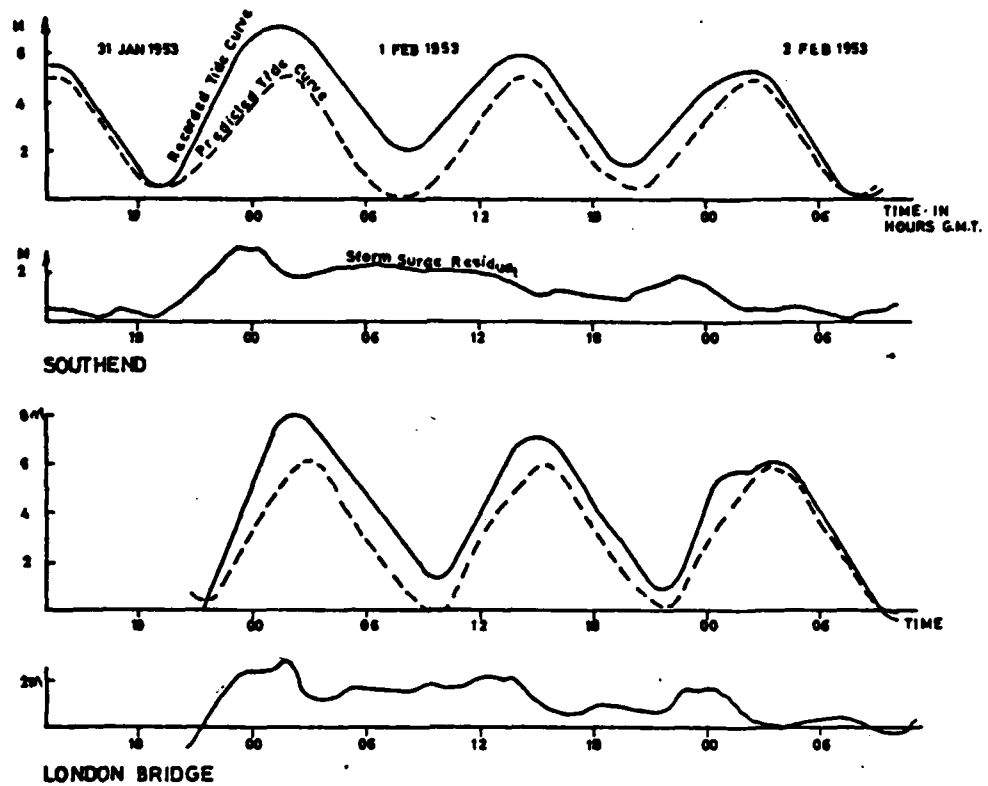
FIG.1·1–THE STORM SURGE OF FEBRUARY 1953 (Taken from GLC's first report
of studies 1969)
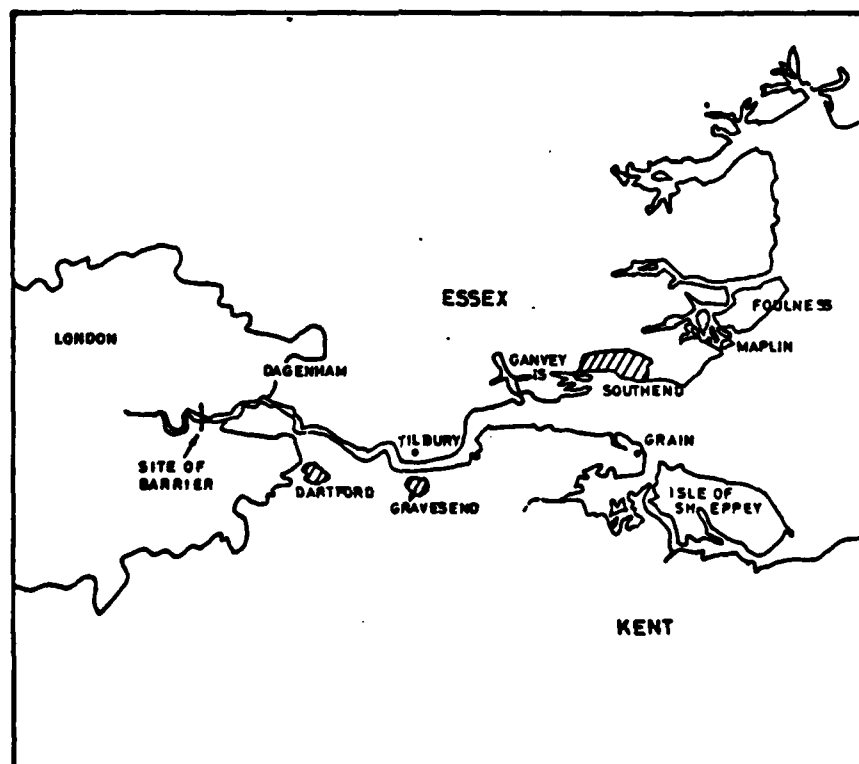
FIG 1·2   MAP OF THAMES ESTUARY FROM ORDNANCE SURVEY
1:625,000, SOUTH

1.2 The Thames Flood Embankments

In February 1953 an unusually deep depression, Peters, 1953, moved in an easterly direction past the North of Scotland and turned south-west towards North Germany. The strong winds associated with this storm generated a surge in sea level which became sharper and steeper as it entered the converging straits of the Channel and the Thames estuary, Farquharson, 1953. Tide readings at Southend and at London Bridge for the duration of the storm are shown in Fig. 1.1, taken from the GLC's second report of studies, GLC, 1970. The storm surge in the Thames took the form of an irregular step increase in water level of approximately 2m in height and approximately 28 hours duration. The storm caused extensive damage in Holland and on the east coast of England. At several places the flood embankments along the Thames were breached.

Several alternative proposals have been made in the last half century to provide a flood barrier across the Thames to protect the capital from flooding by severe storm tides. The Thames Barrier actually under construction at Silvertown, Fig. 1.2, is a half tide barrage with rising sector gates, Horner, 1978, which offers little hindrance to shipping or to the normal fluctuations of the tide except when a storm surge is predicted. In this case the gates may be closed and will result in higher maximum water levels downstream. On account of this effect and the greater safety margins required for the new work, the design peak tide levels downstream of the barrier have been increased by up to 2m, Marsland and Powell, 1977.

Until 1953, storm surges of a severity expected to occur several times a century had breached the defences at some point or another. Although serious, the resulting flooding usually inundated only agricultural land. In this century the marshes have been increasingly inhabited: housing estates and industry occupy land which would become flooded if the flood defences were breached. The river flood embankments require regular

STORM H.W.L.

ORDINARY H.W.L.

NEW BANK

EXISTING BANK

NEW BERM

MARSH

GRAVEL
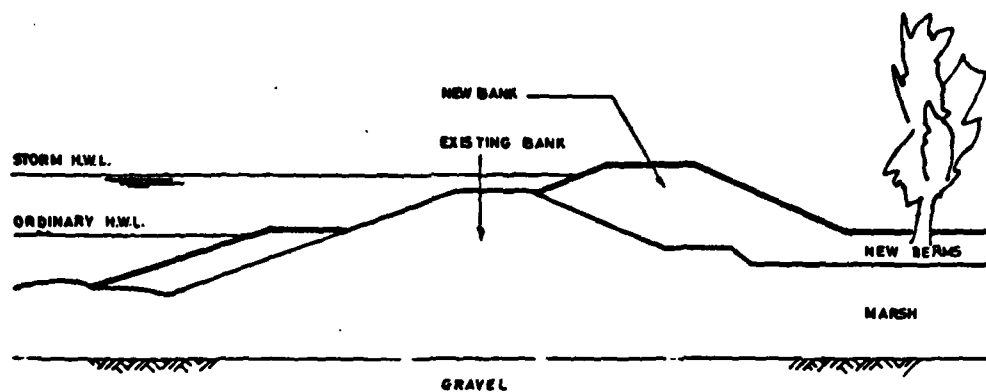
FIG 1·3 FLOODBANK PROFILES DOWNSTREAM OF THAMES BARRIER

ALLUVIUM & SILT

GRAVEL

THAMES

CHALK
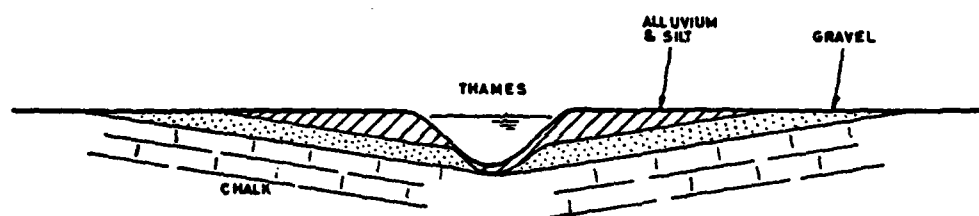
FIG 1·4 SCHEMATIC CROSS SECTION THROUGH THAMES AT DARTFORD

CLAY BANK AVERAGE DENSITY 1·6 γ_w

PEAT AND PEATY CLAY AVERAGE DENSITY 1·2 γ_w

PEAT AND PEATY CLAY AVERAGE DENSITY 1·15 γ_w

RIVER THAMES

SAND AND GRAVEL

CHALK
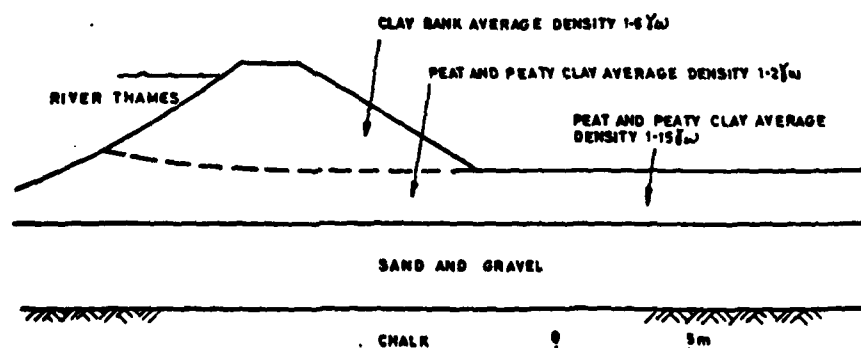
FIG 1·5 SECTION THROUGH FLOODBANK AT DARTFORD LOCK BREACH
(Taken from Marsland, 1961)

maintenance. In the last half century major works have been required approximately every twenty years. On each occasion the level of the banks has been raised, but the protection offered by these embankments has remained approximately constant. The reason for this is a combination of settlement and disiccation of the upper layers of soil of the embankments, settlement of the marsh by drainage and the general rise in sea level.

It was not until 1972 that interim bank raising restored a suitable freeboard at low points in the GLC's flood defences, after the serious flood of 1953. Recently, the Thames Barrier project has necessitated the comprehensive rebuilding and strengthening of the river walls and embankments downstream to meet new design levels which have been based on computer predictions and model tests.

In many places along the Thames the alluvium of the marshes has been too soft to sustain the rapid construction of the new embankments. Where this is the case wide loading berms, Fig. 1.3, have been built in advance of the main embankment raising. The loading berms consolidate and strengthen the subsoil before bank raising, and later in times of flood, stabilise the embankment against underseepage and uplift induced failure.

A reference to part of the work with which the Building Research Establishment (BRE) has been concerned is to be found in the papers by Marsland, 1961, 1968, 1973. In the 1961 paper he discusses the geology of part of the southern part of the estuary at the level of the Crayford marshes, shown schematically in Fig. 1.4. The chalk bedrock is overlain by a gravel layer approximately 7m in thickness. Close to the river Thames the gravel is overlain by a layer of recent alluvium up to 11m thick which now forms the marshes. This clay/peat alluvium thins away from the main river and eventually about one kilometre from the river the gravel outcrops. The layer of alluvium consists of soft interbedded clays, silts and peat.

The same general pattern is found along the creeks and inlets which feed
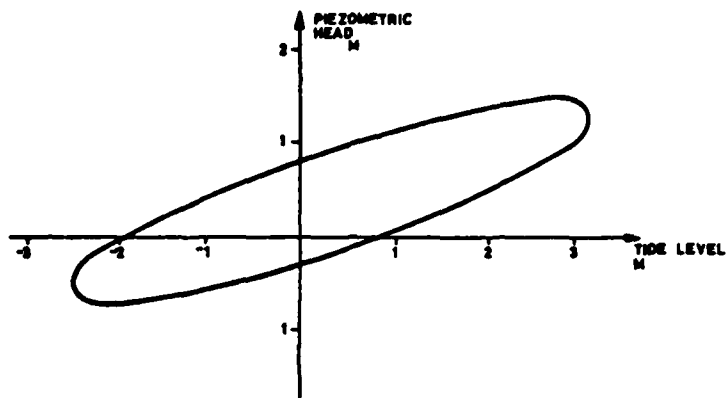
FIG. 1·6 VARIATION OF WATER HEAD IN GRAVEL
WITH TIDAL FLUCTUATIONS.
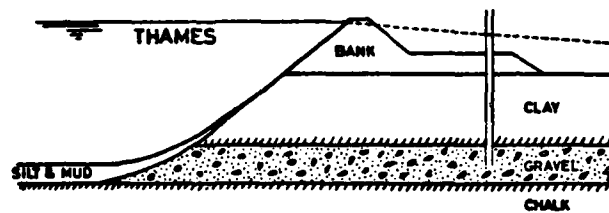
FIG. 1·7 IDEALISED RIVERBANK CROSSECTION
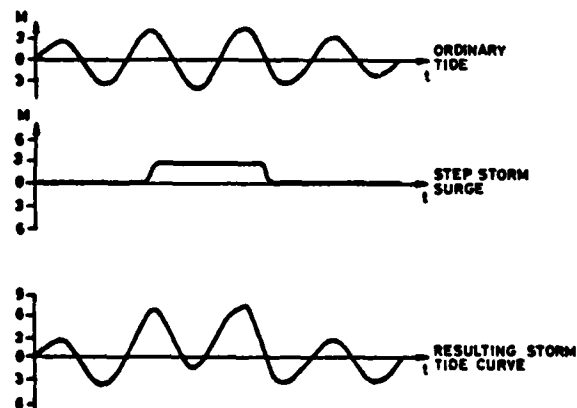
FIG. 1·8 TIDE CURVES USED IN ANALYSIS
(Taken from Marsland & Randolph, 1978)

the Thames, except that the alluvium is not so thick on the banks of a creek as it is along the Thames. Marsland found that at Dartford Lock at the site of a breach in 1953, the alluvium was locally only 1.8m thick and consisted of a lightweight mixture of peat and peaty clay, Fig. 1.5.

The gravel which underlies this alluvium outcrops in the creek, and excess pore water pressures in the gravel under the marsh are closely coupled to the outside water level. Measurements reported by Marsland and Randolph, 1968, at the nearby Crayford marshes, Fig. 1.6, show that the water pressure in the gravel under the marsh lags the tide by about two hours. The magnitude of the water pressure is usually attenuated by the finite permeability of the gravel stratum, and by layers of silt and mud on the river bed, Fig. 1.7. Randolph used these data to develop a mathematical model for the response of the pore water pressures in the gravel to fluctuations in tide level in the river. He then used the model to predict the magnitude of the pore water pressures which would be developed during a storm surge superimposed on a peak spring tide. He found that the pore pressures predicted for a twelve hour step surge, Fig. 1.8, were considerably higher than those predicted by a simple extrapolation of the ordinary sinusoidal tidal response.

Randolph calculated the ratio of alluvium weight to excess pore pressure in the gravel, Fig. 1.7, to give a factor of safety against flotation of the marsh. His results are shown in Fig. 1.9 for the tide conditions shown in Fig. 1.8. The factor of safety is in places less than unity and is nowhere greater than 1·2. At some distance from the river, where the pore pressures are attenuated, the factor of safety is still critical since the depth of the alluvium decreases further from the river.

The inescapable conclusion from these calculations is that during a long storm surge the alluvium in the low-lying marsh may well be floating and in extreme cases may heave, store water under pressure until it bursts, and so flood the marsh.
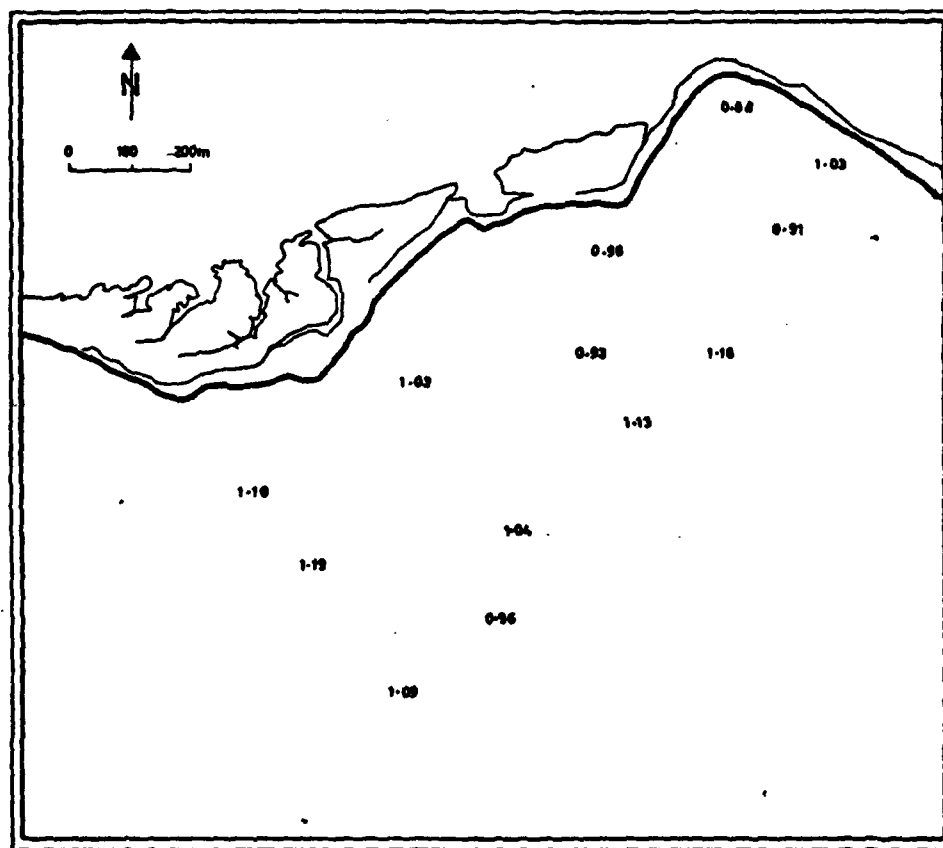
FIG 1·9 SAFETY FACTORS AGAINST UPLIFT FAILURE FOR CRAYFORDNESS
FOR 3m STEP STORM SURGE LASTING 12 HOURS AT SPRINGS
(Taken from Marsland & Randolph, 1978)

The uplift water pressures act also on the foundation of the flood embankments and can have a serious effect on their stability. At least one failure in 1953 was caused by "uplift interaction" and occurred at Dartford Lock where the alluvium was locally very thin as mentioned above, Marsland, 1961. The danger that uplift pressures may precipitate a failure is increased at a particular site if the height of the bank is increased. Many uplift failures were probably avoided in 1953 because the banks were simply overtopped or breached by seepage. If the banks had remained intact the maximum flood stage would have been greater, generating thereby higher uplift pressures.

The enlarged Thames flood embankments downstream of the barrier are provided with loading berms to ensure stability during construction. In areas of critical uplift large berms have been built which are intended to reduce the danger that the uplift will precipitate a failure of the back slope of the bank. The design of these berms has been based on limiting assumptions about the behaviour of the bank/marsh system under selfweight and uplift loading. The BRE gave advice to the designers of the new embankments.

A trial embankment has recently been built at Littlebrook on the south bank of the Thames to test the assumptions made in design concerning shear strength and consolidation of the soil, Marsland and Powell, 1977. Although the level of this bank was raised until a slip occurred it was not possible in this type of full scale test to input the effect of uplift pressures. No uplift failure has ever been observed in progress and little is known of the mechanisms of deformation that are involved.

An attempt was made to fill this gap by Hird, Marsland and Schofield, 1978, who constructed a series of 1/60 scale models which were tested on the Geotechnical Centrifuge at the University of Manchester, Institute of Science and Technology (UMIST), Hird 1974. The geometry of these models was
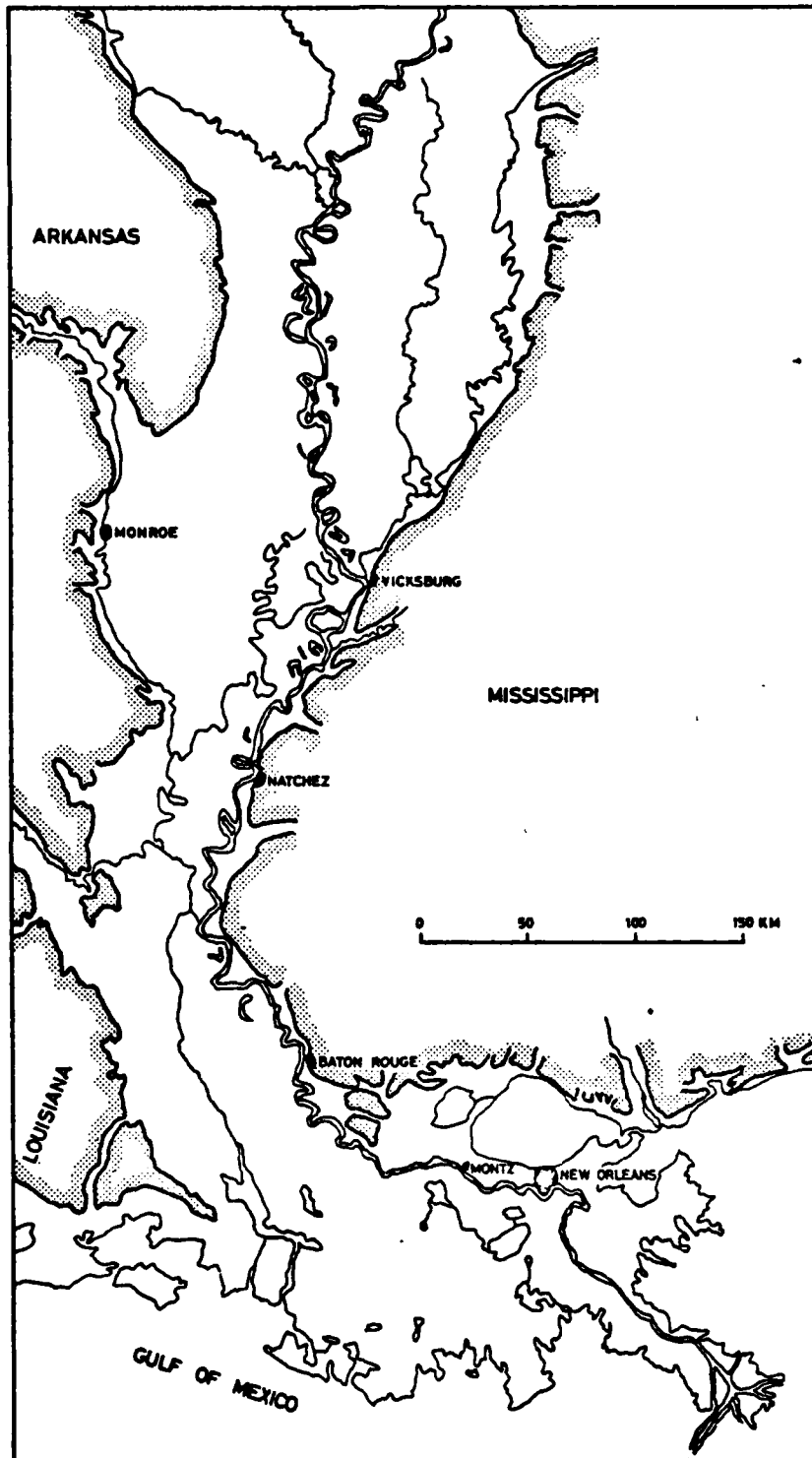
FIG 1·10 THE LOWER MISSISSIPPI VALLEY, PLEISTONE
BLUFFS AND THE MISSISSIPPI RIVER DELTA.

scaled from the typical embankment and marsh cross section which is to be
found along the south bank of the river Thames at the level of the Crayford
marshes (where the alluvium is thicker than at Dartford). The tests
provided data relevant to some of the assumptions made by the designers of
the new flood embankments and indicated that uplift was not a problem
along the main river where the alluvium was relatively thick.

The tests at UMIST did not explore the behaviour of a bank/thin marsh
system and as a consequence did not observe an interaction failure. A thin
marsh geometry is critical for several reasons. The embankment is high in
relation to the marsh thickness and so the head of water which may be stored
in the river is large in comparison with the thickness of the marsh alluvium.
Secondly, the zone of intense shear stress responsible for the stability of
the embankment will be closer to the gravel interface if the marsh is thin.
Increased pore pressures in the interface layers will reduce effective
stresses and hence the strength of the sheared zone and may bring the bank
to failure before the pressures are high enough to float the marsh.

The investigation reported in this thesis into the stability of model
Thames flood embankments took three forms:

In Chapter 2, theoretical predictions are presented concerning the modes
of failure which are to be expected to result from the interaction of uplift
and self weight loadings on an idealised model embankment founded on alluvial
layers of different thicknesses. The experimental details are give in
Chapter 3 of the centrifuged model embankments designed to test the hypotheses
presented in Chapter 2. In Chapter 4 the results of the experimental model
series are presented. Finally, in Chapter 5 the results of the initial
predictions are discussed in the light of the experimental data. Conclusions
are presented in Chapter 6.

1.3 The Mississippi River Banks

The problem of Mississippi river bank stability came to the attention
of A. N. Schofield in the winter of 1974 when he was guest of the U.S. Army,
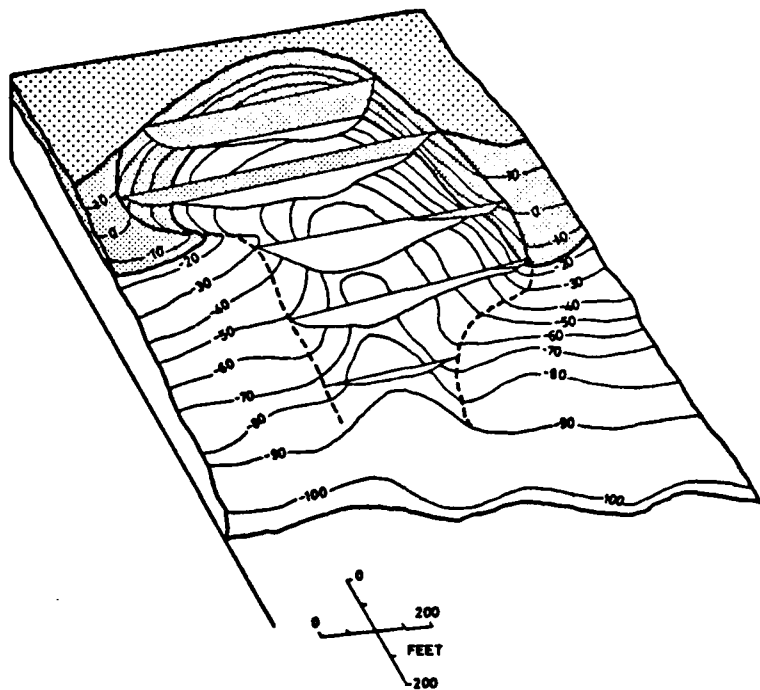
FIG. 1·11 ISOMETRIC VIEW OF THE FAILURE AT MONTZ, LA 1973 (Torrey & Strohm, 1976)
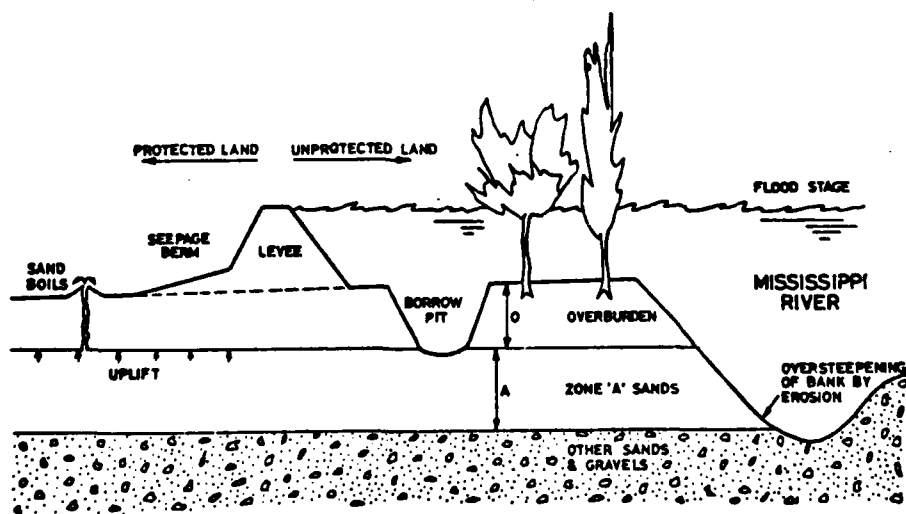
FIG. 1·12 THREATS TO THE STABILITY OF THE RIVERBANK

Corps. of Engineers at the Waterways Experiment Station (W.E.S.),
Vicksburg, U.S.A. One year previously an exceptional flood had tested to
the limit the flood defences of the Mississippi River, Fig. 1.10, and
caused a particularly dangerous flowslide in the river bank at Montz, a
few miles upstream from New Orleans, Fig. 1.11.

Although the flowslides occur frequently in the Mississippi river
banks, this flowslide failure underlined the need for an understanding of
the phenomenon, since this was the closest occurrence of a flow-failure to
the low-lying and densely populated region of New Orleans. The flood
embankments, or 'levees' as they are called in the U.S.A., are built
extremely close to the river at New Orleans and are very sensitive to
river bank failure.

At times of flood the river defences are endangered in three main ways,
Fig. 1.12. Firstly, the embankments may be damaged by overtopping. Hydraulic
and computational models of the river are used to predict maximum river level
or 'stage' as it is called, for a given flood discharge and this data is used
to determine the design height of the flood embankments. If the predictions
underestimate the floodstage, the embankments may be damaged by overtopping
which causes erosion on the backface. Secondly, as is the case for the
Thames flood embankments, the landward face may be endangered by underseepage
which may cause piping and undermining of the embankment. Sand drains and
cutoffs have been installed to solve this problem wherever particularly
dangerous conditions have been identified. Thirdly, with a high flood
discharge there is intense erosion along the river bank itself which is
difficult to control. The river can be trained to some extent by the
provision of groins and revetment but the erosive power of the river at
flood-stage is sufficient to undermine even woven concrete revetment and
leave it flapping in the stream.

The U.S. Army, Corps. of Engineers were made responsible for the
Mississippi River flood defences after the disastrous flood of 1927 and, with
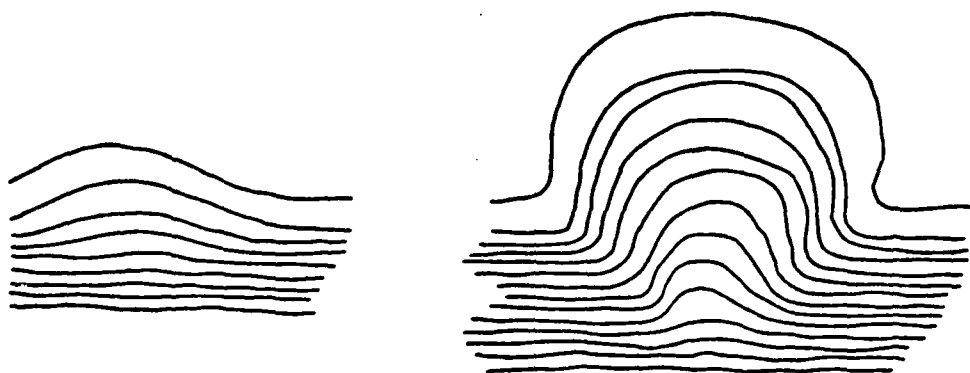
a. SHEAR TYPE FAILURE   b. FLOW TYPE FAILURE

FIG. 1·13 SCHEMATIC CONTOUR PLANS OF FAILURE TYPES

LEVEE

OVERBURDEN   O

ZONE "A" SAND   A

OTHER SAND & GRAVEL

ZONE B & LOWER SANDS
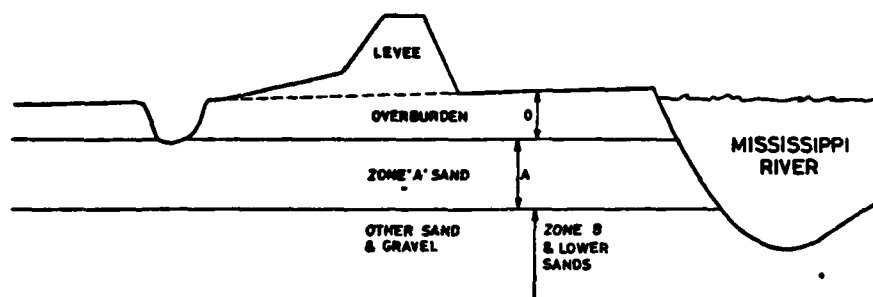
MISSISSIPPI RIVER

FIG. 1·14a SCHEMATIC SECTION OF RIVERBANK

O

$O/A > 1·4$ STABLE

$0·85 < O/A < 1·4$ UNCERTAIN

$O/A < 0·85$ SUSCEPTABLE TO FLOW SLIDING

A
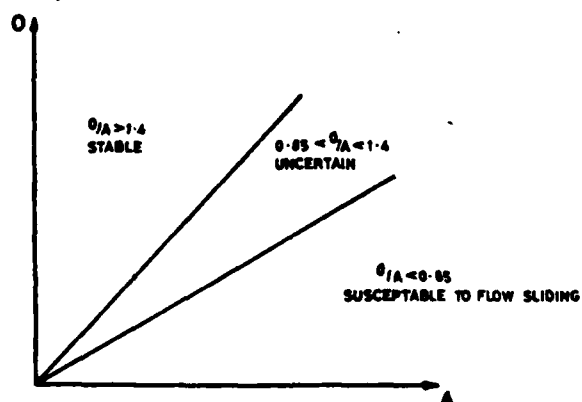
FIG. 1·14b THE "EMPIRICAL CRITERION" OF RIVERBANK STABILITY

the Mississippi River Commission, have undertaken research at the
Waterways Experiments Station since 1929 into the circumstances of the
dangerous bank failures.

Flow failures which are able to erode huge scars into the river bank,
sometimes threatening the main levee, appear to occur only on specific
sections of the river bank. The essential form of the two most common
types of failure is shown in Fig. 1.13. When undermined by erosion at
flood stage sections of river bank with a relatively thick cover of
overburden collapse to form a small crater in the river bank, thereby
generating what is known as a 'shear type failure', Fig. 1.13a. A 'flow
type failure', Fig. 1.13b, appears to occur only where the overburden is
relatively thin. The soundings often show that the shape of the flow
failure is bottlenecked, widening further from the river bank. In many
intermediate cases it is difficult to decide whether a failure is of the
flow or shear type, but principally a 'shear type' failure has its greatest
dimension parallel to the river bank whereas a 'flow type' failure is
oriented perpendicular to the river.

In searching for a means to identify potentially sensitive sections of
river bank the Corps of Engineers have developed a simple empirical
criterion based on the data from thousands of borings made since 1929. The
criterion pinpoints certain sections of old 'point bar' material which
appear from the records particularly susceptible to flow sliding. A point
bar is the deposit of sand and clay which normally builds up on the convex
bank of a bend on a meandering river. The development of these features will
be described in Chapter 7.

The criterion, referenced here as 'The Empirical Criterion' is the most
successful of a series of correlations made by the Corps of Engineers, WES,
1956. Referring to Fig. 1.14a the criterion states that if the overburden
layer is thin with respect to the layer of fine 'Zone A' sand, the deposit
is susceptible to flow sliding. The relation is shown in Fig. 1.14b where

it may be seen that the site is potentially unstable if

$O/A < 0.85; \quad A < 8m$

The absolute thickness of zone A sand is found to be important. Layers of sand thinner than 8m do not generate flowslides. The boundaries between overburden, zone A sands and the coarser underlying materials, Fig. 1.14a, are often diffuse. The classification is based exclusively on grain size distribution as shown in the following table:

Material	Criterion
Overburden soil	More than 20% passing No. 200 sieve
Zone 'A'	25% or more passing No. 60 sieve
Zone 'B'	Less than 25% passing No. 60 sieve
Lower sand	Less than 50% passing No. 40 sieve

The criterion does not predict where flow failure will occur, but where it may occur given the right conditions. In the 1973 emergency the criterion proved to be invaluable to the Corps, being used to predict lengths of bank which required guarding. The criterion was successful in predicting each length where failure actually occurred. The Potomology Reports (e.g. WES 1976) entitled 'Verification of the Empirical Criterion of River Bank Stability' give details of all the bank failures since records began in 1929.

The empirical criterion was developed from correlations of data in the lower Mississippi Valley and its application to the deeper formations on the delta near New Orleans depends on questions of scaling which presupposes knowledge of the processes involved. It is important to know whether the physical processes which give rise to the data summarised by the empirical criterion depend on a critical property of the point bar material itself or on the geometry of the mechanisms which develop when the river bank collapses.

In his paper in 1936, Casagrande explained the occurrence of flowslides in terms of the susceptibility to liquefaction of the sand deposits. The liquefaction event was seen as the result of the propagation of a collapse of structure in sand which was looser than a certain 'critical density'.

The influence of effective confining pressure was realised but not quantified. Geuze, 1948, later identified a higher critical density for a particular value of confining pressure beyond which no volume contraction occurred with shear. More recently Castro, 1969, 1975, and Casagrande, 1976, have reported tests which quantify the effect of confining pressure and express the results of undrained stress controlled triaxial tests in e,lnp space as shown in Fig. 1.15 where distinct regions may be plotted where limited liquefaction and full liquefaction are found to occur. Durham and Townsend, 1973, have published similar work on a Mississippi River sand on the basis that the flowslides along the Mississippi are believed to be caused by the collapse of loose sand deposits.

In a review paper, WES, 1956, Hvorslev reported the state of knowledge concerning the flow failures. In this review Hvorslev stressed the role of the zone A sands and in his recommendations for the identification of potentially dangerous sites suggested the use of the empirical criterion. The approach to be presented in this dissertation highlights two points in Hvorslev's argument. Firstly, he discussed briefly the role of the cohesive overburden in blocking the potential flow of sand away from a failure and in this connection cited the empirical correlations which are presented here as Figs. 1.14b and 10.4. He did not develop this theme and it seems to have been dropped. Secondly, the mechanisms of flow initiation within the zone A sand layer were discussed solely within the context of the collapse of loose sand strata (below the 'critical density' defined by Casagrande). No mechanism was proposed whereby a sand layer of density greater than the critical density may be caused to flow; indeed this was not seen as an alternative. More importantly, however, no consideration was given or has since been given to the manner by which sand, however liquefied, is transported away from the scar of the failure. This neglected aspect of the mechanics of a flowslide would seem to be fundamentally important, since no matter how loose a sand deposit may be, a catastrophic

I   LIMITED LIQUEFACTION
II   LIQUEFACTION

VOIDS RATIO AFTER CONSOLIDATION

EFFECTIVE MINOR PRINCIPAL STRESS AT FAILURE

KN/M²
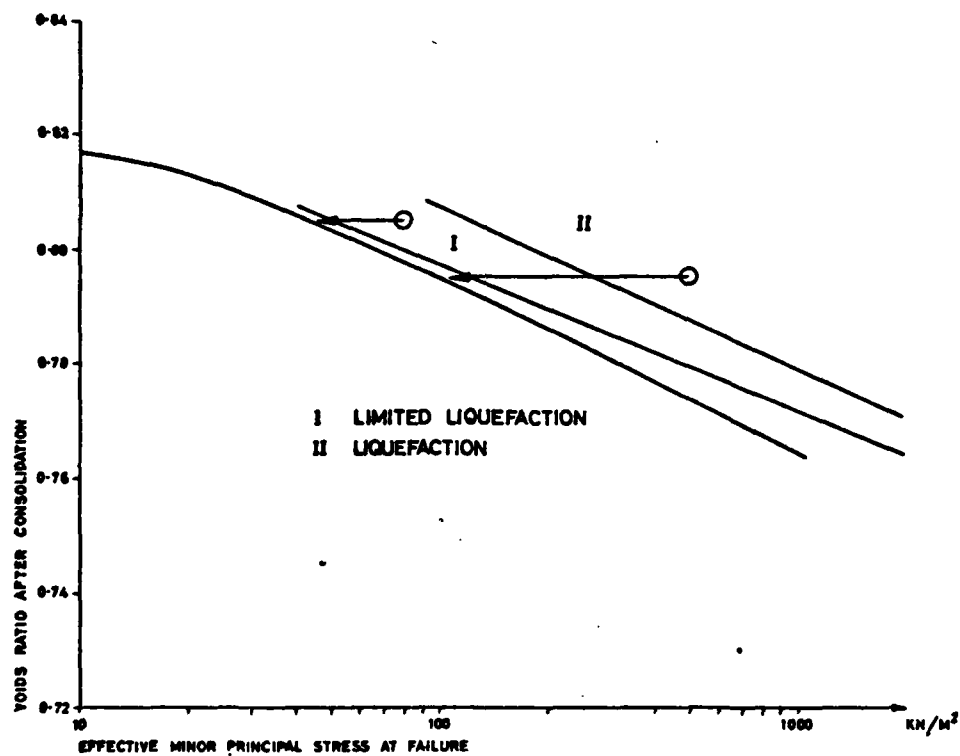
FIG. 1·15 LIQUEFACTION SUSCEPTIBILITY OF SAND FROM THE
REID BEDFORD BEND, MISSISSIPPI RIVER. DATA FROM
STRESS CONTROLLED TRIAXIAL TESTS.
(Taken from Townsend & Durham, 1973)

flow failure will only result if the material is able to set itself in motion and maintain its transport away from the scar.

Current research at WES into the flowslide problem involves careful quantitative measurement in triaxial tests of the 'critical density' of the prototype sands under differing conditions of loading. This approach improves our understanding of the spontaneous collapse of structure which may develop in loose sands, and bears direct relation to the research into the response of sands of supercritical density to oscillating loadings, (e.g. Seed, 1976).

The empirical criterion is a geometrical condition which makes a simple statement about the relative thickness of two layers. This apparent contradiction between on the one hand the research into the liquefaction susceptibility of sands at differing densities and stress levels, and on the other the unresearched simple geometrical criterion, led Schofield to hypothesise that the physical meaning of the criterion was to be found in the geometry of the mechanisms which develop when the overburden and the sand layer interact in failure. If suitable mechanisms can be observed and the hypothesis substantiated then one inference from this new approach is that the sand layer in a zone A formation may be susceptible to liquefaction almost wherever it occurs, but only susceptible to flowsliding when covered by a thin overburden. In that case it is the behaviour of the cohesive overburden that allows the propagation of a failure in certain circumstances and not in others.

In June 1975 a research proposal was submitted to the U.S. Army European Research Office, to fund a centrifugal model investigation of the phenomenon of flowsliding on the Mississippi river banks. The proposal was accepted and a grant made to support the work presented in this dissertation on 1 April 1976. In the proposal two important postulates were made. Firstly, it was suggested that sites where the zone A sands are potentially liquefiable are not uniquely identified by the empirical
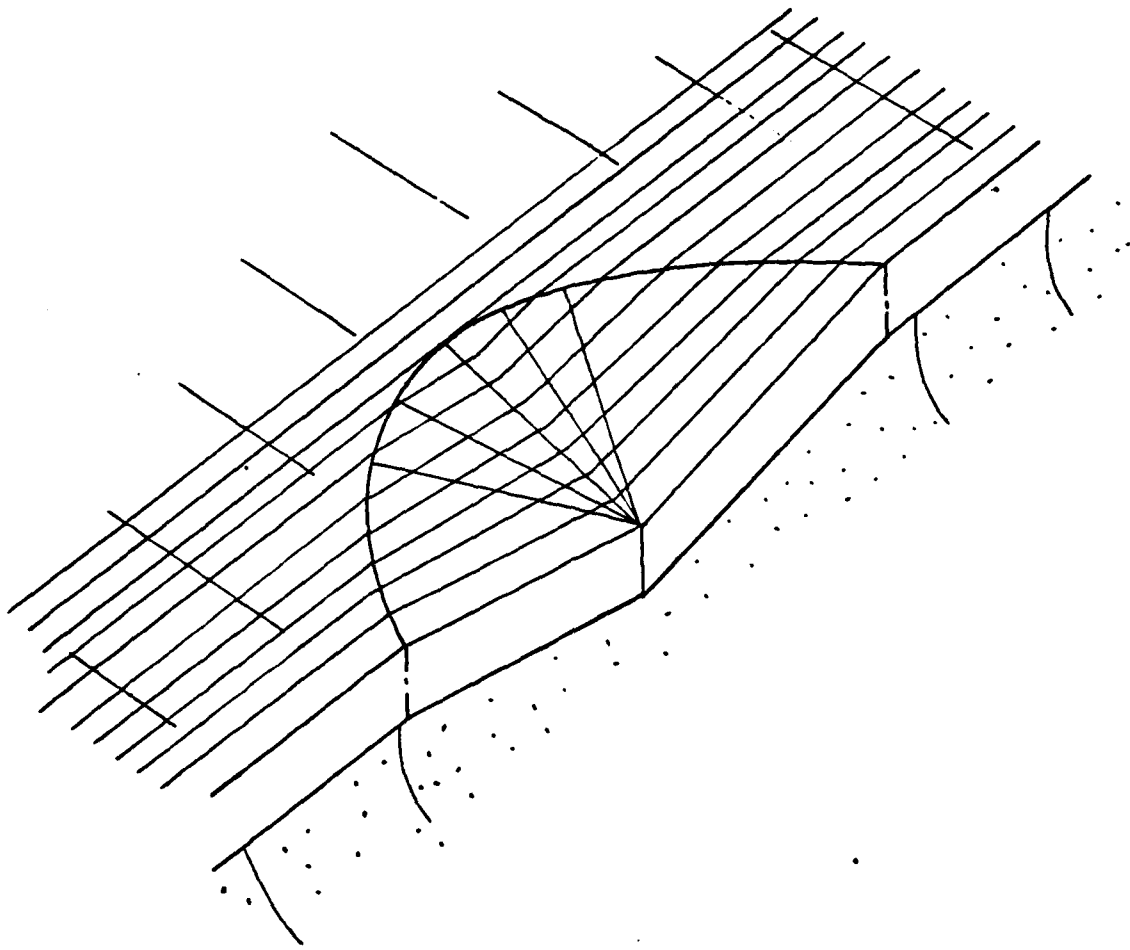
FIG. 1.16 HYPOTHETICAL MODE OF FAILURE OF OVERBURDEN

criterion. In other words, that sand under thick layers of alluvium may also be able to generate a liquified flow, but not able to propagate a flowslide. Secondly, where the river bank is composed of point bar deposits the factor which decides whether or not a slump results in an extensive flow failure may be related to the geometry of fracture and plastic deformation of the overburden, Fig. 1.16. At that stage the phenomenon of flowsliding was believed to occur only where loose sand layers were to be found.

With the benefit of hindsight after performing an extensive series of exploratory centrifuge tests, it is clear that the following conditions are necessary for the development of a flowslide failure:

(a) The granular material deforms, fails and becomes liquefied.

(b) The liquefied layer is able to flow away from the failure and does not remain choking up the outlet of the flowslide scar.

(c) Overlying layers do not, by their deformation, restrict the flow or block the outlet of the failure.

The primary aims of the model series were, at the outset:

1. to model a flowslide, and

2. to investigate the effect of different thicknesses of overburden. As a result of the preconceptions about the nature of the processes in flowsliding, rather too much emphasis was placed at the start of the model series on the attempt to model a flowslide by the achievement of liquefaction.

In July 1976 the author made a visit to the WES at Vicksburg to present the results of the first fifteen tests on the centrifuge, to gain an impression of the Mississippi River and site conditions, and to study the available literature. The staff at WES were chiefly interested in the modelling of a liquefaction flowslide; the interaction of the two layers was seen there to be of secondary importance. It was apparent, however, that the mechanics and development of a flowslide were not at all well understood. In that case the modelling of a flowslide is an entirely

speculative enterprise since the proper scaling may be calculated only once the physical properties are understood. The author supported the view of James* and others who believed that a mechanism of flowsliding should be possible whereby dense sand is enabled to dilate and then be set in motion. It became evident during the study reported here that the initiation of liquefaction, condition (a) was a necessary process but subordinate in the development of a flowslide to the ability of the debris to flow unhindered from the site of failure, condition (b). A study was made of the literature concerning the flow of liquefied debris and it became apparent that several features of the experiments which were not understood at the time can be put into perspective by a good understanding of the flow of granular materials. With this understanding it is seen that the existence of a loose deposit is not in itself a sufficient prerequisite for the propagation of a flowslide, nor indeed a necessary one.

Part II of the dissertation is devoted to a study of the flowslide phenomenon. In Chapter 7 the origin and nature of the point bar deposits is described in its relation to the processes of erosion and deposition in the river. Also in Chapter 7 the literature is reviewed that concerns the ability of suspensions of granular sediments to flow under gravity. In Chapters 8 and 9 the experimental investigation is described and conclusions are drawn regarding the role of the overburden in controlling whether or not a small failure will develop into a flowslide. The understanding gained by the review in Chapter 7 and by the experiments in Chapters 8 and 9 is used in Chapter 10 to develop new analyses which describe rather well the development of a retrogressive flowslide in a dense, dilatant sand.

1.4 Centrifugal Model Testing

In the laboratory testing of soil models it is often possible to scale prototype processes such that the mechanisms involved in the laboratory bear

---

*R. G. James, 1976, personal communication.

direct relation to the full scale. This is true for example of many groundwater flow problems, footings and the laboratory testing of material properties. Soil properties such as permeability and strength may be scaled by using artificially compounded soils in the laboratory, but it is not possible without the possession of extremely heavy minerals, downward fluid drag or a centrifuge to recreate at model scale the stress distribution found in a massive prototype.

The use of a centrifuge to raise the self weight loading of a soil model was reported by Pokrovski, 1936, and has been widely used in the Soviet Union. The technique was adopted by Avgherinos and Schofield, 1969, and has advanced rapidly. The development of the technique has been described recently by Endicott, 1970, Hird, 1974, Craig, 1974 and Scott, 1977. The latter author gives an exhaustive bibliography.

Linear measurement, density, energy, time etc., scale variously on the centrifuge depending on their dimensions. Mechanisms of deformation scale depending on the type of process involved; for example, scaling for the viscous flow of liquefied sand will be discussed in Chapter 10. For a soil model where stability and diffusion of groundwater are of interest, two scaling rules are of primary importance.

1. If a model is constructed of a homogeneous prototype soil to a scale 1/n and is subjected to n gravities in the centrifuge, then within the limitations of the model and its boundary constraints the effective stress distribution within the model will be equal to that in the prototype. If the prototype is stable, so will be the model.

2. Consolidation times are given by the dimensionless number $T_v = \dfrac{C_v t}{H^2}$ where a characteristic dimension H on the prototype is scaled on the model to H/n. The time taken to achieve a particular state of consolidation after a perturbation (equal values of T_v) will be n^2 less for the model than for the prototype.

Of the several approaches which may be taken in centrifugal modelling the attempt to model a particular prototype situation is perhaps the most complex. It must be possible in this case to show that the material properties scale appropriately for the process involved and that they take the correct values at the outset of the test.

If a model soil specimen has been through a cycle in which it has been unloaded and then reloaded by acceleration, the stress history will not correspond in detail to the stress history of the prototype, which may cause differences in behaviour, particularly at failure.

The complex process of the modelling of prototype behaviour is possible in principle but is to some extent a second generation task. This type of modelling is only unreservedly useful when the scaling relations are known for the mechanisms which are involved, and this in turn only becomes possible when the mechanisms themselves have been observed and are well understood.

The machine is used in this investigation in one of its most basic modes - the investigation of mechanisms of deformation of highly simplified and idealised models. The behaviour of the models is then examined and analysed in its own right. Any conclusions which derive from this analysis may then be applied to the prototype by analogy.

In general the most persistent criticisms of the centrifuge apply also to any laboratory test on soil whether the test is a simple triaxial determination of material properties, or a centrifugal model study of the mechanisms of deformation of an embankment. In comparison with some laboratory tests the centrifuged model often has the advantage that it is relatively large. Nevertheless, the following criticisms are valid and represent cautions rather than refutations of the laboratory technique of testing small samples and models.

1. Particle sizes do not scale properly. The argument that a sand grain may represent a cobble at 1/100 scale is valid but not relevant provided that there are statistically many sand grains involved in the process under study.

2. An increase in strain rate causes an increase in observed undrained strength, e.g. Parry, 1972, Bjerrum, 1973. This argument applies for example, to the measurement of the undrained shear strength of soft clay by triaxial tests where a process which takes, say, four months in the field is performed in the laboratory in 20 minutes. Parry suggests that on average the measured peak strength drops by 3% for every tenfold reduction in strain rate in an undrained test.

    If settlement processes are considered at model scale (1/n) on the centrifuge or on the laboratory floor then the strength may be expected to be increased by a factor of the order $3\log_{10}(n^2)$%. in the present case the factor is perhaps 12%. However, the results of the model tests are not related to any specific prototype and no contradiction is involved.

3. For a small scale model, ruptures may not be modelled properly, Palmer and Rice, 1973. Kaolin in the overconsolidated state softens under shear along discrete rupture planes and it is this material that has been used in the present investigation. Bassett, 1973, has remarked that rupture is not modelled using prototype soils and blames particle size effects. The soils to which Bassett refers are organic with fibrous and peaty inclusions which are large compared with the scale of the model and are likely to have a marked effect. The criticism highlights the observation that different clays respond in different ways to a change in model scale.
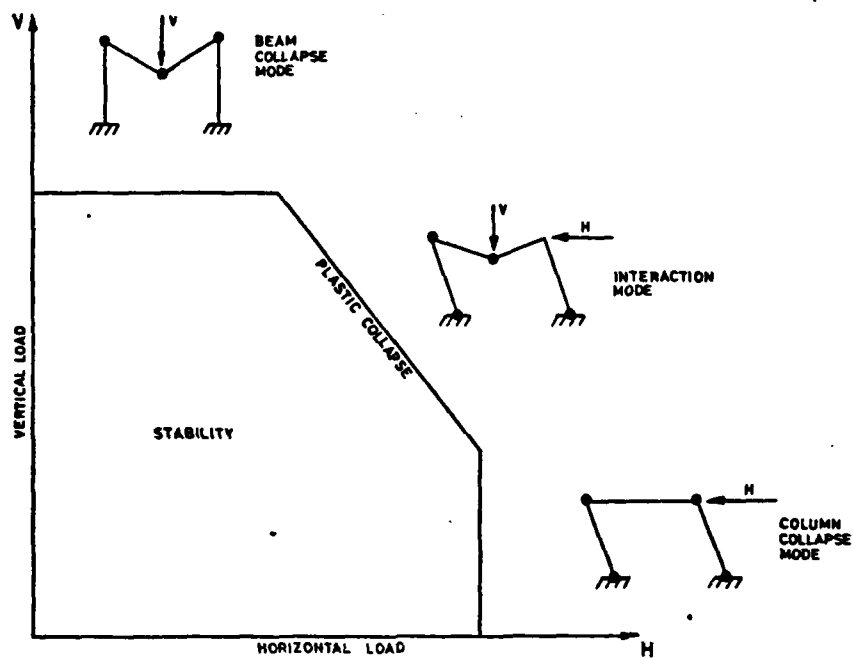
FIG. 2·1 INTERACTION DIAGRAM FOR THE COLLAPSE OF
A STEEL PORTAL FRAME BY THE DEVELOPMENT
OF A MECHANISM WITH PLASTIC HINGES

CHAPTER 2

THAMES FLOOD EMBANKMENTS - SIMPLE PREDICTIONS

2.1 Introduction

In this chapter a simple analysis is presented which predicts the character of the interaction that will occur between uplift and self weight loading on an embankment. In particular the analysis predicts the behaviour of a series of centrifuged model clay embankments.

2.2. Presentation of Data of Failure in the Form of an Interaction Diagram

Bolton, English, Hird and Schofield, 1973, proposed that model test results for uplift induced embankment failures should plot on an interaction diagram of the sort familiar in the theory of plasticity. For the well-known portal frame example, Fig. 2.1, there are three distinct faces to the interaction diagram which represent the three possible combinations of plastic hinge. A load combination which plots anywhere within the diagram is stable, but plastic collapse occurs if the loading combination probes outside the diagram. The mechanisms of interaction involved in the embankment collapse were not considered closely by Bolton et al. and no data was presented to support their hypothesis.

First, in this section, very simple mechanisms are considered that are involved in the failure of a bank of almost impermeable but frictional material, to show how the failure load combinations may be plotted on an interaction diagram. Later in this section attention will be given to a more realistic situation.

Consider, by way of introduction, a block of material supported by a saturated elastic frictional foundation of unit surface area, Fig. 2.2a. The forces on the block are shown in Fig. 2.2. W is the weight of the block and u is the upward force per unit area exerted by the pore water pressure in the foundation (shown diagramatically by the standpipe). R_F is the
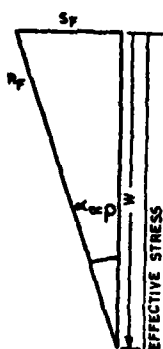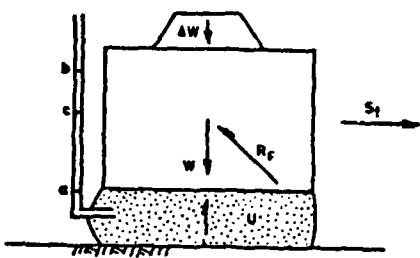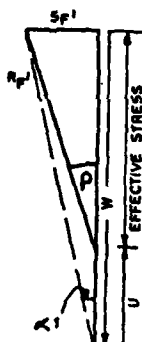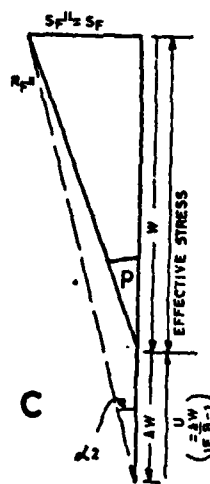
FIG. 2·2 RESISTANCE TO MOVEMENT OF A MASSIVE
BLOCK ON A FRICTIONAL FOUNDATION

resultant of the effective normal stress transmitted to the foundation and the frictional shear resistance in the limiting case. S_F is the force required to move the block laterally. If the water pressure $u = 0$ then the water head in the standpipe is at level (a) in Fig. 2.2 and the polygon of forces in Fig. 2.2a applies where

$$S_F/W = \tan\alpha = \tan\rho = \text{constant} \qquad (2.1)$$

where

ρ = angle of friction for this material

When the water head rises to level (b) in the standpipe a pressure u is exerted on the base of the block and the polygon of forces in Fig. 2.2b applies where the reduced value of S_F' is given by

$$S_F'/W = \tan\alpha_1 = \frac{(W-u)\ \tan\rho}{W} \qquad (2.2)$$

Alternatively, if the weight of the block is increased by ΔW, without allowing drainage in the foundation, then the extra weight will cause an increase in pore water pressure Δu (level (c) in the standpipe) as shown in the polygon of forces, Fig. 2.2c. In this simple analysis it will be assumed for simplicty that $\Delta u = \Delta W$. In other words it is assumed that the pore pressure parameter $\overline{B} = \Delta u/\Delta\sigma_v = 1$ which can be true for example for a lightly overconsolidated silty clay. The basic argument is unaffected by $\overline{B}$. The combination of ΔW and Δu causes the angle α to alter to α_2 where the value of S_F'' is given in the general case by

$$\frac{S_F''}{W+\Delta W} = \tan\alpha_2 = \frac{(W+\Delta W-\Delta u)\ \tan\rho}{W+\Delta W} \qquad (2.3)$$

In the particular case that $\Delta u = \Delta W$

$$\frac{S_F''}{W} = \frac{S_F}{W} = \tan\rho \qquad (2.4)$$

the shear resistance S_F has not been changed by the alteration in W.

a

SLIP CIRCLE DIVIDED
IN SLICES FRICTIONAL
RESISTANCE BY
FRICTION CIRCLE METHOD

SURPLUS LATERAL
FORCE AVAILABLE

COMPLETE
POLYGON
OF FORCES—
STABLE

b

SOIL LAYER IN
EQUILIBRIUM

SOIL LAYER WITH
EXCESS PORE
PRESSURES

DEFICIT OF
LATERAL FORCE

POLYGON
OF FORCES
INCOMPLETE—
UNSTABLE
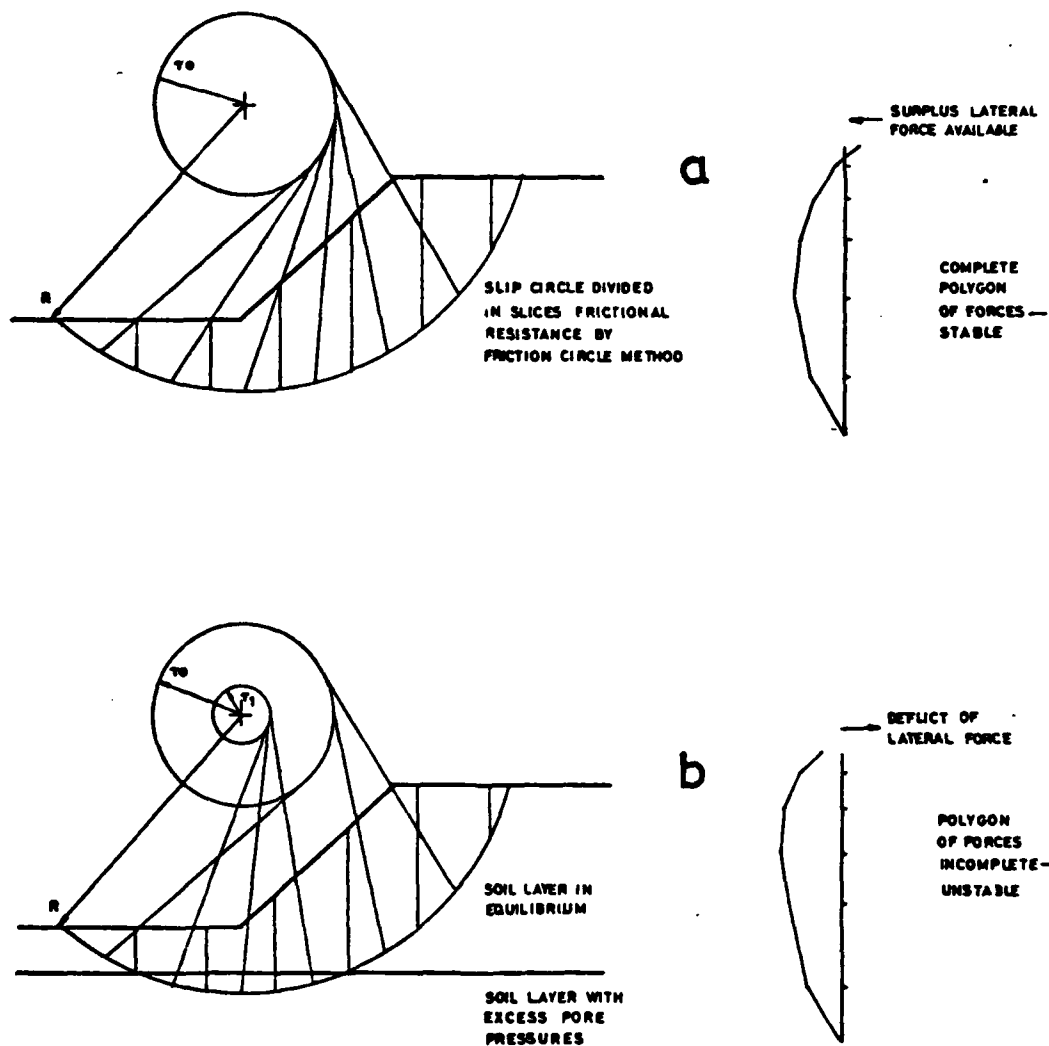
FIG 2·3 RESISTANCE TO SLIP SURFACE FAILURE OF AN
EMBANKMENT OF FRICTIONAL MATERIAL

This type of analysis may now be applied to an embankment of frictional material on a frictional foundation. Ignoring the shear forces between slices it is possible to construct a polygon of forces for a potential sliding mass using the friction circle method, Fig. 2.3a. For a stable bank, a net external side force directed to the left in the diagram would be required to fully mobilize friction on the most critical circle. The radius of the friction circle is given by

$$r_o = R \sin\varphi \tag{2.5}$$

where R = radius of the potential slip circle.

If the deepest part of the circle passes through the layer of soil with excess positive pore pressures, Fig. 2.3b, the conditions described above and in Fig. 2.2b, are realised. For these slices the friction circle will be of a smaller radius,

$$r_1 = R \sin\alpha = R \sin \left(\tan^{-1} \left(\frac{(W-u)}{W} \tan\varphi\right)\right) \tag{2.6}$$

where W is the weight of a slice. A net external side force may be required to the right at the top of the polygon of forces to maintain equilibrium even with fully mobilised friction. If this extra reaction is not available, the slope will fail.

Similar behaviour will occur during an undrained increase in self weight. In this case W increases to $W + \Delta W$ and the pore pressure in the foundation increases from zero to $\Delta u (=\Delta W)$. This is the case discussed above and shown in Fig. 2.2c. α is altered to α_2 and the shear resistance remains unaltered by the increase in W. The radius of the friction circle that applies in this case throughout the embankment is given by

$$r_2 = R \sin\alpha_2 = R \sin \left(\tan^{-1} \left(\frac{W \tan\varphi}{W+\Delta W}\right)\right) \tag{2.7}$$

where the parameters are those defined above. By means of such increases in pore pressure and self weight a previously stable bank may be brought to failure.

In this way it is seen that an increase in either of the two types of loading considered above reduces the stability of the embankment. The two perturbations may be characterised as follows:

1. Undrained increase in material self weight due to an increase in material density or gravitational acceleration (increases disturbing forces without materially altering strength).

2. Undrained increase in excess pore pressure in a foundation layer (reduces shear resistance of soil).

These independant loadings may act separately or together. When they act together they may produce a more severe loading condition than when either acts independantly. This particular combined loading may result in a mechanism of failure characteristic of the interaction of the two loadings, called an "interaction mode" failure.

The material properties so far ascribed to the embankment relate more closely to a sand than to a clay. Where a silt or a clay is involved time is required for water to drain into or out of the material to effect any softening due to excess pore pressures. The simplest concepts of idealised inelastic friction no longer apply. The value of the preceeding argument is that although it deals with an idealised inelastic frictional material it still illustrates, in simple qualitative terms, the behaviour of a clay embankment on a foundation layer of similar clay material. The relevance of the analogy will be discussed below.

In truly undrained loading where there is insufficient time for even local changes in moisture content of the soil, the undrained shear strength is a unique function of moisture content, Bjerrum, 1954, and Schofield and Wroth, 1968. Even if the clay, as is typically the case, behaves as if it is overconsolidated in the upper layers and in the embankment itself, the undrained shear strength is always a unique function of water content, which is in turn related to the stress history of the soil and the current value of mean effective stress. In practice no loading is totally undrained and

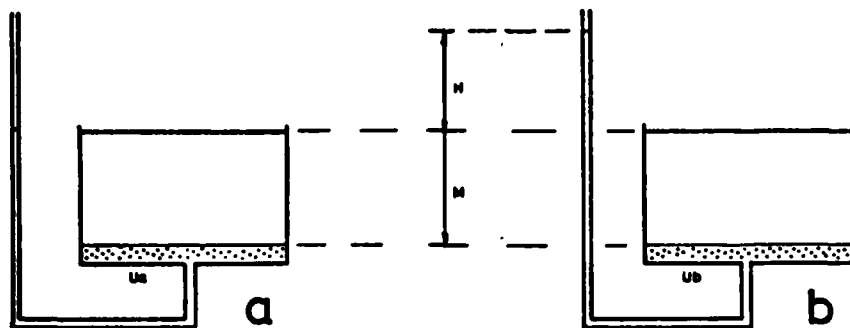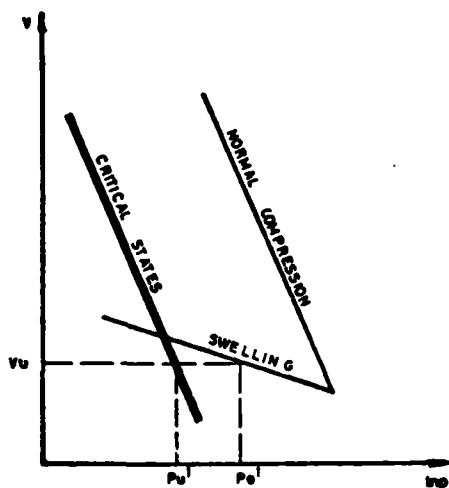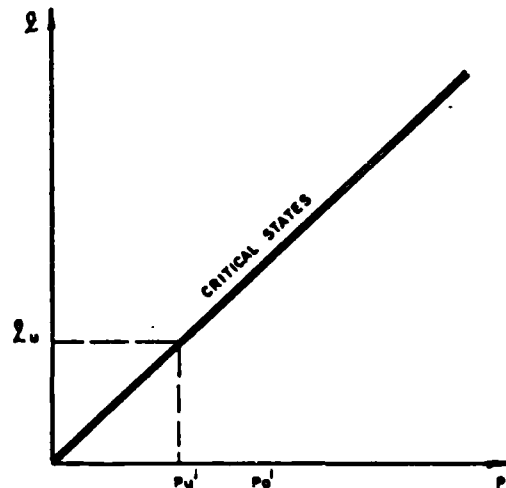FIG 2·4 HORIZONTAL LAYER OF KAOLIN ON SAND DRAINAGE LAYER, UPLIFT
PRESSURE GIVEN BY EXCESS HEAD H

a Imp' GRAPH SHOWING
UNDRAINED CRITICAL STATE
VALUE Pu'

b q, p' GRAPH SHOWING
UNDRAINED CRITICAL STATE
VALUE Qu FOR CLAY AT Po'

FIG 2·5

local moisture content changes are possible at the drained interface.

Consider a layer of clay on a layer of free draining sand, Fig. 2.4a. The water table is at the surface of the clay. If the water pressure in the sand layer is suddenly increased Fig. 2.4b, the clay in an infinitesimally thin layer at the interface will swell vertically to assume a new, lower, value of mean effective stress. This swelling effect will propagate as a wavefront into the clay layer. An individual element in the clay layer will swell progressively towards an equilibrium value of voids ratio that depends on the steady state upward seepage from the sand layer to the surface. The effect at the sand/clay interface itself of the input of pore pressure is to immediately establish a new value of voids ratio and hence of undrained shear strength. At the interface, p' has been reduced by an amount that depends on the elastic properties of the material and the magnitude of the injected pore pressure.

If we identify the critical state strength with the undrained shear strength at any particular voids ratio, Fig. 2.5, then the analogy with frictional material becomes apparent. In qp' space the critical state line passes through the origin and there is no cohesion intercept ($c=0$, $\phi'=\phi'_a$). The shear resistance is determined by the voids ratio of the soil at the time of the test, which for a particular soil with accurately known stress history, is related to the mean effective pressure p'. The major difference between this behaviour and that of the simple rigid/frictional material considered above is that the clay must swell or consolidate to alter the value of voids ratio. These processes are "drained" and require both time and access to water. "Undrained" shear strength is considered because the loading perturbation to failure from the drained equilibrium state of the material is a relatively rapid one.

With these concepts it is possible to develop a model for the response of a clay embankment on a clay foundation in equilibrium to the application of the two independant loadings considered above. Consider a homogeneous clay
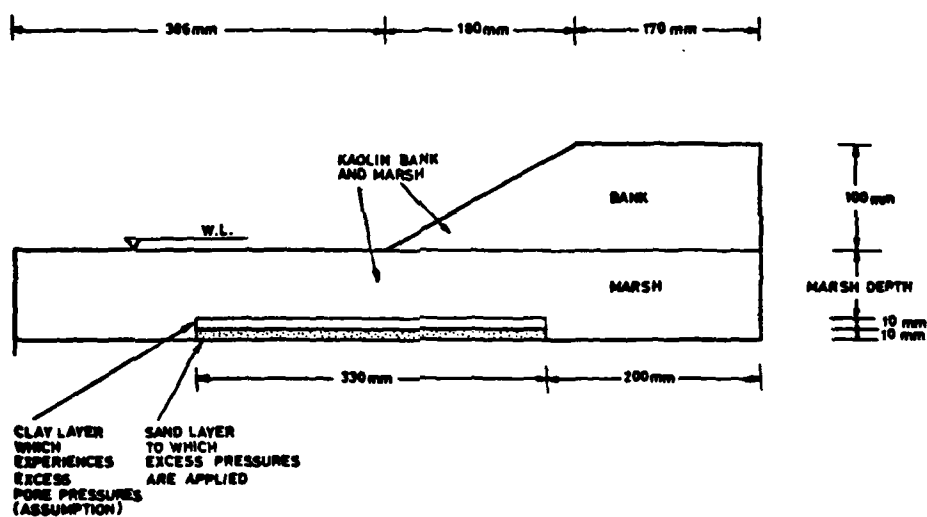
FIG. 2·6 SIMPLE FLOODBANK / MARSH GEOMETRY

embankment on a homogeneous clay foundation (marsh) layer, Fig. 2.6.
The system is subjected to a rapid increase in self weight characterised here
by the general parameter W. The material strength remains unaltered from
its equilibrium value in the bulk of the material, but the disturbing
forces increase with the self weight W. The embankment fails when the
total stresses attain a limiting value. The failure is of the type shown
in Fig. 2.7(I), where a circular slip develops in the bank to a depth that
depends on the material properties: in particular the profile of undrained
strength with depth. There is a range of uplift pressures for which
uplift has no effect on these slip circles and on the mechanism I of failure.

If the uplift is increased independantly of self weight a pressure is
reached eventually at which the marsh begins to float. In Fig. 2.4 the
water pressure, u, at the base of the marsh clay layer of thickness M is
shown in terms of a head of water H above the top surface of the layer.
The marsh layer floats when

$$(H+M)\gamma_w = M\gamma \qquad (2.8)$$

That is when

$$U = \frac{u}{M\gamma_w} = \frac{H+M}{M} = \frac{\gamma}{\gamma_w} \qquad (2.9)$$

which is entirely independant of the value of the self weight W. Any
further increase in the pore pressure u results in a physical lifting of
the marsh and probably failure in tension of the alluvium. Piping may
develop through the ensuing cracks, Fig. 2.7(III).

If the uplift pressures act for an appreciable length of time the
material at the base of the marsh layer may swell and soften. The longer
the uplift is applied the further into the soil will this effect propagate.
This progressive softening alters the material strength profile which may
in turn alter the geometry of the most critical failure surface.

If both types of loading are applied together then a second slip

SELF WEIGHT
COLLAPSE

I

W

'INTERACTION MODE'

II

W

ZONE OF SOIL
INFLUENCED BY
UPLIFT PRESSURES

U

UPLIFT FAILURE

III

U
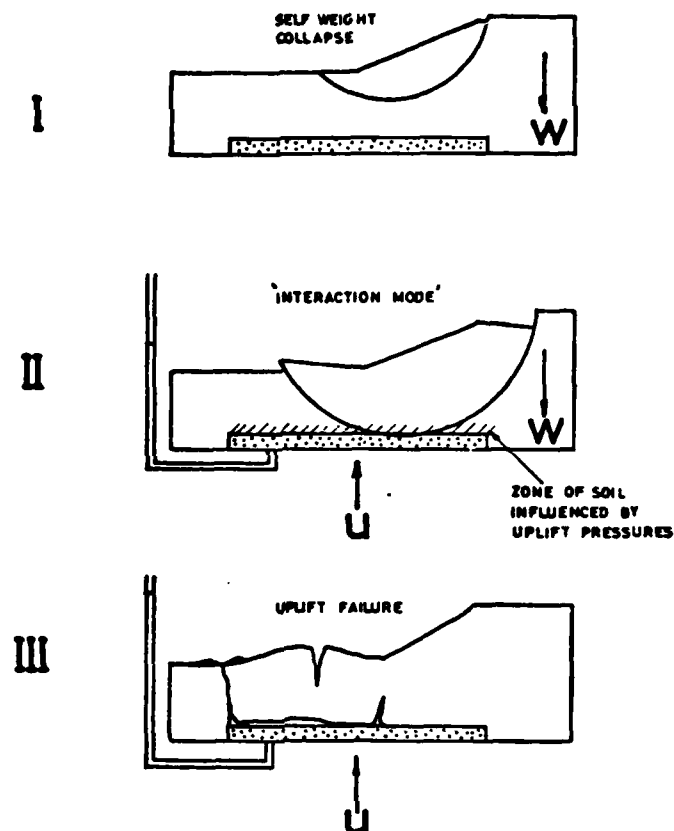
FIG 2·7 THREE POSSIBLE MODES OF FAILURE FOR A FLOODBANK/
MARSH OF FRICTIONAL MATERIAL SUBJECTED TO UPLIFT AND SELF
WEIGHT LOADINGS

W

I

SELF WEIGHT COLLAPSE
OF BANK - INDEPENDENT OF U

SELF
WEIGHT
LOADING

EMBANKMENT

II

INTRACTION MODE

STABLE

COLLAPSE

III

UPLIFT OF MARSH
INDEPENDENT OF W

UPLIFT LOADING U

FIG 2·8 INTERACTION DIAGRAM - LOCUS OF FAILURE STATES FOR
FRICTIONAL BANK AND MARSH SUBJECTED TO INTERACTING LOADING:
UPLIFT AND SELF WEIGHT

self weight loading alone, Fig. 2.7(I) on account of the zone of softened

soil at the uplifted interface. The resulting failure has been termed an

"interaction mode" failure.

The failure states discussed above may be plotted on an interaction

diagram, Fig. 2.8 where the axes represent the two independent systems of

loading. The axes are as follows: The ordinate is the self weight loading,

W, the origin of which is some value of self weight at which all excess pore

pressures have dissipated and the system is in equilibrium. The absissa is

the uplift loading U, the origin of which is zero excess pore pressure at

the equilibrium value of self weight.

For a quantitative consideration of the application of these concepts

to a real clay embankment, in this case a clay model, it is necessary to take

account of several further difficulties. The soil used in the models which

are described in Chapters 3 and 4 was not a simple frictional material nor

an isotropic clay. Therefore it is important to study the actual stress

paths with care to consider the effect of stress history on material behaviour.

2.3 Stress Path Considerations for the Application of Analysis to
Centrifuge Model Tests

In the remaining sections of this chapter the general arguments used above

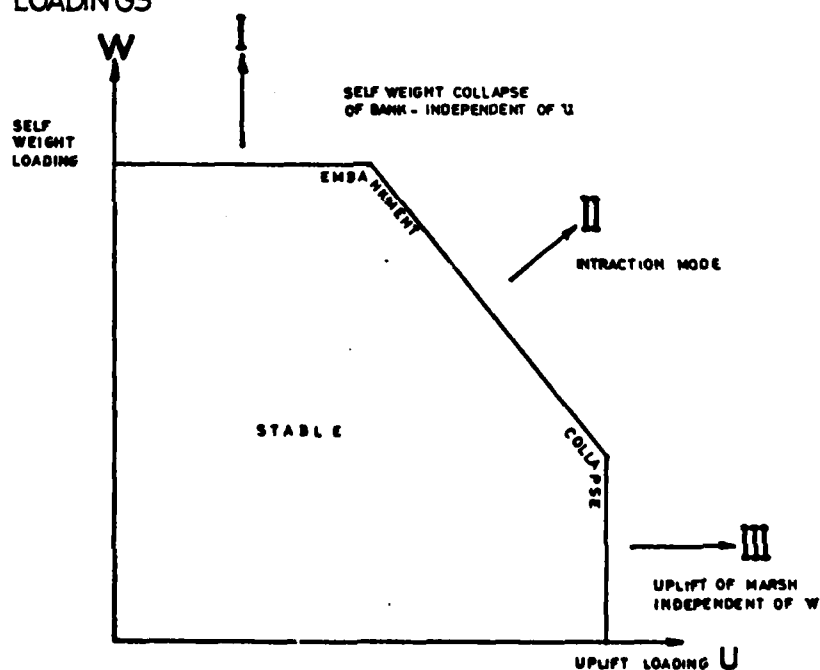are particularised to consider the stability of the idealised centrifuge

model system in plane strain shown in Fig. 2.6. The bank and the marsh layer

were both kaolin. The geometry of the bank was standard in all tests but

different thicknesses of marsh were used. Drainage and uplift to the model

were provided through a sand layer under the clay marsh layer. The aim of

the analysis is to predict the load combinations required to bring such a

centrifuged model embankment to failure. The experimental data of failure

are presented in Chapter 4.

The complicated stress history involved in making and centrifuge

testing to failure a clay model is described in the following sections. The

UNIFORM HORIZONTAL LAYER OF KAOLIN 150mm THICK WITH
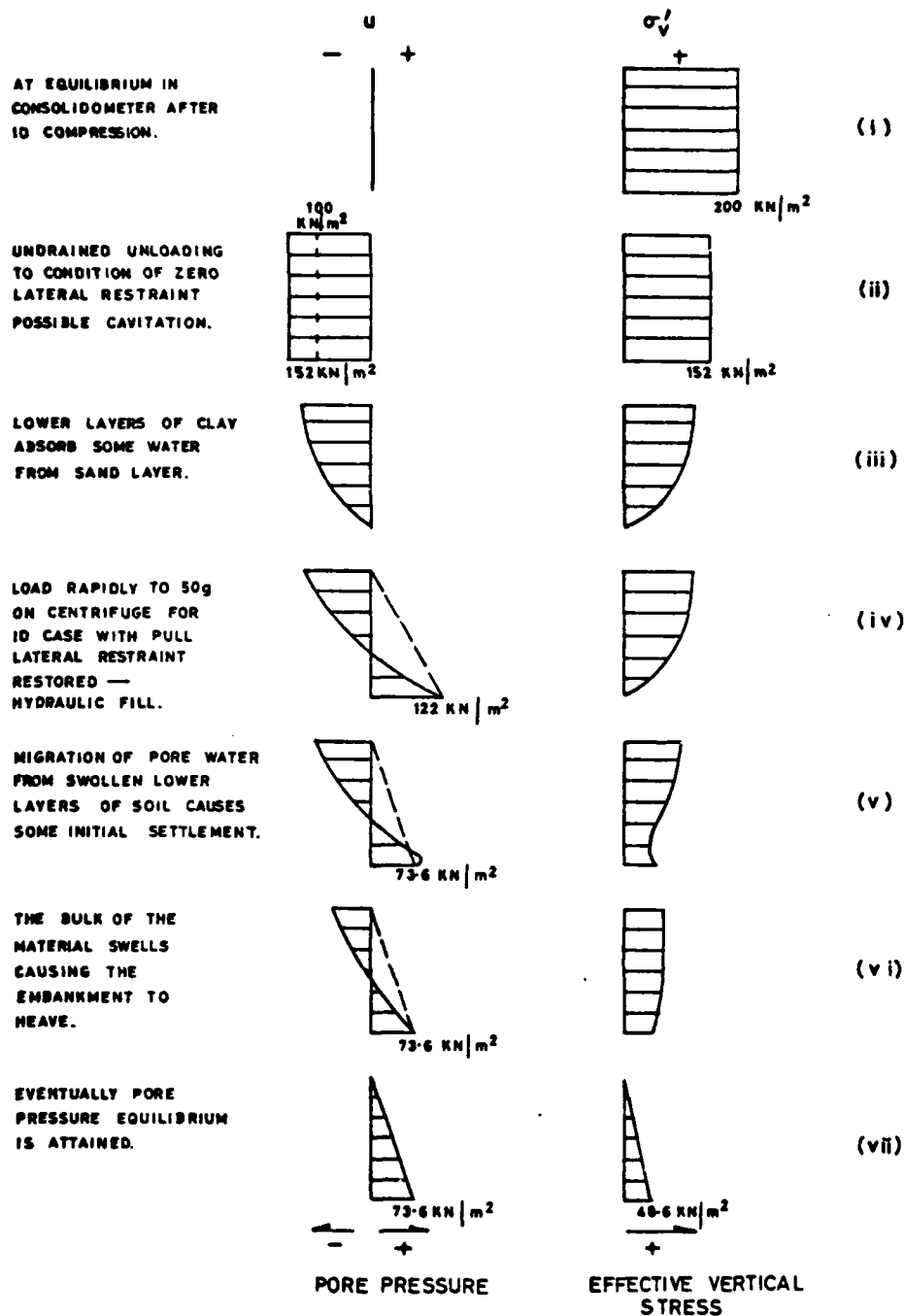UNDERDRAINAGE ONLY.

FIG. 2·9 — PORE PRESSURE AND EFFECTIVE VERTICAL
STRESS DURING CONSOLIDATION, UNLOADING
AND RECONSOLIDATION TO EQUILIBRIUM AT
50g ON THE CENTRIFUGE.

process of laboratory consolidation of the kaolin and swelling to equilibrium

at 50 gravities (50g) on the centrifuge are discussed in Section 2.3.1. In

Section 2.3.2 the stress paths followed by the material during undrained

shear are discussed and relations established for the determination of the

undrained shear strength. In Section 2.3.3 the influence is considered

of the rapid loading perturbations on the behaviour of the model. Finally

in Section 2.4 these considerations are used in the prediction of failure

load combinations for the model embankment. It is shown that the postulate

of Bolton et al, 1973, that such failure load combinations should plot on

an interaction diagram, has a basis theoretically for this type of model.

2.3.1 Stress History in Consolidation and Swelling on the Centrifuge

The stress history of a centrifuged kaolin model from first consolidation

on the laboratory floor to the attainment of equilibrium at the modelling

scale (50g) on the centrifuge, is complex. The clay was consolidated

one dimensionally in the laboratory, unloaded in two stages and then cut to

the required shape on a laboratory bench. Later the model was loaded to

50g on the centrifuge and allowed access to water. The material swelled

at this stress level and eventually achieved equilibrium, at which time it

was loaded to failure.

The pore pressure and effective vertical stress history of a simplified

150mm thick layer of the model is described qualitatively in Fig. 2.9. The

manner in which the changes indicated in Fig. 2.9 can be predicted are set

out in detail below. In summary the stages are the following. The clay is

unloaded from the consolidometer, Fig. 2.9ii and may cavitate. A small

amount of water is available in the sand layer at this stage which may allow

the lower layers of clay to swell slightly during model making, Fig. 2.9iii.

The application of 50 gravities may in the extreme case generate a hydraulic

fill condition where $\Delta u = \Delta\sigma_v$, Fig. 2.9iv which reverts in time to the K_o

condition of effective stress equilibrium, Fig. 2.9v. With a hydrostatic

a

SPECIFIC VOLUME

V

2·8

2·7

2·6

2·5

Critical State Line

1D Compression

V

1D Swelling

X

MAX CONSOLIDATION
PRESSURE
$\sigma_v' = 200$ KN/m^2
$p' = 152$ KN/m^2

p'

50   100   150

MEAN EFFECTIVE PRESSURE KN/m^2

b

AXIAL DEVIATOR STRESS
KN/m^2

150

100

50

-34

-50

Critical State Line

Ko Line
1D Compression

X

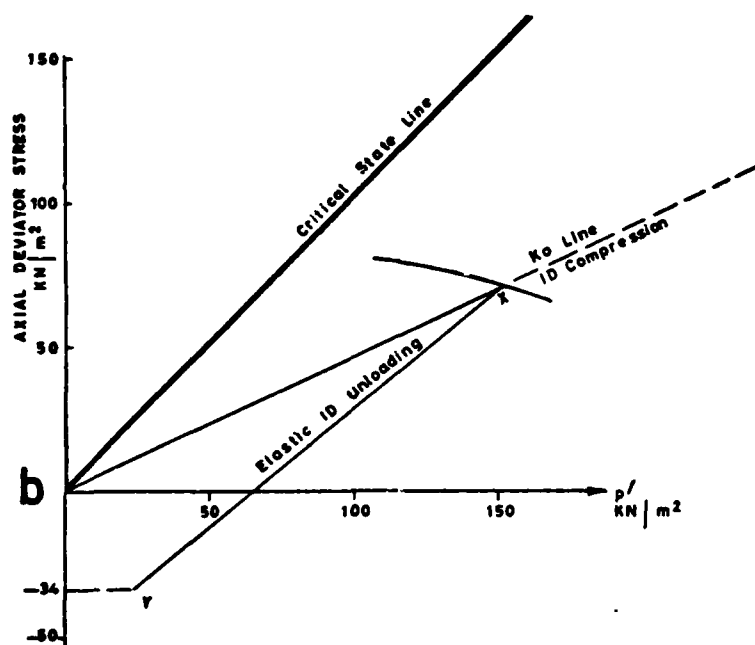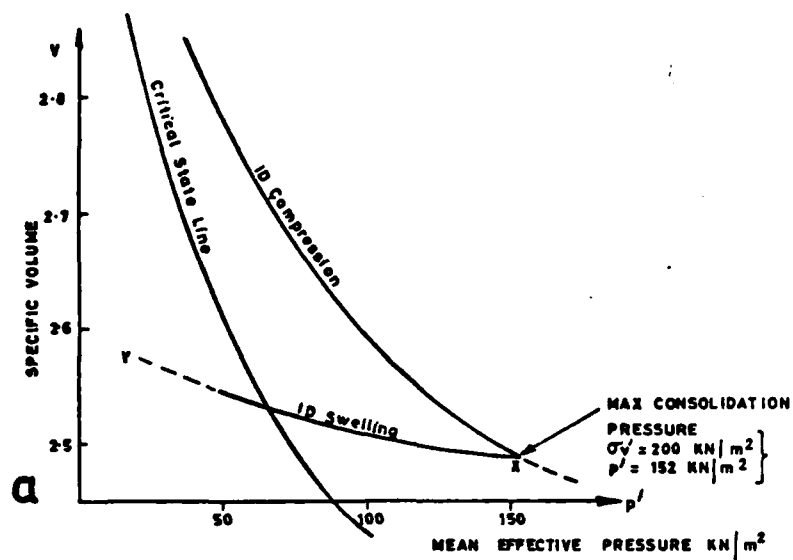Elastic 1D Unloading

V

p'
KN/m^2

50   100   150

FIG. 2·10 – ONE DIMENSIONAL LOADING AND
UNLOADING FOR SAMPLE OF KAOLIN.

water pressure gradient. The first observable effect of the application of 50 gravities, Figs. 2.9iv, v is recompression at the base of the model of the soil that has swollen. The greater part of the embankment swells steadily until it attains pore pressure equilibrium, Fig. 2.9vi, vii. Cavitation if it has occurred inhibits the inflow of water, but during the "consolidation run" at 50g the air and water vapour released from solution at unloading gradually redissolve.

An approximation to the time required for the establishment of equilibrium, Figs. 2.9v, vi, vii, of the layer on the centrifuge at 50g may be calculated using simple consolidation theory. Time is measured from the moment of application of 50 gravities which is also the moment at which the drainage taps are opened. The layer is drained on the bottom only and negative pore pressures are present until a late stage in the consolidation/swelling process. From the standard solution for a uniform surcharge loading it is possible to show that the top of the layer will have achieved 90% dissipation of excess pore water pressures at a time factor

$$T_v = \frac{C_v t}{H^2} = 0.87. \qquad (2.10)$$

Endicott, 1970, gives a value for $C_v = 4 \times 10^{-7}$ m^2/sec for kaolin in a similar state. From the above values the time taken to achieve 90% consolidation in the uppermost part of the layer 150mm thick is $t = 13.6$ hours.

The detailed arguments for the construction of Fig. 2.9 are as follows. The one dimensional consolidation of the kaolin is represented in Fig. 2.10. The 1D consolidation line (normal compression) appears in Fig. 2.10a, in e.lnp' space and is the sloping K_o line of Fig. 2.10b, in qp space. All models were made with a maximum vertical effective stress $\sigma_v' = 200$ KN/m^2. Nadarajah, 1973, gives a value of $K_o = 0.64$ for the normal compression of kaolin. The maximum value of mean effective stress is then

p'_{max} = 152 kN/m^2. The position of the critical state line is derived from data summarised by Schofield and Wroth, 1968, for this type of Spestone kaolin.

λ = 0.26   M = 1.02 Γ = 3.62 (kN/m^2)

κ = 0.05 (average)   PI = 0.32

Initial normal compression to p' = 152 kN/m^2 takes the soil to point X in Figs 2.10a,b.

The unloading curve in e,ℓnp and in q,p space is based on the assumption of full lateral restraint and full drainage to equilibrium. Inside the yield locus the behaviour of kaolin approximates to that of a cross anisotropic elastic material, Parry and Wroth, 1976. The nature of this cross anisotropy is still imperfectly understood and it is convenient to assume that one value of Poisson's ratio and one unique value of Young's modulus adequately describe the behaviour of the material in loading and unloading. Parry and Wroth give a curve that relates Poisson's ratio (ν') to the plasticity index for various clays and from this curve a value of ν' = 0.32 has been obtained for kaolin. A simple elastic calculation involving superposition is sufficient to derive an expression for the lateral stress at any stage during unloading. As presented by Parry and Wroth the expression takes the form

$$K_o = OCR \times K_{NC} - \frac{\nu'}{1-\nu'} (OCR-1) \qquad (2.11)$$

where OCR is defined in terms of effective vertical stress and K_o and ν' take the values mentioned above. This elastic calculation predicts that when σ_v' has dropped to zero the lateral effective stress drops to the small but still compressive value σ_H' = 34 kN/m^2. The applied stress σ_v' = 0, σ_H' = 34 kN/m^2 corresponds to the point Y in Fig. 2.10b, see below.

If the same elastic constants are assumed to apply during undrained unloading, Parry and Wroth show that the effective stress path within the yield locus approximates to a vertical line for which p' = constant. The
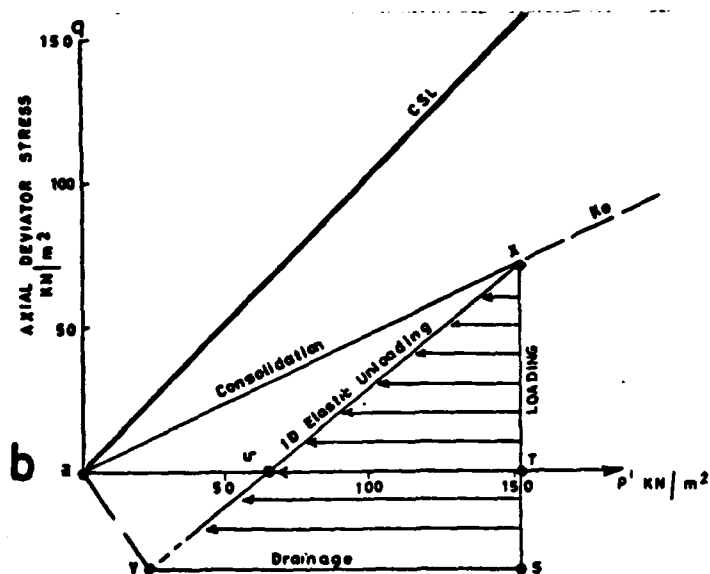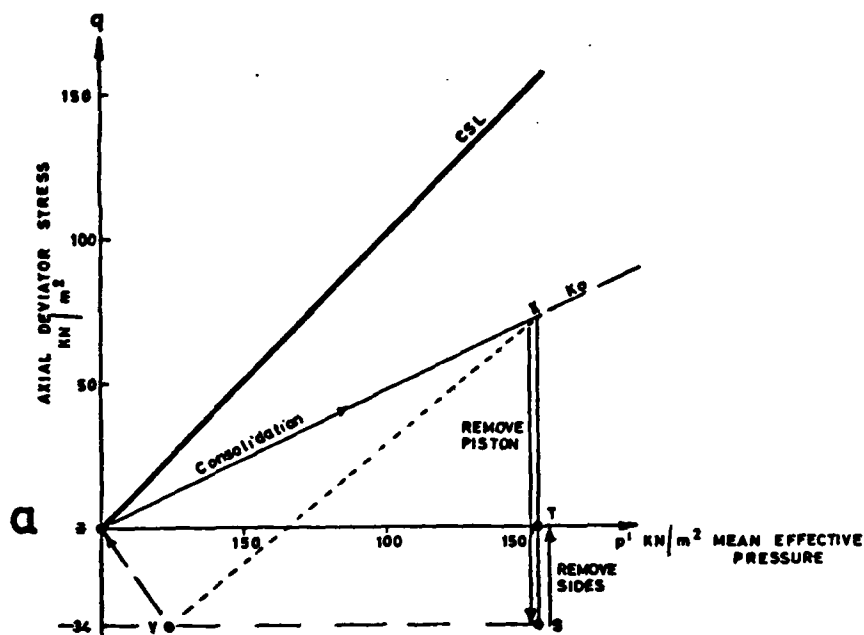
FIG. 2·11 – a. UNDRAINED UNLOADING TO CONDITION OF
ZERO TOTAL STRESS, Z
b. KAOLIN RELOADED WITH SELF WEIGHT STRESS
DISTRIBUTION AND ALLOWED TO SWELL.

ONE DIMENTIONAL LOADING CONDITIONS.

limitations of this assumption are discussed further by Cairncross and James, 1977. With the assumption of full lateral restraint it will be seen that on releasing the vertical effective stress in the consolidometer, the material effective stress state drops down a line p' = constant to q = -34 kN/m^2, point S on Fig. 2.11a. The p' is maintained constant by a negative pore water pressure $u = 152 - \frac{2 \times 34}{3} \doteq 129.3$ kN/m^2 and the total stress state is point Y in Fig. 2.11a. When the sides are .removed from the consolidometer and σ_H' = 0 the material effective stress state reverts to q = 0, p' = 152 kN/m^2, u = -152 kN/m^2. The total stress state is now the point Z in Fig. 2.11a, and the effective stress state is point T. Any drainage into the sample causes the value of p' to fall, Fig. 2.11b, and the material effective stress state to move to the left in the q,p' diagram and out of the plane of the paper following the "elastic wall" or κ line in the $e, \ell np$ plot towards the point U in Fig. 2.11b.

The next assumption is that when the perspex face is fixed on the centrifuge strong box, full lateral restraint is restored to its original value. This implies that any elastic swelling strain laterally in the soil is recompressed by the box sides. The material is subsequently loaded under selfweight stresses at 50g and drainage is permitted. Initially the effective stress states of the material are distributed on the line XS of Fig. 2.11b. Material deep in the layer is heavily loaded and approaches point X and material near the surface approaches the point S. The corresponding points for total stress are found laterally displaced from the effective stress points and on the line XY.

Still with the assumption of a uniform horizontal layer with no possibility of gross shear distortion, the effective stress state of the material, which is loaded to different values of σ_v' (and hence σ_H' and q depending on its depth in the layer) moves to the left in the q,p plane. When swelling is complete the effective stress state points may be expected to lie close to the drained unloading trajectory shown as the line XY in Fig. 2.11b.

a.
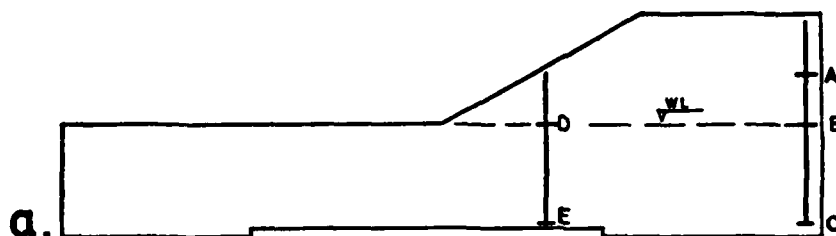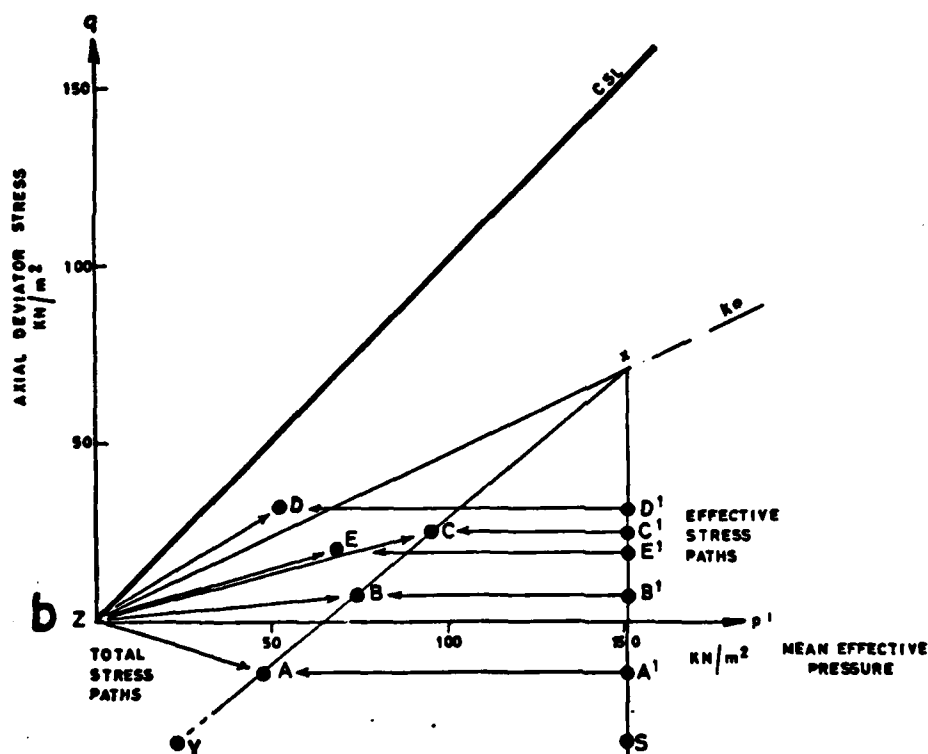
MODEL EMBANKMENT AT 50g

b.

FIG. 2·12.— SKETCH OF THE POSSIBLE INFLUENCE OF SHEAR
ON MATERIAL STRESS STATE.
PROFILE A-C APPROX ONE DIMENSIONAL
DE DEVIATIONS FROM SIMPLE ID CASE

This complex sequence of loading, unloading and reloading may occasion deviations from the theoretical behaviour but the magnitude of the discrepancies is likely to be of the same order as that due to the effects of structural anisotropy and no simple substitute methods of calculation are available.

One further consideration complicates the picture and requires a further assumption. The model is made in the form of a two dimensional homogeneous embankment which is subjected to considerable shear stresses and so the development of shear distortions. The effect of these shear components is to shift the material total stress state off the one dimensional swelling line. As mentioned above, regardless of the applied total stress path the effective stress state is constrained by its elastic properties within the yield locus to move up or down the lines of $p' = $ constant in an undrained loading. If we assume for the present purposes that even in the drained case, p' is unaffected by any deviator stress component due to the shear distortions, then the p' component of the material stress state is fully described (as in the truly 1D case) by the vertical overburden pressure at equilibrium. Some error is implicit in this useful and widespread simplification and it is discussed further in Chapter 5. Qualitatively the situation considered is illustrated in Fig. 2.12. Upon first loading to 50g the total stress state points for elements A-E in Fig. 2.12a move from point Z to the points labelled A-E in Fig. 2.12b. The effective stress state points simultaneously move to the points A'-E' on the line XS. As drainage proceeds the effective stress points A'-E' tend towards A-E as shown in Fig. 2.12b.

The preceding argument has sought to establish that given sufficient time to swell completely at 50g on the centrifuge, the p' component of the material stress state of any element of soil in the model is adequately described by considerations of one dimensional elastic unloading. Quant-
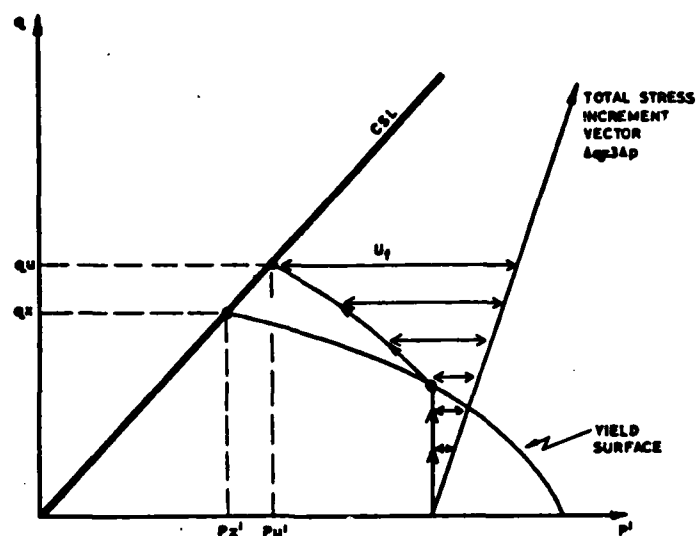
FIG. 2·13 TOTAL AND EFFECTIVE STRESS PATHS FOR
QUICK UNCONFINED COMPRESSION TEST
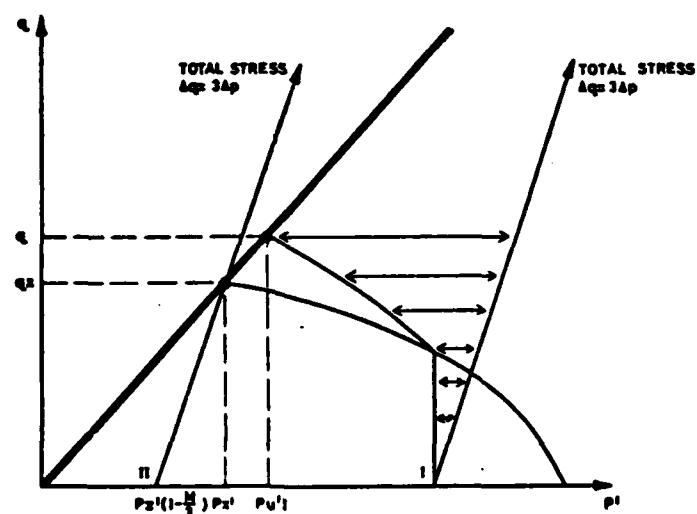ON OVERCONSOLIDATED KAOLIN
(ISOTROPICALLY CONSOLIDATED)

FIG. 2·14 TOTAL AND EFFECTIVE STRESS PATHS FOR
QUICK UNCONFINED COMPRESSION TEST
ON THREE SAMPLES OF ISOTROPICALLY
CONSOLIDATED KAOLIN
TEST I Po'>Px'
TEST II Po'<Px'

itatively p' may be determined from the equilibrium value of σ_v', σ_v'(max) and K_o. To a close approximation the specific volume of the material is then determined uniquely and an estimate can be made of the undrained shear strength.

2.3.2   Undrained Shear Strength Parameters

The point was raised in the previous chapter that an undrained loading or unloading of an element of overconsolidated soil results in an approximately vertical effective stress trajectory in q,p space. In Fig. 2.13 is shown the total stress path, $\Delta q = 3\Delta p$, of triaxial compression with constant cell pressure. The effective stress point rises with the deviatoric component of total stress until it meets the yield locus. Up to this point pore water pressure has developed such that $\Delta u = \Delta q/3$, or the pore pressure parameter $\bar{B} = \Delta u/\Delta\sigma_v = 1/3$. Once the effective stress path meets the yield locus it moves along the state boundary surface on a plane $v = constant$, for which $\bar{B} \approx 1$, until it approaches the critical state at (q_u, p_u') where unlimited shear distortion may develop with no further increase in deviator stress. The rate of development of pore water pressure during these two stages of loading has been discussed recently by Parry and Wroth, 1976, and earlier by Schofield and Wroth, 1968. Lightly overconsolidated specimens may be said in general to deform elastically, yield and proceed towards the critical state with the generation of positive pore pressures.

Heavily overconsolidated specimens are those whose effective stress origins lie to the left of the critical state point (q_x, p_x') on the q,p diagram of Fig. 2.14 and move to the right in q,p space during the latter phase of deformation and typically approach the critical state with the generation of negative pore pressures. (The point at which negative pore water pressures are developed depends on the orientation of the total stress increment vector). The behaviour of heavily overconsolidated specimens is however not homogeneous. Discrete surfaces develop which

FIG. 2·15 EFFECTIVE STRESS PATH FOR UNDRAINED
SHEAR OF HEAVILY CONSOLIDATED KAOLIN
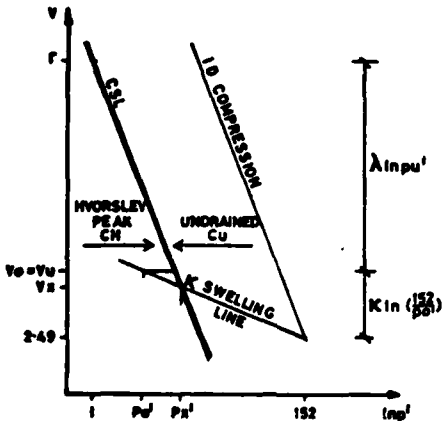
FIG 2·16a EFFECTIVE STRESS
PATH IN UNDRAINED SHEAR
FOR HEAVILY OVERCONSOLIDATED
KAOLIN
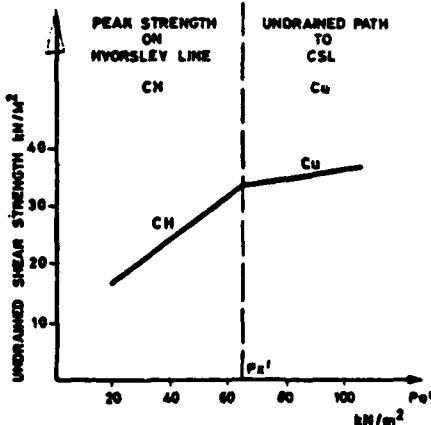
FIG. 2·16b VARIATION OF
UNDRAINED SHEAR STRENGTH
WITH CONFINING PRESSURE

soften and deform towards the critical state. The mode of failure is one
of rupture rather than plastic deformation and the critical state strength
(q_u, p'_u) of the intact material at its initial uniform voids ratio is no
longer a good estimate of the undrained shear strength. The peak shear
strength attained by the material at rupture denoted here by

$$c_H = \frac{q_{(peak)}}{2} \qquad (2.12)$$

is often described in q,p space by a set of "Hvorslev lines" as shown in
Fig. 2.15. These lines are sections on v = constant of the "Hvorslev
surface".

The point v = 2.49, p' = 152 kN/m^2 on the normal compression line of
Fig. 2.16a was determined experimentally, (cf. Endicott, 1970). The point
(q_x, p'_x) is the critical state point on the swelling curve. From the
figure

$$2.49 + \kappa \, \ln \left(\frac{152}{p'_x}\right) + \lambda \, \ln p'_x = \Gamma \qquad (2.13)$$

$$p'_x = \exp. \left\{ \frac{\Gamma - 2.49 - \kappa \, \ln 152}{\lambda - \kappa} \right\} \qquad (2.14)$$

$$= 65.7 \text{ kN/m}^2$$

$$q_x = Mp_x = 67.0 \text{ kN/m}^2 \qquad (2.15)$$

One Hvorslev line is shown thicker than the others in Figure 2.15. This
line passes through the point (q_x, p'_x) and has an equation:

$$2c_d = q_{peak} = k + 0.58 \, p' \qquad (2.16)$$

The gradient of this line has been estimated after study of other pub-
lished work on the subject (e.g. Sketchley, 1972 and Hird, 1974). An effect-
ive stress path that originates from p'_o to the left of p'_x peaks on a
Hvorslev line that lies below the thick line appropriate to p'_x since p'_o lies
on a plane $v_o > v_x$. The relevant Hvorslev line for any p'_o passes through
the point (q_u, p'_u) on the critical state line where, from Figure 2.16a

$$v_u = \Gamma - \lambda \ln p'_u = 2.49 + \kappa \ln \left(\frac{152}{p_o}\right) \tag{2.17}$$

$$p'_u = \exp. \left\{\frac{\Gamma - 2.49 - \kappa \ln 152 + \kappa \ln p_o}{\lambda}\right\} \tag{2.18}$$

$$= \exp. \frac{0.8788 + 0.05 \ln p'_o}{0.26} \tag{2.19}$$

From Equation 2.16 and the equation of the critical state line

$$q = Mp' \tag{2.20}$$

it is possible to derive a value for the intercept k of the general Hvorslev line

$$k = p'_u \ (M-0.58) \tag{2.21}$$

whence from Equations 2.12, 2.16, 2.19, 2.20 and 2.21

$$c_H = 0.21 \exp. \left\{\frac{0.8788 + 0.05 \ln p'_o}{0.26}\right\} + 0.29 \ p'_o \tag{2.22}$$

The effective stress path bifurcates at peak with part of the material swelling and softening towards the critical state at the expense of the bulk of the material which remains undeformed. The peak strength is used for heavily overconsolidated soil in the slip circle analysis of Section 2.4.

As discussed above, for lightly overconsolidated specimens for which $p'_o > p'_x$ the critical state strength is given by Equations 2.19 and 2.20:

$$c_H = \frac{q_u}{2} = \frac{Mp_u}{2} = 0.56 \exp. \left\{\frac{0.8788 + 0.05 \ln p'_o}{0.26}\right\} \tag{2.23}$$

In summary, the undrained strengths used in the analysis of Section 2.4 are shown in Fig. 2.16b where the influence of the two distinct classes of behaviour is evident. It now finally becomes possible to show why the value of deviator stress, q (at equilibrium of the material before undrained loading) is not strictly relevant to the consideration of undrained strength. Effective stress paths rise vertically within the yield locus

and meet the critical state line or peak strength envelope at points that depend on p_o' and v but not on q. The relevance of these points to the particular conditions of a centrifuge model is discussed in the following section.

2.3.3 The Influence of the Loading Perturbations on the Undrained Shear Strength

In previous sections two independent types of loading perturbation have been considered. The effect of these two types of loading on the effective stress state of the model is considered in this section. The same simplifying assumptions are made regarding one dimensional behaviour. The detailed changes in effective stress are considered by means of an example.

Consider an idealised marsh layer 95 mm thick as a uniform horizontal stratum of clay founded on a permeable sand layer. The water table is at the surface of the clay. The layer is in equilibrium at 50g and has an average bulk density of $\gamma = 1.66$ tonnes/m^3. The effective and total vertical stresses are shown in Fig. 2.17A. At the base of the clay layer

$$\sigma_v = 77.35 \text{ kN/m}^2$$
$$= \sigma_v' + u = 30.75 + 46.6 \text{ kN/m}^2$$
$$\sigma_H' = K_o \sigma_v' = 33.9 + 0.47 \sigma_v' = 48.35 \text{ kN/m}^2 \text{ (from Equation 2.11)}$$
$$p' = 42.5 \text{ kN/m}^2$$

If the centrifuge speed is now increased such that the layer experiences 120 gravities, the additional bulk weight may, in the extreme, be taken as a hydraulic fill loading. The resulting total and effective vertical stresses are shown in Fig. 2.17B with the initial drainage into the sand layer and out of the top surface of the clay layer. At the base of the clay

$$\Delta\sigma_v = \Delta\sigma_H = \Delta u = \Delta p = 108.29 \text{ kN/m}^2$$

TOTAL AND EFFECTIVE VERTICAL STRESS AND POREPRESSURE
DURING PERTUBATIONS ON THE CENTRIFUGE   (SCHEMATIC)

a EQUILIBRIUM AT 50g

DEPTH

Us σ_v

STRESS
46·6   77·4   kN/m²

DEPTH

σ_v'

30·8   kN/m²

b INCREASE TO 120g

DEPTH

Us   U σ_v

111·8   154·9   185·6   kN/m²

DEPTH

σ_v' σ_v'

30·8   73·6   kN/m²

c UPLIFT TO U = 1·60

DEPTH

U σ U

111·8   154·9   185·6   kN/m²
178·9

DEPTH

σ

PEAK IN σ_v' PROPOGATES INTO MATERIAL

σ_v'
6·7   30·8   73·6   kN/m²
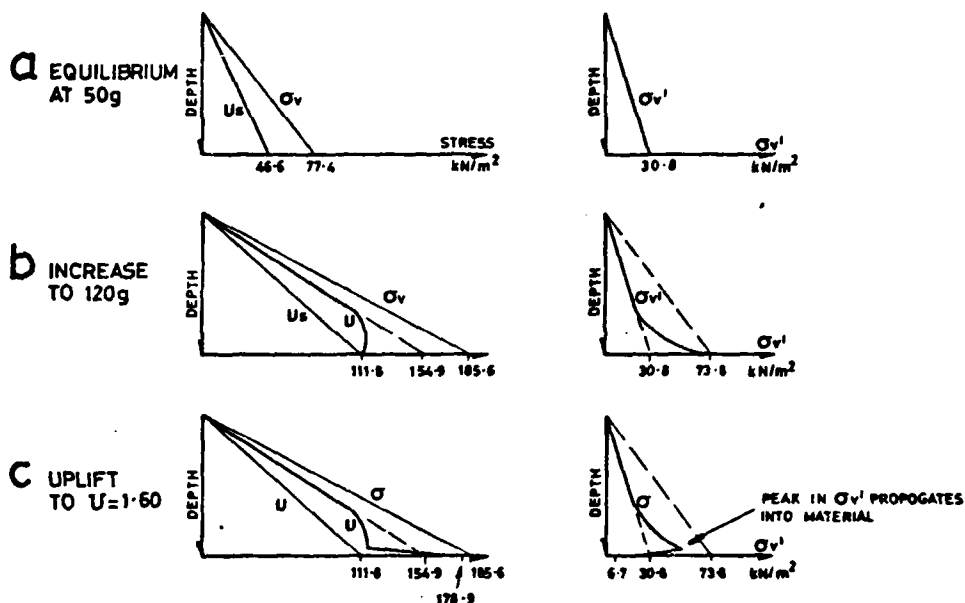
FIG. 2·17 SELF WEIGHT INCREASE PRECEEDS UPLIFT

a EQUILIBRIUM AT 50g

DEPTH

Us σ_v

STRESS
46·6   77·35   kN/m²

DEPTH

σ_v'

30·8   kN/m²

b UPLIFT TO U = 1·60

DEPTH

Us σ_v U

STRESS
46·6   77·35   kN/m²
74·8

DEPTH

σ_v'

2·75   30·8   kN/m²

c INCREASE TO 120g

DEPTH

Us σ_v U

111·8   154·9   185·6   kN/m²
178·9

DEPTH

σ_v'

TROUGH IN σ_v' PROPOGATES INTO MATERIAL

σ_v'
30·8   kN/m²
2·75   6·7
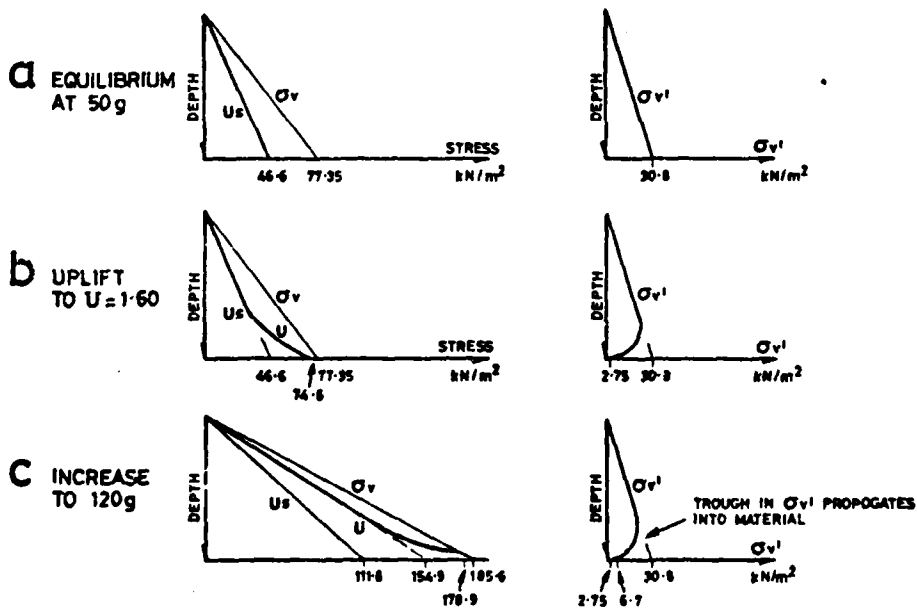
FIG. 2·18 UPLIFT INCREASE PRECEEDS SELF WEIGHT

Material at the interface itself will consolidate rapidly to a new value

$$\sigma_v' = 73.8 \text{ kN/m}^2$$
$$\sigma_H' = 68.6 \text{ kN/m}^2 \qquad p' = 70.3 \text{ kN/m}^2$$

This effect propagates rapidly into the material, strengthening first the layers of soil close to the interface. The effective stress profile some moments after the speed increase is shown in Fig. 2.17B.

If at this point an uplift pore pressure is applied to the sand layer, the consolidation behaviour will be modified. Uplift was defined in Section 2.2 as

$$U = \frac{H+M}{M} = \frac{u}{M\gamma\omega} \qquad (2.9 \text{ bis})$$

where the parameters were defined again in Figs 2.4 and 2.6. For this soil an uplift of $U = 1.66$ would cause flotation of the marsh. Consider the application of $U = 1.60$. In that case

$$H = M(U-1) \qquad (2.24)$$

$$\Delta u = Hng = Mng(U-1) \qquad (2.25)$$

$$= 67.1 \text{ kN/m}^2 \text{ at } 120g$$

The total and effective stresses are now as shown in Fig. 2.17C. The effective vertical stress at the base of the layer has been reduced towards the point Y. It is possible that the layers closest to the interface will yield and the strength parameters used above are then an overestimate.

A new perturbation propagates upwards into the clay layer. This time causing progressive swelling. At the interface itself the effect is almost instantaneous but further into the material time is required for swelling. As a crude indication of the time required for swelling by a thin layer close to the boundary it is sufficient to use the standard solutions for the consolidation of a uniform layer with bottom drainage under a surcharge loading. The time taken to achieve 50% consolidation at a depth of 10 mm

into the layer of kaolin is approximately 5 minutes.

The effect of these perturbations on the undrained shear strength has been the following: At the base of the layer at 50g,

$$p_o' = 42.5 \text{ kN/m}^2 \ (< p_x = 65.7 \text{ kN/m}^2 \text{ from Equation 2.15})$$

In that case the material is heavily overconsolidated and Equation 2.22 applies whence

$$c_H = 0.21 \ \exp . \left\{ \frac{0.8788 + 0.05 \ \ln p_o'}{0.26} \right\} + 0.29 \ p_o' \qquad (2.22 \text{ bis})$$

$$= 25.0 \text{ kN/m}^2$$

After the speed increase to 120g the material at the base of the layer has strengthened by the increase in effective stress to a value

$$p_o' = 70.3 \text{ kN/m} \ (> p_x)$$

In that case the material is lightly overconsolidated and Equation 2.23 applies whence

$$c_u = 0.56 \ \exp . \left\{ \frac{0.8788 + 0.05 \ \ln p_o'}{0.26} \right\} \qquad (2.23 \text{ bis})$$

$$= 37.3 \text{ kN/m}^2$$

Finally, the application of uplift has reduced p' to

$$p_o' = 26.9 \text{ kN/m}^2 \ (< p_x)$$

in which case the material is again heavily overconsolidated and from Equation 2.22

$$c_H = 19.42 \text{ kN/m}^2$$

In the event that uplift is applied at 50g and the model subsequently accelerated to 120g the effective and total stresses at the various stages are shown in the Figures 2.18A,B,C. In this case a very small trough in the effective stress profile propagates up the thickness of the clay but the effective stress at the interface after both perturbations have been applied is the same in both cases. In both cases also the effective stress
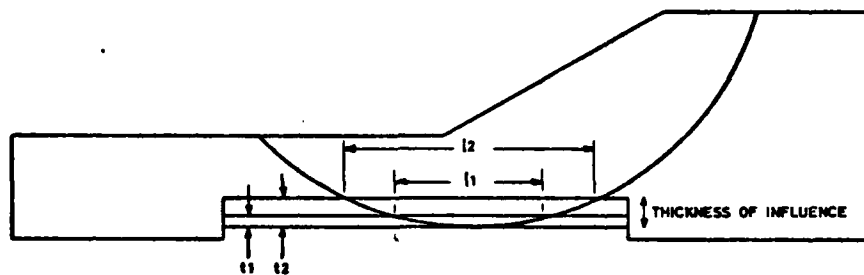
FIG. 2·19 INFLUENCE OF THE THICKNESS ASSUMED FOR
THE CLAY LAYER AFFECTED BY UPLIFT
PRESSURES

(and hence the undrained shear strength) increases with depth in the layer until close to the sand interface where it drops sharply.

In the general case the effective stress on the sand/clay interface for soil lying entirely below the water table is reduced by the application of uplift to

$$\sigma_v' = \sigma_v - u_{static} - \Delta u \tag{2.26}$$

where

$$\sigma_v = 1.66 \ hng \ kN/m^2$$

$$u_{static} = hng \ kN/m^2$$

$$\Delta u = M(U-1)ng \ kN/m^2 \tag{2.25 bis}$$

$$\sigma_v' = ng \ (0.66h - M(U-1)) \tag{2.27}$$

Provided that $1 \le U \le 1.66$

then $0.66 \ Mng \le \sigma_v' \le 0$

But if $U > 1.66$ then σ_v' vanishes and horizontal cracks may propagate in the material if there is no tensile strength.

In contrast to the rapid response of the thin interface layer of clay and sand, the effective stress in the bulk of the layer is unaffected by an increase in either gravitational self weight or uplift. The effective stress of this material starts to alter only once the perturbation of the isochrones caused by the change in boundary conditions has reached the material in question.

2.4 Slip Circle Calculations

These calculations are intended to be simple predictions of model behaviour presented before the model test results in order to give the reader an impression of the events to be expected in the model series. The simple calculations relate to what are by analogy full scale bank failures induced by self weight and uplift loadings. Linear dimensions are small but densities are extremely large.
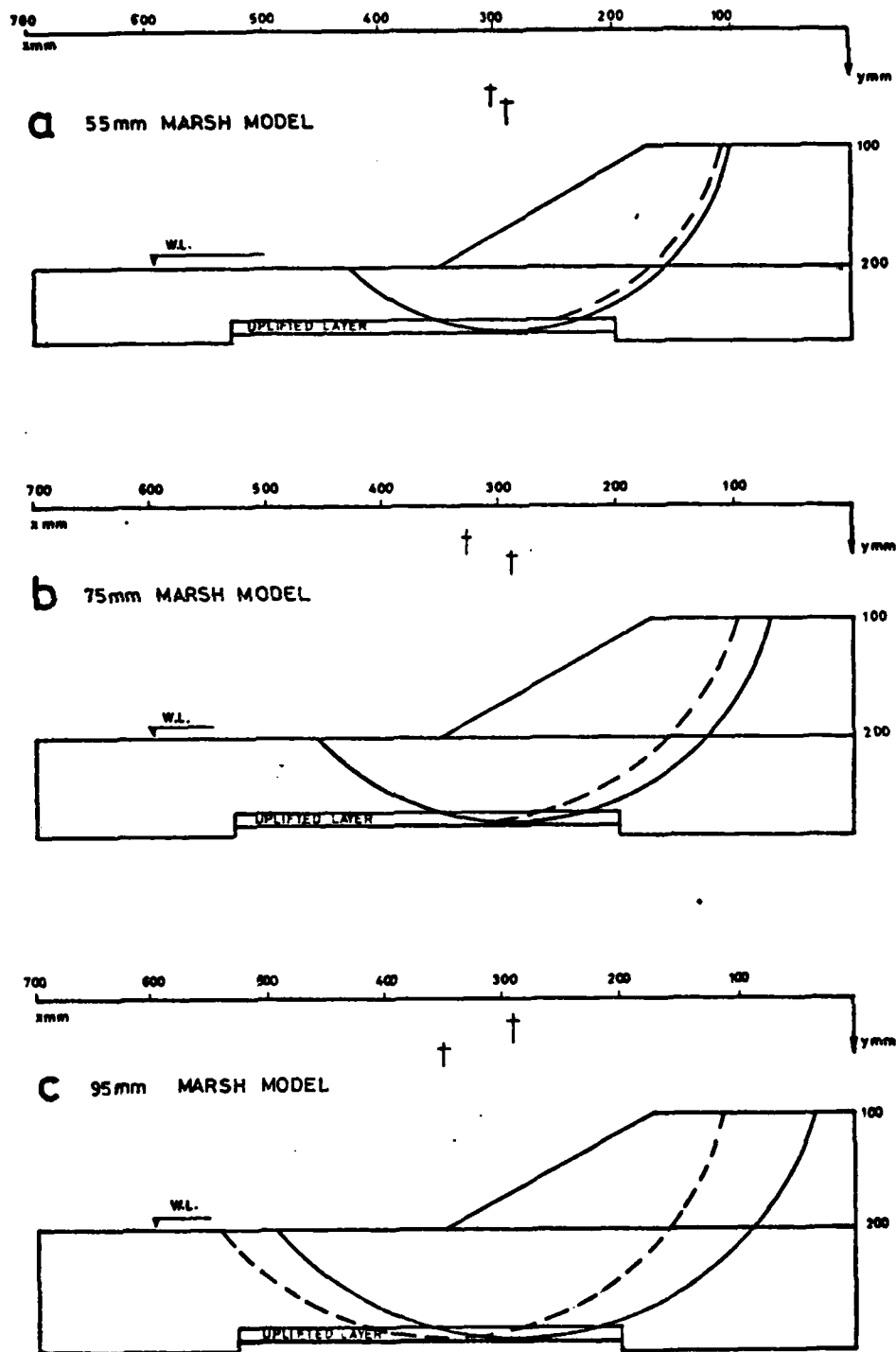
FIG 2·20 SOIL LAYERS USED IN SLIP CIRCLE ANALYSIS

NOTE:

---- BROKEN CIRCLE: MEDIAN POSITION OF EXPERIMENTAL SLIP SURFACES

—— FULL CIRCLE: THEORETICALLY MOST CRITICAL CIRCLE

The behaviour of the models during consolidation and swelling on the centrifuge has been discussed in Section 2.3.1 and it is here assumed that at the time of testing by load increase the models were in pore pressure equilibrium. The prediction of undrained shear strength was discussed in Section 2.3.2 and in Section 2.3.3 an example was given of the prediction of undrained shear strength of the material in the body of the model and on the sand layer interface when the self weight and/or the uplift are increased rapidly. The same techniques were used to determine the material properties of the models in these slip circle calculations.

It has been hypothesised by Cooling and Marsland, 1953, that a sliding mechanism involving the translation of a long horizontal wedge of soil would develop under uplift conditions. In this case the thin softened zone along the sand interface would facilitate sliding, but the mechanics of this type of mechanism were not obvious before the model tests were undertaken. For the purpose of these calculations it is possible to introduce a device by which a simple slip circle is influenced by uplift pressures in such a way as to show the general pattern of behaviour.

It is assumed that a layer of finite thickness rapidly achieves the same new equilibrium value of effective stress as does the interface layer itself. The depth chosen for this layer has a considerable influence on the stability of the slip circle as shown in Fig. 2.19. In these calculations a depth of 10 mm was chosen as giving a suitable compromise between the conditions of the actual tests and the object of the calculations themselves which was to indicate the general pattern of behaviour.

The geometry of the models was introduced in Section 2.2, Fig. 2.6, and is shown in detail in Fig. 2.20. The mechanics of the slip circle are shown in Fig. 2.21. The slices are of variable width and are disposed such that slices 3-5 pass through the artificial "uplift softened layer". The water level is at marsh surface elevation and so full bulk density was used above and submerged bulk density below the water table to determine the effect-
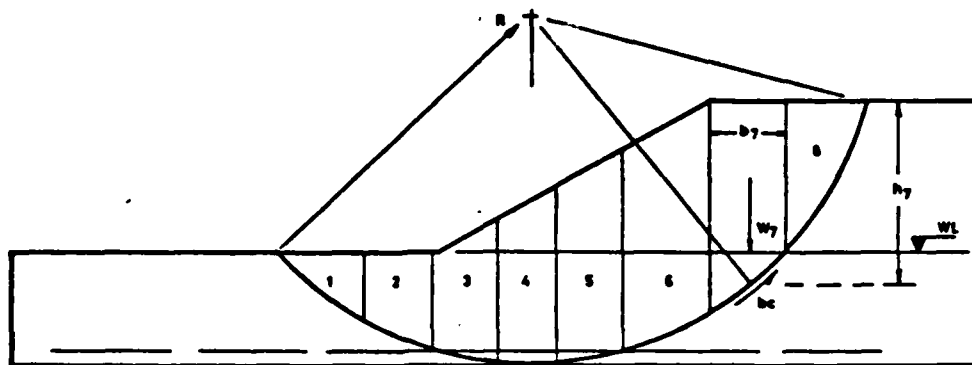
$$Fs = \frac{\Sigma bc \sec \alpha}{\Sigma W \sin \alpha} \quad \text{where} \quad \begin{array}{l} W = bh\gamma ng \text{ at ng gravities} \\ \text{and} \quad \gamma = \text{total density of soil (tonne/m}^3) \end{array}$$

FIG 2·21 SLICE GEOMETRY USED FOR SLIP CIRCLE ANALYSIS FOR SOIL OF
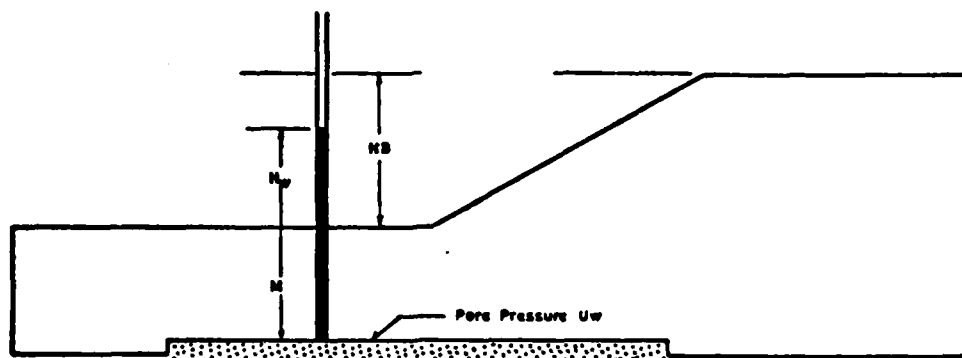UNDRAINED SHEAR STRENGTH C

Pore Pressure Uw

FIG 2·22 THE UPLIFT PARAMETER $U = \dfrac{Hw+M}{M} = \dfrac{Uw}{M\gamma w ng}$

- 38 -

ive vertical stress at the sliding surface. From this value of σ_v', the appropriate value of undrained shear strength (c_u or c_H) was calculated in the manner of Section 2.2.3. This is described in detail in the Appendix.

Calculations were performed on a "Texas" programmable pocket calculator TI58 and involved only one circle for each model geometry, Fig. 2.20. This circle was chosen on the basis of the experience of the model tests and of a comprehensive series of slip circle calculations performed on an IBM370 computer which are not presented here. The equation used for the factor of safety is one of simple moment equilibrium, in effect the simplified Bishop method without the friction angle ϕ, Fig. 2.21. Spencer, 1967, has shown that moment equilibrium methods of this kind are reasonably accurate in comparison with more rigorous methods.

For presentation of the results of these calculations on an interaction diagram it is convenient to use two non-dimensional loading parameters. The uplift parameter U has been defined in Section 2.2 and Fig. 2.22 and the self weight loading parameter F replaces the general parameter W used in Section 2.2

$$U = \frac{\text{Water head in sand layer}}{\text{Marsh thickness}}$$

$$F = \frac{\text{Current value of ng}}{\text{Equilibrium value of ng}}$$

(2.28)

In the above mentioned comprehensive series of calculations it was shown that the safety factor Fs varies linearly with the value of U in the artificial "uplift softened layer" at any particular value of F (ng). The interaction diagram is essentially the locus of loading combinations for which Fs = 1. It was sufficient for the purpose of determining the shape of the interaction diagram to calculate the value of U required to give a value of Fs = 1 at various values of ng. At any particular value of ng the safety factor was determined at U = 1.00 and U = 1.60
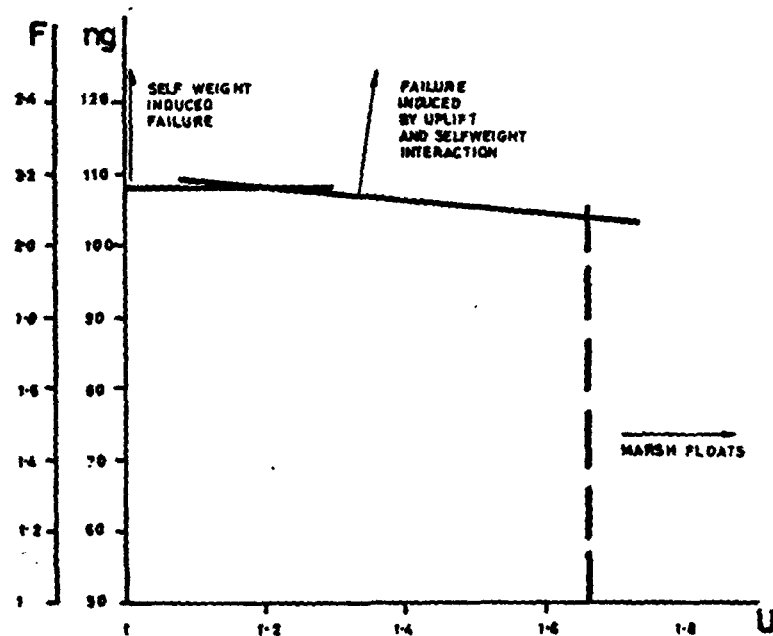
FIG 2·23 INTERACTION DIAGRAM AS CALCULATED IN SLIP CIRCLE ANALYSIS

and then by interpolation between the two values of Fs, the value of U
was determined for which Fs = 1. In this way the boundary between stable
and unstable states (Fs = 1) on the interaction diagram was determined
for values of

F =   1   1.4   1.8   2.2   2.6

ng = .50   70   90   110   130

Calculations were performed for all three model geometries shown in
Fig. 2.20 for the loading conditions described above. One such calculation
is tabulated in Appendix 1. The results for the three geometries were
found to agree within 5% and so have not been presented separately. The
portion of the results that fall within the range of interest $1 \leq U \leq 1.66$
is shown in Fig. 2.23.

One further calculation was performed and that involved a shallower
circle which penetrated to only 0.045 m into the marsh. This circle
passed entirely through material that was unaffected by consolidation or
softening at the sand interface and was found to be marginally more crit-
ical than the base circle at U = 1.0. No attempt was made to locate the
most critical circle, but this one circle generates the horizontal line
on the interaction diagram of Fig. 2.23 at 108g.

The vertical line U = 1.66 represents flotation of the marsh as
discussed in Section 2.3.3.

2.5   Conclusions

Bolton, English, Hird and Schofield, 1973, proposed the interaction
diagram representation for the failure states of an embankment founded on
a marsh alluvium layer which was subjected to uplift water pressures. Their
proposal was not confirmed by any analytical or experimental evidence.
Later Hird, 1974, sought to demonstrate the interaction failure experiment-
ally, but his marsh/bank geometry was thick and no interaction was obser-
ved. The analyses presented in this Chapter have confirmed, at least

theoretically, that the concept is valid when applied to an idealised model geometry, and using physical properties expected to be realised during a centrifuge test. The demonstration has been effected with the aid of slip circle calculations. The interaction diagram representation that has been derived and is shown in Fig. 2.23 shows that an interaction mode of failure becomes more critical than either of the two modes of failure due to the simple loadings, and results in a "cutoff" corner on the diagram.
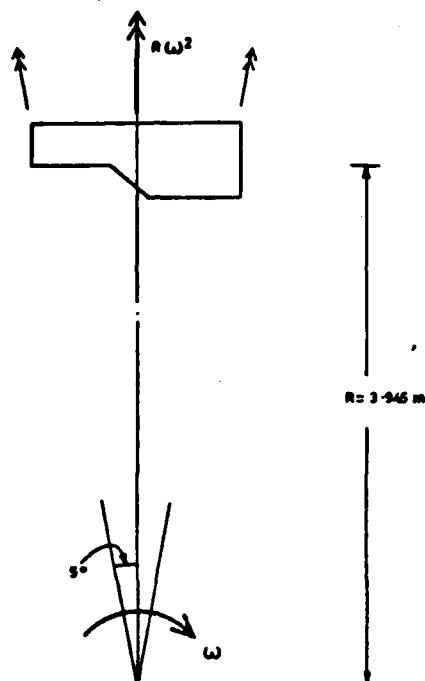
FIG. 3·1 PLAN VIEW OF MODEL ON CENTRIFUGE ROTOR
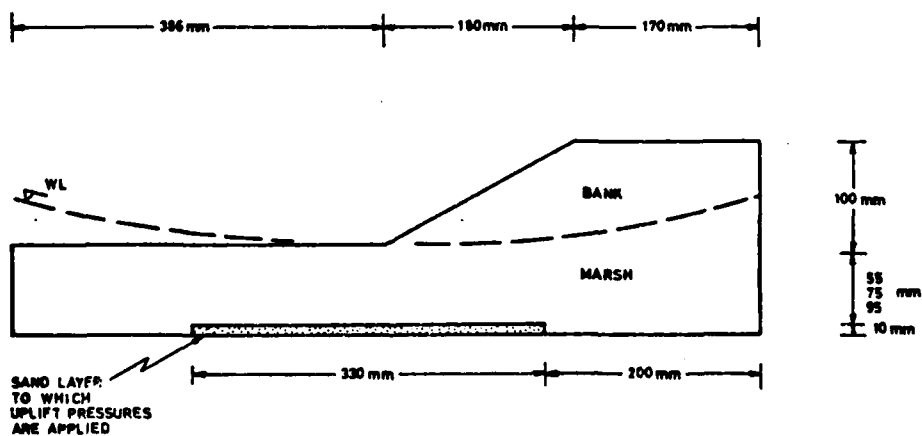AS SEEN FROM VERTICALLY ABOVE THE MACHINE

FIG. 3·2 SIMPLIFIED SECTION OF FLOODBANK MODEL

CHAPTER 3

THAMES FLOOD EMBANKMENTS

MODEL PREPARATION AND EQUIPMENT

3.1   Outline of the Test Program

To test the hypothesis developed in Chapter 2 that the loading conditions at failure for an uplifted embankment under self weight loading may be plotted on an interaction diagram, a series of models was tested on the geotechnical centrifuge at Cambridge. Such an experimental investigation has only one precedent, Hird, 1974, discussed in Section 1.2.

The model configuration adopted at UMIST by Hird was three dimensional and curved to take account of the radial accelerational field of the centrifuge. Furthermore, Hird used two different clays to model the marsh and embankment soils in an attempt to simulate the behaviour of the prototype embankments along the Thames. Both of these features lead to complications.

The models tested in the course of the investigation presented in this dissertation were two dimensional slices of a long embankment. The model was spun on the centrifuge with the cross section perpendicular to the axis of the rotor, facing upwards in the earth's gravitational field, Fig. 3.1. The radial disposition of the field involved errors along the line of the slice on a flat model rather than along the line of the embankment as in Hird's work.

There is no advantage in this. The radius of the rotor of the Cambridge centrifuge is sufficiently large to make the radial divergence negligibly small (5°) and so it was considered unnecessary to curve the model. However, the water table is curved and rises towards the edges of the model, as shown in Fig. 3.2.
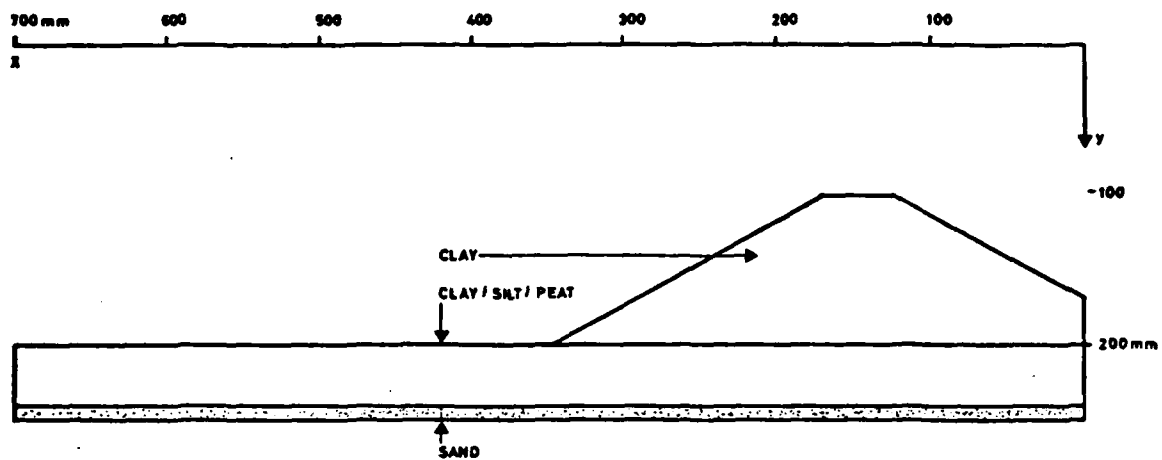
FIG. 3·3 (2DF 1,2) PROTOTYPE GEOMETRY AT DARTFORD - LOCK BREACH
SCALED TO $^1/50$

This curvature implies that the head of water in the porous sand layer shown in Fig. 3.2 increases towards the edge. In the present investigation an excess pressure was applied to this sand layer to uplift the overlying marsh alluvium. On the centrifuge the curved gravitational potentials cause a greater uplift to be felt further from the model centre line. To minimise this effect the sand layer was made central in the model and of only 330 mm length, such that the greatest error in the height of the water table was only 3.3 mm or 6% of the depth of the thinnest marsh (55 mm).

There were certain advantages in the use of two dimensional model tests. They involved lighter models which required less time to prepare than large three dimensional models. Although the boundary errors are more important in a narrow two dimensional slice, the process of data retrieval is very much simpler than for a large three dimensional model. The Cambridge centrifuge had been built specifically for two dimensional tests where the upper face of the strong box can be a perspex window through which the deformation of the model cross section is followed and photographed.

Two strong boxes were already available which had been used by Avgherinos, 1969, Endicott, 1970 and Beasley, 1973, on the centrifuge hired from the British Aircraft Corporation at Luton. These were used for the two preliminary tests after only slight modification. In the middle of the period of this investigation the Cambridge centrifuge was modified to take swinging platforms which could accommodate large three dimensional model strong boxes. New strong boxes were designed by the author for the two dimensional tests. These were constructed in the University Engineering Department workshops. Mounted on the swinging platforms of the Cambridge centrifuge the new boxes were used for twelve of the fourteen tests. The new boxes were built with the same internal dimensions as the old so that the existing consolidometers and liners could be used for the sample preparation. The design of the new strong boxes also benefited from some
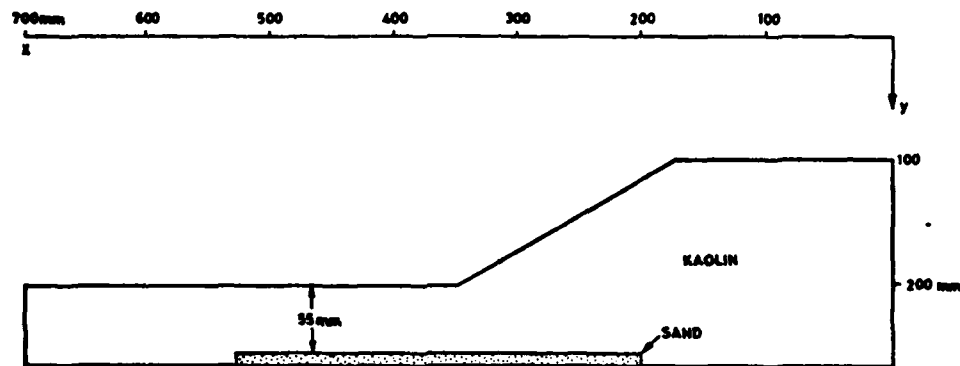
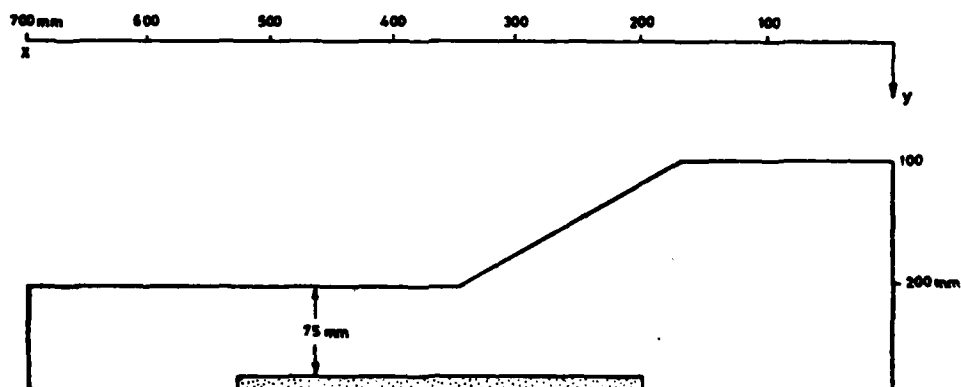FIG. 3·4a THIN MODEL GEOMETRY TESTED (2DF 4,5,6,13,14)
(55mm MARSH MODEL)

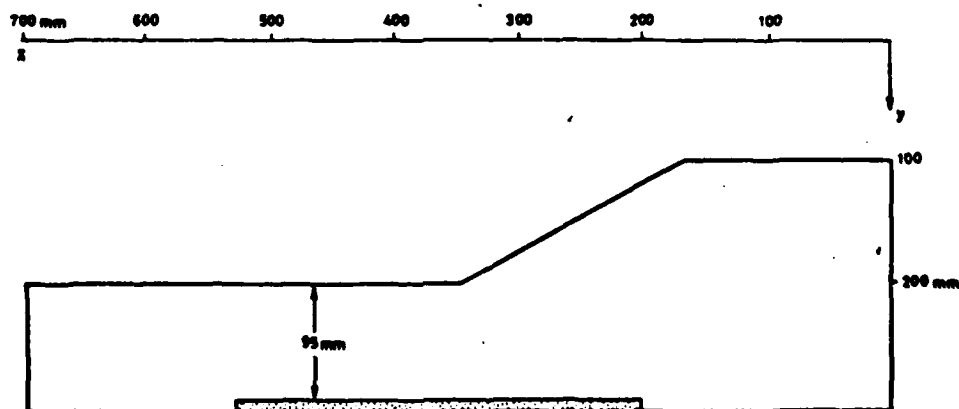FIG. 3·4b INTERMEDIATE MARSH THICKNESS (2DF 7,10,11,12)
(75mm MARSH MODEL)

FIG. 3·4c THICK MARSH MODEL TESTED (2DF 8,9)
(95mm MARSH MODEL)

experience with the old boxes. The stressing calculations and detailed drawings were prepared and will be discussed by Goodings*.

Three-dimensional floodbank tests were planned but were never executed. The apparatus for these tests was designed by the author and built for the purpose but was completed so late that no time was available for the tests.

The model scale chosen for the tests was 1/50. Model bank geometry was largely based on the bank cross section at the Dartford Lock, which scaled to 1/50, gives a model bank 102 mm high on a marsh layer 36 mm thick, Fig. 3.3. This was used in the first two tests. The three different model geometries tested in the main series of experiments employed a 100 mm high bank on three alternative marsh thicknesses (55, 75 and 95 mm), as shown in Fig. 3.4. A layer of sand 10 mm thick and 330 mm long underlay the marsh and was connected to a variable head reservoir. The level of the water in this reservoir was normally controlled such that the water table in the model stood at the marsh surface. When uplift pressures were required, the water level in the reservoir could be rapidly raised.

In theory, once the models had achieved pore pressure equilibrium at 50 g in the centrifuge, the effective stress and pore pressure distributions in the model were equal to those in a full scale embankment of the same material. For the sake of continuity of a series of models and simplicity of analysis, each model was cut out of an intact block of consolidated kaolin. No attempt was made to model the precise soil parameters found at Dartford Lock.

The tests were entitled "Two Dimensional Flood Embankment" tests and are each given code numbers beginning 2DF for ease of reference in centrifuge planning. Fourteen centrifuge experiments were performed (Tests 2DF1-14) in each of which two models (Red and Blue) were tested, one on either end of the centrifuge balanced arm. The members of a pair were usually struct-
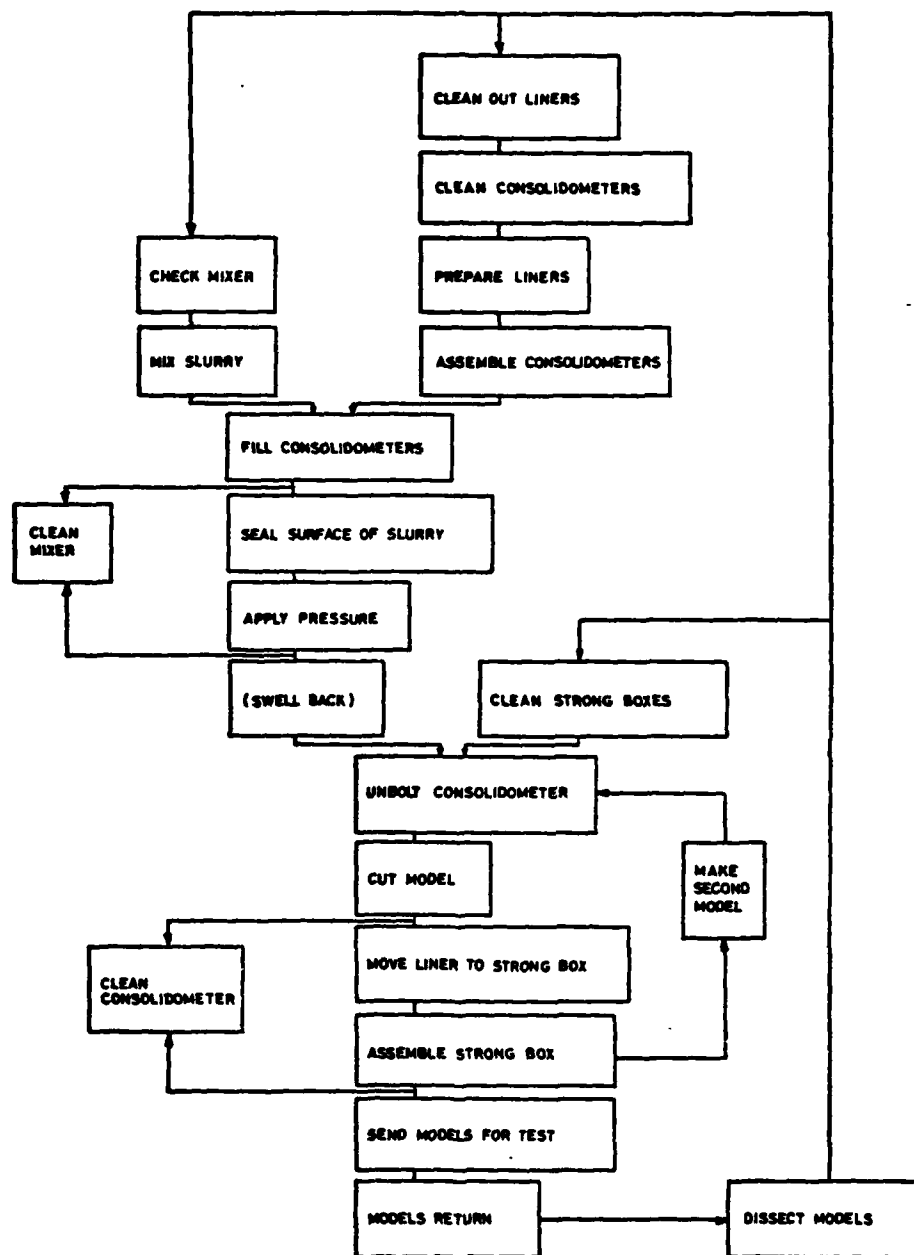
---

*Goodings, D., Ph.D. Thesis in preparation (1979).

FIG. 3·5 FLOW DIAGRAM OF OPERATIONS INVOLVED IN
MODEL PREPARATION

urally idential and for Tests 2DF4-14 were always made according to the same routine to minimise differences between the models. The only important difference between the members of a pair was the value of uplift pressure applied during a test. Both models necessarily suffered the same acceleration history, being on either end of the one centrifuge rotor.

The routine was based on a regular three week cycle of testing in which the models were prepared at the main laboratory in Cambridge, sealed into their strong boxes and transported to the centrifuge facility where they were tested. The individual items of equipment are described in the following sections, together with the procedures developed for their use. The sequence of operations involved in model making is shown in the flow diagram, Fig. 3.5.

Briefly, the routine was as follows. Slurry was mixed overnight and transferred into the two prepared consolidometers, Section 3.2, where it was consolidated under five increments of loading over eight days. On Monday and Tuesday of the test week, the consolidometers were opened and the models made from the blocks of kaolin, Section 3.3. They were then sealed into their strong boxes, Section 3.4, and transported to the centrifuge, Section 3.5, where the plumbing, Sections 3.4, 3.9, and electrical transducers were installed. The boxes were mounted on the swinging platforms of the centrifuge and tested on Friday. The test run, Section 3.7, started at 06.00 hrs and was usually finished by 15.00 hrs. The failed models were brought up from the centrifuge chamber onto a workbench in the centrifuge building where an investigation of model properties, Section 3.10, was conducted immediately after a test: this usually involved working until about 18.00 hrs on the day of the test.

3.2   Liner and Consolidometer

The liner, Fig. 3.6, is an open sided box of aluminium which serves to

SIDE VIEW

SIDE VIEW
CENTRAL SECTION

19 mm

276·9 mm

771·5 mm

RECESSES INTERCONNECTED
BY DRAIN

BOTTOM
VIEW

149·2 mm
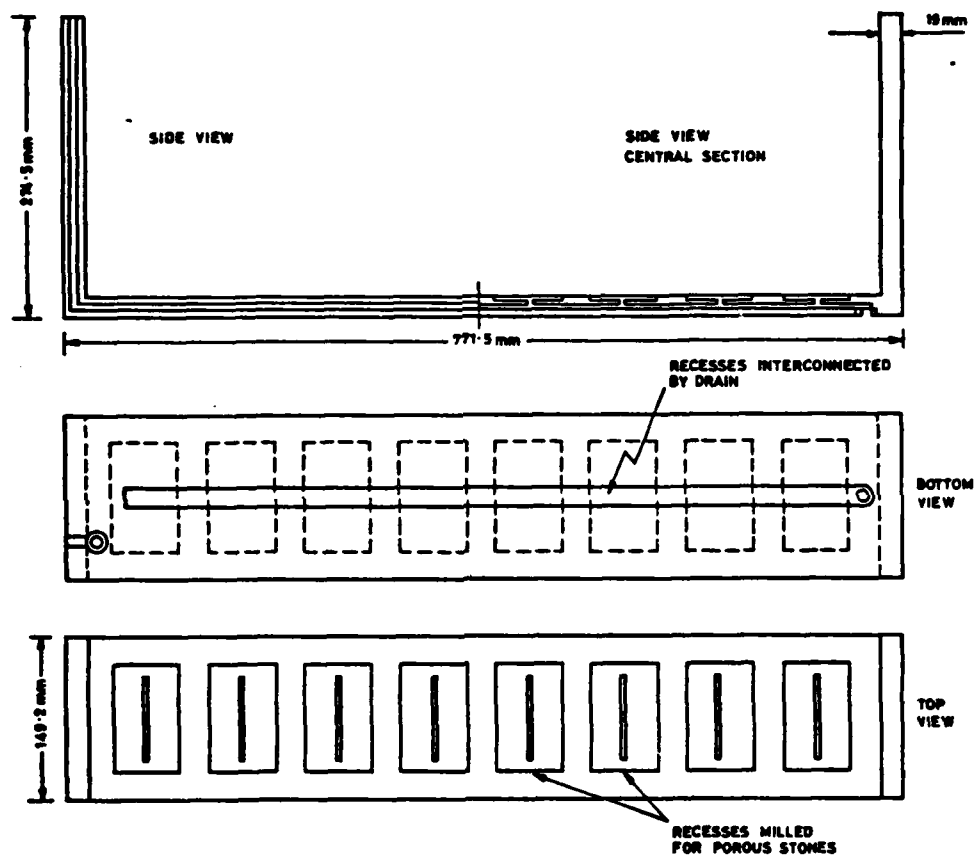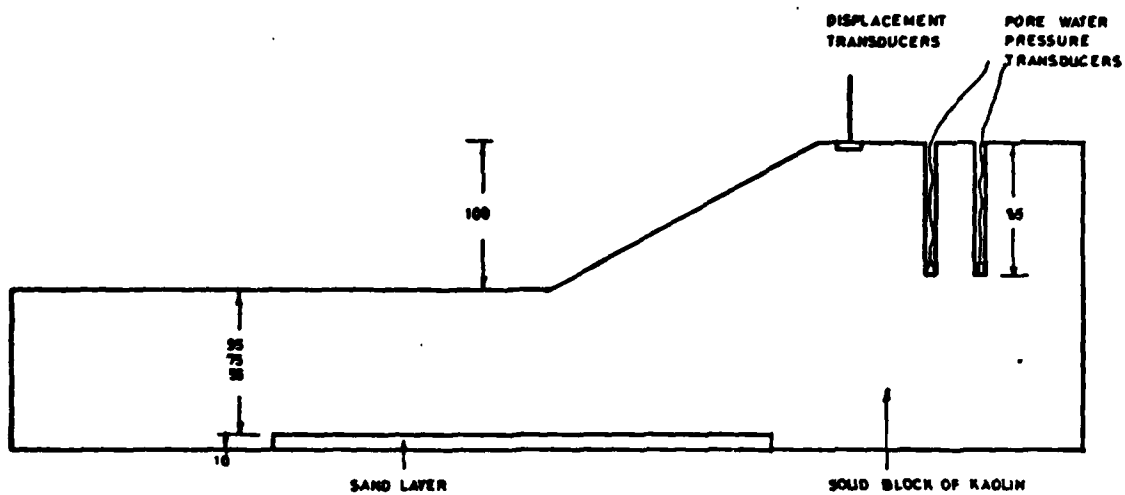
TOP
VIEW

RECESSES MILLED
FOR POROUS STONES

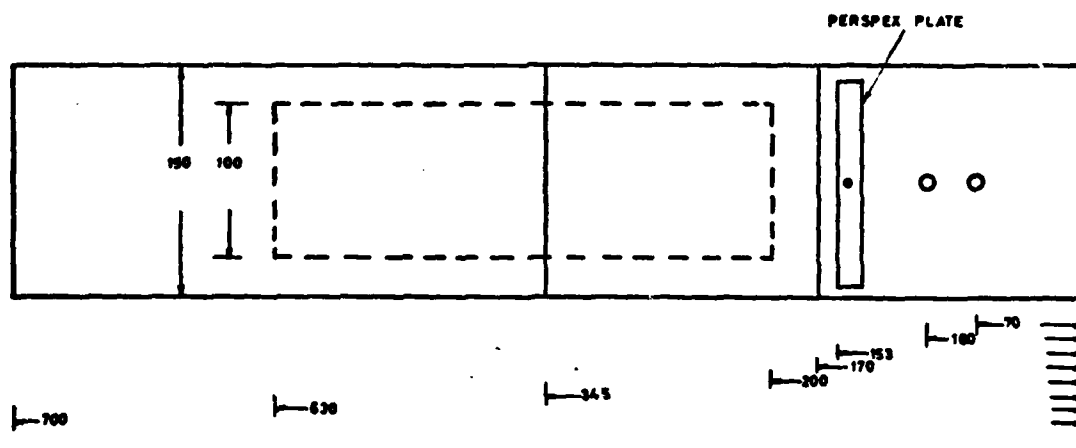FIG. 3·6 ALUMINIUM LINER FOR 2D STRONG BOX

transfer consolidated clay from the consolidometer, Plate 3.1, to the strong box. The consolidometer and the original liners were designed by Avgherinos, 1969. The liners shown in Fig. 3.6 are similar to those of Avgherinos, except that the plumbing has been simplified. Included in the thickness of the metal is all the plumbing required by the model. On the base of the liner are eight drainage points covered by porous stones which connect to a tapping on the underside. For the purposes of the Flood Embankment tests, the central six drainage points were surrounded by a stainless angle frame 10mm deep, Plate 3.2, which was filled with two layers of sand: a layer of course sand 8mm thick and an upper layer of fine sand 2mm thick. This sand layer provides the surface of permeability contrast at which uplift will be applied.

The liner is shown installed in the consolidometer in Plate 3.3 where it may be seen that between the sand box and the side walls of the consolidometer was a 15mm gap on either side which became filled with consolidated clay, Fig. 3.7. The purpose of this clay fill was to seal within the sand layer the excess uplift pressures which would otherwise dissipate uselessly. It was practically convenient to place the sand in a dry state in the sand box, but this had the unfortunate consequence that it was not possible to ensure full saturation of the sand layer after the clay slurry (at 160% moisture content) was poured over it.

The surfaces of the liner were carefully degreased before consolidation to ensure good adhesion and Adsil spray was used to grease the sides of the consolidometer to reduce friction. Load was applied by pneumatic pressure on a ram in increments over eight days to a maximum vertical pressure of 200 kN/m^2 chosen such that the models would be stable at 50g and be over-consolidated throughout their depth at this stress level. Water expressed during consolidation collected above the piston and in a reservoir connected to the tapping on the underside of the liner. The first two tests differed in certain respects from the procedure described above. The first test, 2DF1

DISPLACEMENT
TRANSDUCERS

PORE WATER
PRESSURE
TRANSDUCERS

100

95
75
55

10

SAND LAYER

SOLID BLOCK OF KAOLIN

45

VERTICAL SECTION THROUGH ₵

PERSPEX PLATE

196 100

700

630

345

200

170

153

100

70

PLAN OF FLOODBANK MODEL
DIMENSIONS IN MM

FIG 3·7

involved two consolidations, the first with a small quantity of kaolin to supply the ring of clay which surrounded the sand layer and the second consolidation to form the body of the bank and marsh. 2DF2 employed a removable sand box made of aluminium honeycomb and the sample was prepared in one consolidation. Both of these methods were awkward to use. The sand layers were prone to disturbance and leakage during the tests. In the third pair and in all subsequent models the fixed sand box was used.

In the first three tests, 2DF1-3, the clay was allowed to swell to $50 kN/m^2$ in the consolidometers before the models were made. The swollen clay was found to be too soft, as will be described below, and in Tests 2DF4-14 the clay was not allowed to swell in the consolidometers.

3.3   Model Making

When the load had been taken off the block of clay the consolidometer was dismantled and the clay transferred, in the liner, to the workbench, Plate 3.1. Every effort was taken to deny the model access to water until the last moment before the model was subjected to 50 g on the centrifuge although nothing could be done to prevent cavitation.

The final embankment profile was cut using a cheesewire, guided by steel templates, Plate 3.4. Fig. 3.7, which was shown above, illustrates cross sections of a typical model. A perspex plate which extended over 140 mm of the 150 mm width of the model served to distribute the load of the displacement transducer spindle. The plate was countersunk to such a depth in the clay surface that the weight of the transducer had no net influence. Two pore water pressure transducers were located inside the model bank. They were pushed into holes which had been previously augered into the clay. The holes were backfilled with thick kaolin paste squeezed into the bottom of the hole with a syringe. Two transducers were used side by side in order to give comparable readings to allow a check on the repeatability of the data. The clay surface was greased to inhibit the loss of
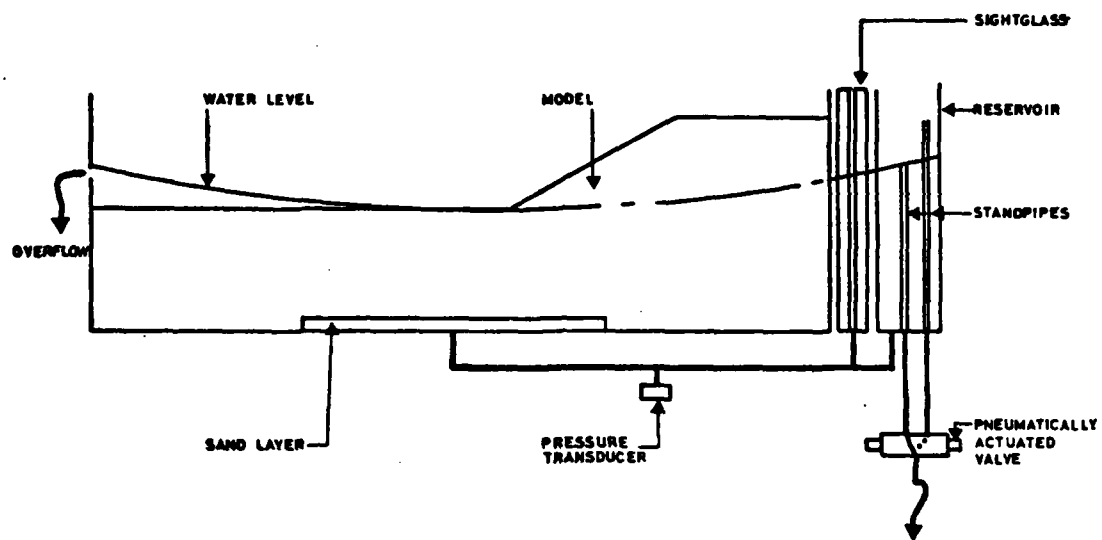
FIG. 3·8   PLUMBING FOR FLOODBANK TESTS 2DFI-14

moisture and the model was placed in the strong box.

The strong box was tipped onto its back and a template positioned over the model, Plate 3.5. With the aid of this template, silvered perspex balls were pressed into the surface of the embankment cross section in a regular square grid at 15 mm centres. The perspex front of the box was then clamped in place, Plate 3.6, and the model was transported to the centrifuge.
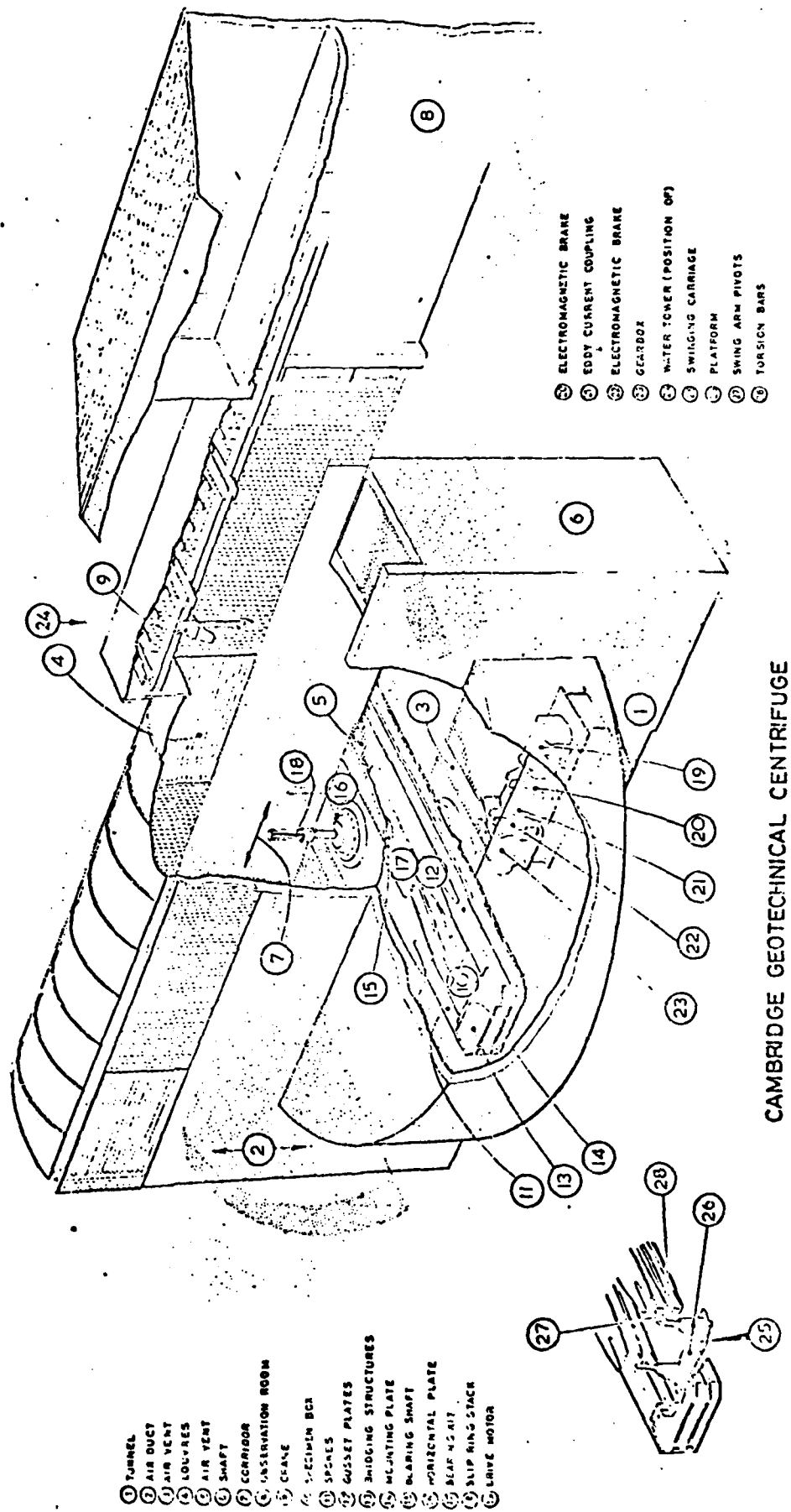
Moisture content samples were taken from the block of clay which was removed in the course of cutting out the embankment profile. · Samples were taken immediately the consolidometer was opened and also at the end of the model making process. The sample block was covered when the model was covered and exposed when work was in progress on the model to measure desiccation that occurred during this time. Average values taken for all the Tests 2DF-14 show a moisture content, w = 56% ($\pm$0.5) after consolidation which agrees well with data given by Endicott, 1970. Averaged over the whole model the clay dried by w $\approx$ 0.5% during the model making process, although drying was more serious on the outside of the block (up to 1%).

3.4 Strong Boxes

Tests 2DF1, 2 were performed in the existing strong boxes. These boxes have been described by Avgherinos, 1969, and later workers and were mounted on their backs on fixed platforms on the centrifuge. The boxes were modified slightly for these tests.

The new boxes were designed specifically for the new swinging platforms of the Cambridge centrifuge, and are shown in Plates 3.6 and 3.7. The cellular grillage which stiffened the back of the box was used to mount valves and electrical connections. The water reservoir was mounted on one side of the grillage with water lines passing inside the box section to connect up to the underside of the liner.

The plumbing circuit within the box is shown schematically in Fig. 3.8. All

CAMBRIDGE GEOTECHNICAL CENTRIFUGE

FIG 3·9

① TUNNEL
② AIR DUCT
③ AIR VENT
④ LOUVRES
⑤ AIR VENT
⑥ SHAFT
⑦ CORRIDOR
⑧ OBSERVATION ROOM
⑨ CRANE
⑩ SPECIMEN BOX
⑪ SPOKES
⑫ GUSSET PLATES
⑬ BRIDGING STRUCTURES
⑭ MOUNTING PLATE
⑮ BEARING SHAFT
⑯ HORIZONTAL PLATE
⑰ BEARING UNIT
⑱ SLIP RING STACK
⑲ DRIVE MOTOR

⑳ ELECTROMAGNETIC BRAKE
㉑ EDDY CURRENT COUPLING
㉒ ELECTROMAGNETIC BRAKE
㉓ GEARBOX
㉔ WATER TOWER (POSITION OF)
㉕ SWINGING CARRIAGE
㉖ PLATFORM
㉗ SWING ARM PIVOTS
㉘ TORSION BARS

valves were $\frac{1}{8}$" Atlas Copco spindle valves actuated by 80psi pneumatic pressu₁

and spring return. Pneumatically controlled valves of this type were found t

be very versatile. The head of water in the reservoir which was connected

directly to the sand layer in the base of the model was altered by switching

the outflow from one standpipe to another and by varying the inflow of water

the reservoir. The height of the standpipes was chosen to correct for the sha

of the free water surface on the centrifuge (paraboloid). This water level

could be monitored visually using a sight glass on the front face of the mode

Plate 3.6, and also electrically using a strain gauged diaphragm transducer.

This transducer was mounted in a $\frac{1}{4}$" BSP plug and installed in a manifold at

the base of the box. Throughout the consolidation phase of a run the water

level in the reservoir was kept such that the water level in the marsh layer

was at ground level in the centre of the model. Excess water was removed

from the model ground surface through a drain in the end wall of the liner.

A projecting bracket was mounted above the water reservoir, Plate 3.7, whe

bulkhead connectors made the union between the internal plumbing of the box

and the centrifuge services. The brass fittings on the top of this bracket

were connected into the pneumatic lines to trap any slugs of water or oil whic

may find their way into the pipework from the hydraulic slip rings on the

centrifuge.

3.5   The Centrifuge

The general arrangement of the Cambridge centrifuge is shown in Fig. 3.9

The rotor is 10m in diameter and is housed underground in a reinforced

concrete lined pit. The radius to the working surface of the swinging plat-

forms is 4.125m. The platforms are of aluminium hollowed on the underside

to form a stiff grillage. They are mounted on roller bearings such that when

the machine is at rest they hang under earth's gravity and swing up to the

horizontal between 8 and 12g depending on the position of the centre of grav-

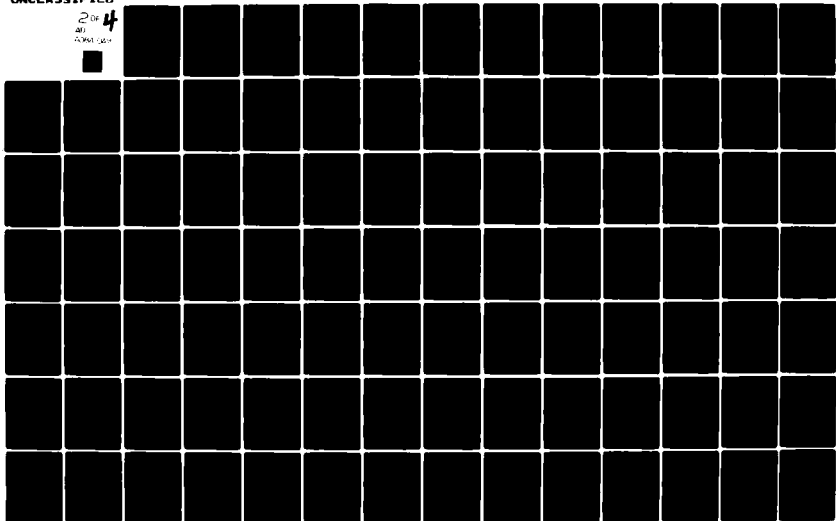ity of the model package. The bearings of the platforms are mounted eccen-

2 OF 4
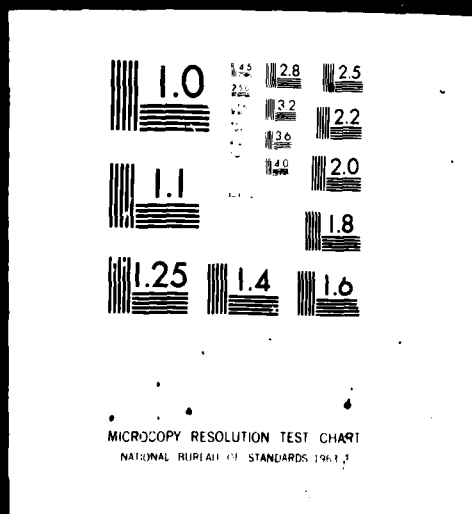AD
A084 049

MICROCOPY RESOLUTION TEST CHART
NATIONAL BUREAU OF STANDARDS 1963 A

trically on torsion bars such that with increasing centrifuge speed the platforms move radially outwards until they meet the face of the centrifuge arm by which they are supported as the acceleration is increased.

The machine is driven by a synchronous motor operating through an eddy current coupling. The motor delivers 225 kw and is capable of driving the rotor at 189 rpm which generates an acceleration of 165 g at the surface of the swinging platforms. The maximum package mass allowed is 900 kg which at 165 gravities gives the centrifuge a capacity of 148 g tonnes. Package size is limited to approximately 0.9 × 0.9 × 1 m. Certain stringent require-ments are made regarding the position of the centre of gravity to ensure that no part of the centrifuge is overloaded and that the platform swings up accurately.

Hydraulic and electrical services are available to the package in flight. The hydraulic lines may be used to conduct compressed air or fluids from the control area to the model. Sixty electrical channels are available to send power to and receive signals from transducers which monitor behaviour of the model. Both electrical signals and hydraulic services are trans-mitted to the centrifuge rotor and thence to the model package in flight through a stack of slip rings.

3.6 Data Output from the Model

Several classes of data were recorded from each model.

1. The geometry of the model was chosen before the test was started. Similarly, the combination of self weight and uplift loading was chosen before the test. The time lag in real-time interaction with the model was too large to make decisions in flight and so the planned loading path was always followed.

2. Photographs of the models were taken at various stages in the consol-idation process and after important events in the tests. Subsequent superposition of two photographs allowed displacement diagrams to be

drawn for the movement of the silvered perspex balls.

3. Two different types of electrical pore water pressure transducers were mounted within the model bank. The output from these transducers was recorded on paper tape by a data logger and could be monitored on a digital voltmeter.

4. One displacement transducer, mounted on the strong box, followed the displacement of the crest of the embankment. The output was recorded by the data logger.

5. The water level in the reservoir connected to the sand layer was monitored visually using a sight glass on the front of the strong box and electrically using a water pressure transducer in the water line which connected the water reservoir to the sand layer in the model. This pressure was recorded by the data logger.

6. An accelerometer was mounted on the face plate of the centrifuge. The output was recorded by the data logger.

7. The events of a test were related in time using a clock that was mounted within and recorded by the data logger.

8. Moisture contents, and in early tests, vane strengths, were measured as soon as practicable ($\frac{1}{2}$ - 1 hour) after each test.

9. Failure slip surfaces were traced from the side of the model onto tracing paper.

3.7 The Test

As an illustration the progress of one test (2DF5 Blue) will be followed from beginning to end. The geometry of this model was as shown in Fig. 3.4a where a 100 mm bank was founded on a 55 mm marsh. The model was made and mounted on the centrifuge in the normal way, described in Section 3.3. The taps were opened at 05.45 hrs on Friday 8 October, 1976 to allow water from the water reservoir into the sand layer. The machine was started at 05.55 and speed built up slowly to approximately 38 rpm. As
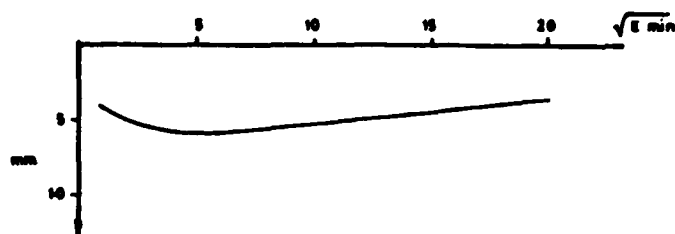
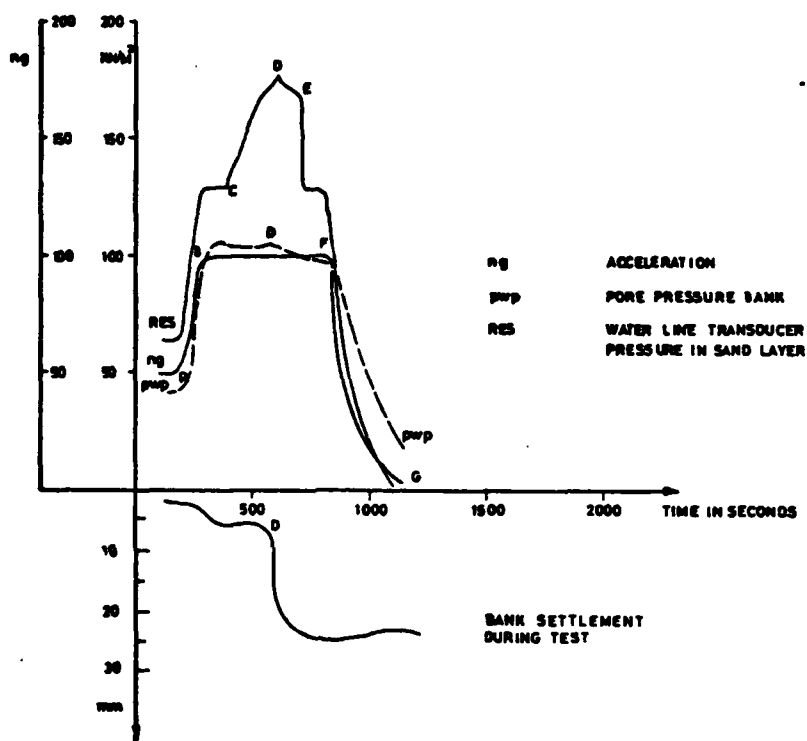FIG 3·10 BANK SETTLEMENT AND HEAVE DURING 8 HOUR CONSOLIDATION
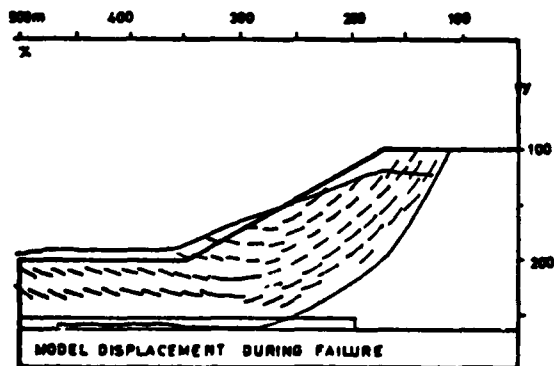
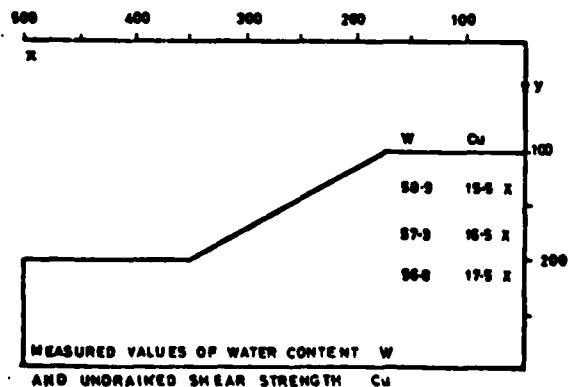

FIG 3·11 TRANSDUCER OUTPUTS DURING TEST

FIG 3·12a

FIG 3·12b

predicted the platforms swung up to the horizontal at this speed which pro-
vided a check on the accuracy of calculation of the centre of gravity of
the package. By 06.00 the machine was running at 107 rpm (50 g) and the
data logger was recording scans of all transducer outputs every five min-
utes. The consolidation run lasted eight hours.

The presentation of data used for this test is common to the present-
ation used in Chapter 4 for the entire test series, although the diagrams
presented here are reduced in size and are intended only as an illustration.
In Fig. 3.10 the embankment settlement during the eight hour period at 50 g
is plotted against the square root of time. In Fig. 3.11 four transducer
outputs are presented for the loading phase of the test on the upper half
of the diagram the accelerometer output, (green), the pressure in the water
line to the sand layer, (red) and the pore water pressure within the embank-
ment, (blue); on the lower half of the diagram, the embankment crest settle-
ment. In Fig. 3.12a the main deformations observed during the test are
presented to scale. These deformations have been drawn by superposition of
two successive photographs. In Fig. 3.12b the results are presented of the
model vane strength determinations and the water content at the same three
locations.

Polaroid photographs and glass plate negatives were taken of the models
at intervals throughout the eight hour consolidation run, and the water level
was checked with the aid of the Polaroid photograph. Throughout consolid-
ation, Fig. 3.10, settlement of the banks was plotted against the square
root of time to follow the progress of the model towards equilibrium. The
bank is seen to settle in this case for 35 minutes, and thereafter to heave
steadily. As discussed in Section 2.3.3 the clay adjacent to the sand layer
was able to swell during the unloading and model making period. At 50 g
this clay at the base of the model was recompressed causing the initial
settlement of the embankment. The bulk of the bank however required to
swell, which caused the crest to heave as water became available to the kaolin.
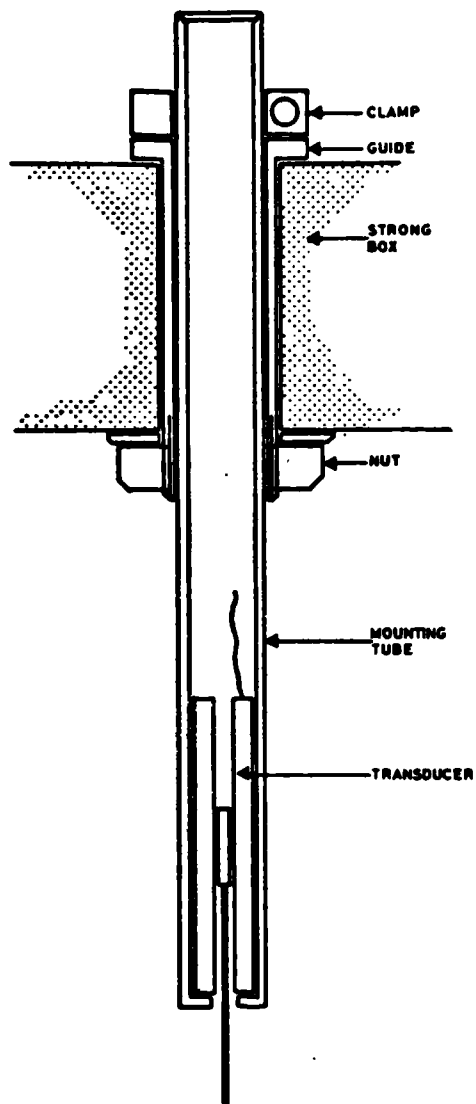
FIG. 3·13 MOUNTING FOR DISPLACEMENT
TRANSDUCER

At 14.30 preparations were ready for the application of the loading perturbations; the data logger was switched to rapid scan, the flow rate of water into the reservoir was increased and the compressed air reservoir charged. Final photographs were taken of the model. The test path that had been chosen in this case was to uplift the model to failure at 100 g. The machine speed was therefore increased as rapidly as possible to 147 rpm (100 g). It will be seen, AB in Fig. 3.11, that this acceleration took 90 seconds. Shortly afterwards, the valve in the strong box was actuated to switch the outflow from the consolidation standpipe to a longer one in the reservoir. The water level started to rise, C, and at a certain level the bank collapsed, D . The collapse was indicated, as shown in Fig. 3.11, by the sudden settlement of the bank, ___ (which typically took about 10 seconds) and by the sharp change in slope of the pore pressure reading in the bank ___ . Failure occurred in this case due to an increase in the water pressure in the base layer. The value of U in this layer at failure was calculated from the reservoir transducer output, see Section 3.8.3 and was found to be U = 1.91 at 100 g. This value of U is unusually high and suggests that there might have been some blockage in the pipework to contain these high pressures. However, the model did experience uplift as will be seen in Fig. 3.12, which shows that the mode of failure involved a long sliding surface along the uplifted interface, referred to in this disser-tation as the "interaction mode" failure mechanism. The collapse evidently caused some leakage since the reservoir transducer trace shows a change in slope at failure, D . Uplift was reduced at 100 g, E, to give a check on the calibration of the transducer, photographs were taken of the model and the machine was stopped, FG.

As soon as the centrifuge had come to rest the water taps were closed and the packages removed from the swinging platforms. The plumbing and transducer leads were disconnected and the liner, with the collapsed model, was removed from the strong box. The investigation of model properties
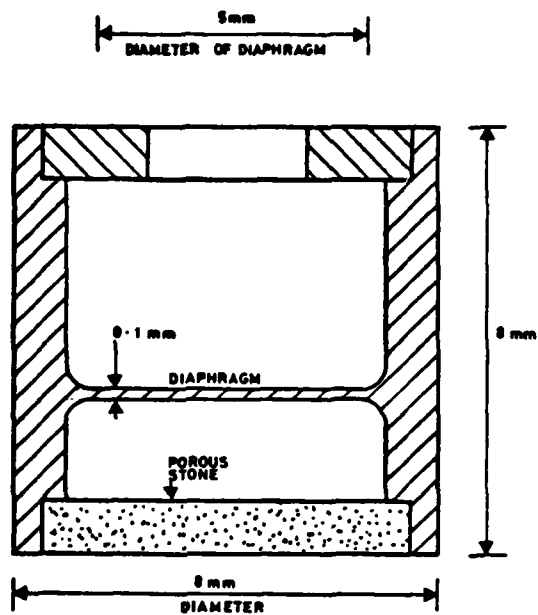
FIG. 3·14 STAINLESS PORE WATER
PRESSURE TRANSDUCER

was complete by 17.30 and the moisture content samples were weighed and in the oven by 18.30.

3.8   Transducers

3.8.1   Displacement Transducers

The displacement transducers were standard 30 mm stroke linear variable transformer type displacement transducers with internal circuitry to convert the DC power to AC and to reconvert the AC output signal to DC. They were supplied part-assembled by Sangamo Weston Ltd so that light weight spindles could be fitted at Cambridge. The mountings are shown in Fig. 3.13 and were designed to fully support the transducer and be rapidly adjustable.

3.8.2   Pore Water Pressure Transducers

Two types of pore water pressure transducer were used. The first type, available commercially, were manufactured by Druck Ltd of Leicester and have been described by Hird, 1974. The membrane is a single silicon crystal into which is diffused a strain gauge. The transducers were expensive (£100) but early versions gave trouble through leakage. The transducers which survived the rough handling involved in centrifuge modelling demonstrated high sensitivity and rapid response.

A second type of transducer was used in the Tests 2DF5-14 as a backup to the Druck transducers. These were designed by the author and are illustrated in Fig. 3.14. They used a thin machined stainless steel membrane with a diaphragm strain gauge on the back. The transducers were very small and gave excellent results in the water line to the reservoir. In the soil, however, their response was poor, possibly because the diaphragm was large and sensitive to air bubbles.

Both types of pore water pressure transducer suffered from the cavitation which was unavoidable when kaolin under a vertical stress of 200 kN/m^2 was unloaded completely.
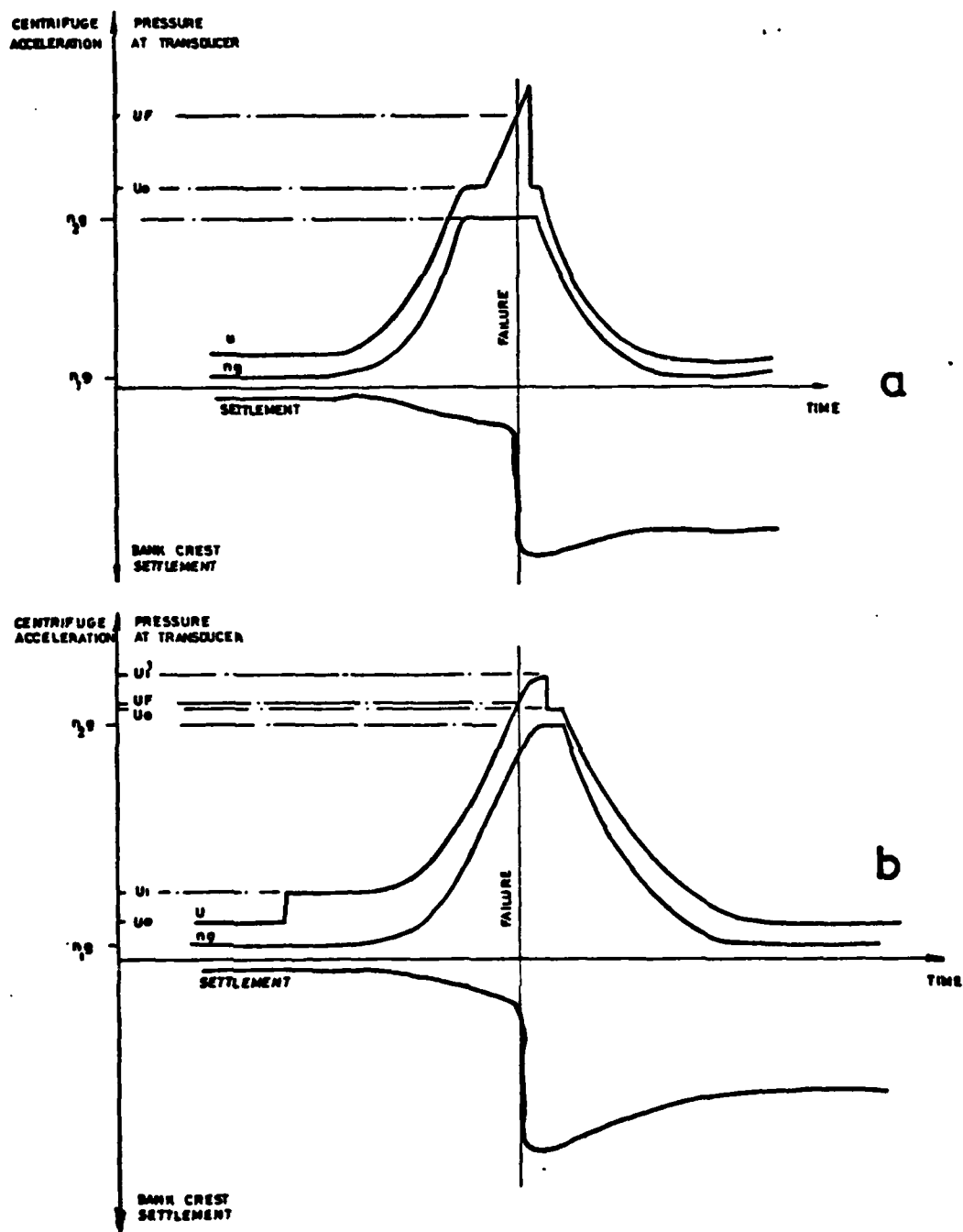
FIG 3·15 SKETCH OF TRANSDUCER OUTPUTS DURING TEST PHASE TO ILLUSTRATE CALCULATION OF Ư

During the consolidation run at 50 g on the centrifuge, the air
bubbles redissolve, but judging by the unreliable traces recorded in many
of the tests, the air takes a considerable time to go back into solution.
There is very little that may be done to improve the performance of trans-
ducers under these circumstances, other than to allow sufficient time to
elapse at 50 g before the application of test perturbations for the model
to come fully into pore pressure equilibrium, by which time the air bubbles
should be fully dissolved. This topic is further discussed in Sections
4.4.14.2 and 4.4.14.5.

3.8.3   Calculation of Uplift Value, U

The value of uplift at failure, U, had to be calculated for each model
test after the transducer outputs had been processed on the computer and
plotted against time. There were two types of loading path as illustrated
in Figs 3.15a,b. In the first case the model was uplifted to failure at
constant elevated speed as was the case in Test 2DF Blue, described in Section
3.7. In the second case the model was uplifted at 50g and then accelerated
to failure. The diagrams in Fig. 3.15 show in each case

1.   The water pressure recorded by the transducer in the water line
     that connects the reservoir to the sand layer, u. (RED)

2.   Gravitational acceleration, ng. (GREEN)

3.   Bank settlement.

These readings were approximately zeroed at the start of a test but
since the zeros drifted during a run and even during a speed increase, the
zero value taken for the determination of U at failure was obtained from
the transducer output as close as possible to the event of failure. These
zero readings are indicated as u_o on the diagrams. In the case of
Fig. 3.15a the uplift was unity (U = 1) immediately after the centrifuge had
attained n_2g, but before the uplift had been applied. Uplift was again
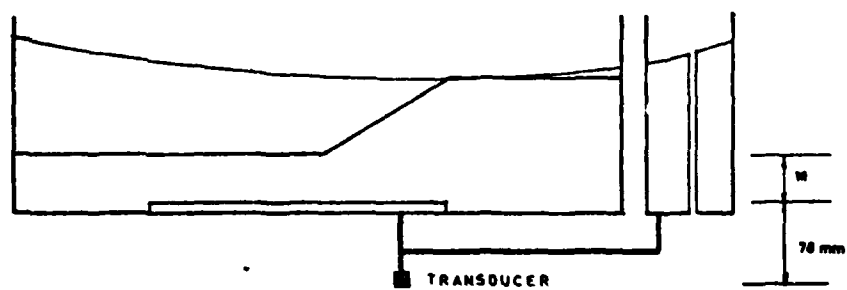unity during the few moments in between the reduction of uplift after

FIG 3·16 SKETCH SHOWING PRESSURE TRANSDUCER
LOCATED BELOW SAND/CLAY INTERFACE

failure and the reduction in centrifuge speed from n_2 to n_1g. In the case
of Fig. 2.15b two zeros were again available, one before uplift was app-
lied at n_1g and one after the moment of failure at n_2g. The pressure
value at the moment of failure, u_f, could be simply interpolated from the
data output.

Fig. 3.16 is a diagram of the model showing the water line transducer
below the reference level of the top of the sand layer. The pressure
measured by the transducer was therefore greater than that in the sand
layer by an amount that depended on the value of ng. The parameter
$U = (H+M)/H$ (as defined in Section 2.2) was known to be unity at $u = u_o$
since the water level in the sand layer was controlled at marsh surface
elevation by the standpipes. Consequently, it was possible using the u_o
value to zero the transducer output for a determination of U at $u = u_f$.

3.9   Ancilliary Equipment

3.9.1   Electrical Equipment

Electrical power was supplied by units in the control area of the
centrifuge building, through the cabling and slip rings of the centrifuge
to the transducers in the model package. Transducer output was read
directly by a data logger and could be monitored at any time on a digital
volt meter. The data logger was set to scan the outputs every half hour
overnight before the consolidation run started, every ten minutes during con-
solidation, and every six seconds during the test. In this way, though some
degree of real time monitoring of the model was possible, most of the inform-
ation concerning pore pressures and settlement was not available until the
paper tape had been processed on the computer and the transducer outputs
plotted some days later. Included on the paper tape record were: time,
ng value, input voltages, and for each model: settlement of the bank crest,
two pore pressures readings in the bank and the water pressure in the water
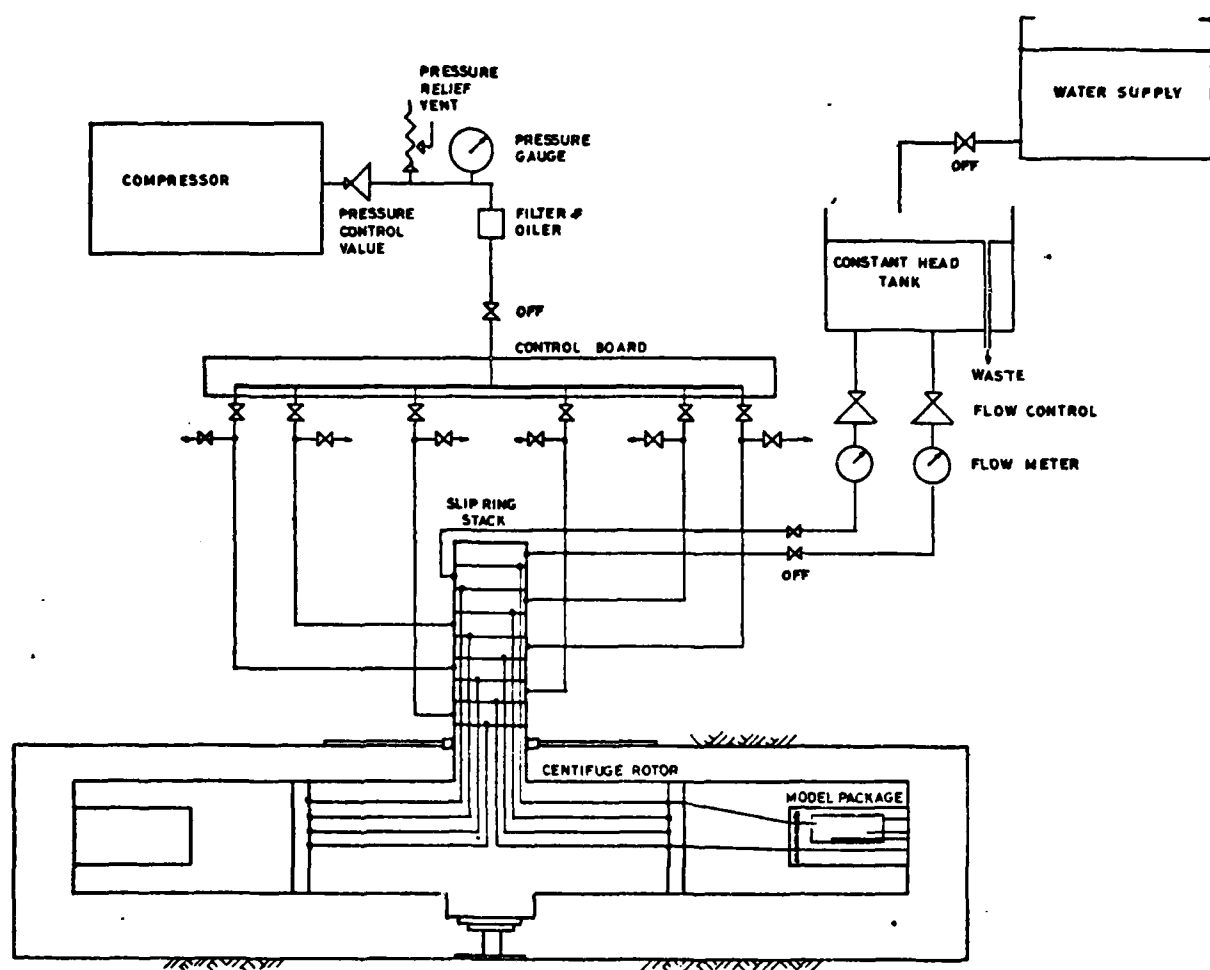line from the reservoir to the sand layer.

FIG 3·17 SERVICES REQUIRED ON CENTRIFUGE

The data logger was introduced for Tests 2DF4-14. For the three development tests a variety of chart recorders was used in an attempt to supplement the manual logging of readings. It was found that the recorders available drew too much power from the transducers. Voltage offsets and attenuation proved also a continual source of worry during a test and were abandoned in favour of the data logger.

3.9.2 Photographic Equipment

The photographic system has been modified several times, but is essentially the simple system developed for Test 2DF1. A camera (at first a Lindhof 5" x 4" plate camera and later an automatic Hasselblad 500 EL/M) was mounted above the steel decking over the centrifuge chamber. Perspex windows were let into the decking for the camera and for the flash gun of a stroboscope.

The stroboscope supplied a 20 Joule flash of approximately 2 μsec duration triggered by a mechanical microswitch on the axis of the centrifuge. Photographs were recorded on glass plates and on Polaroid positives. The Polaroid photographs were used in the absence of a television system to give visual confirmation of model behaviour.

The glass plate negatives were later projected in an enlarger onto a sheet of white paper where the positions of the balls were marked with a pencil. Superposition of two of these records gave the type of displacement diagram shown in Fig. 3.12a.

Sophisticated film measuring equipment is available in Cambridge which can provide input data to computer programs which calculate shear and volumetric strains. That approach was not considered suitable in this test series since the important consideration was failure and not the analysis of small strains for which the computer program is uniquely suitable.
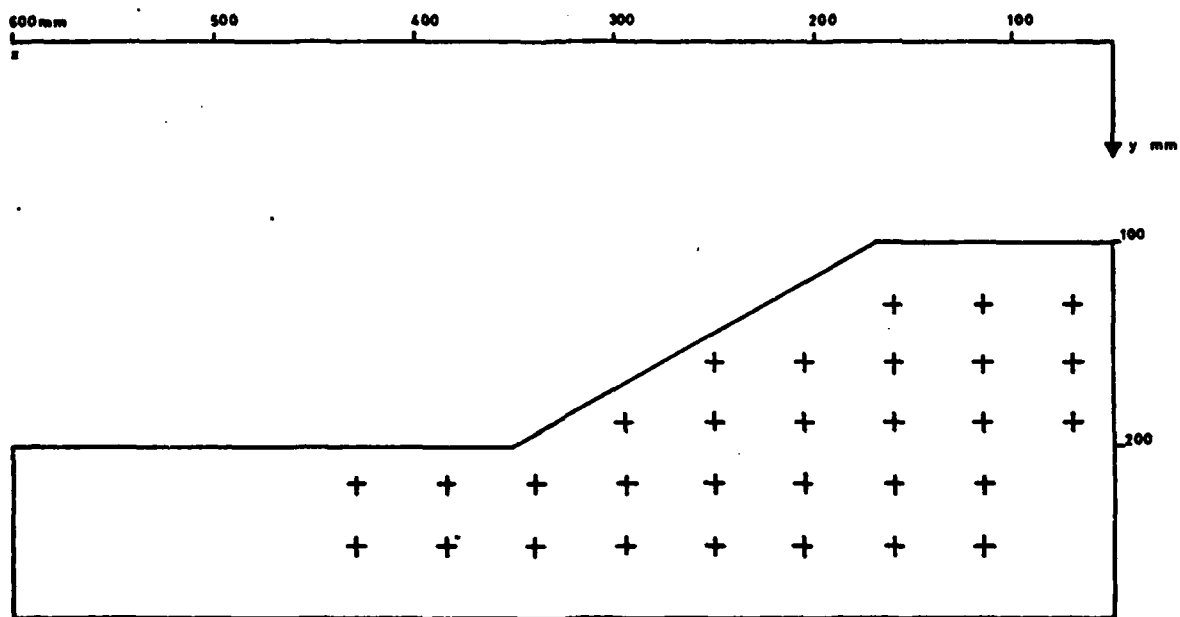
FIG. 3·18 POSITIONS AT WHICH MOISTURE CONTENT SAMPLES TAKEN
FLOODBANK TESTS 2DF 10-14.

3.9.3   Hydraulic Systems

The pneumatic system shown in Fig. 3.17 was developed for Test 2DF1 and was retained with slight modification throughout the test series. Water supply was controlled manually from a reservoir. The flow rate was monitored visually by making the water drip feed through a glass "dribbler". Both water and compressed air are transmitted to the centrifuge through the slip rings shown schematically in Figure 3.17.

3.10   Investigation of Model Properties

After the test run was over the strong boxes were removed from the centrifuge and opened on a work bench. The profile of the failure was drawn on tracing paper and the model was photographed. In Tests 2DF1-9 the model was then investigated using a pocket vane to measure the undrained shear strength at three points (40, 80, 120 mm below the crest of the embankment). Moisture content samples were taken at the sites where strength measurements were made. The miniature vane measurements were rejected for Tests 2DF10-14 in favour of a comprehensive array, Fig. 3.18, of moisture content samples taken with the aid of a sampler and a perspex template. To take these samples the models were cut in half with a cheesewire and the samples were obtained from the central section of the model. The shortcomings of the vane measurements are discussed in Section 4.4.14.5. One slice of the model was retained on a board and allowed to dry for later examination.

CHAPTER 4

THAMES FLOOD EMBANKMENTS

DATA FROM THE TESTS

4.1 Outline of the Two Dimensional Flood Embankment Tests

In total 27 models were tested in fourteen separate centrifuge runs which may be divided into three groups.

I Two preliminary embankment tests (2DF1,2)

The initial hypothesis was that interaction between the self weight and uplift loadings would be observed in a centrifuge model test if a model geometry was chosen such that an embankment was supported by a relatively thin marsh. It was hypothesised that in the tests performed by Hird, 1974, the marsh layer was so thick that at no stage did the deeper slip mechanism along the uplifted interface become more critical than the shallow circle. The first two tests, 2DF1-2, employed a bank geometry copied directly from Hird, but the marsh thickness was chosen to be approximately half the thickness used by Hird - that is, the depth to which the slip circles penetrated in Hird's tests.

II One exploratory test (2DF3)

For various reasons to be discussed in Section 4.3.5, this was the last of the preliminary tests. The models were failed by rapid draw down. The embankment geometry was changed and the clay was consolidated to a greater pressure than had been used in the two previous tests.

III Main series of eleven two dimensional flood embankment tests (2DF4-14)

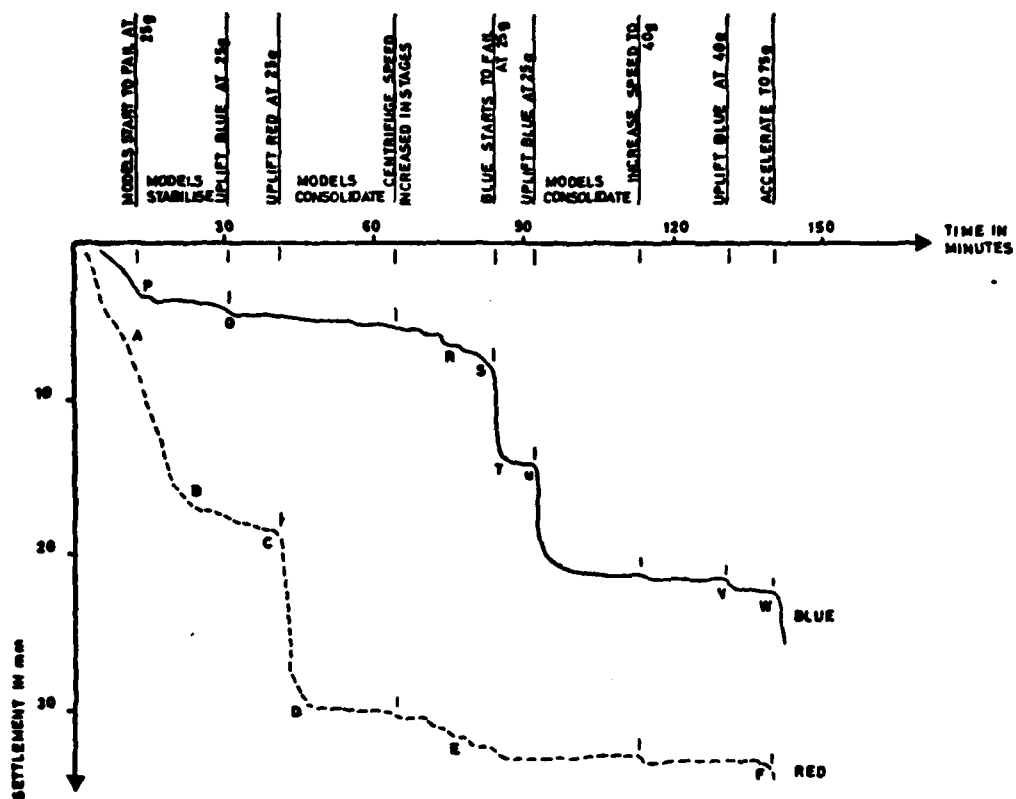These tests were executed according to the routine described in the

MODELS START TO FAIL AT 15g

UPLIFT BLUE AT 25g

UPLIFT RED AT 21g

CENTRIFUGE SPEED INCREASED IN STAGES

BLUE STARTS TO FAIL AT 35g

UPLIFT BLUE AT 25g

INCREASE SPEED TO 40g

UPLIFT BLUE AT 40g

ACCELERATE TO 75g

MODELS STABILISE

MODELS CONSOLIDATE

MODELS CONSOLIDATE

TIME IN MINUTES

30   60   90   120   150

SETTLEMENT IN mm

10

20

30

P
A
Q
R S
B
T U
C
D
V W BLUE
E
F RED

FIG. 4·1 PLOT OF BANK CREST SETTLEMENT AGAINST TIME
FOR MODELS 2DF1

previous chapter. Model geometry was standardised and the models were sub-jected to a rapid increase in either gravity loading or uplift pressure or both. The models in this series were not allowed to swell in the consolido-meters and were allowed no access to water until subjected to 50g on the centrifuge.

Table 1 (bound at the end of this dissertation) gives the important parameters for all the tests.

4.2   Preliminary Embankment Tests

4.2.1   Test 2DF1

In this test, embankments of the same geometry as those used by Hird, were tested on a thin marsh layer (102 mm bank, 48 mm marsh). Kaolin slurry was consolidated to a vertical pressure of 128 kN/m^2. This stress level was chosen such that the clay would be overconsolidated throughout its depth at 50g, and so that the strength of the model would be such that it could be brought to failure with an admissible increase in speed of the centrifuge. The clay was allowed to swell to 50 kN/m^2 in the consolidometer and after model making the soft clay models were reconsolidated on the centrifuge. This method was preferred initially since it was expected that the expulsion of water by the model on the centrifuge would be less often frustrated by airlocks and bubbles in the pipework than water uptake with its associated risk of cavitation. The plumbing arrangement in the strong boxes was essentially that shown in Fig. 3.8.

Only eight hours was allowed in this case for the whole experiment and so consolidation increments at 10, 25, 40 and 50g were of very short duration – only 13% consolidation could be expected at the end of any inc-rement. As a consequence the embankments started to fail as they approached 25g as will be seen in Fig. 4.1, where settlement of the crest is plotted against time. The behaviour of the two models in this test which were nominally identical and were called Red and Blue, will be described together.
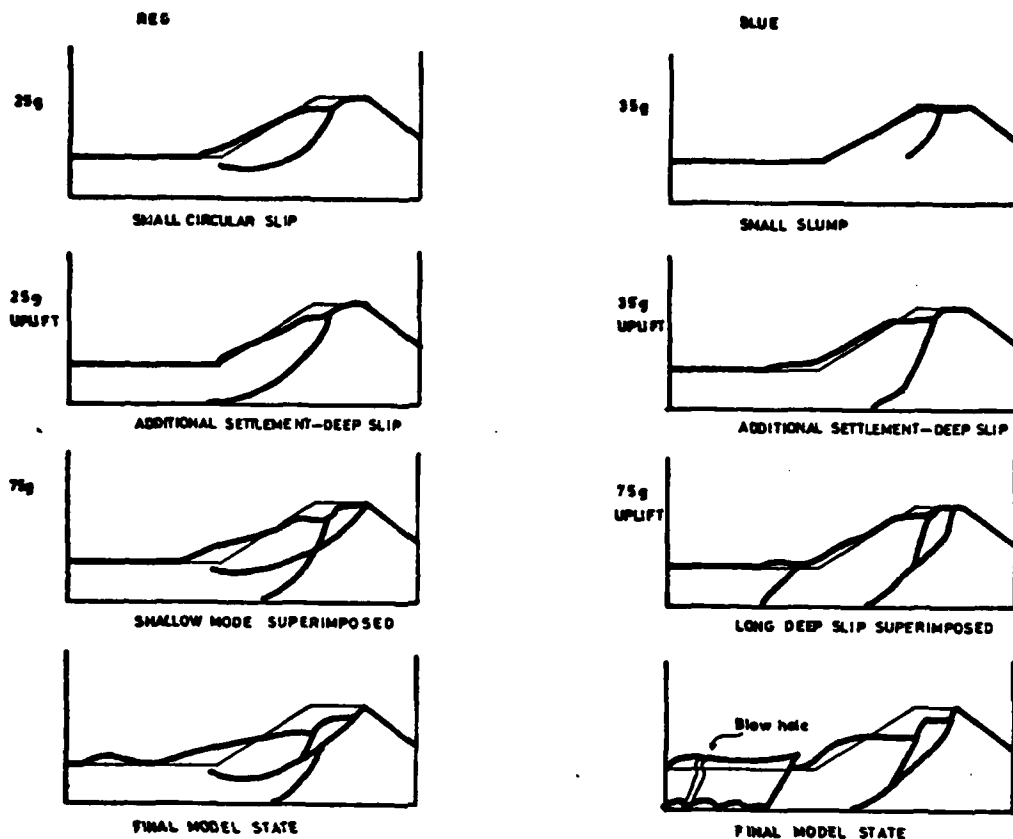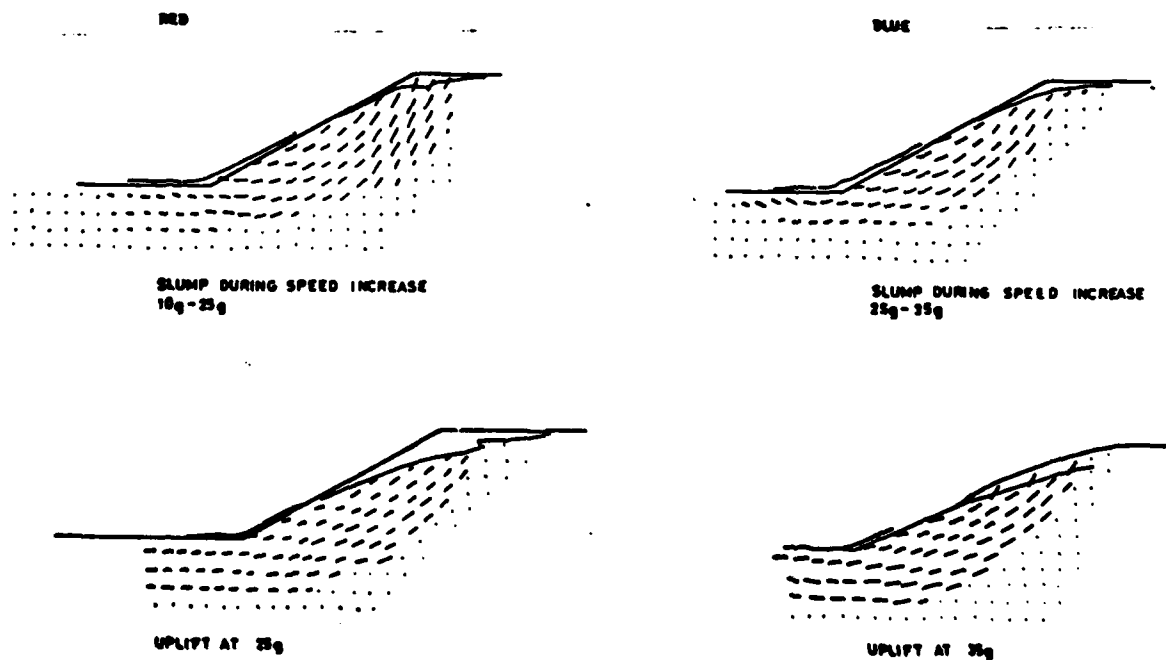
RED

25g
SMALL CIRCULAR SLIP

25g
UPLIFT
ADDITIONAL SETTLEMENT—DEEP SLIP

75g
SHALLOW MODE SUPERIMPOSED

FINAL MODEL STATE

BLUE

35g
SMALL SLUMP

35g
UPLIFT
ADDITIONAL SETTLEMENT—DEEP SLIP

75g
UPLIFT
LONG DEEP SLIP SUPERIMPOSED

Blow hole
FINAL MODEL STATE

FIG 4·2 SEQUENCE OF EVENTS FOR 2DF1

RED

SLUMP DURING SPEED INCREASE
10g - 25g

UPLIFT AT 25g

BLUE

SLUMP DURING SPEED INCREASE
25g - 35g

UPLIFT AT 35g

FIG 4·3 FLOODBANK MODEL 2DF1

Blue model suffered only a little damage at 25g (P) but the Red bank (A) continued to settle for ten minutes before stabilising (B). Both embankments were then known to be in a limiting condition of equilibrium, though Red model, for unknown reasons, appeared to be more unstable than the Blue model.

Uplift was applied to Blue model (Q) and resulted in a small additional settlement. Uplift was then applied to Red model (C) which resulted in a large settlement (D). The centrifuge speed was increased in stages until Blue model started to fail at 35g (S). The settlement stabilised (T) and the model was again uplifted (U) whereupon a further large settlement occurred. Uplift was applied again at (V) and the models were accelerated to 75g (F,W).

The sequence of events sketched in Fig. 4.2 shows the type of deformation which occurred in each of the settlements described above. The displacements are shown in greater detail in Fig. 4.3 which shows the interesting result that the initial slip, associated with general instability of the bank, occurred on a very shallow circle. When uplift was applied the slip surface moved deep into the marsh and along the base of the clay layer as predicted in Section 2.4.2. Plate 4.1 shows the slice of Blue model which was allowed to dry. The slip surfaces show up clearly. The relief in the surface of the slice is due to non-uniformity in the clay caused probably when filling the consolidometer with slurry.

4.2.2 Test 2DF2

The Blue model of this pair was accidentially dropped and damaged before the test run and so only Red model was tested. Data from the test are limited to the displacement diagrams shown in Fig. 4.4, since there were problems with the interfacing of the transducers to the chart recorders, and no reliable record of displacement was made.

Test preparation was similar to 2DF1 except that 12 hours were allowed for the experiment. The model started to show signs of distress during the increment from 40-50g but stabilised in the slightly slumped condition shown in Fig. 4.4a. After three hours consolidation at 50g the valve which switched

a
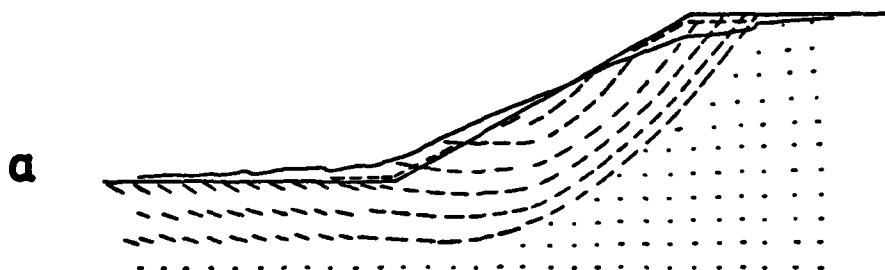
BANK FAILURE DURING FINAL CONSOLIDATION INCREMENT   40-50 g

b
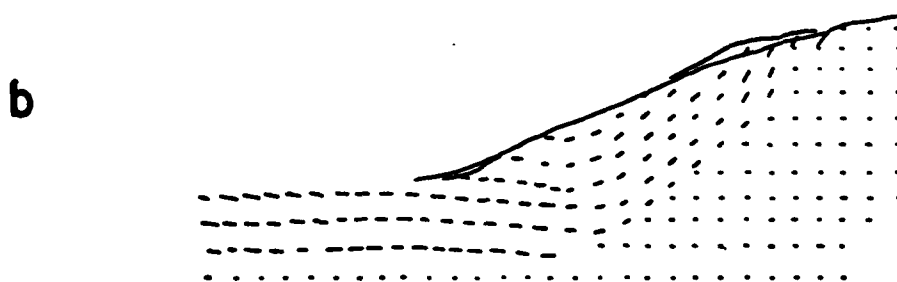
UPLIFT AT   50 g.

FIG. 4·4   FLOODBANK   MODEL   2DF2

outflow from the reservoir between the standpipes was observed to have suddenly operated. It was later discovered that a slug of water had found its way into the pneumatic signal line. The column of water had actuated the valve and caused the model to be uplifted. The uplifted bank failed at 50g on a long sliding surface along the interface with the sand layer, Fig. 4.4b. In this case the depth of the two types of failure were not appreciably different.

4.2.3   Conclusions to Preliminary Embankment Tests

1.   In the first test two distinct mechanisms were observed as predicted in Chapter 2. The deeper, long sliding failure became more critical when uplift pressures were high. However, the evidence of Test 2DF2 suggests that the most critical circular self weight slip is not necessarily shallow.

2.   Models which were consolidated to 128 kN/m^2 and allowed to swell to 50 kN/m^2 were very soft. The vane strength measured after Test 2DF2, was 6-9 kN/m^2 and the moisture content was 61-64%. Model making was difficult and the banks were so soft that extreme care had to be taken in consolidation on the centrifuge to avoid excessive deformations. The consolidation period allowed at each increment of loading on the centrifuge was so short that insufficient strength had developed at each load level to support the subsequent increment.
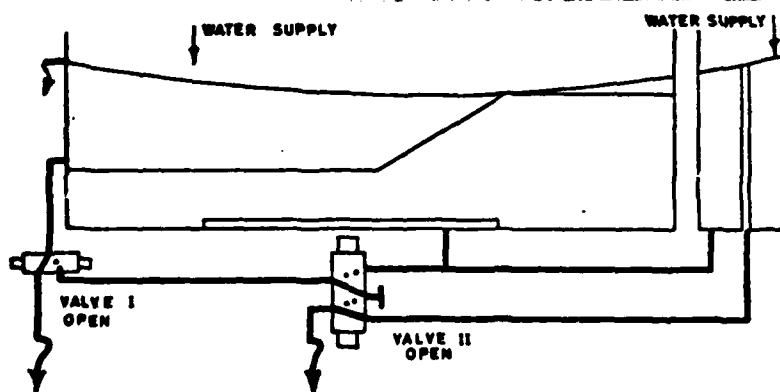
3.   The signals from the transducers were conditioned for input to the data recording instruments by an inadequate temporary assemblage of resistors. If chart recorders were to be used then offset and attenuation circuitry would have to be readily adjusted and accurately calibrated.

4.2.4   Changes of Policy

It was decided to consolidate the clay for the next test to 200 kN/m^2 in order to increase its strength during model making, and in the runup to . 50g. The clay was again allowed to swell in the consolidometers to 50 kN/m^2. The consolidation run had not been long enough in the first two tests and despite difficulties in manning the centrifuge it was decided to consolidate the models

WATER SUPPLY   WATER SUPPLY

VALVE CLOSED

VALVE CLOSED — CONSOL^n
VALVE OPEN — DRAWDOWN
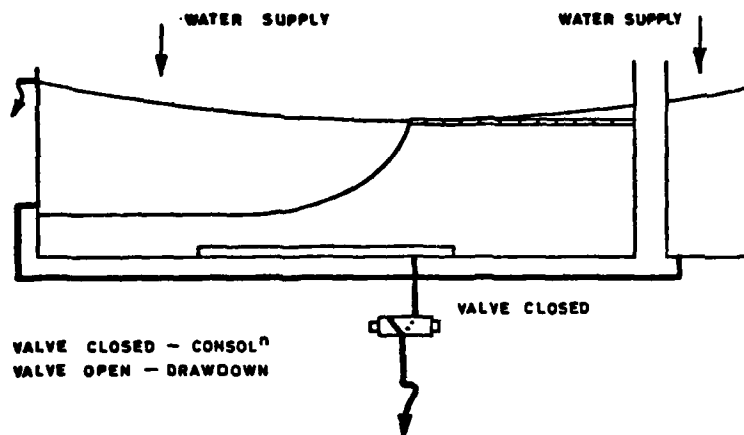
SOKOLOVSKYS IDEALISED SLOPE MODEL

WATER SUPPLY   WATER SUPPLY

VALVE I
OPEN

VALVE II
OPEN

CONSOLIDATION :	VALVE I CLOSED	VALVE II CLOSED
DRAWDOWN :	OPEN	CLOSED
UPLIFT :	OPEN	OPEN

FLOODBANK MODEL

FIG. 4·5 PLUMBING FOR MODELS 2DF3.

of Test 2DF3 in increments overnight and allow for a 20 hour consolidation period.

An alternative perturbation was sought which would induce controlled failure and would replace the perturbation used in the first tests - rapid increase in centrifuge speed. It was decided to investigate whether rapid draw down of an embankment would constitute a viable perturbation of embankment stability. Using this technique the bank and marsh would both be consolidated subaqueously and the water level subsequently drawn down. This subaqueous consolidation had two potential advantages. Firstly, the shear stresses within the model would be less for a subaqueous bank and so deformations during consolidation were likely to be less serious. Secondly, the bank and marsh would both be consolidated subaqueously and there would be no problems of saturated soil developing complex pore pressures on account of its position above the water table.

The transducers and data recording facilities available at the time were unreliable. The most accurate and potentially the most versatile data which could be retrieved from the tests was obtained from analysis of the photographs. However, the analysis of strain is most significant if the material deforms as a continuum rather than along discrete slip planes. For this reason, one of the models of Test 2DF3 was constructed with such a profile that subject to certain assumptions the slope was theoretically in limiting equilibrium everywhere. The theoretical basis of this design will be discussed in the following section.

4.3   Exploratory Test 2DF3

4.3.1   Introduction

In this test the clay was consolidated to 200 kN/m and allowed to swell to 50 kN/m in the consolidometer. The new strong boxes were used in this test for the first time. Pore water pressure transducers and displacement transducers were employed but the electrical systems on the centrifuge were still elementary and the data was unreliable. All four water pressure transducers failed during consolidation.
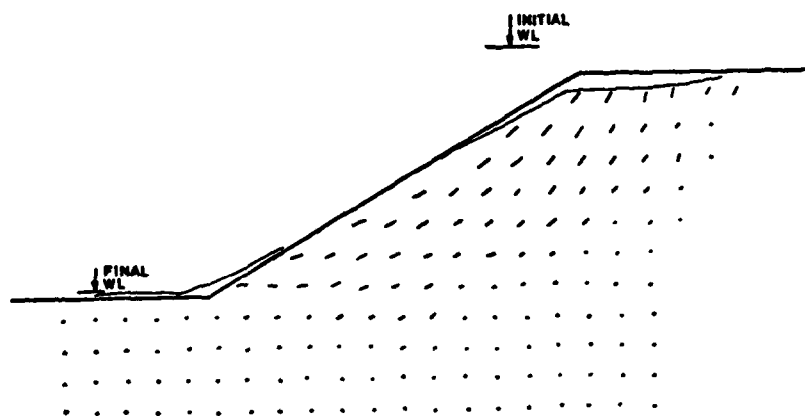
FIG. 4·6 DISPLACEMENTS IN MODEL EMBANKMENT
ENSUANT UPON DRAWDOWN 2 DF 3

Minutes before the consolidation run was started the models were immersed and were consolidated subaqueously in increments of loading to 50g throughout the night.

The two models were dissimilar and they will be treated independently below.

4.3.2   2DF3 Subaqueous Embankment Model

The plumbing for this test was modified, Fig. 4.5a, to allow independent control of the water level against the bank surface and in the underlying sand layer, although in this particular test the water levels were coupled. The process of drawdown took three minutes.

The theoretical account of the drawdown process given by Taylor, 1948, indicates that for a sliding wedge the effect of the draw down is to increase the disturbing forces by effectively increasing the density of the clay from the buoyant weight to the saturated weight, without altering the material strength. The resulting additional loading on the slip surface represents a valid loading perturbation which should be able to interact with an uplift loading.

In the test the subaqueous embankment survived intact to 50g with only 3mm settlement. Upon draw down, the failure was shallow, Fig. 4.6, and did not affect the bulk of the bank. It is possible that the simultaneous application of an uplift loading would have caused the embankment to fail by the development of a deeper slip surface but this was not attempted. Plate 4.6 shows the failure of the front of the slope.

4.3.3   Sokolovsky's Theoretical Slope Profile in Limiting Equilibrium

In a purely cohesive soil body where limiting equilibrium is described by the stress difference in the Mohr's circle, as in Fig. 4.7a, it is not generally possible to determine from known boundary stresses the values of the principal stresses everywhere within the body. Two equations of equilibrium

T SHEAR STRESS

K

POLE

(σ'_y, τ_{xy})

σ'_{min}

2ϕ

Σ'

σ'

EFFECTIVE STRESS

-K

s

a MOHR'S CIRCLE REPRESENTATION OF STRESS

b PRINCIPAL STRESS AXES

(ϕ)

Σ'

σ'_{min}

x

y

C CHARACTERISTIC DIRECTIONS

(ϕ)

x

d_x

d_y

(s, ϕ)

$\frac{\pi}{4}$

α

$(s+ds, \phi+d\phi)$

$\frac{dy}{dx} = \tan(\phi - \frac{\pi}{4})$

β

$\frac{dy}{dx} = \tan(\phi + \frac{\pi}{4})$

y

FIG. 4·7 CHARACTERISTIC DIRECTIONS FOR COHESIVE SOIL

describe the three unknowns (σx, τxy, σy). In the work of V.V. Sokolovsky, 1965, expounded in Critical State Soil Mechanics, Schofield and Wroth, 1968, a third postulate is made: that the stress is limiting everywhere. With this postulate the equations are determinate.

Two parameters are defined:

$$\xi = \frac{S-\gamma y}{2K} + \phi$$

$$\eta = \frac{S-\gamma y}{2K} - \phi \qquad (4.1)$$

where the symbols are illustrated in Figs 4.7 and γ = density.

The parameters have the property that loci may be found within the material along which ξ (β characteristic) and η (α characteristic) are constant. These characteristics are shown in Fig. 4.7c and are inclined such that

$$\frac{dy}{dx} = \tan\left(\phi + \frac{\pi}{4}\right) \text{ along a } \beta \text{ characteristic}$$

$$(4.2)$$

and $\frac{dy}{dx} = \tan\left(\phi - \frac{\pi}{4}\right)$ along a α characteristic.

If ξ has a constant value throughout the region, then all the α characteristics become straight lines of equation

$$\frac{y-y(\phi)}{x-x(\phi)} = \tan\left(\phi - \frac{\pi}{4}\right) \qquad (4.3)$$

Schofield and Wroth consider the limiting shape of a slope in cohesive soil, Fig. 4.8b. Along the top surface is a surcharge loading and at any point on the curved free face of the slope the principal stress is parallel to the slope. The equation of the slope is found to be

$$\frac{\gamma x}{2K} = \ln \frac{\sin(\beta_o + \gamma y/2K)}{\sin\beta_o} \qquad (4.4)$$

and has a horizontal asymptote

$$\frac{\gamma y}{2K} = \pi - \beta_o \qquad (4.5)$$

where $\beta_o = \left(\frac{\gamma}{2K} + \frac{\pi}{2} - 1\right) \qquad (4.6)$
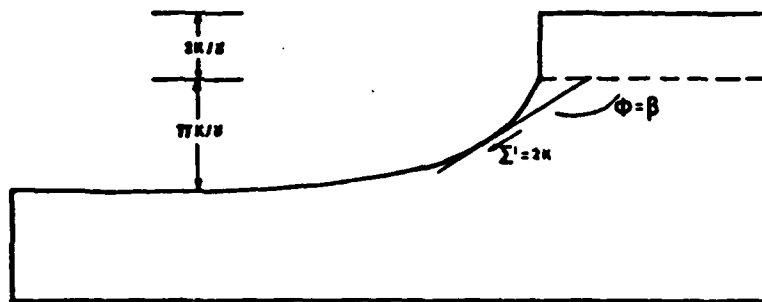
FIG. 4·8a LIMITING SHAPE OF SLOPE IN COHESIVE SOIL
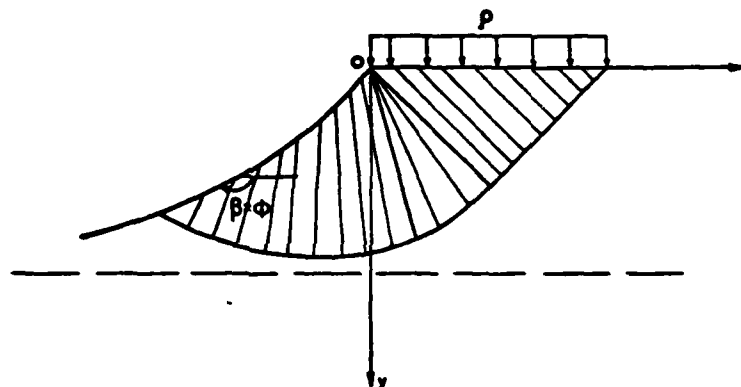
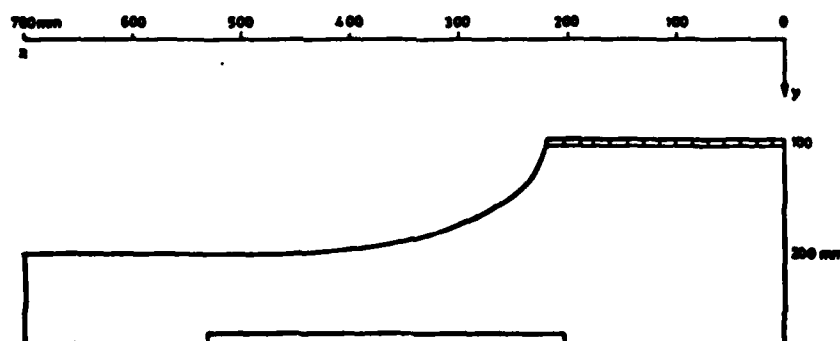FIG. 4·8b GENERAL LIMITING SHAPE OF SLOPE IN COHESIVE
SOIL

FIG. 4·9 DESIGN OF LIMITING SLOPE FOR MODEL TEST
KAOLIN BANK - BRASS SURCHARGE

In the case where the surcharge loading is in fact soil then the slope may take the form shown in Fig. 4.8a, where $\beta_o = \pi/2$ and the slope equation is

$$\frac{\gamma x}{2K} = \ln \cos\left(\frac{\gamma y}{2K}\right) \tag{4.7}$$

For the centrifuge model test a surcharged slope design was used for which the height of the slope was 100mm, and the surcharge loading was provided by lengths of brass bar 150 x 25 x 6 mm. The slope was designed to be stable at 50g and to fail in draw down. An average value of $C_u = K = 14$ kN/m^2 was taken for the kaolin at that stress level. The resulting slope profile is shown in Fig. 4.9. Evidently even if the design is safe at 50g, the material may soften in the long run up to 50g.

4.3.4   Test of Sokolovsky's Limiting Slope Profile

The design of this slope was discussed in Section 4.3.3. At 25g the slope was initially stable as shown in Plate 4.5a, but after a period (unknown) at this stress level the tip of the crest fell and came to rest further downslope, Plate 4.5b. By 50g a considerable portion of the slope had likewise degraded.   During draw down the whole slope reduced to a rubble and the brass surcharge strips buried themselves in the clay, Plate 4.5d.

The effect seen between Plates 4.5b and 4.5c was characteristic of the behaviour of this model. An overconsolidated clay exhibits a softening tendency under drained shear. In reality the material does not dilate uniformly but takes in water along distinct surfaces from the surrounding material, Henkel, 1956. As a result, the continuum breaks up into a rubble of blocks, Plate 4.5d, which slide over each other. The frictional resistance along the softened bands is extremely low in comparison with the undrained shear strength of the intact soil.

The aim of this test was frustrated in so far that for the overconsolidated clay used, a uniformly yielding slope was not produced. However,

the result was informative. For a truly cohesive material a profile of the type used here may develop if the material at the base of a slope is regularly removed, for example by a river. Some natural materials approximate closely to the truly cohesive soil, e.g. soft clay. This type of profile is well known in geomorphology where the lower part of a slope is regularly swept clear of debris. It is interesting that no reference to this analysis may be found in the relevant literature. If, however, the cohesive material breaks up into a rubble where the resistance between the blocks is less than the resistance of the intact mass to shear then no steep faces can develop and the theory is not appropriate.

4.3.5 Change of Policy

It had become important by this stage in the investigation to rapidly settle on a standard test procedure and to perform a series of tests prepared according to the same routine. The Sokolovsky slope was not repeated and the test by draw down was rejected in favour of a rapid increase in self weight. Attention was focussed in the remaining tests on models of the Thames Flood embankment type subjected to uplift and self weight loading perturbations. The search for a uniformly yielding model was adjourned in favour of the discrete planes of failure which develop in tests using over-consolidated clay. For these model failures simple slip circle analyses were considered appropriate.

Pore water pressure transducers had proved unreliable up to this point. Without pore pressure measurements nothing was known experimentally about the effective stress state of the model at the beginning of the test perturbations. Also, without the pressure transducers, the only indication of the progress of the model towards pore pressure equilibrium at 50g was the record from the displacement transducer on the crest of the bank. A new type of pore pressure transducer, described above in Section 3.8.2 was designed to attempt to solve the problem.
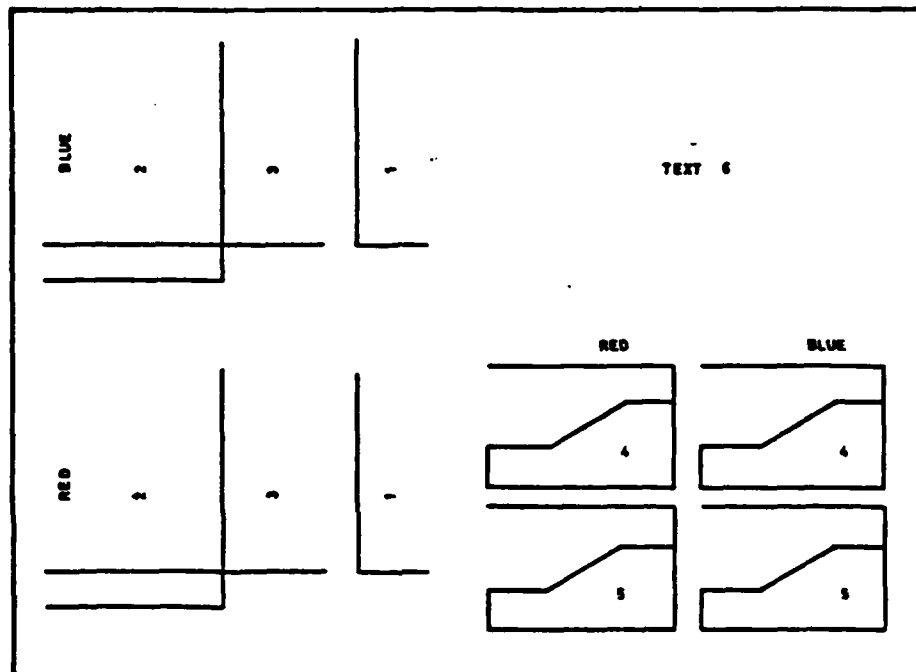
FIG. 4·10 SCHEMATIC REPRESENTATION OF THE DOUBLE
PAGE LAYOUT USED TO PRESENT DATA FROM
FLOOD EMBANKMENT TESTS

It was decided to continue using kaolin that had been consolidated to a maximum vertical stress of 200 kN/m^2 and not to allow any swelling until the model experienced 50g. The maximum time available for the consolidation run was eight hours which meant that in none of the tests had the models attained full pore pressure equilibrium. However, at the end of this time the moisture contents were sufficiently close to the equilibrium values to generate reasonable values of undrained shear strength.

4.4 Main Series of Two Dimensional Flood Embankment Tests

4.4.1 Outline of the Test Series

In all these tests an identical test procedure was followed. The clay was consolidated to 200 kN/m^2 in the laboratory and not allowed access to water until subjected to 50g on the centrifuge. The machine was accelerated from rest directly to 50g and the models were consolidated for 8 hours at 50g. Each test involved an increase in uplift or acceleration or both until the models failed. The data from each of these tests is presented in Sections 4.4.3 - 4.4.13. The form this presentation takes is described in Section 4.4.2.

4.4.2 Data Presented for Each Test

It will be seen from the following pages that the data from each test is presented on one double page, shown diagrammatically in Fig. 4.10. The presentation takes the following form.

1. Bank settlement or heave plotted against the square root of time during the consolidation run at 50g on the centrifuge. The processes behind this behaviour were described in Sections 2.3.3 and 3.7.

2. A graph showing in analogue form the output of three transducers:

    (i) Accelerometer output is shown with a thick line and labelled (ng), (green)

    (ii) Pore water pressure within the bank is labelled (pwp). Since it was rare that both pore water pressure transducers within the bank

gave full response in any one test, in each graph only the most informative trace is shown. For all the water pressure trans-ducers the zero was uncertain at the beginning of each test. The zero which is used on the graphs is chosen for clarity to be the value of pressure that the transducers would be reading if the model were at equilibrium at 50g at the end of the eight hour consolidation run. (Red)

(iii) The output of the transducer in the water line to the sand layer is labelled RES. The transducer was mounted in the base of the strong box and therefore records higher pressures than the others. This record was used to calculate the value of U defined in Section 2.2 and explained in Section 3.8.3. (Blue)

3.   The output of the displacement transducer which records embankment crest settlement during the test perturbations.

4.   A diagram showing the slip surfaces as traced from the face of the model after the test. Also on this diagram are the displacements recorded to scale by superimposing photographs taken before and after failure.

5.   The moisture content distribution for models 2DF10-14. For models 2DF4-9 the limited vane strength/moisture content distribution is given.

6.   In the text the events are described which occur in each test. In certain cases reference is made to plates bound at the end of the volume which show either the dried slice of a model after failure or the failed model immediately after the test.

7.   Data of failure are shown plotted on an interaction diagram in Fig. 4.37 and given in Plates 4.10a,b,c which fold out at the end of the volume. For each model the loading conditions at failure are shown by one point, for example, the failure of 2DF5 Blue model, which was a model with a 55mm marsh, occurred at 100g by an increase in uplift. The failure point is labelled in Plate 4.10a as 5B with an arrow to show that the model failed by an increase in uplift. The build-up of the test series is best followed by noting the

position of each failure point on these diagrams.

8.   Data of failure and model geometry are given in tabular form in Table 1 which folds out at the end of the dissertation.
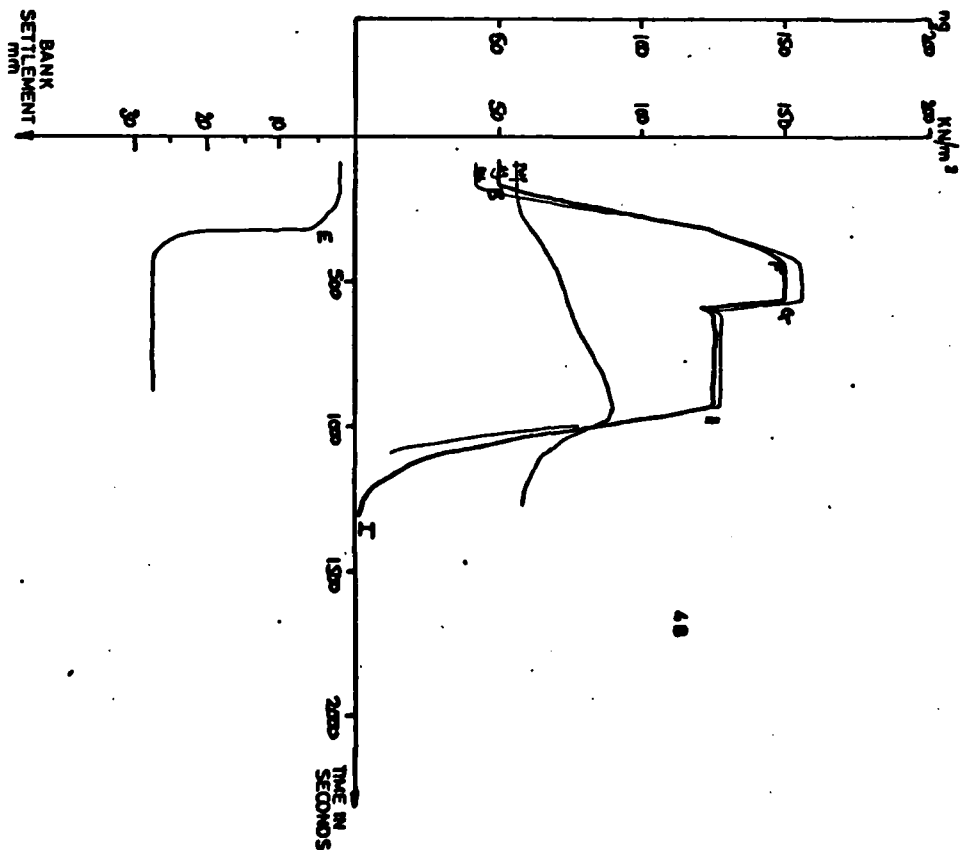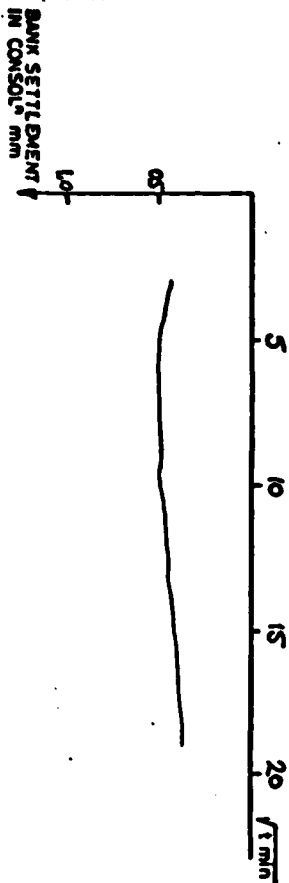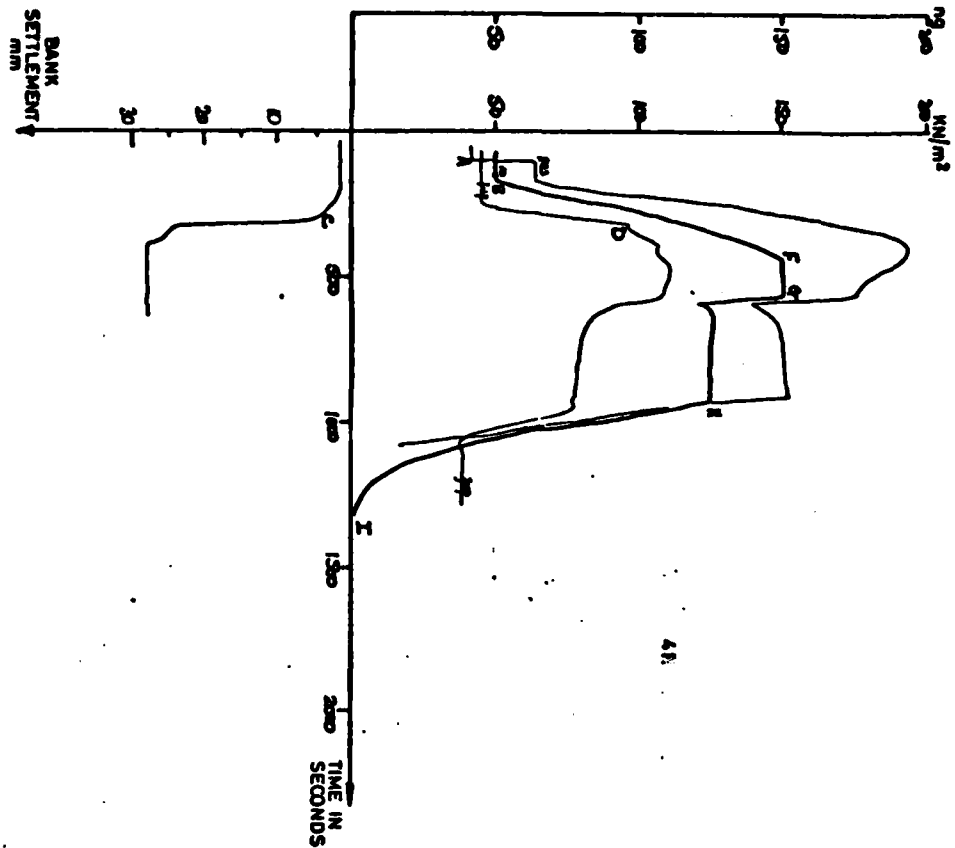
BANK
SETTLEMENT

BANK SETTLEMENT
IN CONSOL⁰ mm

TIME IN
SECONDS

BANK
SETTLEMENT
mm

BANK SETTLEMENT
IN CONSOL⁰ mm

FIG 4.11

TIME IN
SECONDS
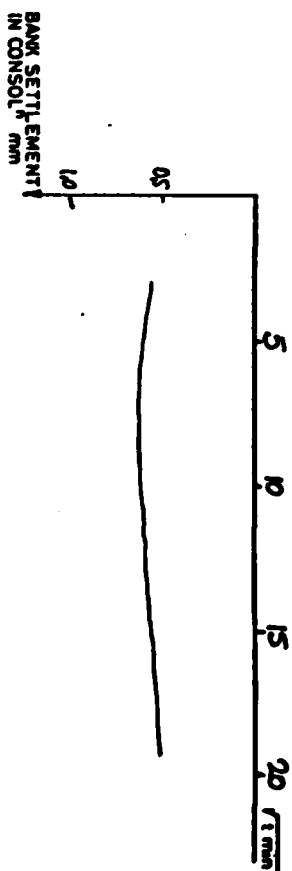
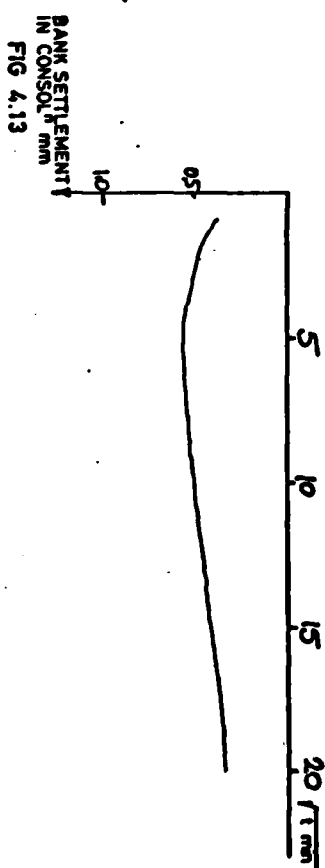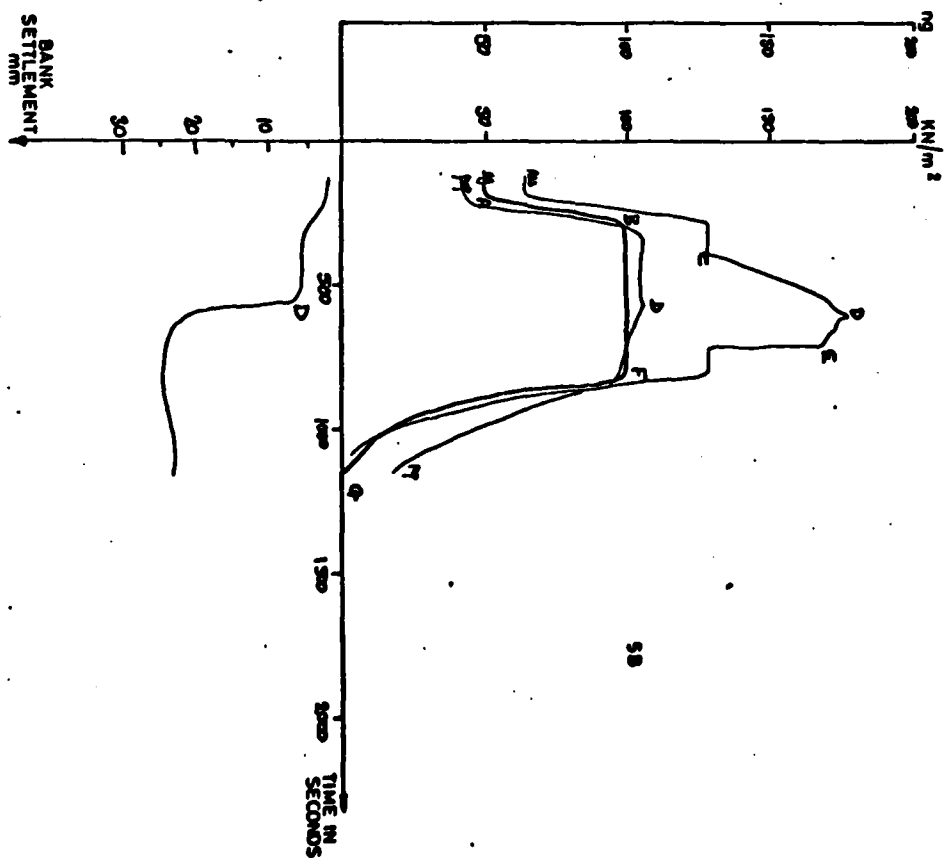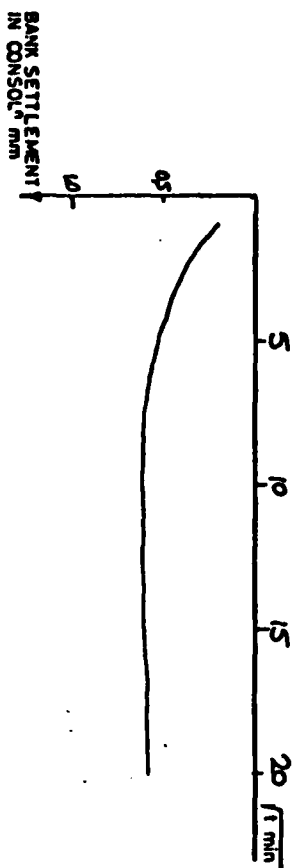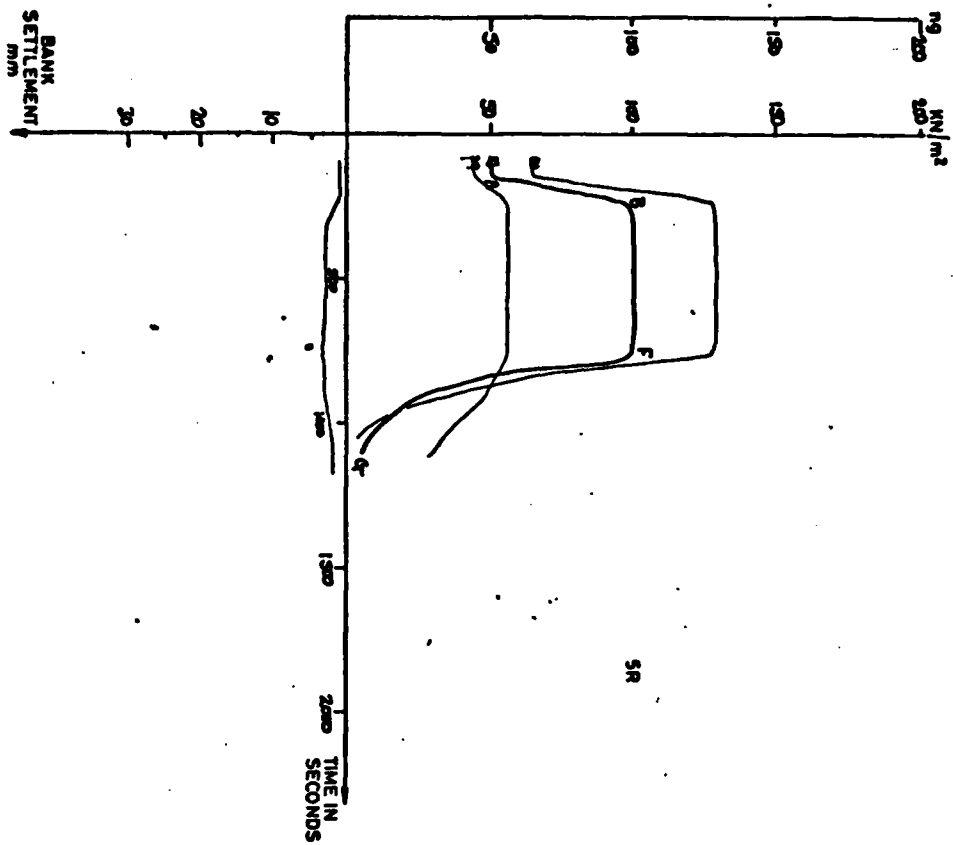### 4.4.3 Two Dimensional Flood Embankment Test 2DF4

55mm Marsh

Red model failed by an increase in self weight in the uplifted condition and Blue model failed by an increase in self weight with no uplift.

Events in Test

A   Red model uplifted at 50g

B   Centrifuge speed starts to increase

C   Red bank fails at 117g, U = 1.58

D   Red failure registered by change in pore water pressure trace

E   Blue bank fails at 122g, U = 0.83

F   Centrifuge speed rises to 150g

G   Speed dropped to 125g to take photographs

HI   Machine stopped.

Notes

1. Due to an oversight the water level in the models were 16mm below the level of the marsh and so the material was correspondingly stronger than was planned.

2. Settlement was followed after approximately ½ hour at 50g, by heave of the embankment crest.

3. The long sliding failure associated with uplift was combined in red model with a circular failure. In all probability the interaction mode failure occurred first and was succeeded at high ng, by the circular mode.

4. The test served also as a proof test.

5. Plate 4.2 shows a slice of Blue model after it has been allowed to dry. The slip surface shows clearly.

BANK SETTLEMENT IN CONSOL mm

BANK SETTLEMENT mm

mg

kN/m²

TIME IN SECONDS

SR

BANK SETTLEMENT IN CONSOL mm

BANK SETTLEMENT mm

mg

kN/m²

TIME IN SECONDS

SB
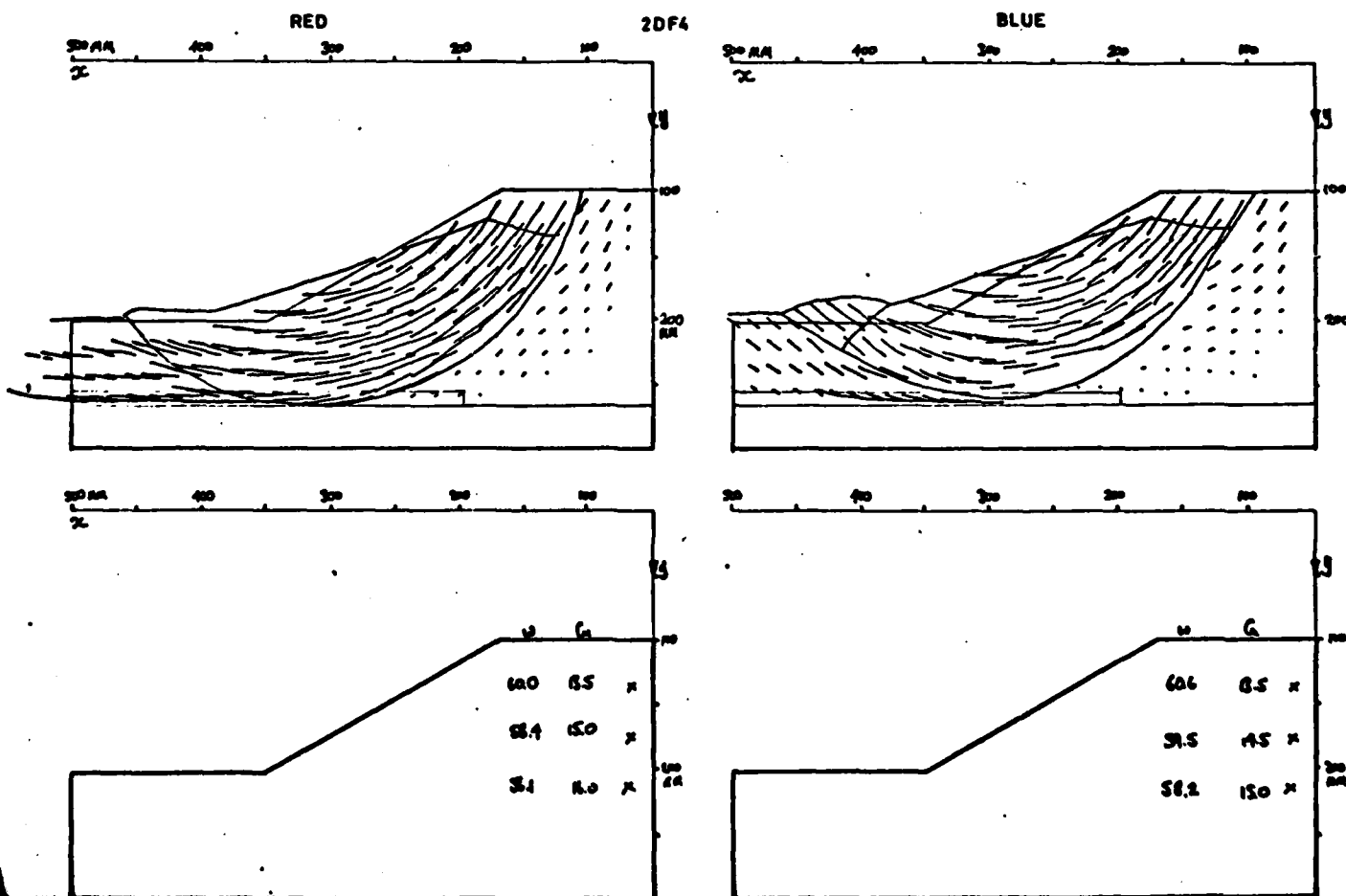
FIG 4.13

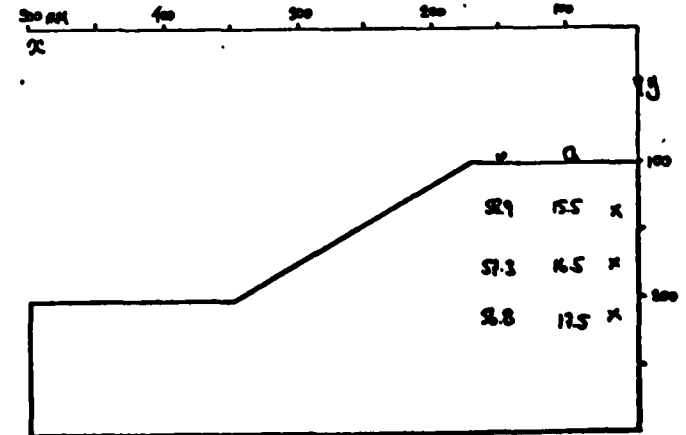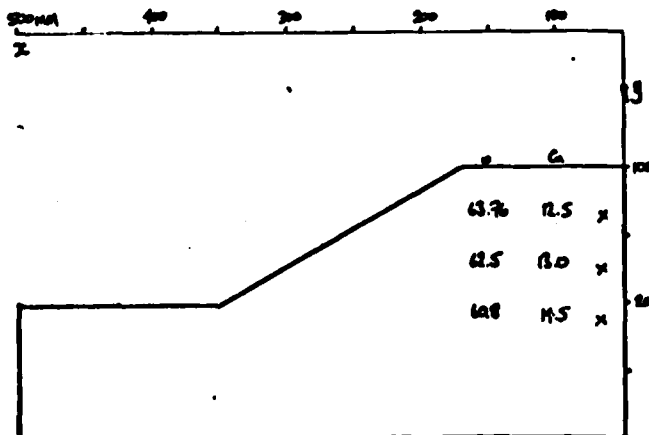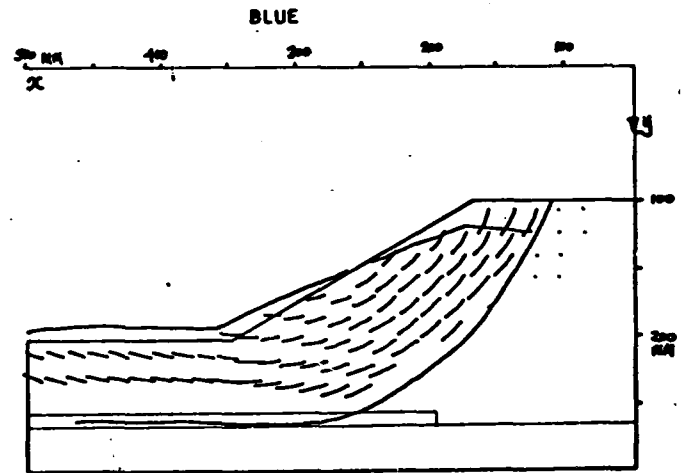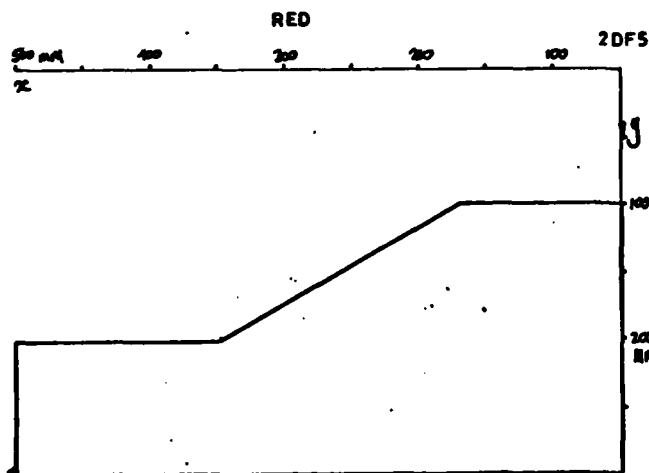#### 4.4.4 Two Dimensional Flood Embankment Test 2DFS

55mm Marsh

Red model was uplifted at 50g without causing any distress. This is not shown in the figures. Blue model failed at 100g by an increase in uplift.

Events in Test

- B_   Centrifuge speed increased from 50-100g
- C   Uplift applied gradually to Blue model
- D   Blue model failure evident in all transducer outputs;   U = 1.91
- E   Reduce uplift to Blue model
- FG   Machine stopped

Notes

1. Behaviour during consolidation at 50g was different for the two models.

2. Blue model failed on a long sliding surface.
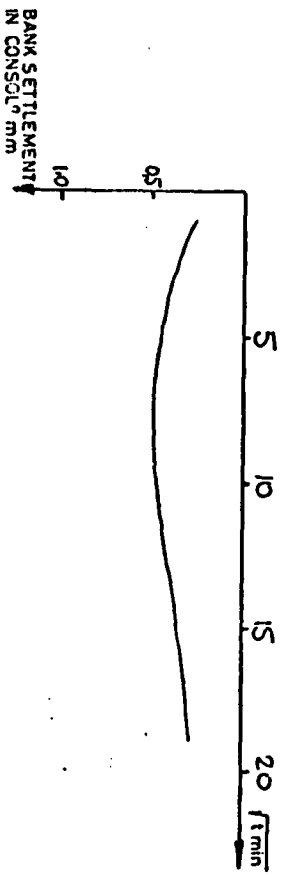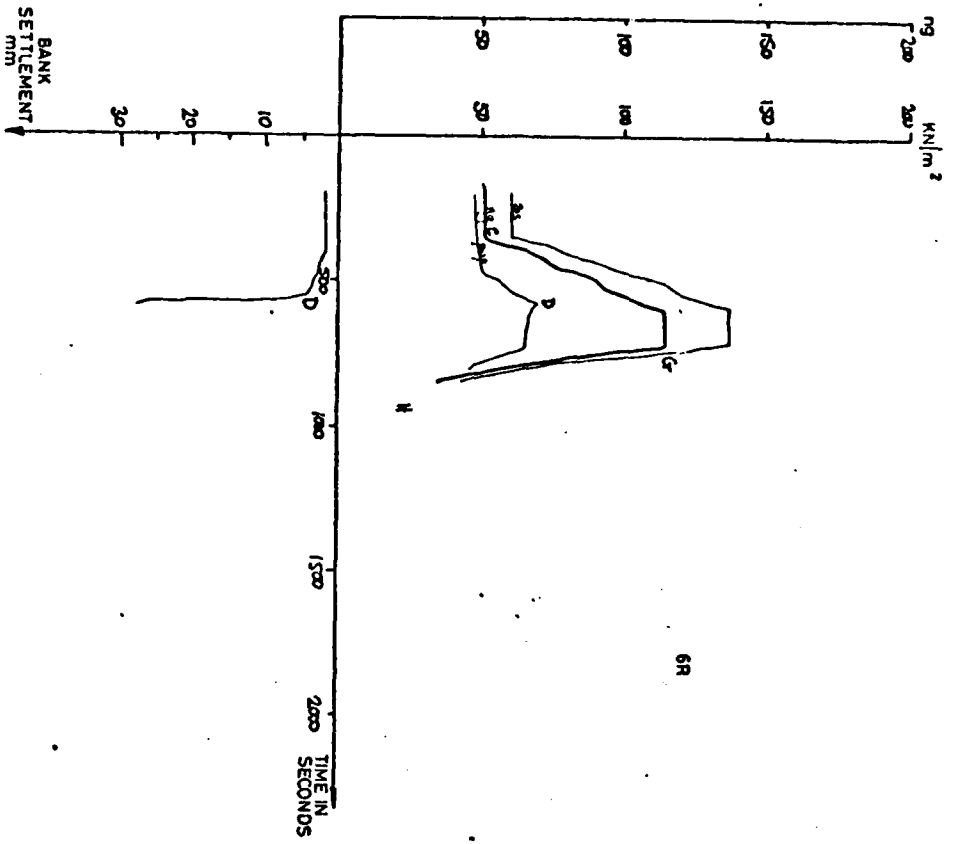
3. Red model did not fail.

BANK SETTLEMENT IN CONSOLⁿ mm

BANK SETTLEMENT mm

mg

50
100
150
200

KN/m²

30
20
10

50
100
150
200

1.0
0.5

5
10
15
20 f min

500
1000
1500
2000

TIME IN SECONDS

6R

D
D
G
N

BANK SETTLEMENT mm

BANK SETTLEMENT IN CONSOLⁿ mm

FIG 4.15

mg

50
100
150
200

KN/m²

30
20
10

50
100
150
200

1.0
0.5

5
10
15
20 f min

500
1000
1500
2000

TIME IN SECONDS

68

B
C
E
G
F
E
F
E
N
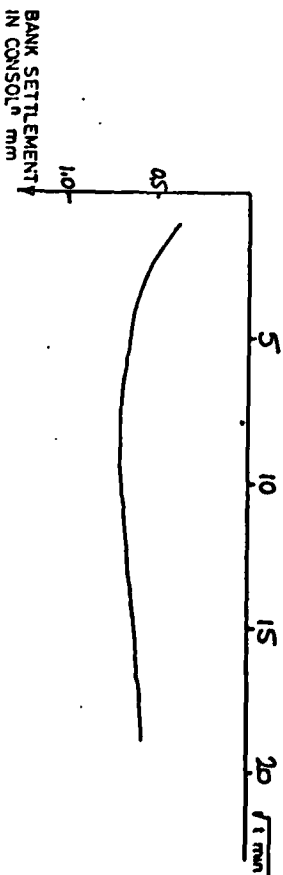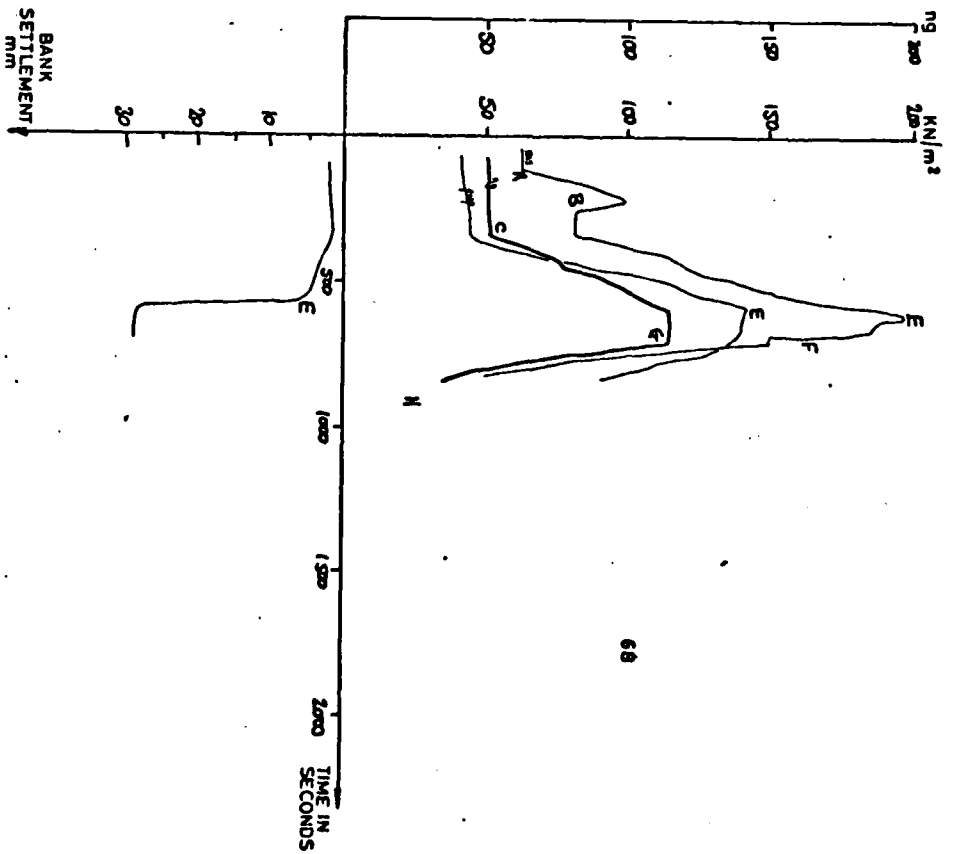
4.4.5 Two Dimensional Flood Embankment Test 2DF6

55mm Marsh

Red model failed prematurely by an increase in self weight with no uplift and Blue model failed by an increase of self weight in the uplifted condition.

Events in Test

A   Blue model uplifted at 50g to U = 1.76

B   Air lock in Blue model plumbing clears and water level settles

C   Centrifuge speed increased

D   Red model fails at 106g with no uplift, U = 1.0

E   Blue model fails at 113g. Some leakage evident in uplift system

F   Uplift reduced to Blue model

GH   Machine stopped

Notes

1. Two distinct types of failure observed for the two loadings.

2. Model behaviour differs slightly during consolidation.

3. The two failures are shown in Plates 4.7 and 4.8 where it is clearly seen that no deformation occurs beyond the point where the circular slip plane intersects the ground surface in Red model, but in Blue model the bank has collapsed without a slip plane intersecting the surface.
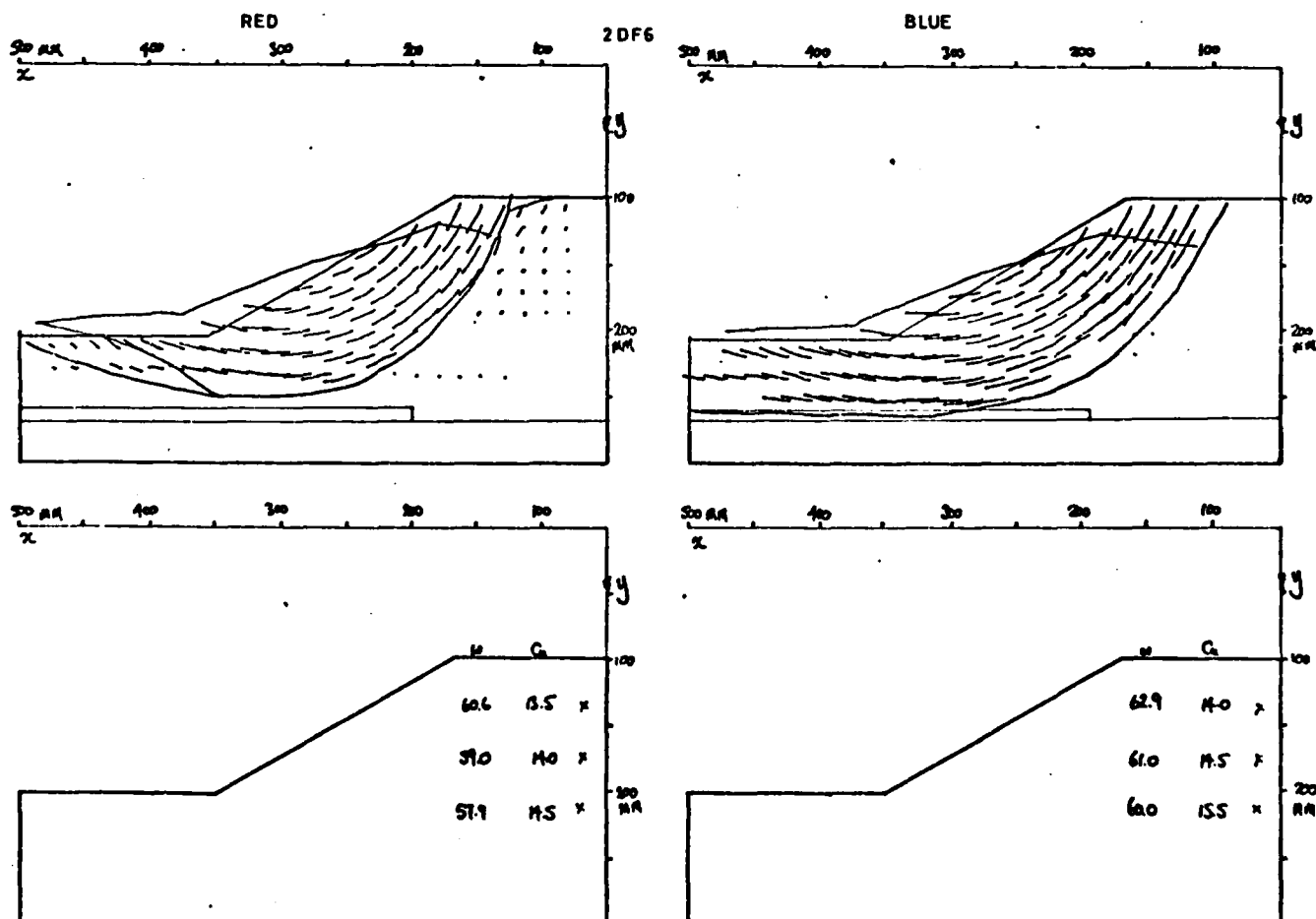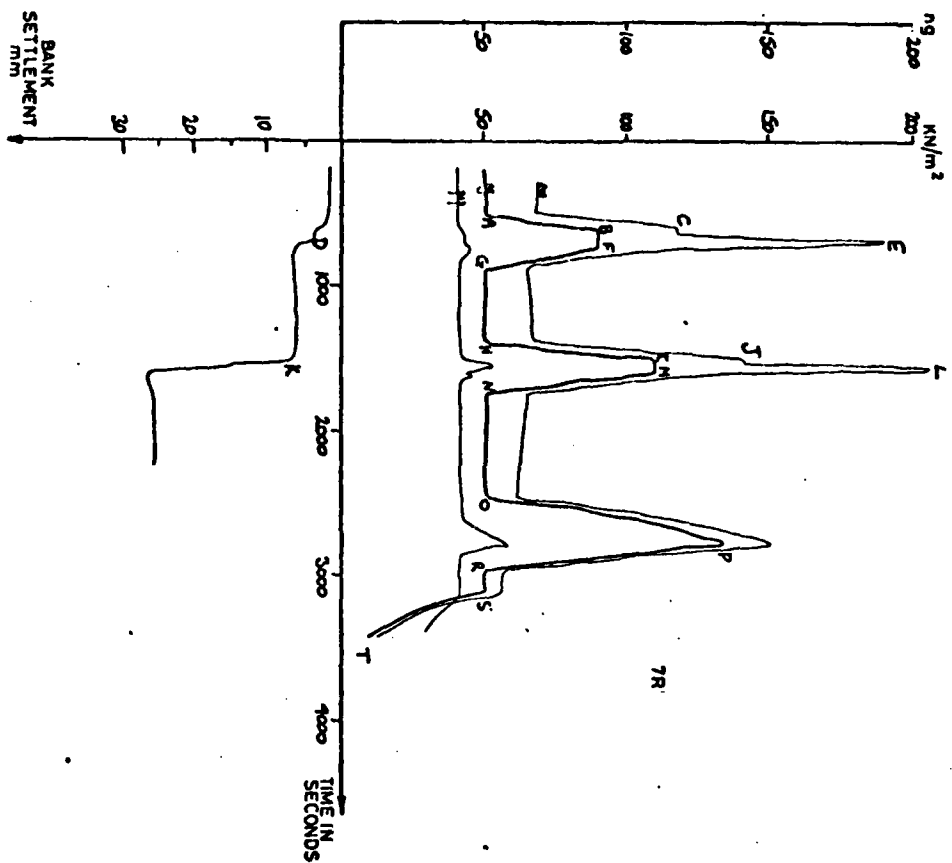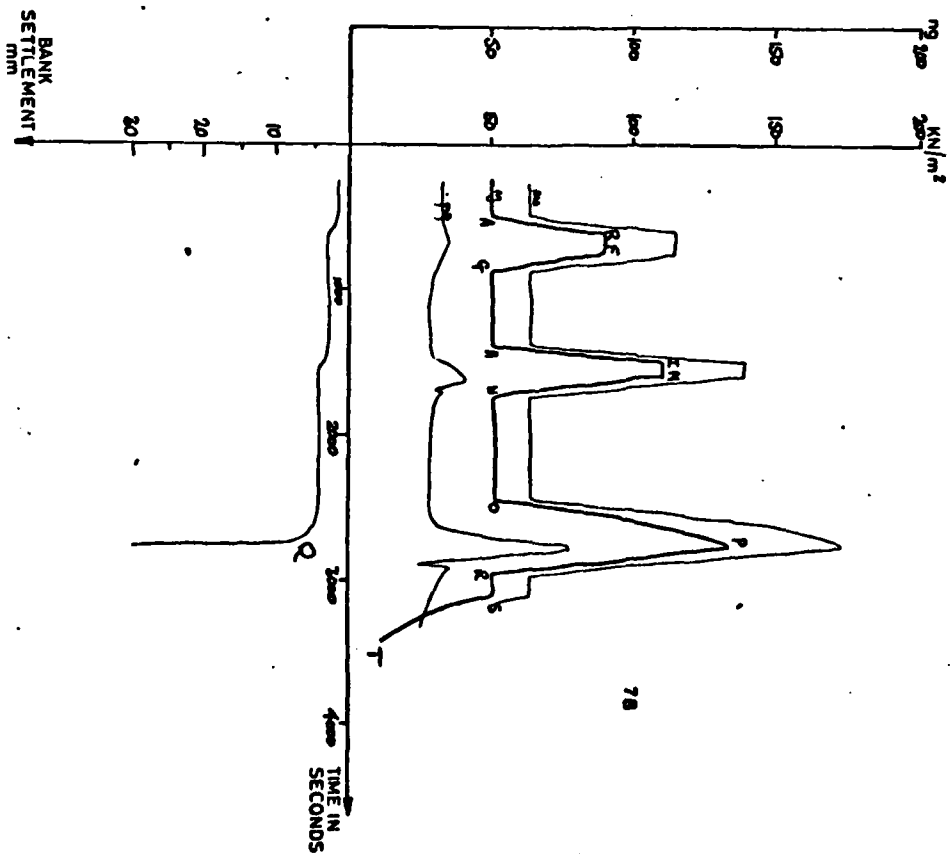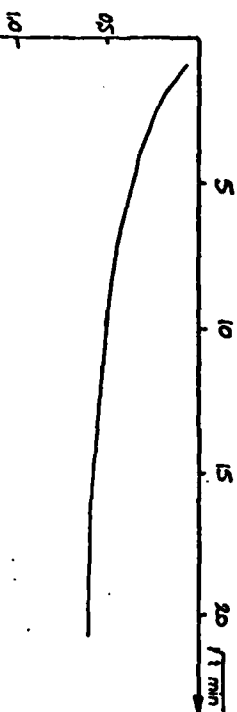

FIG. 4·16.

BANK SETTLEMENT IN CONSOLⁿ mm

BANK SETTLEMENT mm

mg/m²

KN/m²

TIME IN SECONDS

f t min

BANK SETTLEMENT IN CONSOLⁿ mm

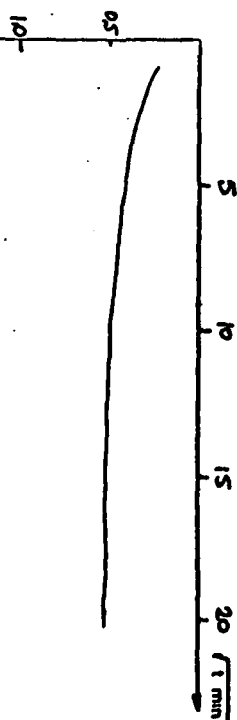BANK SETTLEMENT mm

mg/m²

KN/m²

TIME IN SECONDS

f t min
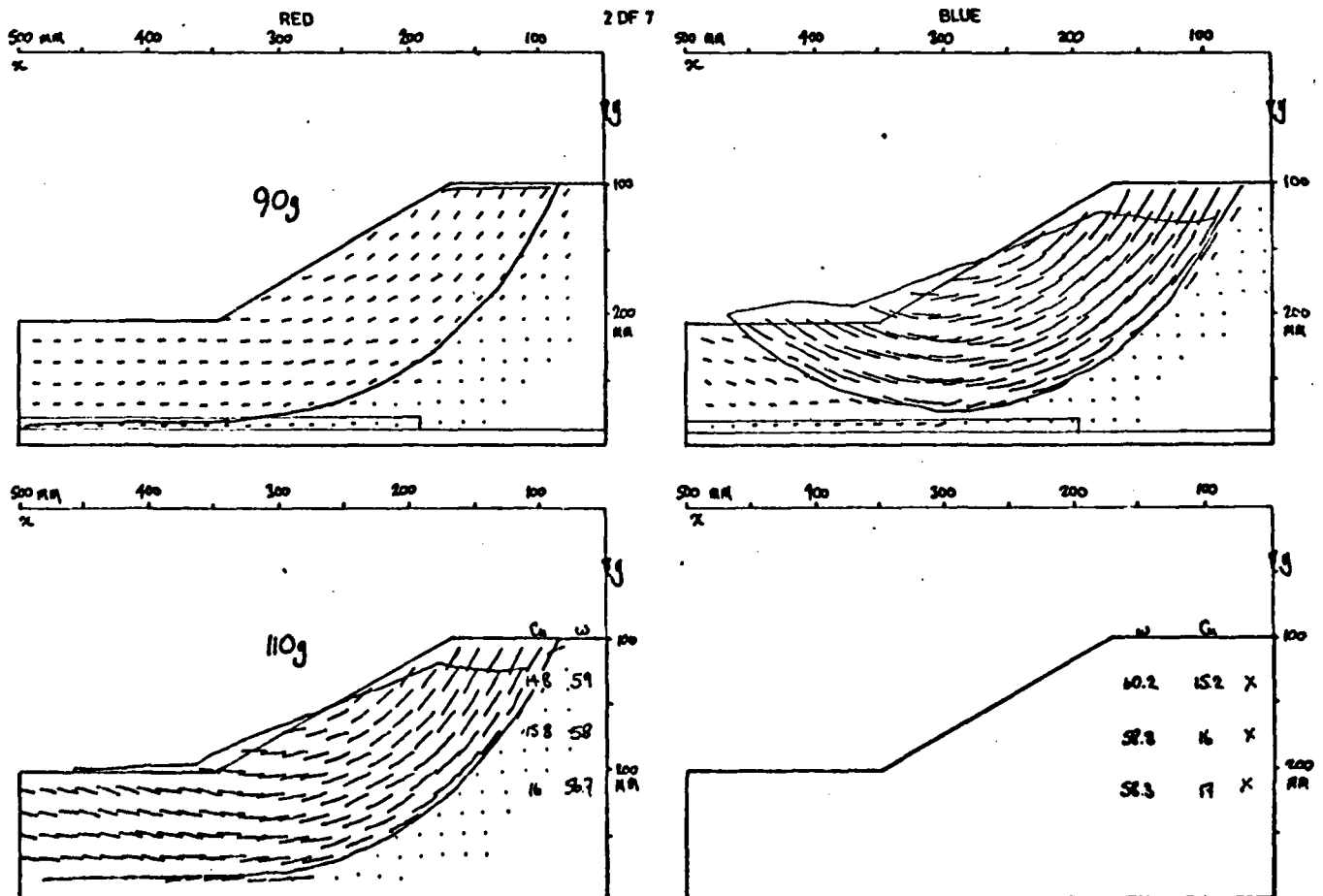
FIG 4.19
/17

75mm Marsh

The test involved three speed increases from 50g. Red model was uplifted at 90g and again at 110g causing limited failure at 90g and total failure at 110g. Blue model was caused to fail by self weight loading only at 130g.

Events in Test

AB   Machine speed decreased from 50-90g

C   Red model uplifted

D   Limited settlement at $U = 1.79$

E   Red uplift reduced

FGHI   Machine speed reduced to 50g and again increased to 110g

J   Red model uplifted

K   Red model fails at $U = 1.79$

L   Uplift reduced

MNOQ   Machine speed decreased to 50g and again increased to 130g

Q   Blue model fails at 130g, $U = 0.75$

PR   Machine speed decreased to 50g

ST   Machine stopped.

Notes

1. Models were stronger than was planned since as in Test 2DF4 an error was made whereby the water level was 20 mm below the level of the marsh.

2. Failure modes distinctive of self weight and interactive failures.

3. No heave observed during consolidation.

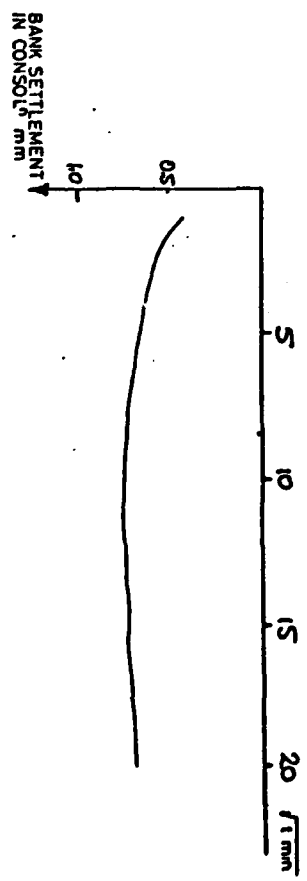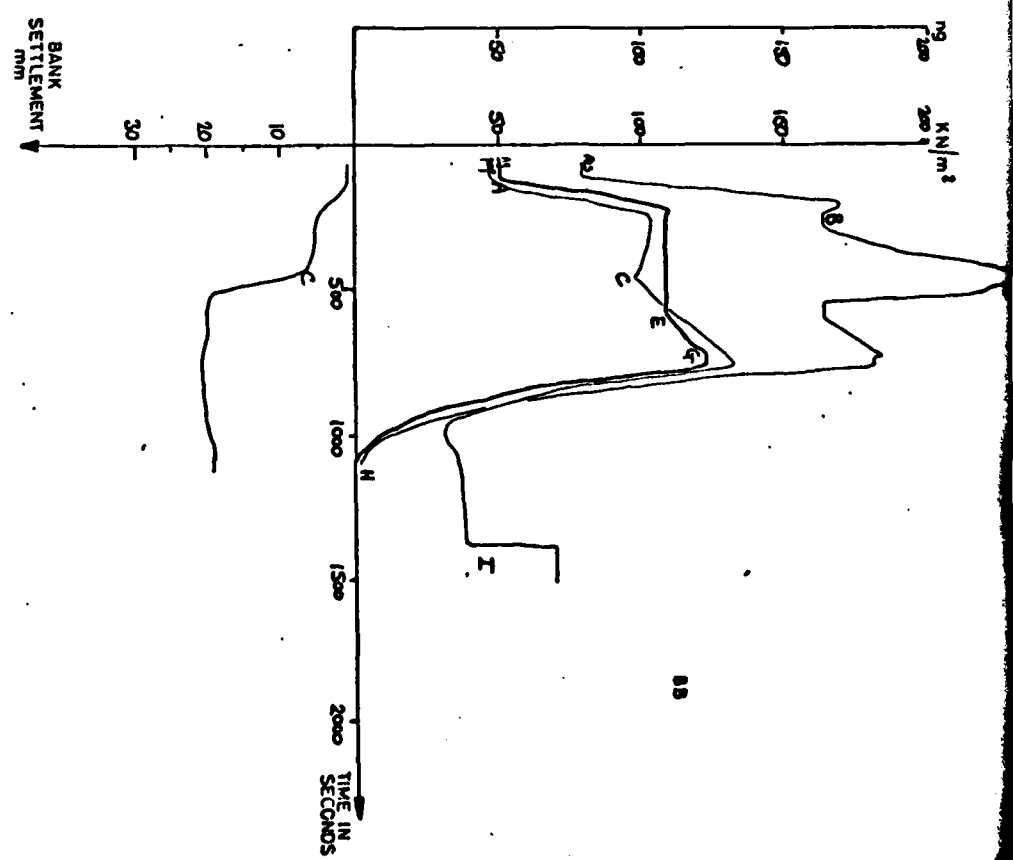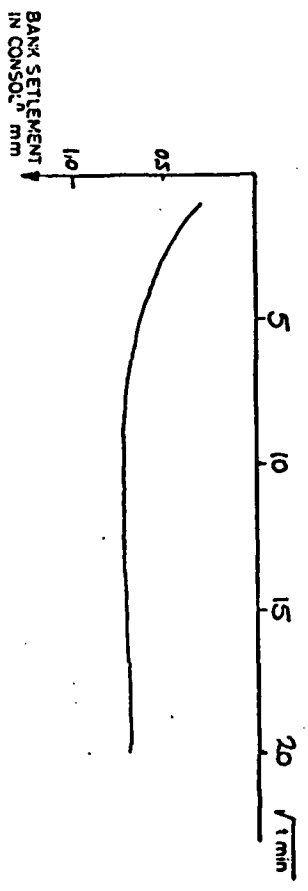4. The two models are shown in Plate 4.9. Note 3 for test 2DF6 applies.
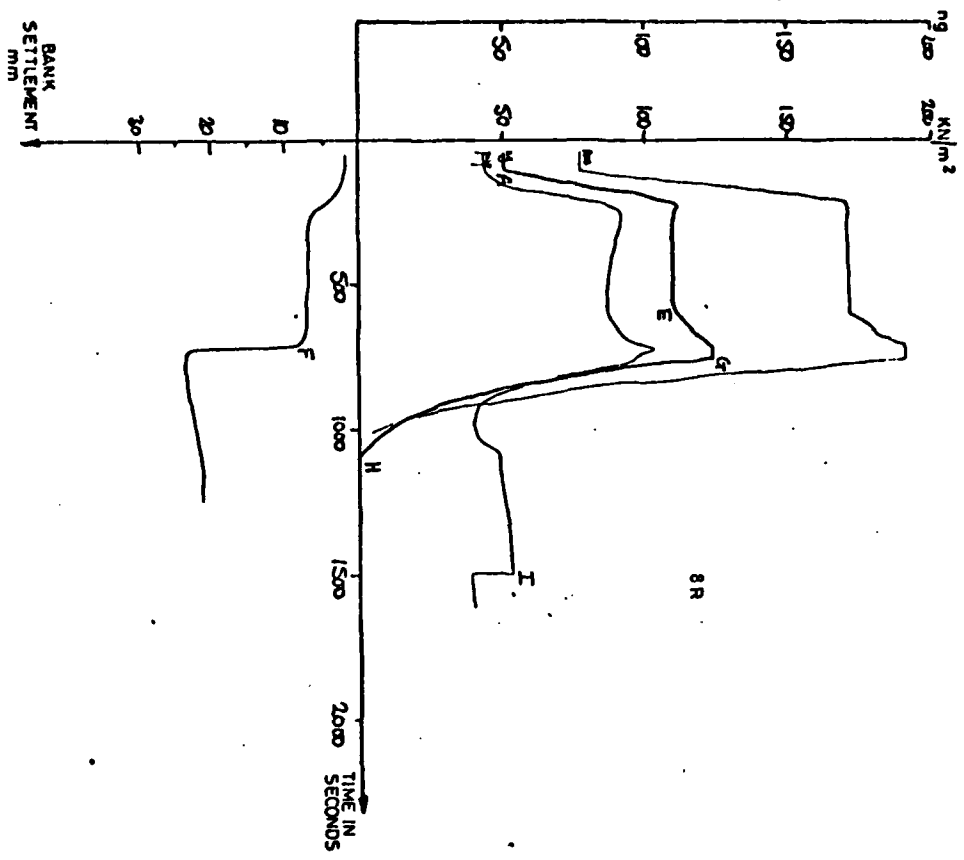

FIG 4.19

FIG 4·19

4.4.7 Two Dimensional Flood Embankment Test 2DF8

95mm Marsh

Red model failed by an increase in self weight alone. Blue model failed at 110g by an increase in uplift.

Events in Test

A   Machine accelerated from 50-110g

B   Blue model uplifted

C   Blue model fails at U = 1.83

D   Uplift reduced

E   Increase centrifuge speed

F   Red model fails at 121g, U = 1.0

GH   Machine stopped

I   Transducers dug out of clay

Notes

1. Stroboscope failure prevented the use of photographs.

2. Very little apparent difference in the shape of failure involved with this deep model for uplift induced and self weight induced failures. In neither case did the failure surface rise to ground surface level at the toe of the slope.
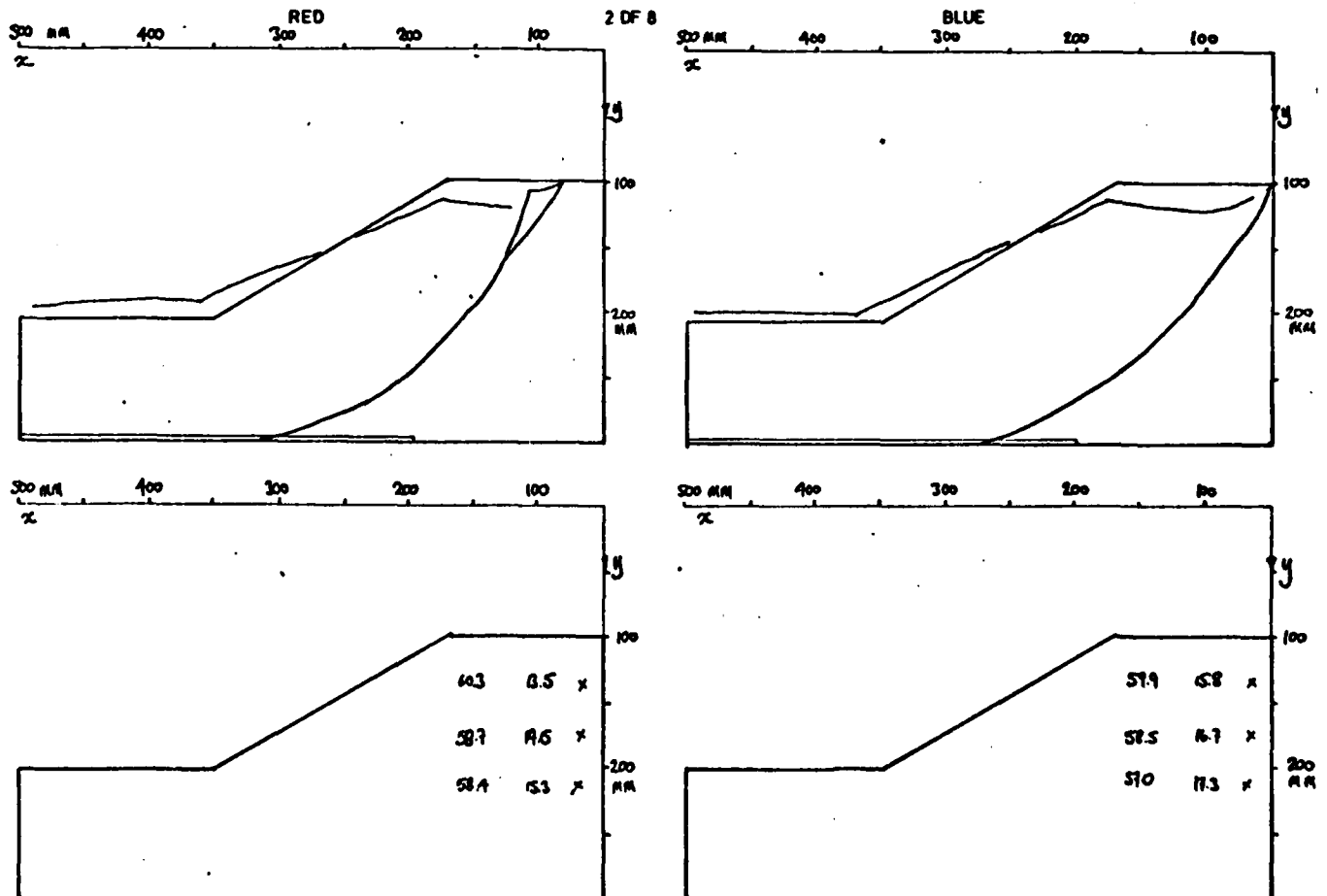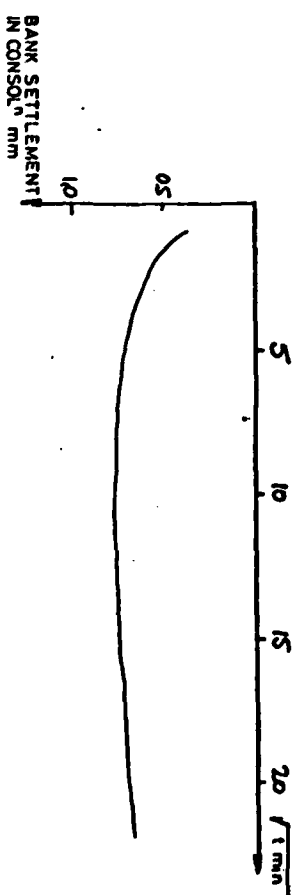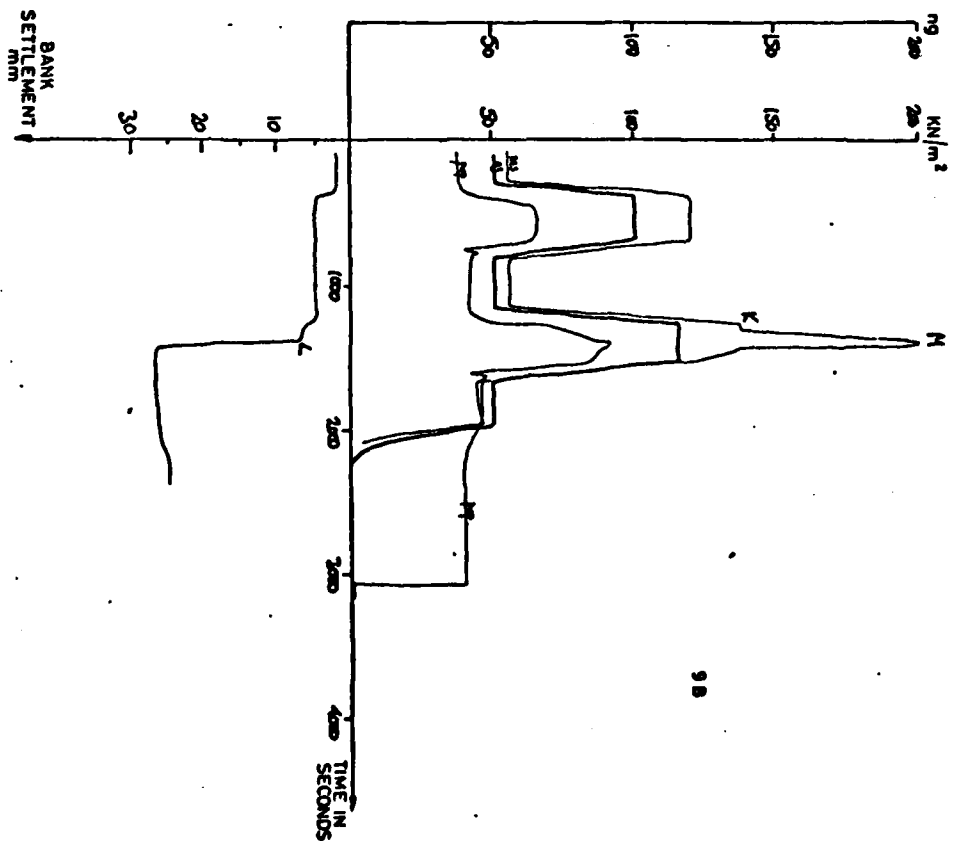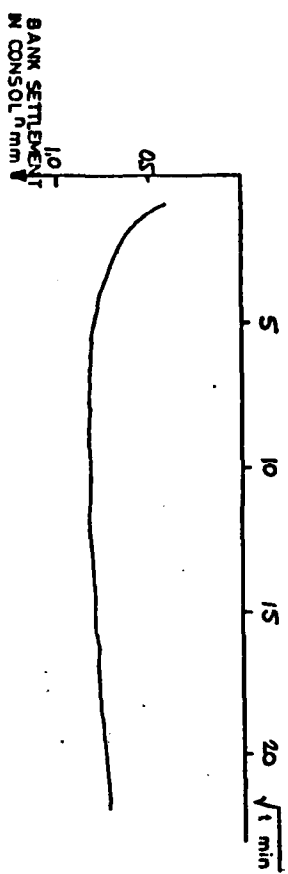

FIG. 4.20

BANK SETTLEMENT mm

ng KN/m²

TIME IN SECONDS
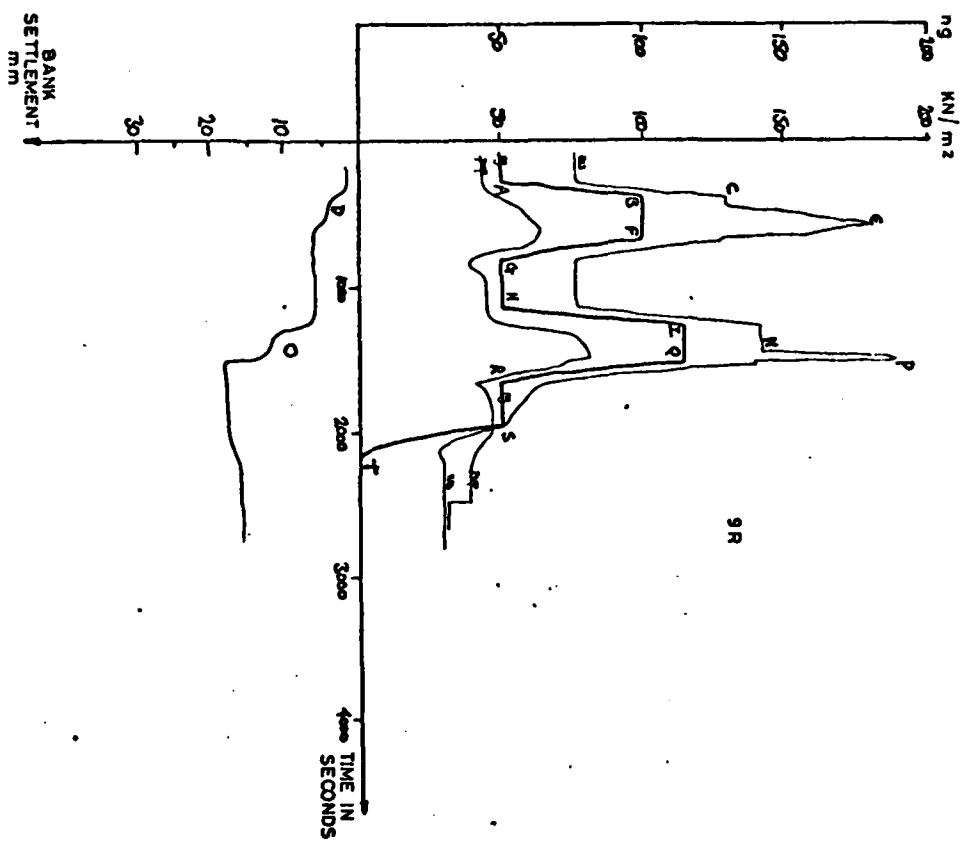
BANK SETTLEMENT IN CONSOLⁿ mm

9R

9B

FIG 4.21

4.4.8   Two Dimensional Flood Embankment Test 2DF9

95mm Marsh

Red model suffered some settlement due to uplift at 100g and failed due to an increase in uplift at 115g. Blue model failed by an increase in uplift at 115g.

Events in Test

AB   Machine speed increased 50g-100g

C   Red model uplifted

D   Some settlement at U = 1.53 - 1.56

E   Red model uplift reduced

FGHI   Machine speed reduced to 50g and again increased to 115g

K   Blue model uplifted

L   Blue model fails at U = 1.48 - 1.54

M   Blue uplift reduced

N   Red model uplifted

O   Red model fails at U = 1.44

P   Red uplift reduced

QRST   Machine speed reduced to 50g and stopped

Notes

1. The models exhibited similar modes of failure.

2. Model behaviour during consolidation was also similar.
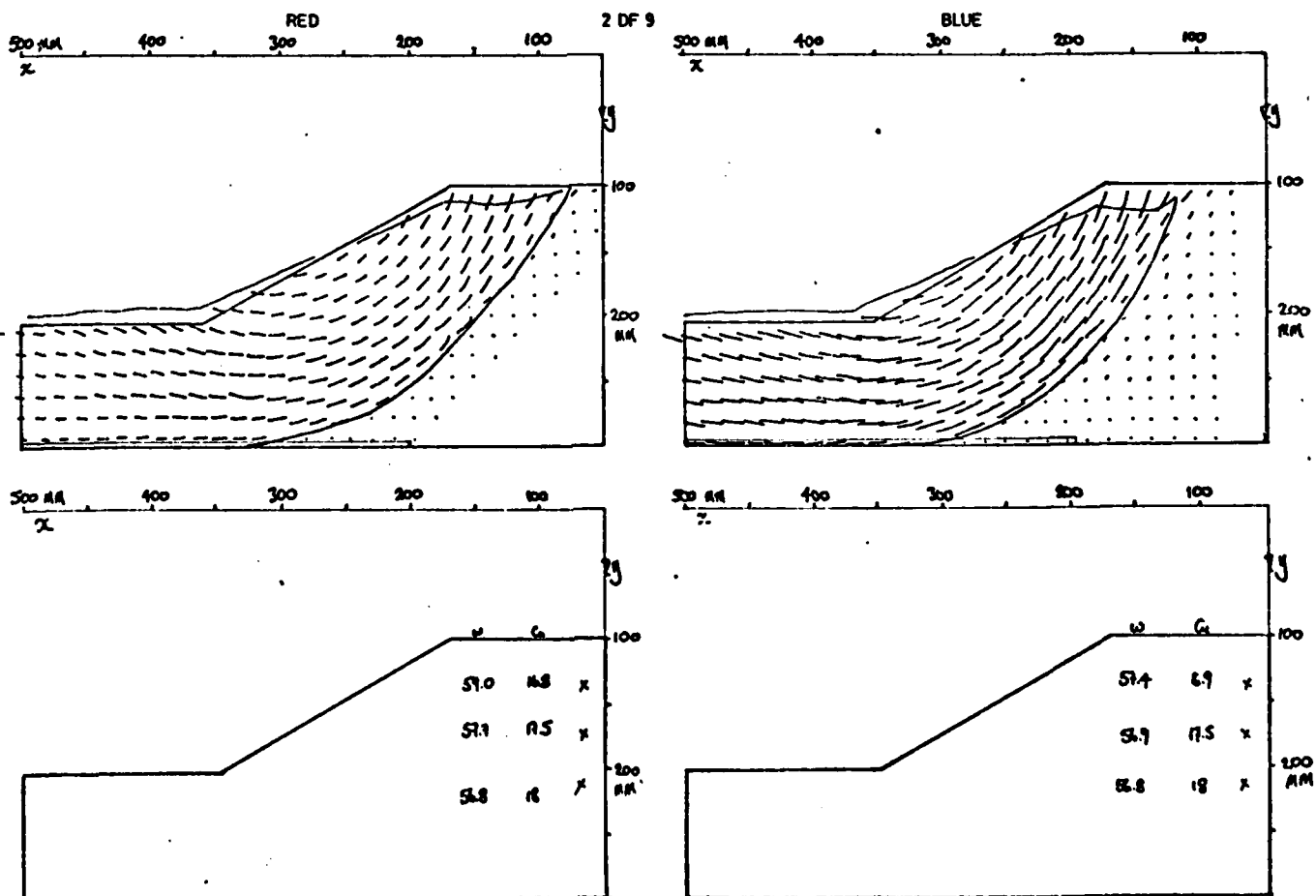
FIG. 4·22
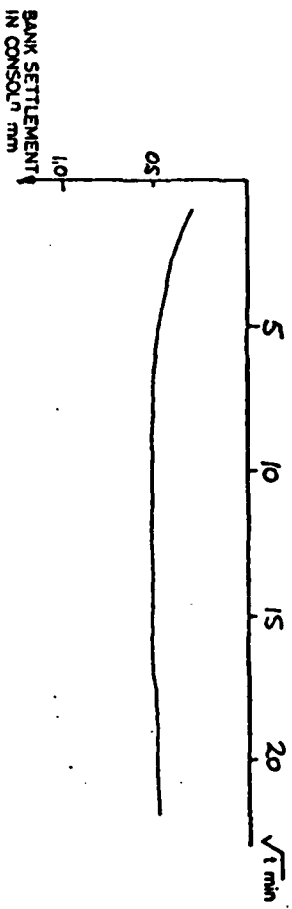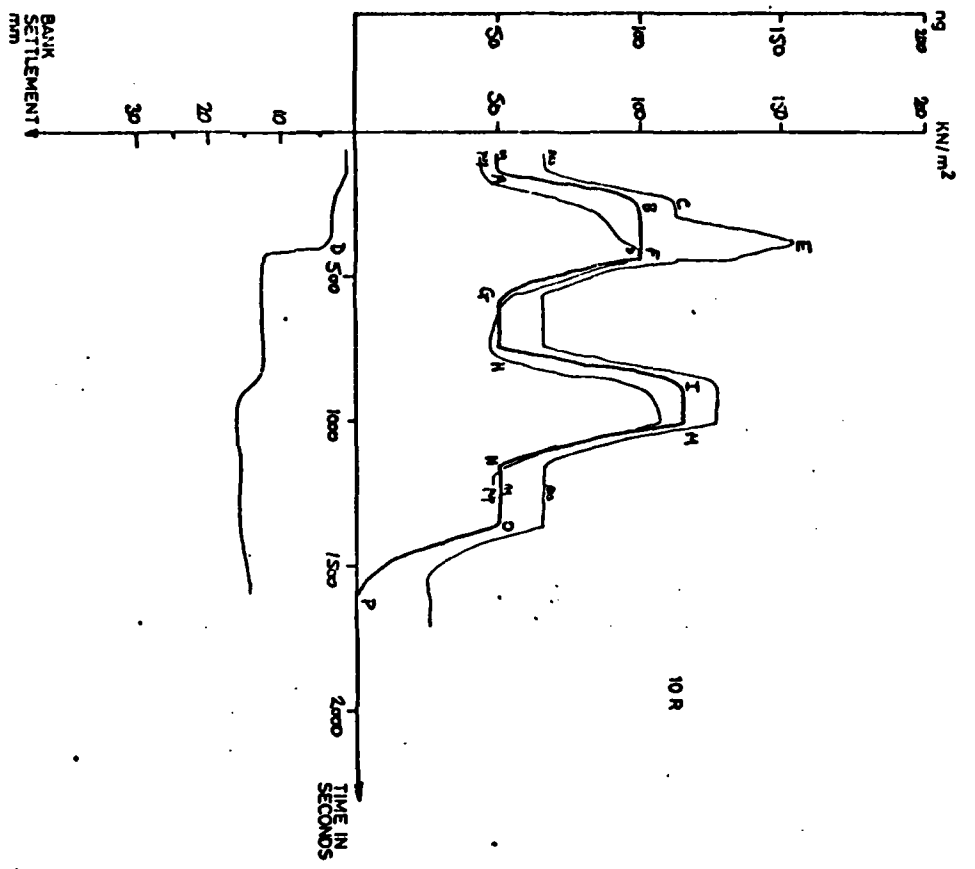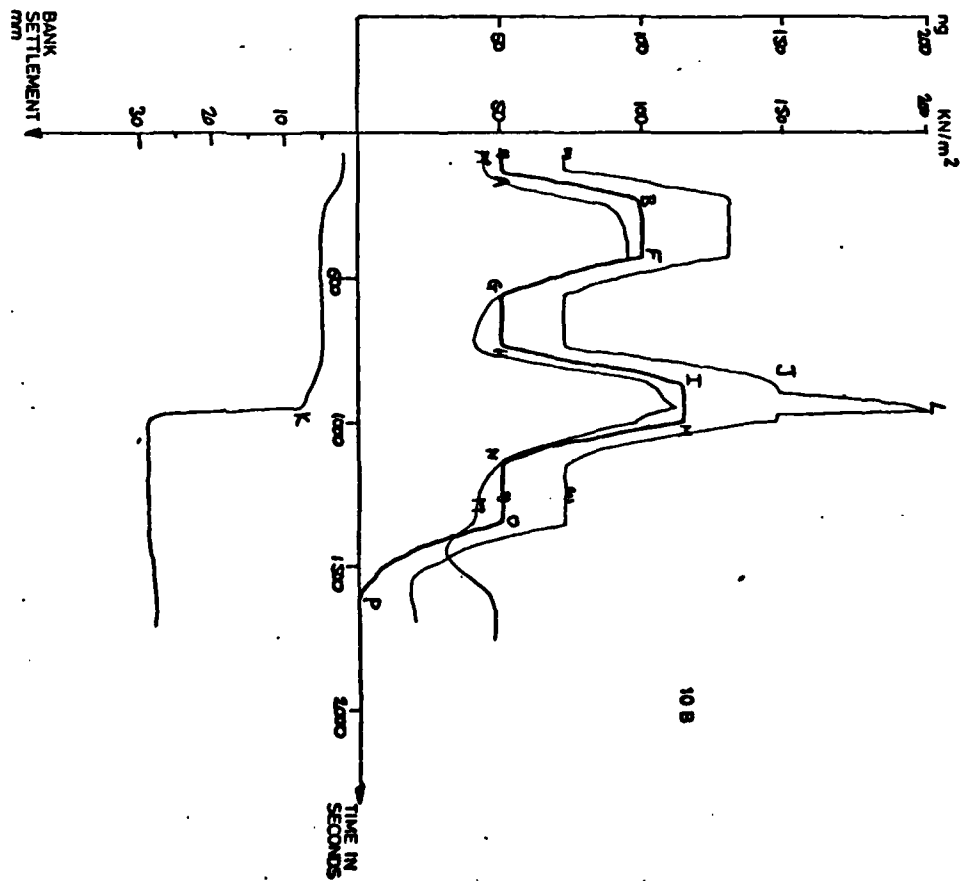
FIG. 4·23

4.4.9   Two Dimensional Flood Embankment Test 2DF10

75mm Marsh

Red model failed due to an increase in uplift at 100g. Blue model failed by an increase in uplift at 115g.

Events in Test

AB   Machine speed increased 50g-100g

C   Red model uplifted

D   Red model fails at U = 1.46 - 1.58

E   Red uplift reduced

FGHI Machine speed reduced to 50g and again increased to 115g

J   Blue model uplifted

K   Blue model fails at U = 1.48 - 1.54

L   Blue uplift reduced

MNOP Machine speed reduced to 50g and stopped.

Notes

1. The modes of failure were similar.

2. Blue model exhibited greater settlement in consolidation than Red model.

3. In this test thirty moisture content determinations were made in place of the three vane strength measurements.
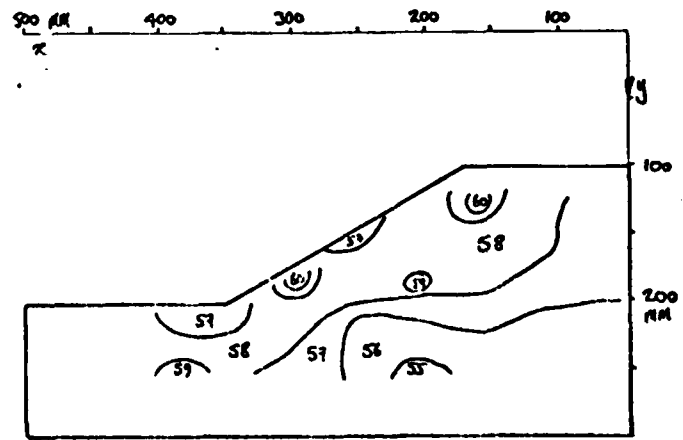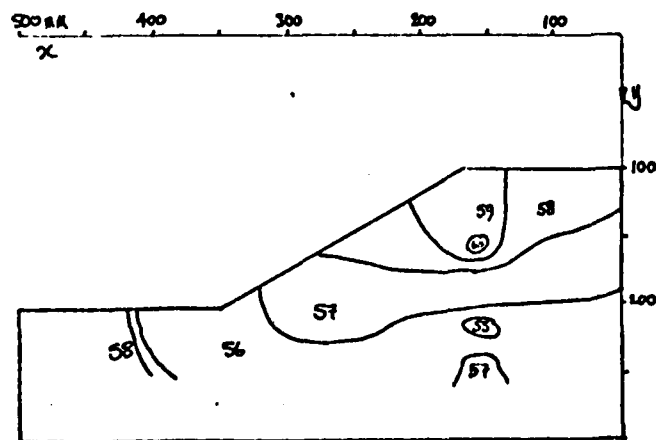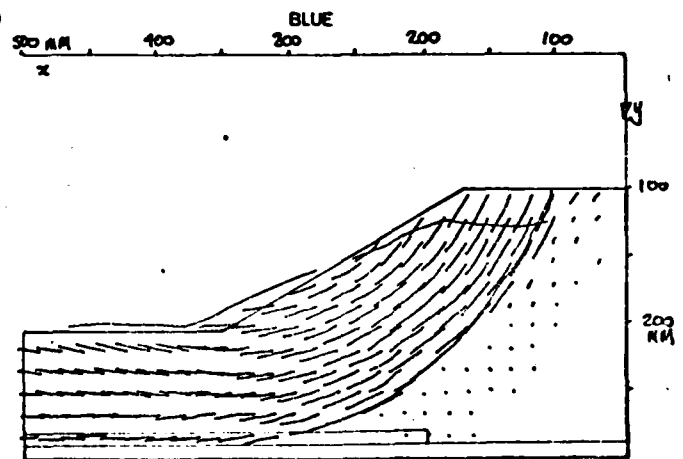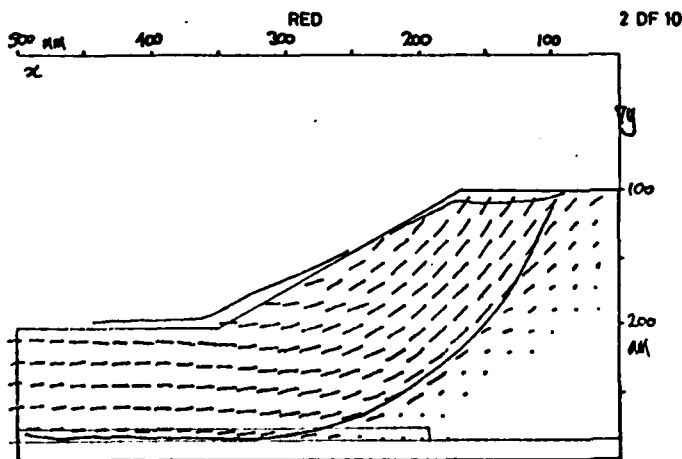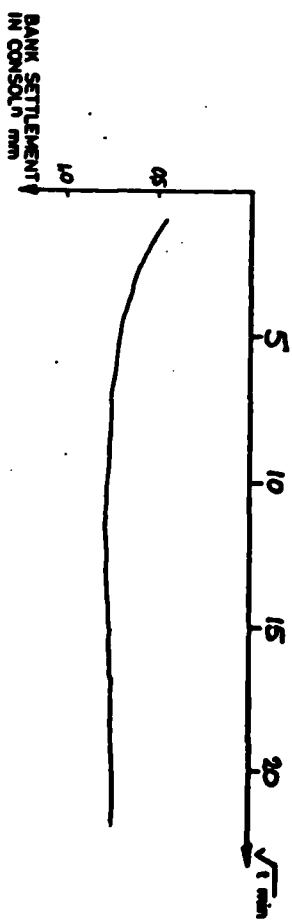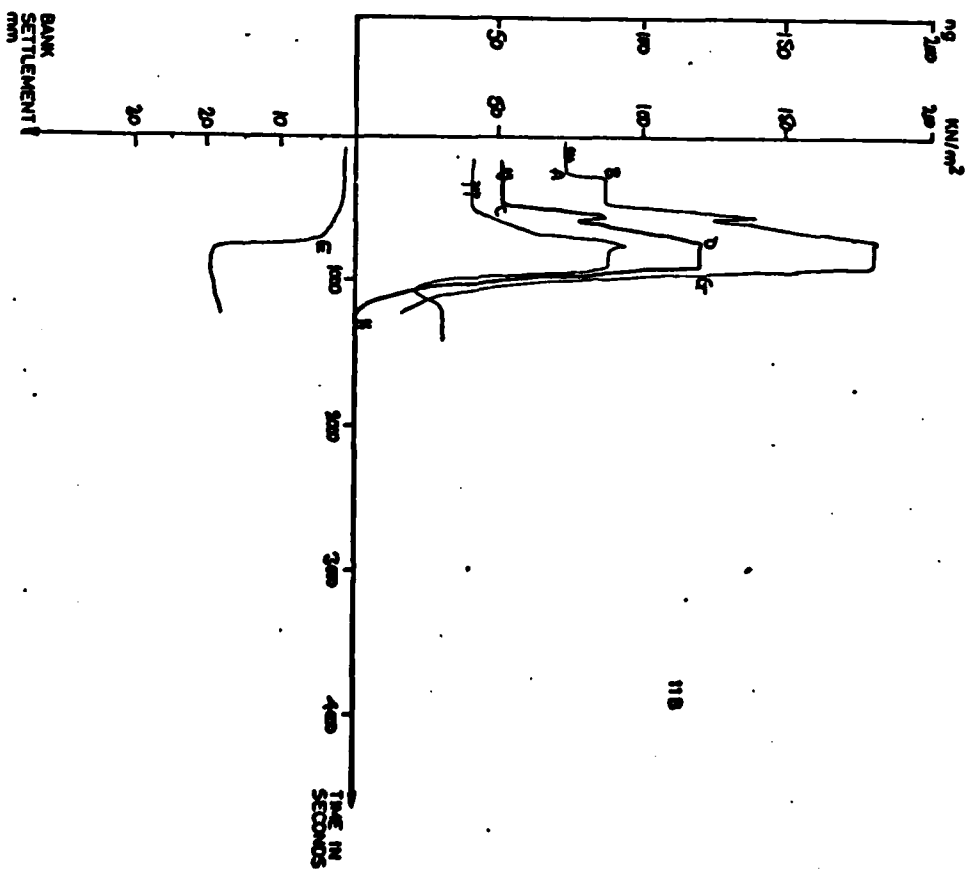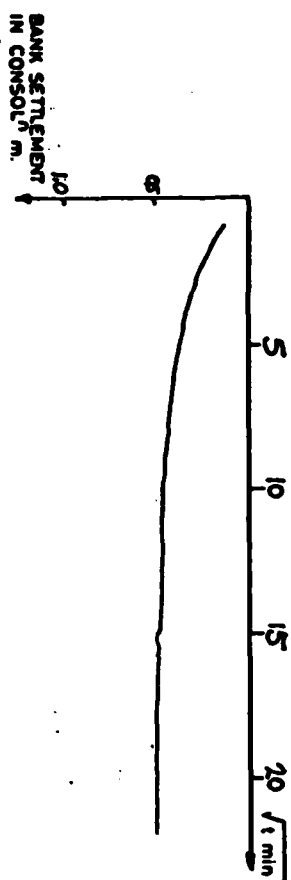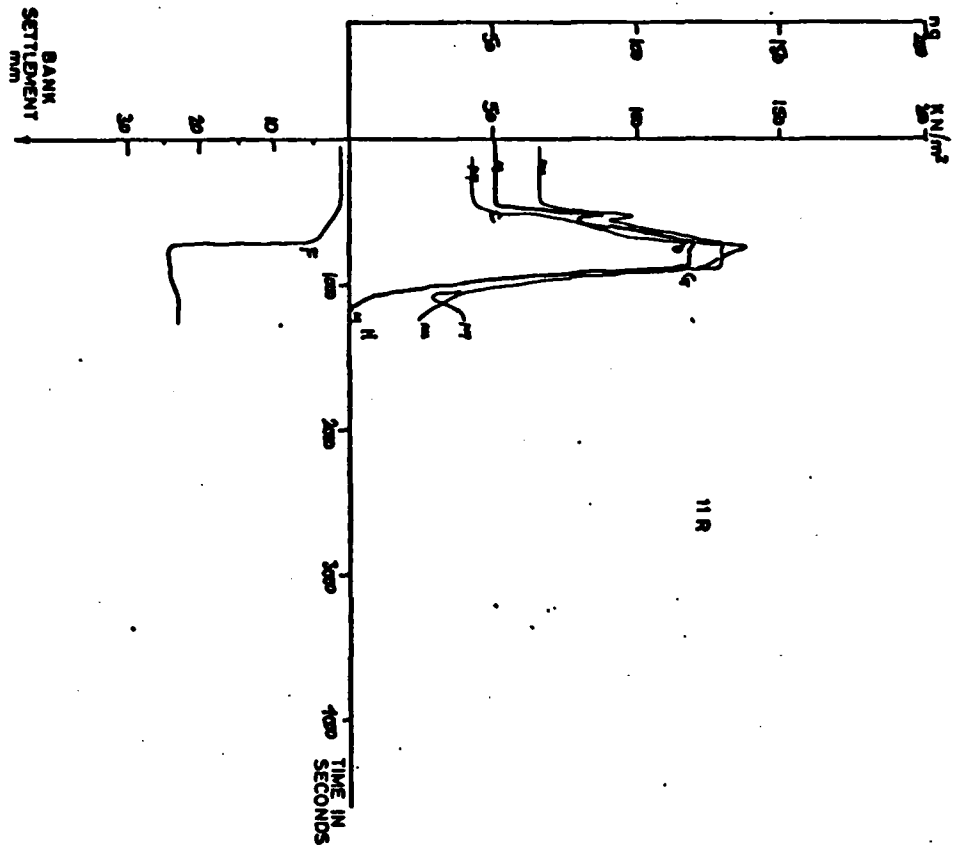
FIG 4·25

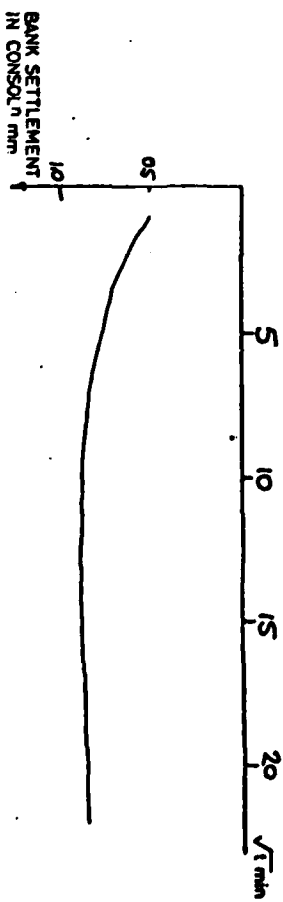### 4.4.10   Two Dimensional Flood Embankment Test 2DF11

75mm Marsh

Blue model was uplifted at 50g and the two models were accelerated to failure. Failure occurred at approximately the same moment.

Events in the Test

AB   Blue model uplifted to U = 1.41

CD   Machine speed increased to 120g

E   Blue model fails at 118g, U = 1.41

F   Red model fails at 119g, U = 1.0

GH   Machine stopped

Notes

1.   The slip surfaces were characteristic of self weight (Red) and uplift interaction (Blue) induced modes of failure.

2.   The slice of Red model that has been allowed to dry is shown in Plate 4.3. The slip surface is clearly visible.

FIG. 4.29

BANK
SETTLEMENT
mm

mg
250
200
150
100
50

KN/m²
250
200
150
100
50

10
20
30

BANK SETTLEMENT
IN CONSOLD mm

10
45

5
10
15
20 √ t min

12 R

TIME IN
SECONDS

500
1000
1500
2000

BANK
SETTLEMENT
mm

mg
250
200
150
100
50

KN/m²
200
150
100
50

10
20
30

BANK SETTLEMENT
IN CONSOLD mm

40
45

5
10
15
20 √ t min

12 B

TIME IN
SECONDS

500
1000
1500
2000
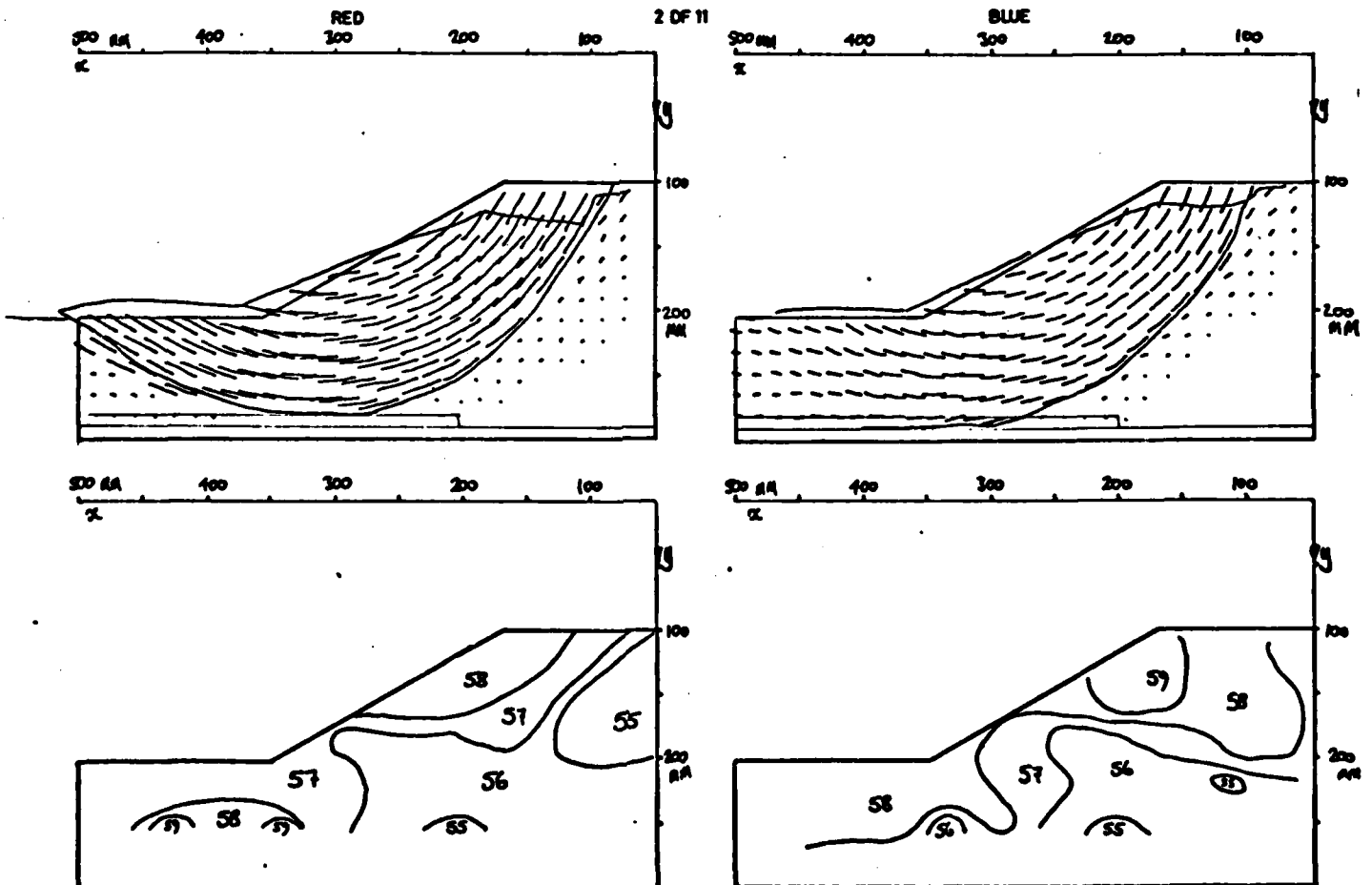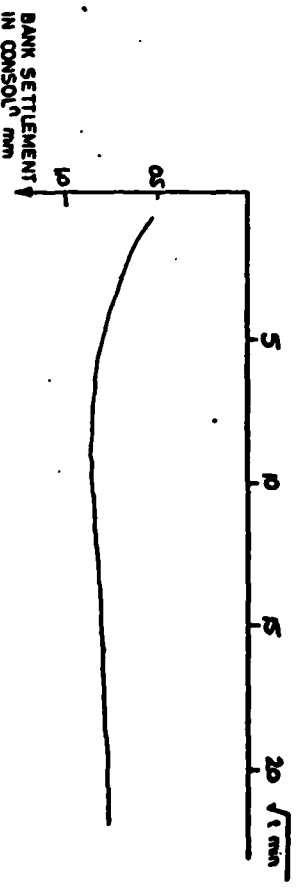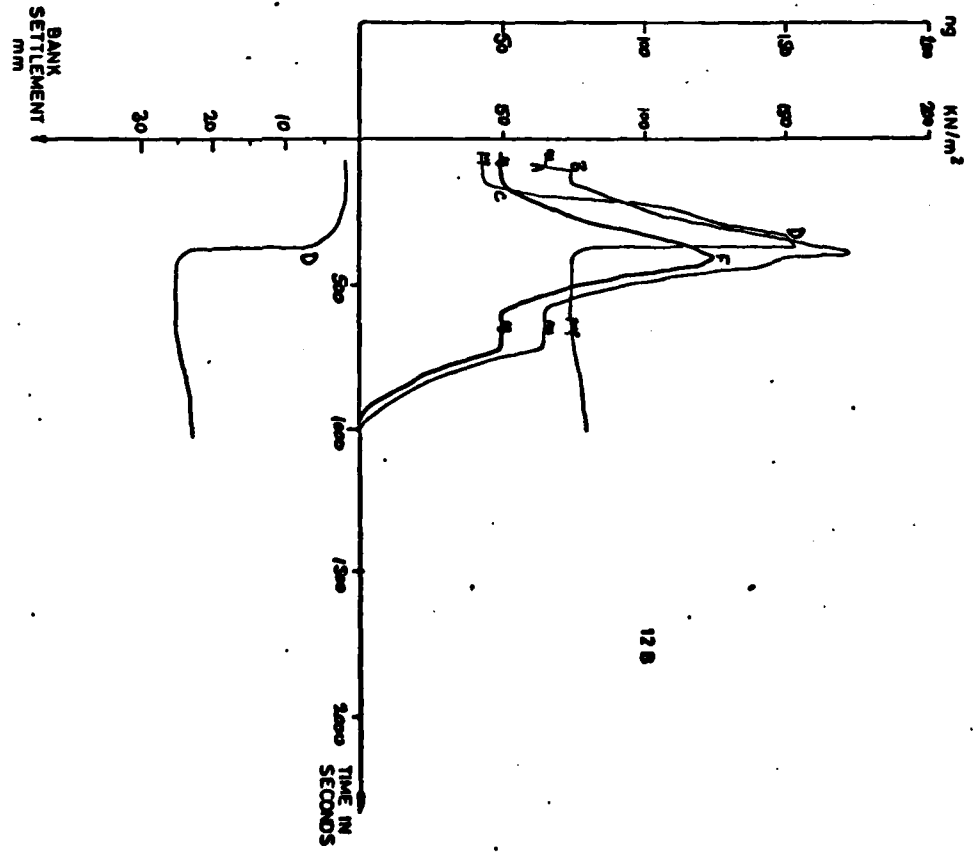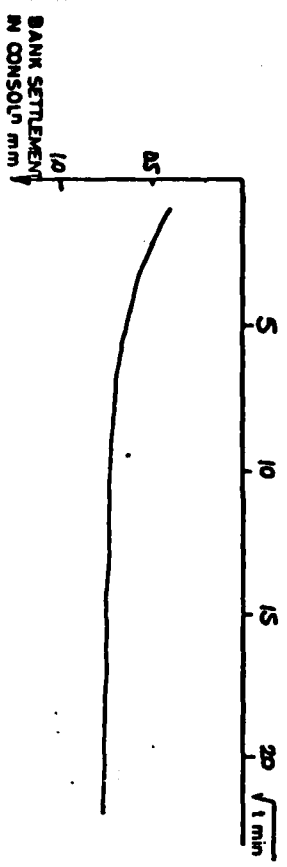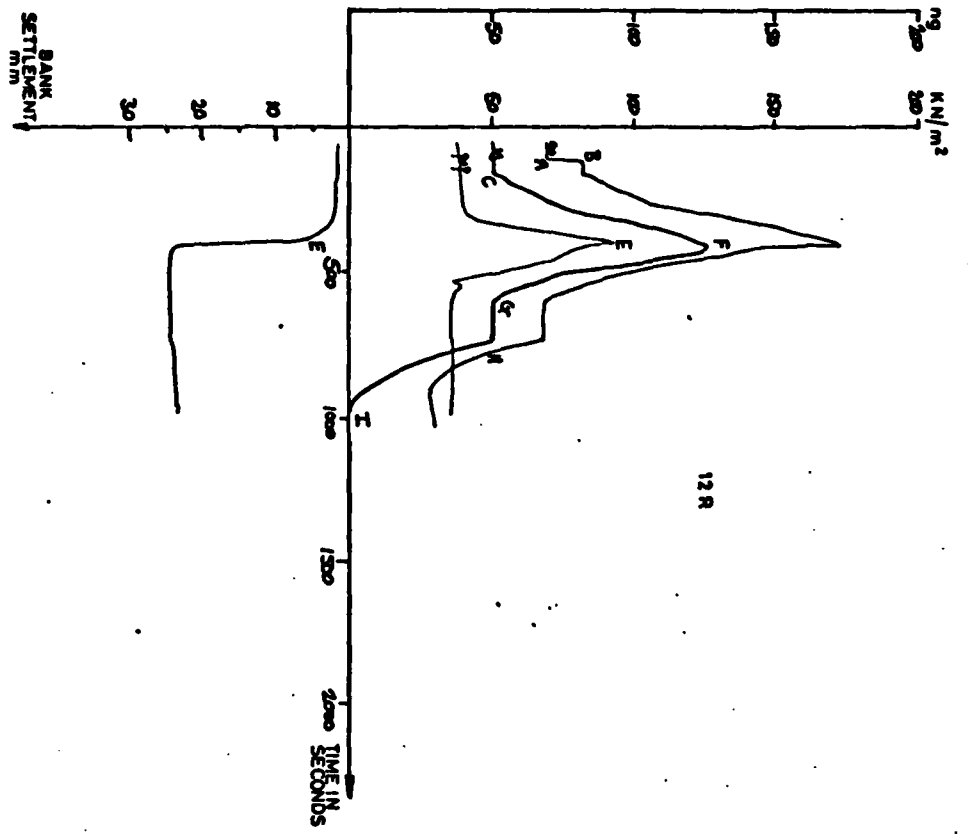
FIG. 4·27

4.4.11   Two Dimensional Flood Embankment Test 2DF12

75mm Marsh

Both models were uplifted at 50g and accelerated to failure.

Events in the Test

AB	Red model uplifted to U = 1.38
	Blue model uplifted to U = 1.26
CF	Machine speed increased to 125g
D	Blue model fails at 119g
E	Red model fails at 122g
FGHI	Machine speed reduced to 50g and stopped

Notes

1. Similar modes of failure were observed.

2. Blue model heaved after 1½ hours of consolidation.

3. The slice of Red model that has been allowed to dry is shown in Plate 4.4. The slip surface is clearly visible.
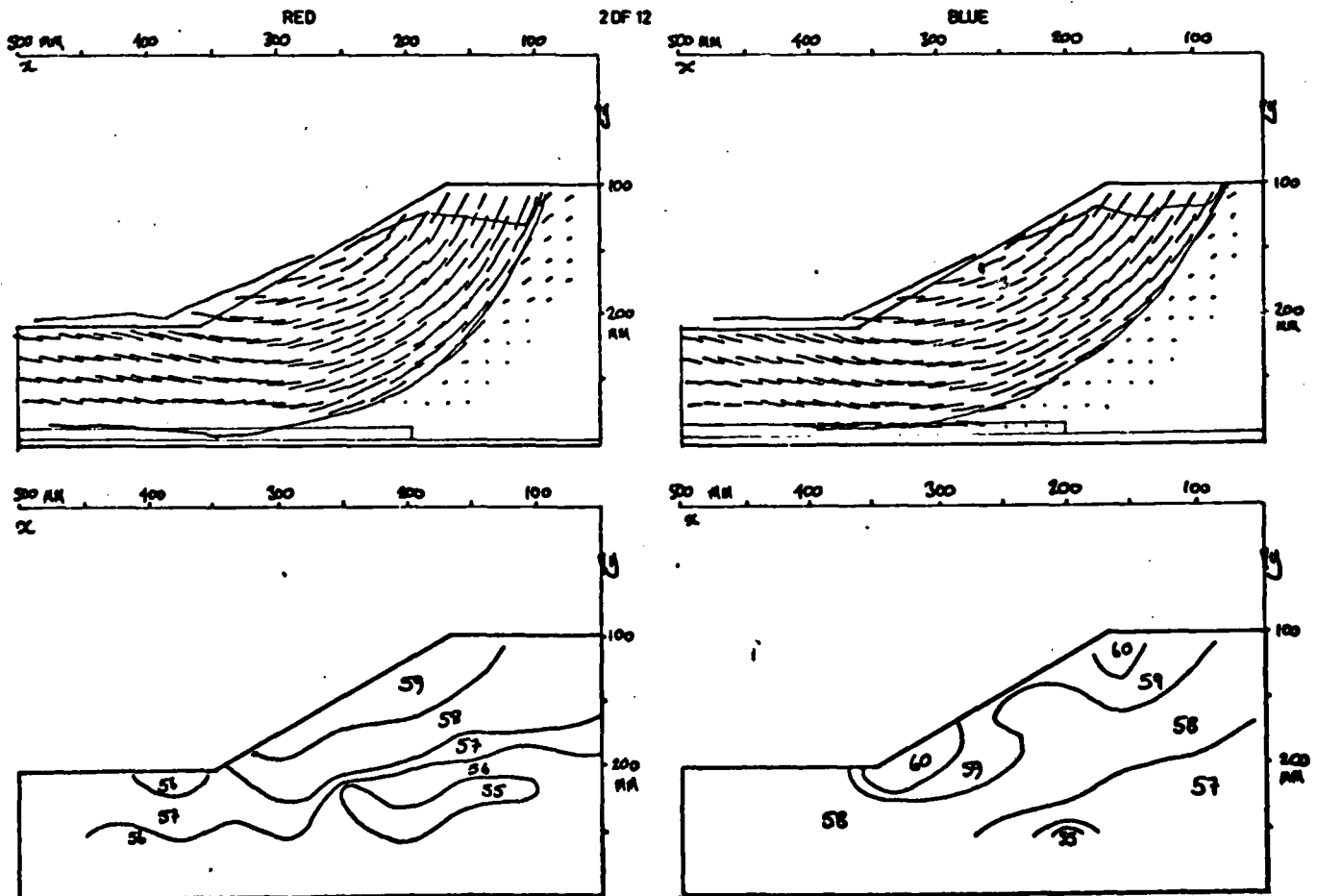
FIG. 4.28
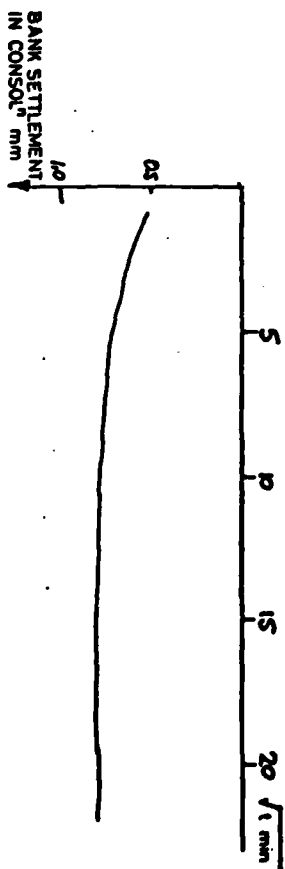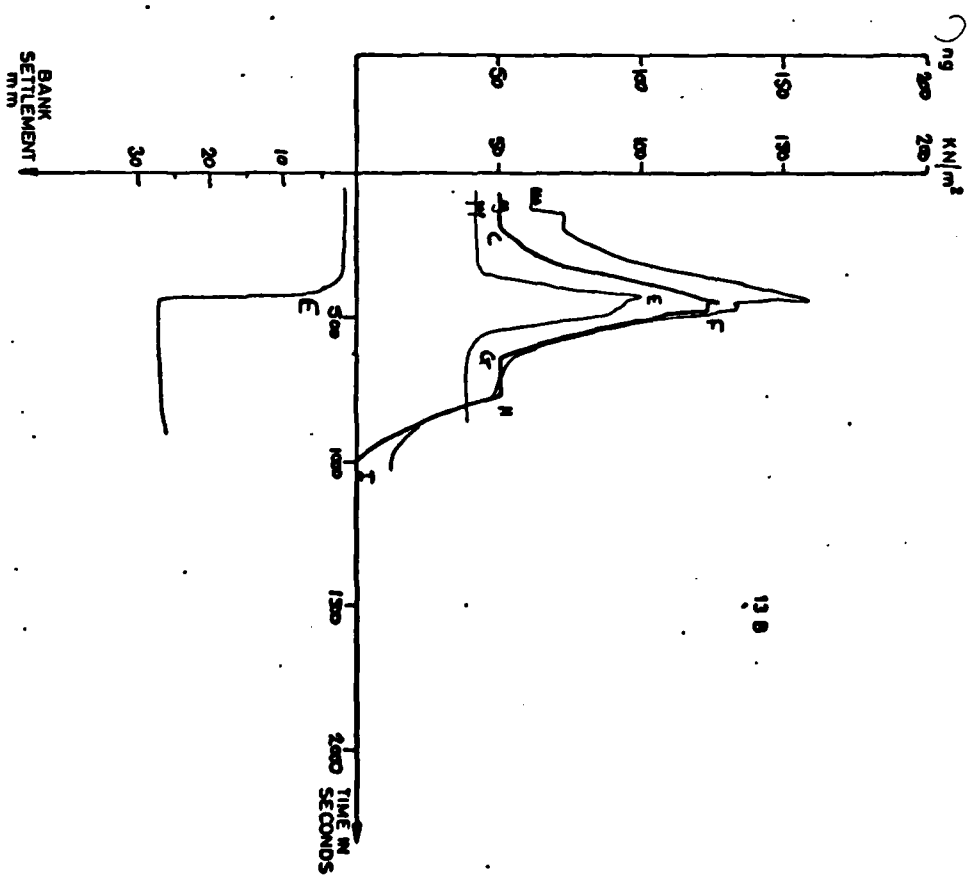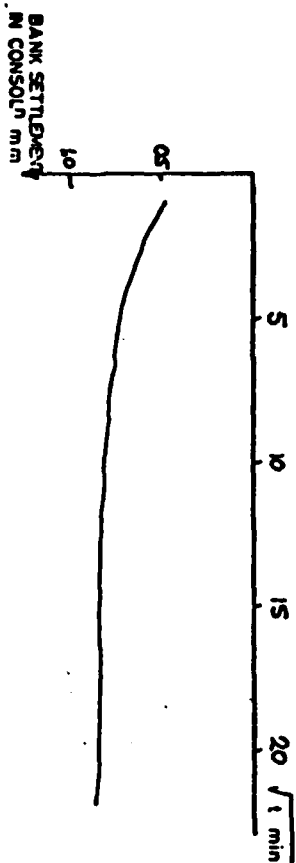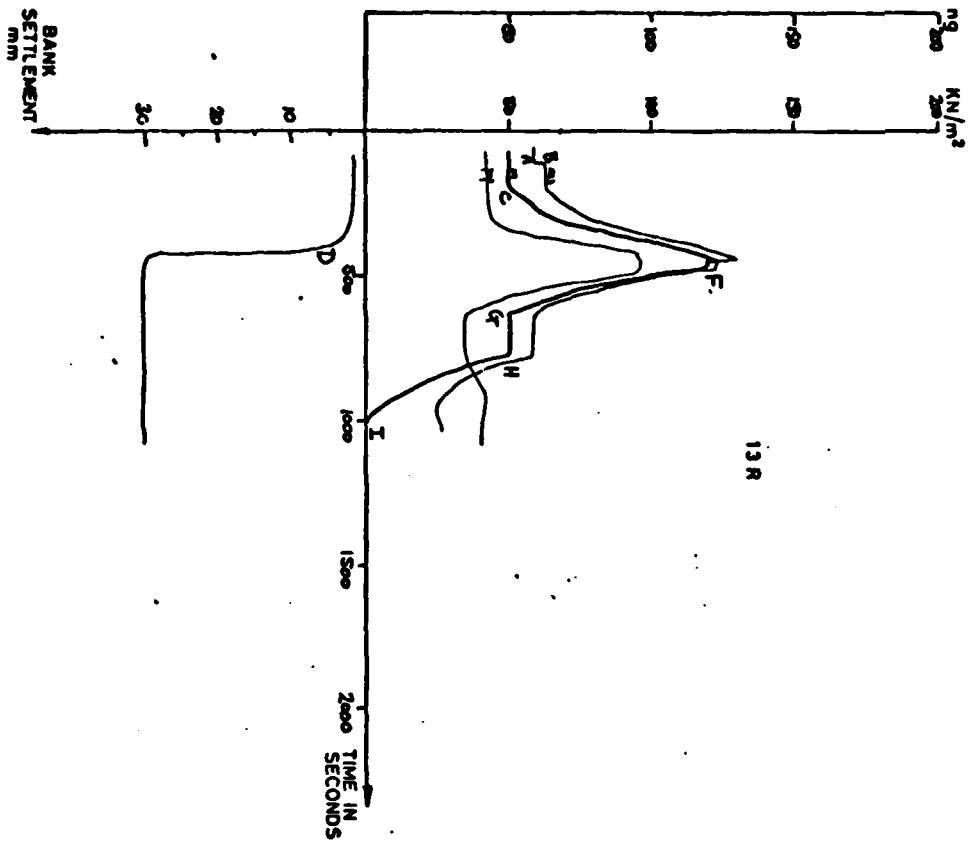
FIG. 4·29.

4.4.12   Two Dimensional Flood Embankment Test 2DF13

55mm Marsh

Both models were uplifted at 50g and accelerated to failure.

Events in the Test

AB   Red model uplifted to U = 1.13

        Blue model uplifted to U = 1.38

CF   Machine speed increased 50g-125g

D   Red model fails at 114g

E   Blue model fails at 117g

FGHI   Machine speed reduced to 50g and stopped

Notes

1. Red model failure shows a combination of circular and interaction modes.

2. Blue model shows no evidence of uplift having been effective. Probable blockage in water line.

FIG. 4.20

BANK
SETTLEMENT
mm

ng 200
KN/m² 300

150

100

50

30

20

10

BANK SETTLEMENT
IN CONSOL? mm

10

0.5

5   10   15   20   √t min

500   1000   1500   2000   TIME IN SECONDS

14 R

FIG. 4·31.

BANK
SETTLEMENT
mm

ng 200
KN/m² 300

150

100

50

30

20

10

BANK SETTLEMENT
IN CONSOL? mm

10

0.5

5   10   15   20   √t min

500   1000   1500   2000   TIME IN SECONDS

14 D
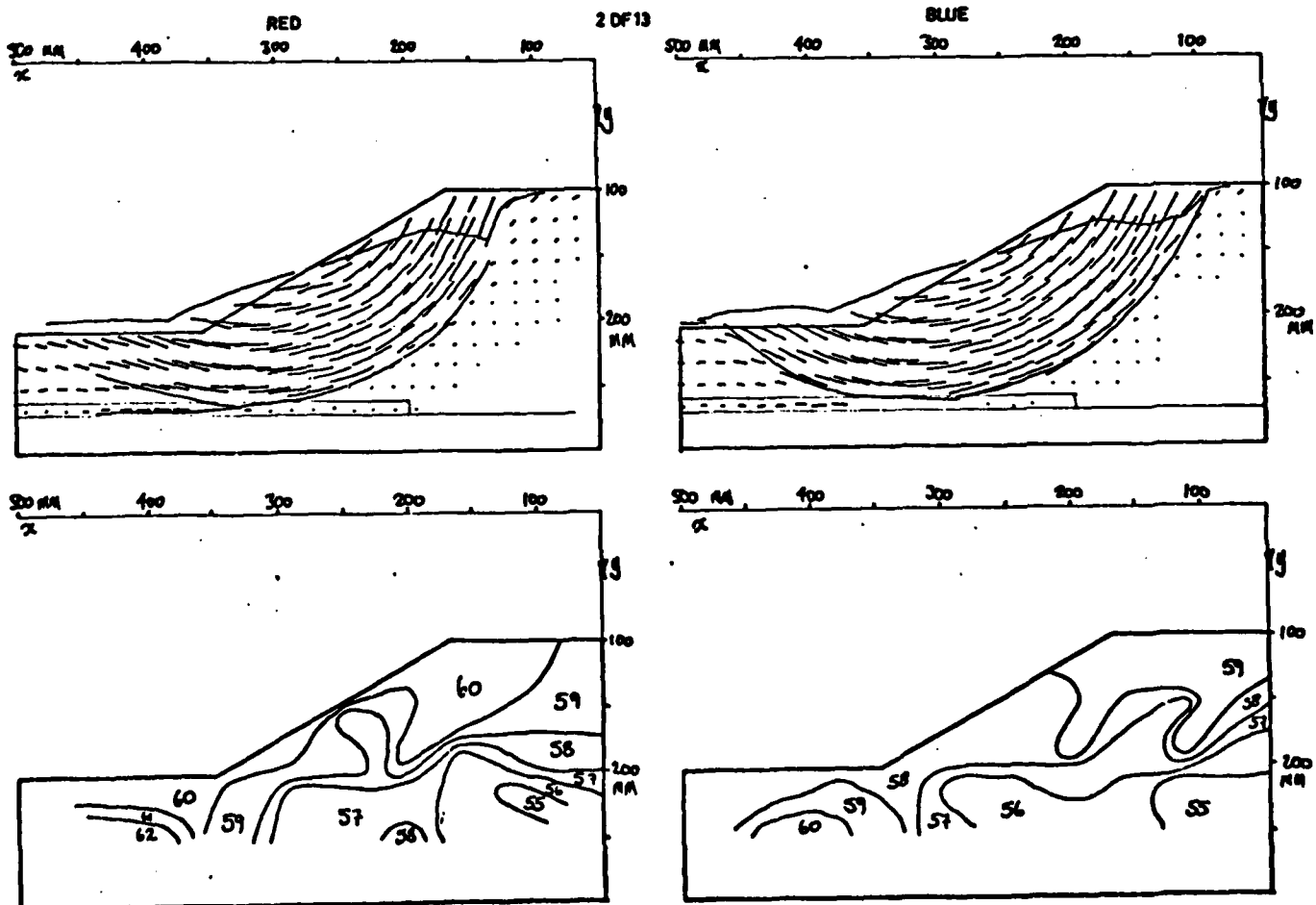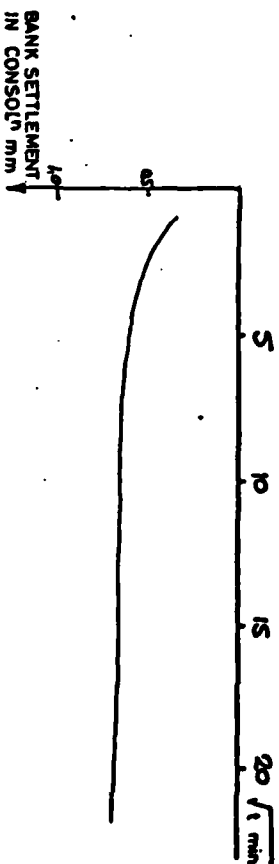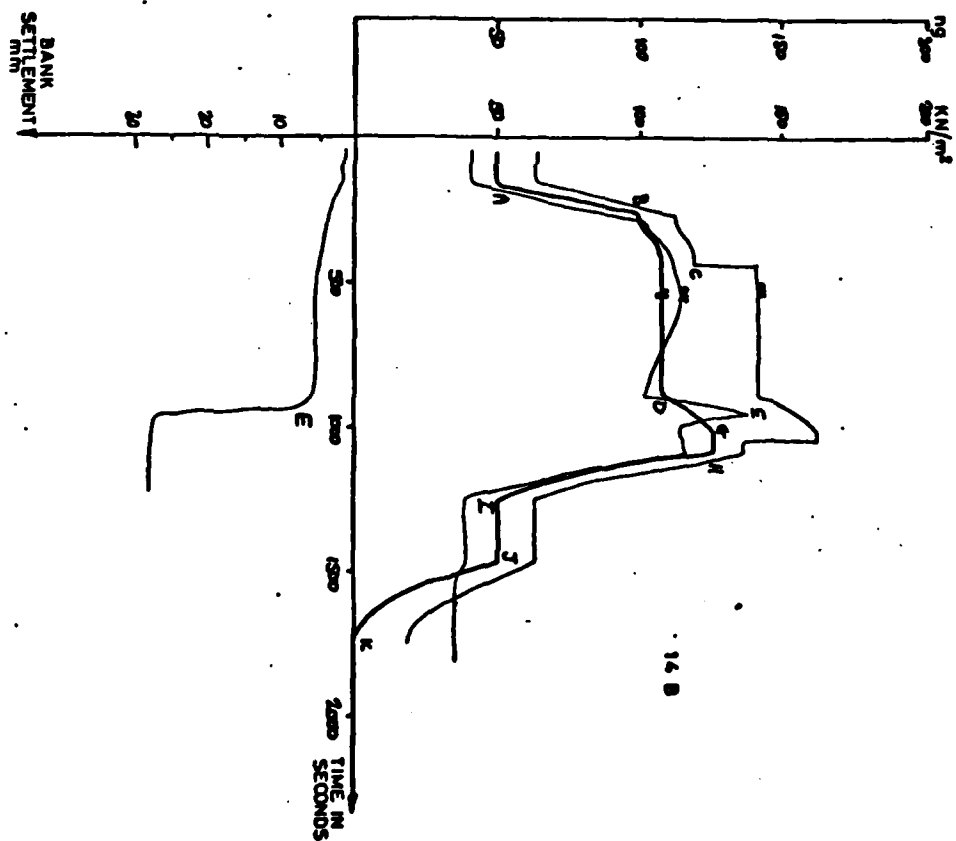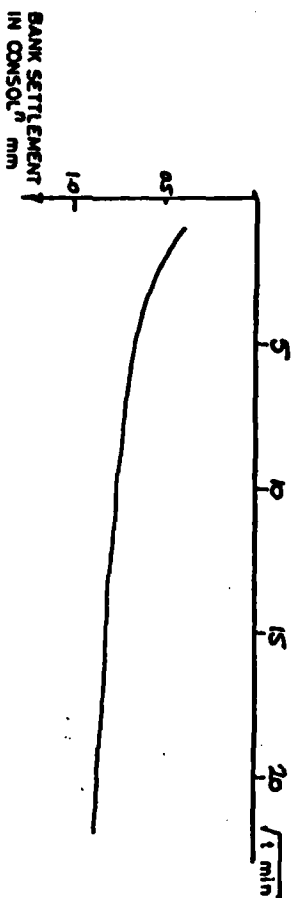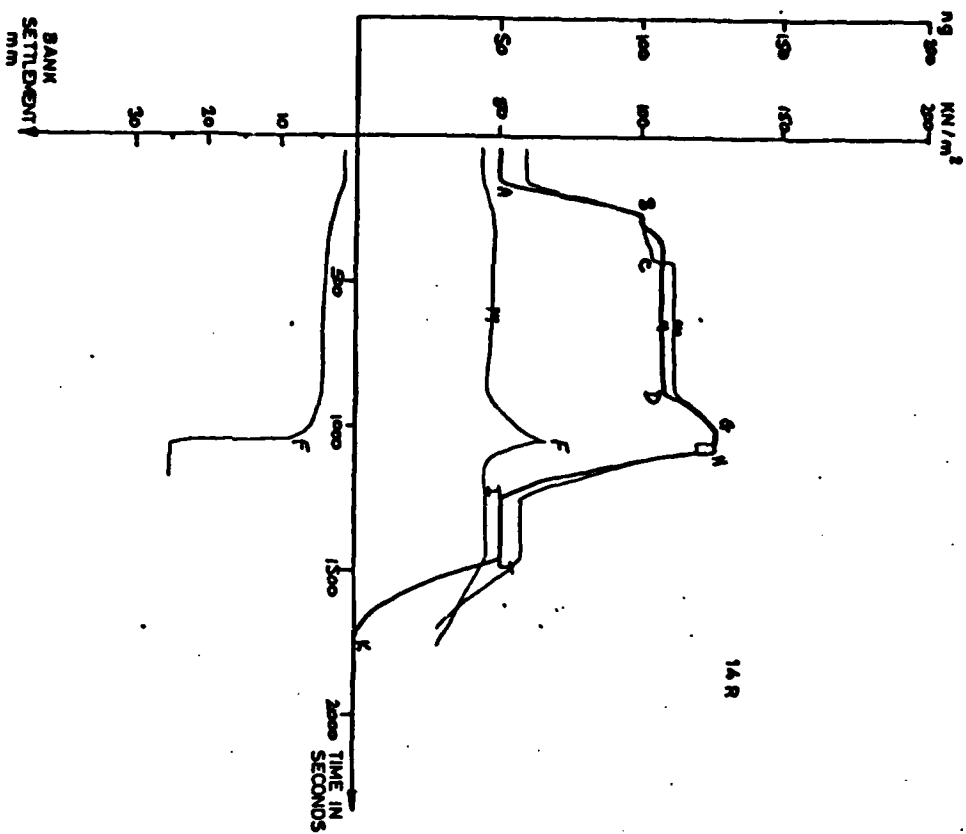
4.4.13   Two Dimensional Floodbank Test 2DF14

55mm Marsh

Uplift was applied at 108g and maintained for 8 minutes. No additional settlement occurred. The uplifted models were accelerated to failure.

Events in the Test

AB   Machine speed increased to 108g

C   Red model uplifted to U = 1.13

       Blue model uplifted to U = 1.38

CD   Uplift maintained for 8 minutes

DG   Machine speed increased 108g-126g

E   Blue model fails at 118g

F   Red model fails at 126g

HIJK   Machine speed reduced to 50g and stopped

Notes

1.   Red model failed with a combination of wedge and circular slip surfaces.

2.   Blue model failed on a deformed slip circle - uplift pressures were again not effective in modifying the shape of failure. (cf. Test 2DF13).

3.   Eight minutes at 108g had the effect of stiffening the models and caused no distress.
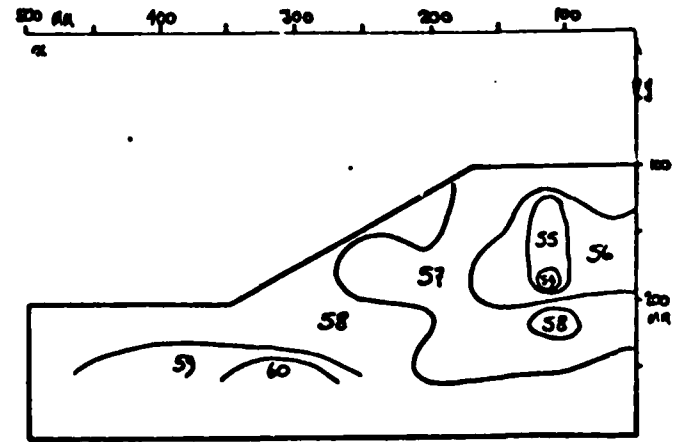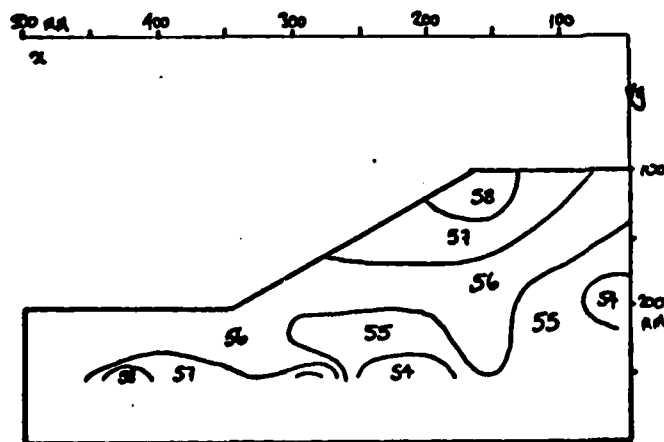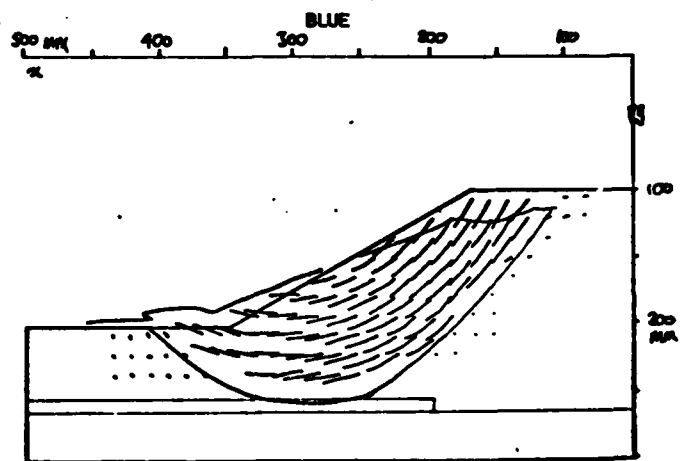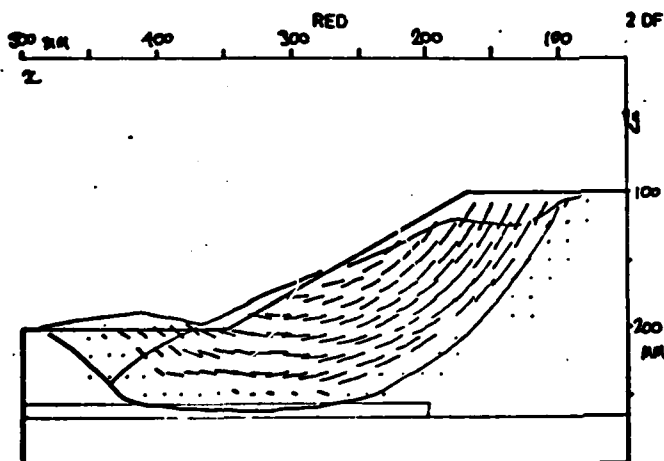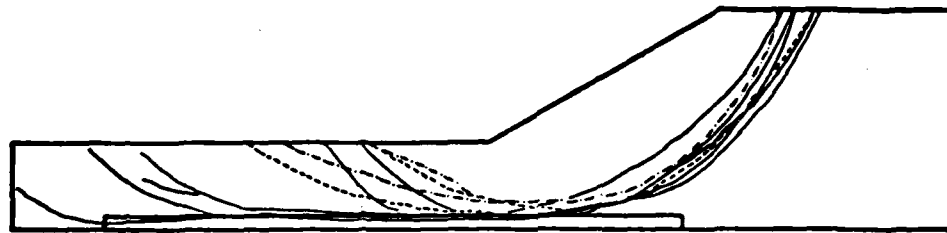
a 55 mm MARSH MODEL

b 75 mm MARSH MODEL

c 75 mm MARSH MODEL

700mm	600	500	400	300	200	100	0
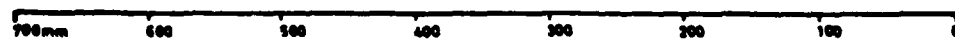
FIG. 4·33 FAILURE SURFACES SUPERIMPOSED FOR ALL TESTS

4.4.14   Discussion of Test Data

4.4.14.1   Bank Settlement

The graphs of settlement against time for the consolidation period show clearly that the models had not come into pore pressure equilibrium after eight hours. In some cases the crest of the bank settled in the first $\frac{1}{2}$ - 1 hour and later started to heave; in other cases no heave occurred. The reasons for this heave are discussed in Section 2.3.3. During the test sudden settlement of the bank crest was taken to indicate the moment of failure.

4.4.14.2   Pore Water Pressures

These transducers behaved badly, possibly because of cavitation and the possibility that air had come out of solution with the negative pressures generated by unloading. The Druck transducers gave the most consistent performance, despite their proneness to failure by leakage. The strain gauge transducers did not perform well in the soil. The transducer records were erratic during the consolidation run, sometimes rising and for other models falling with time. However, the records often gave a very precise indication of the moment of failure, as has been noted in the test descriptions.

4.4.14.3   Reservoir Water Pressure and Accelerometer

The value of uplift U applied to the model at any value of ng was calculated from the reading of the transducer in the water line from the reservoir to the sand box, as described in Section 3.8.3. At failure the value of U was plotted against the value of F on the interaction diagrams in Plates 4.10a-c, and Figs 4.37a-c.

4.4.14.4   Displacement Diagrams and Slip Surfaces

The displacement diagrams serve as a visual record to emphasise the type of mechanism that has occurred and often help to disentangle the chaos of a complex failure. The profiles of the failure surfaces are shown super-
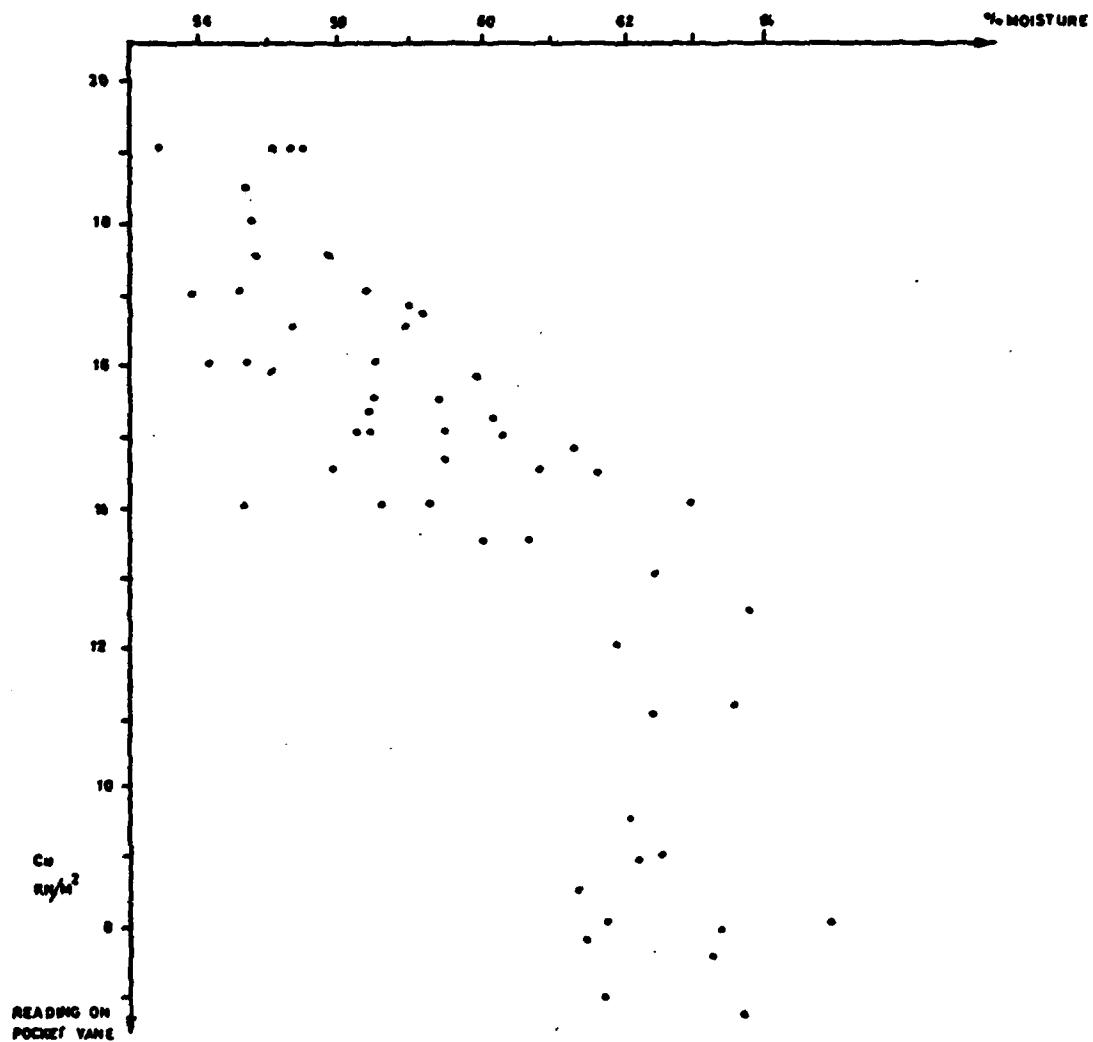
FIG 4·34 CORRELATION OF MEASURED MOISTURE CONTENTS
WITH MEASURED SHEAR STRENGTH

imposed on each other in Fig. 4.33. Although there is some scatter the failures for the three geometries occupy distinct bands such that for the deeper marsh layers more of the bank was involved in the failure. In the case of the 55mm and 75 mm marsh/bank models the circular sliding surfaces are at most 10 mm shallower than the wedge shaped sliding mechanism. In the case of the 95 mm marsh model the surfaces are indistinguishable.

The failure surfaces were curved in plan where they intersected the top of the embankment which testifies to some influence of wall friction and to the effect of the differing foundations in the middle and at the sides of the model. It is of interest to note that in certain cases the slip surface never re-emerges at the toe of the slope. This will be discussed in Chapter 5.

4.4.14.5 Measured Value of Shear Strength

As described above, model properties were measured shortly after the termination of a test. For the first nine tests, three vane strength determinations were made at different depths in the bank. Moisture content samples were taken from the site of the vane tests. The results are plotted in Fig. 4.34 against the vane reading. The plot shows a general though not very precise correlation.

It was realised partway through the series that the values of undrained shear strength measured by the vane measurements were low by up to 50% compared with the strength that was expected theoretically and which was being realised on the centrifuge. Recently Casarin* has investigated this problem and has calibrated the vane on clay samples of known strength. It does indeed appear that the measurements on the soil unloaded from the centrifuge were in error. They appear to differ from triaxial determinations of the strength by up to 50%. This investigation is still underway. In Tests 2DF10-14 the vane was rejected in favour of a more closely spaced

---

*C. Casarin, 1977, personal communication.
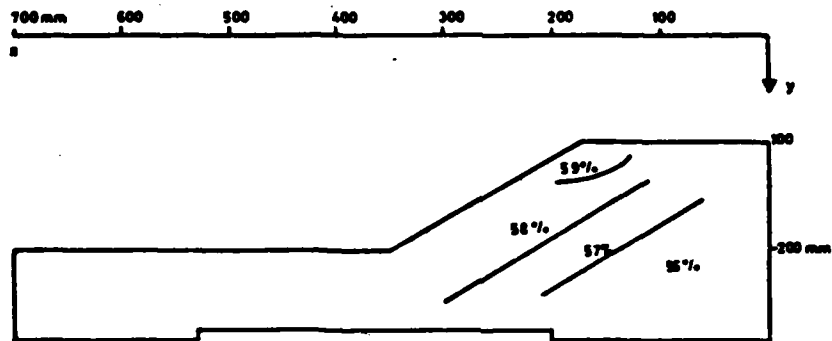
FIG. 4·35 MOISTURE CONTENT DISTRIBUTION OF
AN "AVERAGE" MODEL AFTER TEST
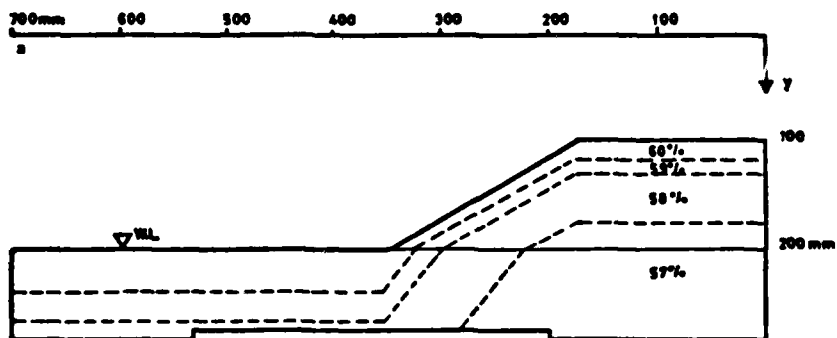
FIG. 4·36 THEORETICALLY DERIVED MOISTURE CONTENT
DISTRIBUTION FOR MODEL IN EQUILIBRIUM
AT 50 g.

grid of moisture content samples.

The vane strengths show only a slight increase in strength with depth. The determinations, which ranged on a typical model from 14-17 kN/m^2 seem too low and the range of values too small. It is possible that the kaolin was not completely saturated and that the pore suctions which should develop when the machine was stopped were not able to do so fully since the small amount of included air altered the elastic properties of the soil. It is likely that the problems experienced in this connection were all due to cavitation effects when the clay was unloaded rapidly from the centrifuge.

In the circumstances this was unavoidable. Hird, 1974, and Mair[*] have both experienced problems of this type when trying to measure the strength of a centrifuged model after the machine had stopped. It was clear that the only certain remedy was to develop a device to measure strength in flight, and indeed a miniature pressure meter has subsequently been developed to measure vertical strength profiles in a centrifuge test[†].

4.4.14.6 Measured Water Contents

By contrast with the measured vane strengths (2DF4-9) the measured moisture contents exhibit a considerable variation with depth. The measured moisture content distribution for each model was shown in the figures accompanying the description of each test. Although these distributions are somewhat irregular a very rough sketch may be made of the distribution in an 'average model' and is shown in Fig. 4.35. This may be compared with the distribution shown in Fig. 4.36 which is derived theoretically using the material properties discussed in Chapter 2. The models are clearly slightly dryer than the predicted equilibrium moisture contents which implies again that equilibrium had not been fully attained after 8 hours at 50g. The discrepancy is, however, not great.

---

[*] R.J. Mair, 1977, personal communication.
[†] R.J. Mair, 1978, personal communication.
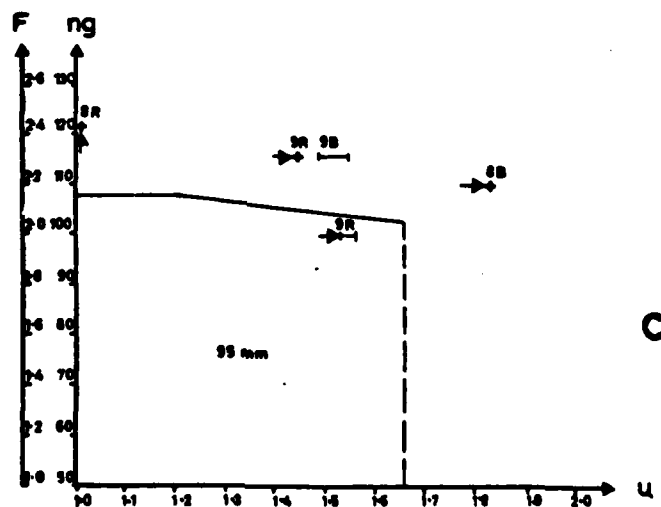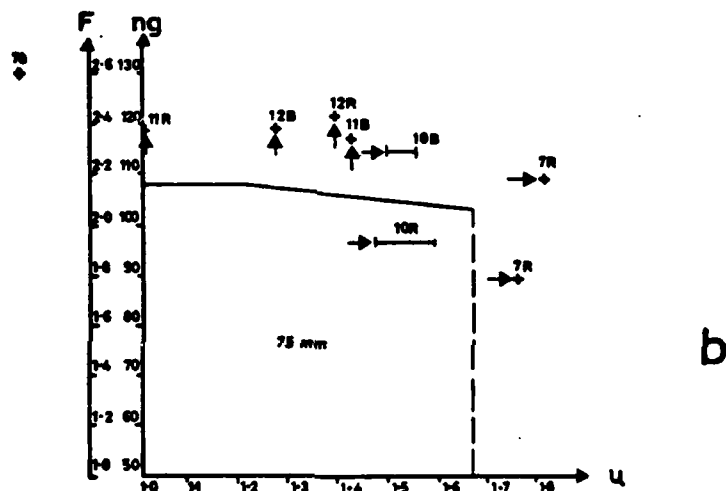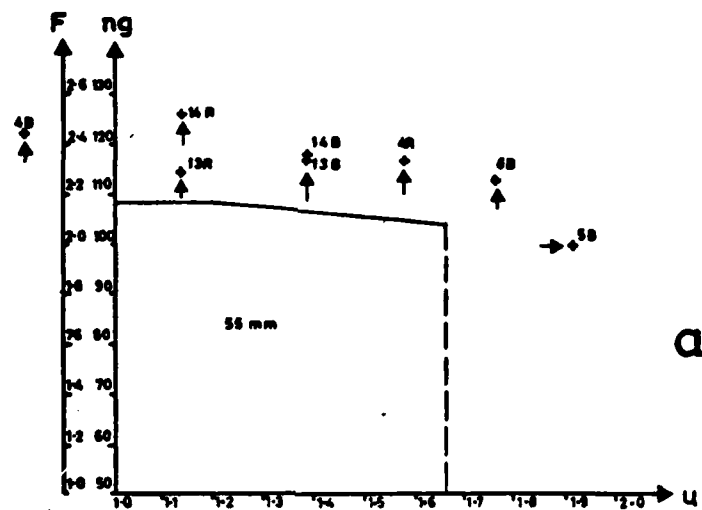
FIG. 4·37   INTERACTION DIAGRAM REPRESENTATION
FOR FAILURE STATES OF MODEL
EMBANKMENTS

4.4.14.7   Interaction Diagram

The data of failure for all tests described under 2DF4-14 may be
gathered onto the three interaction diagrams shown in Fig. 4.37a-c and
Plates 4.10a-c. In certain cases where the embankment becomes critically
stable under two different loading combinations, two data points appear on
the interaction diagram. It will be seen that in the case of all three
model geometries, failure occurred at a lower value of F for a higher value
of U in the foundation, though the effect of uplift is not great on the
value of F at failure. For the thin (55 mm) marsh model an exceptionally
high value of uplift was required to bring the model to failure at 110g.
All the models were able to withstand uplift U > 1.66 at around this value
of F (and lower) which suggests that a mechanism of restraint is acting
in the models that would not be present in the three dimensional condition.
This is further discussed in Section 5.2.

In all cases the experimental points lie outside the predicted locus.
It should be remembered firstly that the interaction mode considered in
the analysis was very different from that observed in the tests, with its
long translational movement on the sand/clay interface. Secondly boundary
restraints would effectively strengthen the model and thirdly the models
were slightly dry of the equilibrium moisture content distribution. With
these considerations in mind the simple analysis gave reasonable predictions.
In Section 2.3.3 it was suggested that the material strength profile is
slightly different in the case of uplift prior to self weight increase than
in the case of prior self weight increase. In the first case a small trough
in the strength profile may be expected to propagate into the material.
If there is a trend in the data points of Fig. 4.37 it is that these models
survived to higher values of ng than did those that were subjected first to
an increase in self weight, so the effect is of no consequence.

CHAPTER 5

THAMES FLOOD EMBANKMENTS

DISCUSSION OF RESULTS

5.1   The Attainment of Equilibrium at 50g

In Section 2.3.3 a simple calculation was presented which showed that a 150 mm thick layer of kaolin as used in the Tests 2DF4-14 would require approximately 13.6 hours to attain 90% consolidation at the top of the layer if drainage was allowed at the bottom only. In fact the largest dimension of the models ranged from 0.155 m to 0.195 m depending on the marsh thickness and so 13.6 hours is an underestimate. It is probable that one other factor increased even further the time that would have been required to obtain equilibrium in the model. The subject of cavitation within the kaolin has been raised at several points in the foregoing discussion. The kaolin was unloaded from a state of one dimensional consolidation with $p' = 152$ kN/m^2 to a state where the total mean normal stress was zero and large negative pore pressures were generated by the elastic rebound of the soil.

Water at these large negative pressures may be expected to boil, but in the fine pores of a soil, Bishop et al, 1975, a state of super-tension may persist to many times the normal maximum. Bishop et al were considering clays that had been consolidated to high pressures within which the pore spaces had been reduced to very small dimensions. The kaolin considered in this study typically consists of flocculated grains which leave relatively large pore spaces at the pressures considered here, and cavitation is a real possibility.

Other factors may also have played a part but it is an inescapable conclusion from the data that the models had not attained equilibrium at 50g by the time the perturbations were applied to the model. In the event this was not too serious since the moisture content of the models was

fairly close to the equilibrium value. However, as mentioned in Section 4.4.14.2, cavitation is held responsible for most of the erratic behaviour of the pore water pressure transducers. Only very occasionally did these transducers give a rapid response during a test. No two tests gave the same record during the 8 hours of consolidation and since none of the models attained equilibrium the initial condition of the different models probably varied somewhat from test to test.

The measured values of vane strength taken after the test are further evidence of cavitation. These measurements were taken as quickly as possible after the completion of a test. Necessarily the models had to be rapidly unloaded from the high stress regime of the centrifuge to a zero total stress state on the laboratory floor. It is likely that cavitation ensued as discussed in Section 4.4.14.5, since the measured values were improbably low. A simple upper bound slip surface calculation using a strength profile determined from the measured values suggests that the embankments would fail at approximately 60g with no uplift. This was manifestly not the case. Typically readings were in the range 14-17 kN/m^2 whereas a uniform undrained strength of 33 kN/m^2 would give a typical embankment a factor of safety of unity at 120g. This value may be compared with the undrained shear strength at the critical state, $Cu = 32.2$ kN/m^2 at $w = 58\%$ which agrees well with the state of the model after the test.

The program that was envisaged at the initiation of this research included a preliminary set of predictions of the kind set out in Chapter 2. It was then intended to run a series of centrifuge tests out of which data would be derived for a comprehensive back analysis. This condition was not achieved. Potentially the most useful source of data was the photographic record of displacement, but the lack of any firm datum has rendered this data useful only for qualitative visualisation of displacement. It has not proved possible to do any more accurate analysis than that presented in Chapter 2.
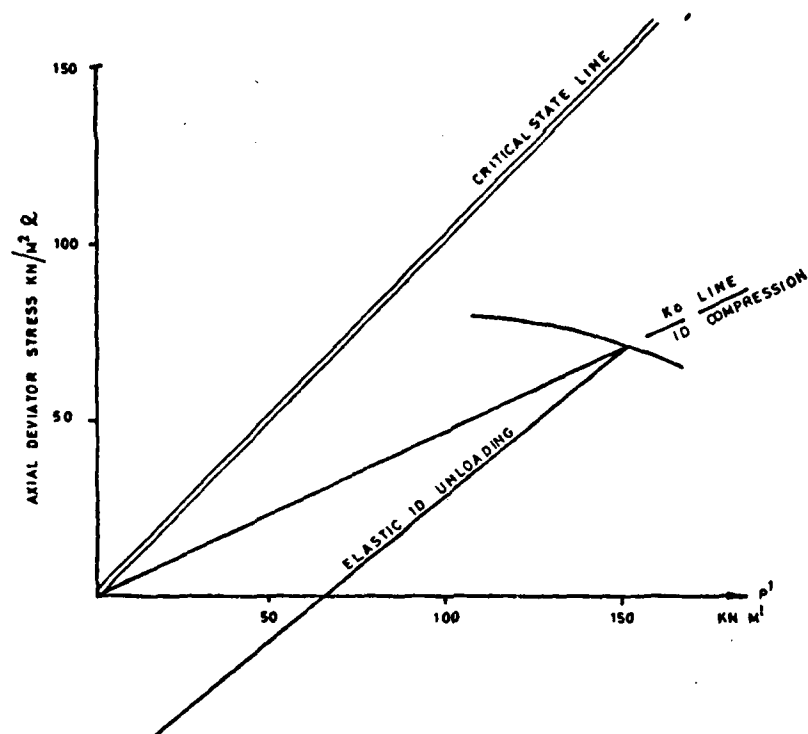
FIG 5·1 ONE DIMENSIONAL LOADING & UNLOADING FOR
SAMPLE OF KAOLIN

It is recommended that in any future work of this kind the test series be planned to achieve equilibrium in each test with no possibility of cavitation. It would have been possible for example to allow the clay to swell slowly in the consolidometer to $\sigma_v' = 100$ kN/m^2 before building and loading the models to 50g on the centrifuge. In this way no cavitation would have resulted and the moisture content changes required on the centrifuge would have been reduced.

5.2 Boundary Effects

In Chapter 2 the assumption was made that the model experienced full lateral restraint in the centrifuge strong boxes. The assumption implies that the material stress state at equilibrium is to be found on the one dimensional elastic unloading line shown in Fig. 5.1. In the model tests it was possible to see that when the perspex front of the strong boxes had been bolted down tightly the perspex was nearly but not quite in contact with the clay. At 50g a distinct line appeared at approximately marsh level which marked the boundary between a darker lower area of close contact between perspex and clay and a lighter, higher area of separation. As swelling progressed this line moved up the visible section of the bank but at no stage did it rise higher than half the height of the embankment.

This observation suggests that lateral restraint was only partially mobilised. This may have had two effects, neither of which is sensibly quantifiable. Firstly the value of effective mean normal pressure at equilibrium would be less with partial restraint than with the full elastic value and consequently the clay would have unloaded to a greater value of specific volume and hence a lower value of undrained shear strength. Secondly, the partial lack of restraint may have affected the material in shear. The additional lateral distortions would be associated with some degree of shear strain and would alter the one dimensional stress state. It appears from the test results that whatever reductions in undrained shear

these influences may have occasioned, the enhancement in strength due to the lack of equilibrium was more than sufficient to compensate.

One other boundary effect made itself apparent in the form of the observed failure surfaces. Almost invariably the failure surface was curved such as to penetrate deeper into the embankment at the centre section of the model than on the two cut faces. The greatest influence was probably wall friction but the geometry of the sandbox may also have had an effect. This wall friction may have had some influence on the overall stability of the models, rendering them artificially stable. In all the diagrams, (e.g. Fig. 4.33) the line given for the failure surface or slip line is that which intersected the plane face of the model.

5.3   In situ Stress Assumptions

The dominant feature in this discussion is the estimation of undrained shear strength from considerations of effective overburden pressure alone. In Section 5.1 it was pointed out that the tests themselves did not yield pore water pressure data that could have answered some of the remaining questions. Almost any of the assumptions are open to challenge. For example, use of the data reproduced by Poulos and Davis, 1974, for the elastic stress distribution within an elastic embankment shows that over a large area the stress ratio is so high that if plotted on the q,p' plane the material stress state would lie outside the yield locus for overconsolidated clay. Evidently there is some truth in these calculations and some amount of yielding and redistribution of stress undoubtedly goes on during the loading of the kaolin embankment. However, the effect of this is not so great as to invalidate the simple assumptions that are necessary to derive an estimate of undrained shear strength.

The influence of shear on the direction of the total stress increment vector is of interest, though strictly relevant only to the magnitude of pore pressure generated during the shearing of the soil. Consider two
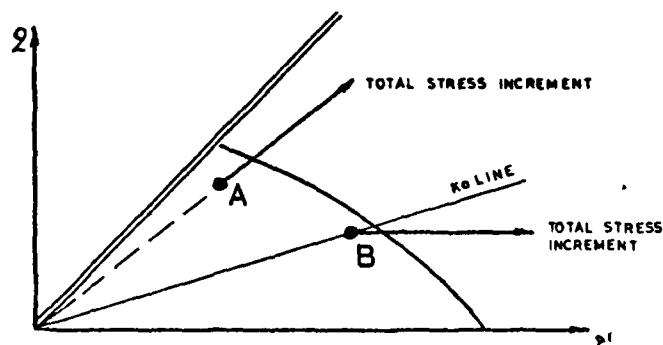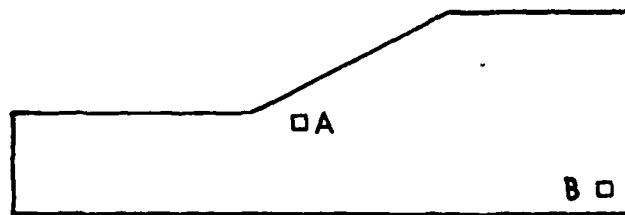
FIG 5·2 POSSIBLE EXTREME STRESS RATIOS FOR
INCREMENTS OF TOTAL STRESS IN UNDRAINED
INCREASE IN SELF WEIGHT

elements of soil A and B within the embankment, Fig. 5.2. Element B is laterally constrained and when subjected to an undrained increase in self weight is able to suffer neither volumetric nor shear distortion. The total stress increment vector has no deviatoric component and the full overburden stress increment is transferred to the pore water. On the other hand, element A is in a region where shear distortion is likely. In this case the total stress increment includes a deviatoric component. It is possible that there is a limiting stress ratio to the total stress incre- ment vector for an undrained increase in self weight, given by a line through the origin and the equilibrium total stress state. At this limit the undrained increase in self weight would cause the deviatoric and mean normal components of total stress to increase proportionally. In this case the pore pressures generated by the undrained loading are in principle calculable since the corresponding effective stress trajectory is known. However, in general this pore pressure depends on the direction of the total stress increment vector which for elements of soil lying between A and B might take a range of values between the extremes of constant q and proportional increase.

5.4 The applicability of Slip Circle Calculations

Al Qassab, 1974, and Fuglsang, 1971, have noted that the occurrence of a discrete failure surface depends on certain characteristics of the stress strain curve of the material. Fuglsang found that an embankment constructed of compacted material with a gently rising stress strain curve tended to flatten out at high ng on the centrifuge. On the other hand an embankment of a material with a peaky stress strain curve collapsed by the development of ruptures. In either case the event of failure may be seen as the response on the part of the embankment to overloading. At failure it unloads to a new geometry of limiting equilibrium. The difference

between the two stereotype materials is that the failure is more catastrophic, more of a jump for the material with a peaky stress strain curve.

Two types of failure surface were observed in the experiments. Where the simple loading of a self weight increase acted in isolation, slip circles developed. The over-consolidated clay ruptured cleanly and symmetrical failure surfaces developed which were well described by the normal slip surface analysis. In particular the clear absence of general plastic deformation in these tests is (for this material) a good defence of slip circle analysis against the reservations raised by Davis and Booker, 1973. Note however that in the case of the 95 mm marsh model there was plastic deformation of the marsh.

The situation is not so clearcut in the case of the failure surfaces that developed in response to overloading by a combination of uplift and self weight. As before, the slip surfaces were sharply defined through the material of the embankment. In every case the surface passed horizontally along the sand/clay interface. The surprising observation is that in these 'interaction mode' failures the failure surface never re-emerged. Instead the slip line visible on the plane face of the model became indistinct and vanished. The material of the marsh was plastically compressed, finishing thicker after the failure than before. This mode of failure was not expected and has never to the author's knowledge been reported in the literature, though it has been observed in practice*.

It should be noted in conclusion that the fact that this interaction mode failure surface passes along the horizontal sand/clay interface means that the mechanism can respond immediately to an increase in uplift. It is sufficient for only the interface layer to swell. Test 2DF14, where uplift was applied at 108g for 8 minutes produced no measurable settlements. The loading was within the failure envelope on the interaction diagram.

---

*P.R. Vaughan, 1978, Personal communication.
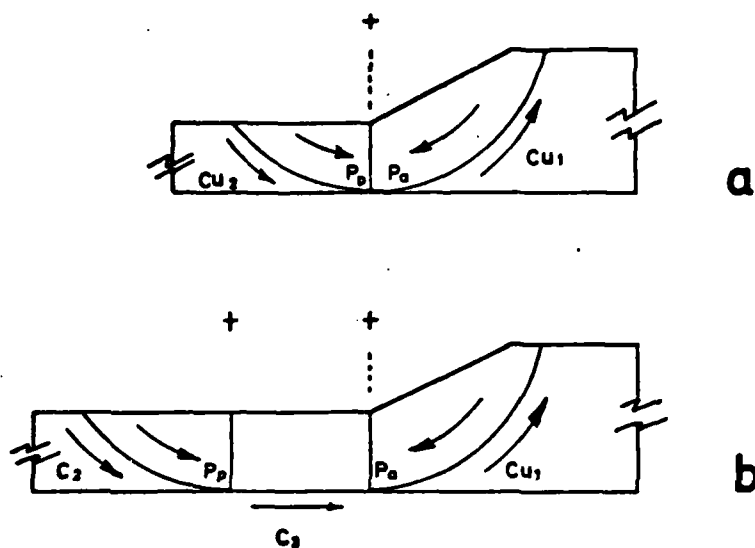
FIG 5·3 SKETCH TO ILLUSTRATE THE ARGUMENT THAT A CIRCLE IS MORE CRITICAL THAN A 'WEDGE' IN UNIFORM SOIL.
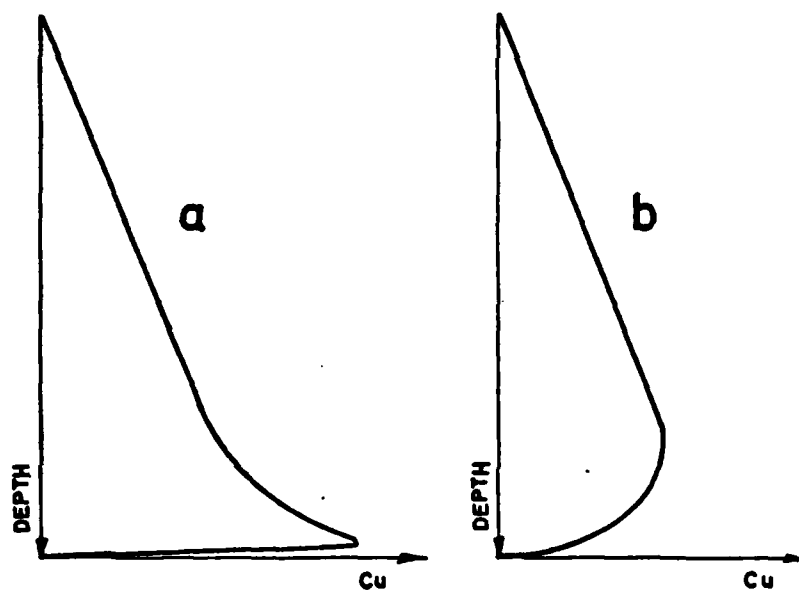
FIG. 5·4 PROFILES OF STRENGTH WITH DEPTH FOR MODELS SUBJECTED TO : a. INCREASE IN ng PRECEEDING u
b. INCREASE IN u PRECEEDING ng

5.5 The Non-Emergent Slip Surface

Consider the two potential slip surfaces in Fig. 5.3. It is evident that in normal circumstances the circle in Fig. 5.3a is more critical than the elongated surface in Fig. 5.3b because in the latter case an additional resisting moment is supplied by the resistance C_3 however small this may be. This problem was at the root of the uncertainty about the nature of the hypothetical 'interaction mode' failure. The centrifuge models have provided a clue to the solution of the problem. It appears that in the case where there is a softened or uplifted layer the failure surface never re-emerges.

In Figures 2.17c and 2.18c the effective stress profile with depth was sketched for the case of uplift applied before increase in self weight and vice versa. These profiles have been redrawn in Fig. 5.4 to show that in both cases there is a peak in the strength-depth curve through which the re-emergent failure surface must penetrate. The important point here is that if the failure surface does not re-emerge immediately it will never do so. In the case of the models with a marsh layer 95 mm thick where the slip surface never re-emerged even in the absence of an uplift softened layer, it is possible that the higher general stress level favoured plastic deformation rather than rupture.

Consider the embankment shown in Fig. 5.5 where a potential slip surface is shown in the body of the embankment. The horizontal thrust generated by this sliding mass of soil calculated in the normal way is P_A and this must be resisted by the marsh material. If the potential resistance of the marsh is greater than P_A then no failure occurs. If the material has a substantially uniform strength with depth and the potential resistance of the marsh is less than the active force of the embankment traditional slip failure is likely to occur with heave at the top. Consider however the case where a discrete layer of soft material forms the foundation of the marsh and embankment. If this is a frictional material the
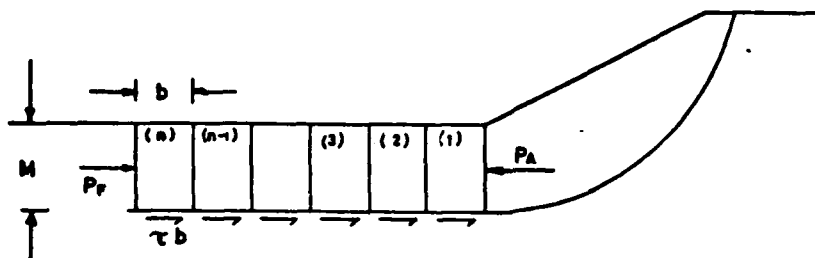
FIG.5·5 n ELEMENTS INVOLVED TO REDUCE THE EMBANKMENT
THRUST P$_A$ TO THE IN-SITU LATERAL THRUST P$_F$.
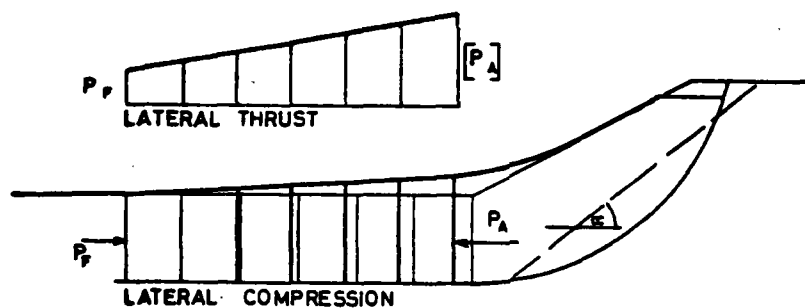
FIG. 5·6 INTERACTION MODE OF EMBANKMENT FAILURE
INFLUENCED BY SOFT LAYER OF SOIL IN
FOUNDATION :— FAILURE SURFACE NEVER
RE-EMERGES AT TOE.

weakness may be due to uplift pore pressures as is the case here, but any weak layer will generate the same effect. Let us say the shear strength of this layer is τ whereas the undrained shear strength of the mass of the marsh is c_u. In Fig. 5.5 the marsh layer has been divided vertically into elements b wide. In equilibrium the right hand element (No. 1) will be resisting the embankment thrust. The maximum possible resistance is

$$P_A = \frac{\gamma M^2}{2} + 2Mc_u \tag{5.1}$$

The horizontal force between elements (1) and (2) is

$$P_{12} = P_A - b\tau = \frac{\gamma M^2}{2} + 2Mc_u - b\tau \tag{5.2}$$

The number of elements involved depends on the values of P_A and P_F, the static K_o condition of the soil. If n elements are involved, each contributing $b\tau$ to the resistance, then

$$P_{n-1,n} = \frac{\gamma M^2}{2} + 2Mc_u - nb\tau = \frac{K_o \gamma M^2}{2} \tag{5.3}$$

This fall off in stress is illustrated in Fig. 5.6.

Beginning now at the left hand side of the diagram and assuming that τ is fully mobilised in all elements it is possible by considering each element in turn to calculate the cumulative horizontal strain. If the horizontal Young's modulus for an element is E and the average stress across the i'th element is

$$(\sigma_H)_i = \frac{1}{M} \left(\frac{\gamma M^2}{2} + 2Mc_u - (i-0.5)\, b\tau \right)$$

$$= \frac{\gamma M}{2} + 2c_u - \frac{b\tau(i-0.5)}{M} \tag{5.4}$$

The cumulative strain is then

$$\Sigma \, \epsilon = \sum_{i=1}^{n} E\{ \frac{\gamma M}{2} + 2c_u - \frac{(i-0.5)}{M} b\tau \} \tag{5.5}$$

Moving from left to right on the diagram there will come a point where the cumulative strain is large enough to generate a horizontal rupture at the sand/clay interface. This rupture will accommodate more and more horizontal movement until it joins with the rupture surface through the embankment. Ignoring distortion of the sliding block the vertical settlement of the crest of the embankment is approximately

$$\rho = b \ E \ \tan\alpha \ \sum_{i=1}^{n} \ (\frac{\gamma M}{2} + 2c_u - \frac{(i-0.5)}{M} \ b\tau) \qquad (5.6)$$

It would appear that in the case where the slip surface doesnot emerge the stability of the embankment is not only calculable but the distortion required to bring an unstable bank into equilibrium is also calculable. In fact the magnitude of P_A reduces as the active wedge rotates and the system quickly finds an equilibrium position where P_A is balanced by the cumulative resistance of the marsh. It is evident from the experiments that some mechanism of this kind is operative. After an interaction mode failure the marsh layer is thicker than before exactly in the manner of Fig. 5.6. Also the rupture surface was clearly seen to vanish towards the left on the diagram in the manner described above.

CHAPTER 6

CONCLUSIONS RELATING TO THAMES FLOOD EMBANKMENTS

6.1 Conclusions

The experimental work of Hird, 1974, had suggested that where flood embankments are built on a thick alluvial marsh foundation, uplift pressures may be expected not to trigger a failure of the bank. However, the proposal of Bolton, English, Hird and Schofield, 1973, that the self weight and uplift loading conditions that would bring an embankment to failure could be plotted on an interaction diagram, remained unqualified. Furthermore it was not evident why an interaction failure mode, say by a sliding wedge, should ever occur in preference to the more obvious circular mode.

The work presented in this dissertation on the uplift interaction problem has shown both analytically and experimentally that an interaction failure mechanism does occur and hence that for the centrifuge loading the interaction diagram representation is valid. The interaction diagram suggests three distinct failure modes. Only two of these were observed in the models. The third mode, marsh uplift, was not observed due to the constraints of the narrow two dimensional model, though it was observed by Hird in his three dimensional models.

The interaction mode mechanism seen on the centrifuge is similar to the mechanism hypothesised by Cooling and Marsland, 1953, for the Dartford Lock breach of that same year. There are several interesting practical features about this new mechanism, among which is the observation that the slip surface never re-emerges from the layer of soil that is weakened by the uplift pressures. The marsh layer suffers plastic compression as the bank crest settles.

Centrifuge experiments have given quantitative data of failure and have revealed and demonstrated mechanisms of collapse which could not have been obtained by any other experimental technique except a very complex

and expensive trial embankment. It should be remembered that each data point on the interaction diagram represents three week's work. But more importantly each point represents also an experimental datum that would have been extremely difficult to obtain even with a full scale trial embankment. One such point at full scale would require the expenditure of considerable resources in comparison with which three week's work is small expense.

The expense and time involved in the process of testing clay models in the centrifuge limited the model series to 21 useful model tests. Of these one or two models failed to provide very useful data due to failures in the apparatus. The anomalous behaviour of other models may be explained by arguing that the boundary values and initial conditions of models of this complexity are not completely understood and that the onset of failure is susceptible to very small influences. Thus the work described here is subject to a clear limitation: that there are too few experimental points to give definite statistical confirmation to the expected trends.

6.2 Further Research

The analysis and experiments reported on the first part of this dissertation have dealt with models of one embankment geometry and one uniform material. This investigation concentrated on the nature of and conditions for interaction. The conclusions proffered are subject to an important caveat: direct application of the results of this research must await the investigation of the importance of certain parameters:

1. Lighter marsh materials, such as peaty clay, or stronger bank materials may considerably alter the shape of the interaction diagram.

2. Geometry of the bank and the provision of loading berms will also alter the loading conditions required to fail the embankment.

3. The models tested were all two dimensional. It is possible that the mode of failure of a real embankment, which is necessarily three

dimensional, is governed by slightly different criteria.

4. It is not entirely clear from the work presented here when and why
    the non-circular mode is more critical under uplift than the circular
    failure mode.

5. Data are available from the centrifuge models to test the validity of
    the analysis outlined in Section 5.5 concerning the non-emergent slip
    surface and this interesting development should be taken further.

PART II

CHAPTER 7

MISSISSIPPI FLOWSLIDES - REVIEW

7.1   Introduction

In Section 1.3 the problem of Mississippi river bank instability was introduced and the flowslides that occur in point bar deposits were described. At the time this study was initiated it was believed that the Mississippi flowslides were associated with some sort of 'spontaneous liquefaction' of relatively loose sands. The physical mechanisms that were at work in the development of a flowslide were entirely unresearched. Consequently it had proved impossible to apply any form of analysis since the events to be described had not yet been identified. In general a modelling exercise is not undertaken in such a speculative climate. It is normal to design a model according to rules of scaling that depend intimately on the physical processes themselves. This was entirely impossible in this case. Initial data comprised sketchy field evidence of the general characteristics of areas where flow failures had already occurred. There were very little data on in-situ sand density or even the properties of the overburden. Only one failure, that at Free Nigger Point, had ever been observed during its development.

The experimental investigation was exploratory and was designed to be flexible: to seek ways either to model the flowslide, to achieve liquefaction or to provide clues to what type of mechanism was likely to be at work on the Mississippi. The model series was time consuming and in certain in satisfactory and inconclusive. It did however provide the clues from two interesting analyses were developed. The model test series is in Chapter 8.

ABANDONED
WALNUT BAYOU
MEANDER BELT

BACKSWAMP

ABANDONED
COCODRIE
MEANDER
BELT

PRESENT MISSISSIPPI
RIVER MEANDER BELT

POINT BAR DEPOSITS

BACKSWAMP DEPOSITS

SANDS & GRAVELS
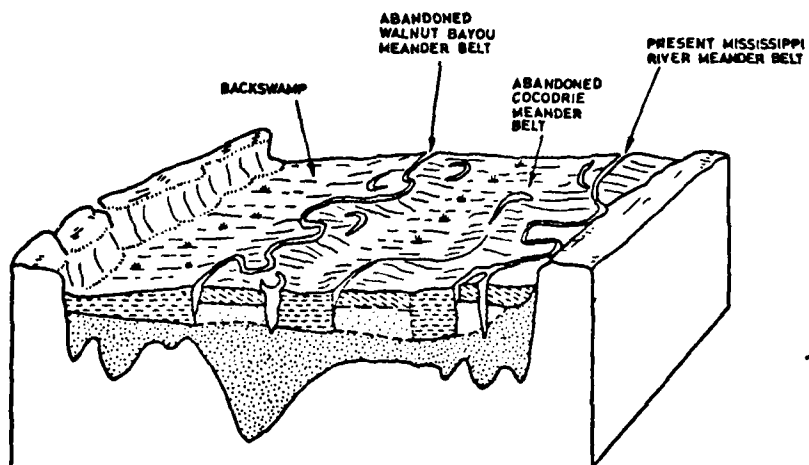
FIG. 7·1 SECTION THROUGH MISSISSIPPI RIVER VALLEY
SOUTH OF NATCHEZ (Taken from Fisk 1947)

a BRAIDED STREAM
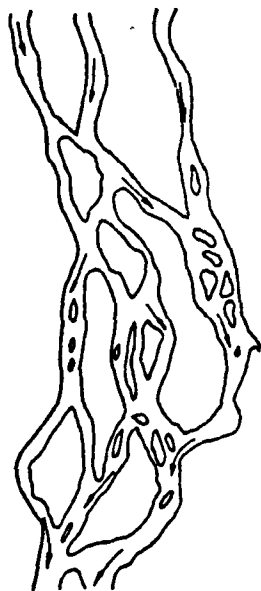
b STRAIGHT BED
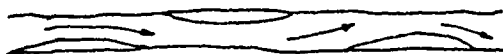
c MEANDERING STREAM

FIG. 7·2 STREAM TYPES

The model tests suggested that the mechanism responsible for the arrest of a flowslide may concern the deformation of the overburden. A simple analysis, presented in Chapter 9, confirms that this hypothesis is reasonable. In Chapter 10 a more complex analysis is presented concerning the distance that a liquefied sand layer is able to flow downhill before it comes to rest. This has provided an almost complete description of the development of an unimpeded flowslide.

Certain preliminary background material is essential to an understanding of this analysis and this is presented for convenience of layout in this dissertation in Chapter 7. The phenomenon of flowsliding is just one of the processes shaping the landscape of the flood plain of a meandering river, and as such is influenced by the behaviour of the river which formed the deposits in the first place. Section 7.2 of this Chapter serves as an introduction to those aspects of river and delta morphology that are relevant to the present problem. The role of sediment transport in the development of a flowslide was introduced in Section 1.3. This topic is resumed in Section 7.3 where the state of present knowledge is reviewed concerning the ability of saturated suspensions of granular material to flow under gravity.

7.2   River Morphology

Ten thousand years ago, at the end of the last ice age, the Mississippi River discharged into a sea, the level of which was some 120 metres lower than at present, Fisk, 1947. Subsequently the ice has retreated, the sea level has risen and the conditions on the lower reaches of the Mississippi have changed. The deeply incised channels which drained into the ice-age sea have been filled with soil and now form a wide alluvial valley, Fig. 7.1. The lower Mississippi River follows a meandering course down this valley, contained between the pleistocene buffs to the east and an abandoned meander belt to the west.

mm/sec

SUSPENDED
TRANSPORT

BED LOAD

10^3

CRITICAL EROSION VEL'Y

CESSATION OF MOVEMENT

10^2

VELOCITY 1m ABOVE BED

DEPOSITION OF SUSPENDED
SEDIMENT

10

10^{-2} 10^{-1} 1   GRAIN DIA.   10   mm
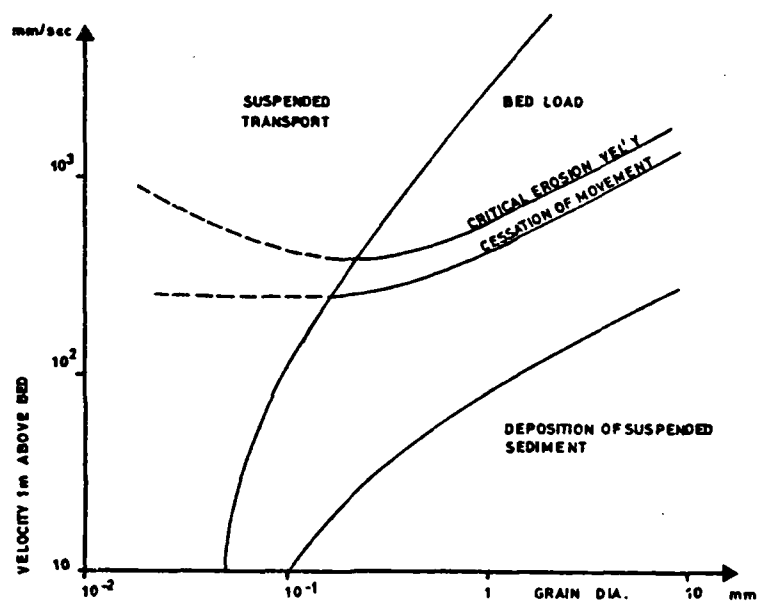
FIG. 7·3 RELATION BETWEEN STREAM VELOCITY,
GRAIN SIZE AND STATE OF SEDIMENT
(taken from Allen 1965)

The meandering of the Mississippi is relevant to the present study. For any particular river, the criterion which determines whether the course will meander or be braided, Fig. 7.2, has been expressed by Leopold and Wolman, 1957, as

$$S = 0.06 \ Q^{-0.44} \tag{7.1}$$

where S = slope of the river bed, Q = fluid discharge of the river. Streams whose conditions lie below this line in QS space (low Q, low S) will meander. All natural meandering streams appear very similar in plan whether they are large or small, Allen, 1965, and although the meander pattern is somewhat irregular the geometry is always a function of the discharge and the suspended sediment load. The present plan of a meandering river is only a moment in a process of continuous and dynamic change.

Within the stream, turbulence increases from the surface to the bed which leads to a stratification in the particle size distribution of suspended sediment throughout the depth. Large particles can be kept in suspension if the vertical velocity component of turbulent eddies is greater than the particle settling velocity. Particles which cannot be suspended, may be carried along by the stream as bed load. On the bed particles in the upper layers of sediment may execute jumps (saltation) and layers deeper down will be sheared by the current drag. Saltation occurs for particles of a certain size when the stream velocity exceeds a critical erosion velocity as shown in Fig. 7.3. The velocity required to erode very fine particles increases with a decrease in particle diameter due to the cohesive effect of interparticle bonds.

The pattern of water flow in a meandering stream is closely related to the formation of point bars. The sinuous nature of the stream is a characteristic of almost any flow over a movable bed. Even in a straight channel the thalweg (locus of deepest points in the cross sections) will be found to cross from side to side of the channel with alternating deep scour
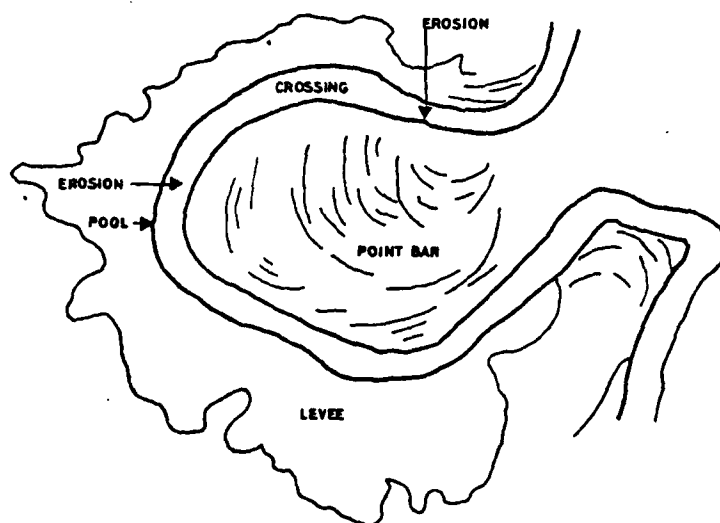
FIG. 7·4   POINT BAR AND NATURAL LEVEE
ACCRETION

pools and shallow crossings. Each meander loop encloses a point bar formed of cusp shaped ridges and troughs ('swales') roughly conformable with the shape of the channel as shown in Fig. 7.4. The ridges comprise an aggregation of bed load material deposited at times of flood when a portion of the stream cut directly across the bend. Between the ridges, the swales often contain marshes and ponds which fill up slowly with finer material. This landscape has been definitively described by Fisk (1944, 47).

The flow pattern on a bend is helicoidal, Fig. 7.5a, due to a transverse pressure gradient from the centrifugal superelevation of the water surface on the outside of the bend. As a result, the current on the stream bed follows a straighter course than the surface current. This secondary cross channel underflow on a bend creates a component of stream velocity down each steep concave bank and up the gently shaoling point bar opposite. The lateral velocity amounts to 10-20% of the downstream velocity and is believed to be largely responsible for the transport of sediment from the steep eroding concave bank to the downstream side of the next point bar downstream. The other factor which is of importance in the formation of point bars (and any other type of bar) is that a reduction in depth generates an instability in the flow which causes material to be deposited from suspension. Further, the flow intensity and turbulence decrease with decreasing depth and so enable finer materials to be deposited from suspension. It is typical of a point bar that the sediment fines upwards in the deposit. The uppermost layers form a cohesive overburden to the lower sandier layers. Significantly, the so-called Zone A sand layer which underlies this cohesive stratum, see Section 1.3, is composed of particles which become entrained close to the minimum erosion velocity. They are the first to be picked up by the river and the first to be dropped. These same particles are also the most easily fluidised and hence are the same that will retain a state of liquefaction for the longest time.
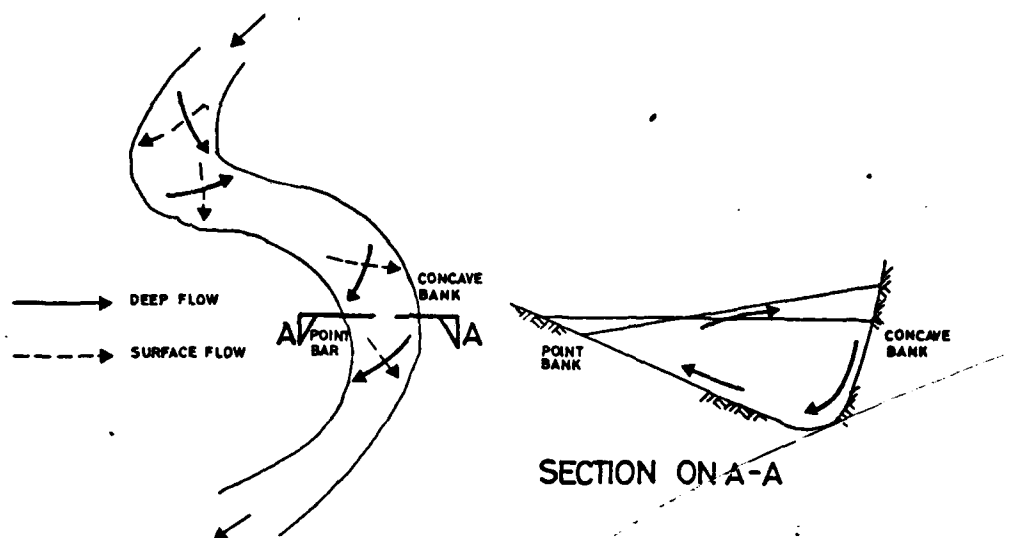
a DEVELOPMENT OF HELICOIDAL FLOW DUE TO CENTRIFUGAL SUPERELEVATION OF WATER SURFACE ON A BEND (schematic)
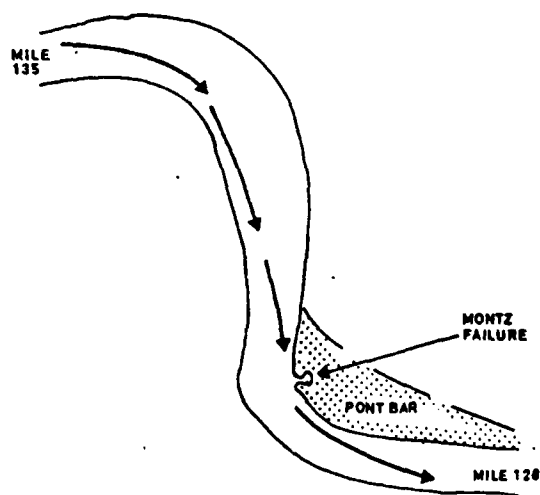
b HYPOTHETICAL MAXIMUM CURRENT VECTOR AT FLOOD STAGE. MONTZ FLOW FAILURE.

FIG. 7·5

Sediment is supplied to the river chiefly by erosion on the steep concave bank of a bend. However, at flood stage, when the transverse flow is intense, deep erosion becomes acute not on the concave bank, but on the leading edge of the convex bank which is often point bar material. This process of erosion and deposition on the next point bar downstream leads to a relentless migration of the meander pattern in the natural stream. The stream is constantly reworking old deposits and since these are irregular the meander pattern is often distorted. It is these processes which engineers seek to control by canalising a river.

The flowslides which are the subject of the second part of this dissertation are only ever found to occur where an actively eroding bank is composed of point bar deposits. Torrey,1975, has shown that the worst failures of recent years have all occurred on the leading edge of active point bars, Fig. 7.5b. As discussed above, the maximum current vector at depth tends to straighten out to cut the corners when the river is in flood. It is reasonable to suppose that this maximum velocity vector strikes the bank just at the point where these failures occur. Powerful eddies are known to develop where the current strikes the bank. The eddies are capable of rapidly excavating a steep sided scour pit in the river bed. Since the scour hole will be very close to the side of the channel, the river bank may be oversteepened and may fail. If the bank material is a fine sand it may be caused to flow into the scour pit and will be very rapidly carried away by the river.

In Section 1.3 it was pointed out that a critical requirement for the propagation of a flowslide is that the material, however it assumes a liquefied state, must be able to flow unimpeded from the site of the failure. The mechanics of the flow of a granular suspension have been researched by sedimentologists and chemical engineers but since this important work is not referenced in the engineering literature on liquefaction it is reviewed in the following sections.

7.3   Flow of Granular Material

7.3.1   Introduction

In this section it is intended to review at some length what is known about the flow of aqueous suspensions of granular material. From this general review will develop several ideas which are of use in reconstructing the events which are experienced in the field as flow failures.

There is an extensive engineering literature on liquefaction. Of the many review papers those by Seed, 1976, and Casagrande, 1976, have discussed the mobility of granular materials under static and dynamic loading. Terzaghi, 1950, discussed the classification of landslides; Koppejan et al., 1948, Bjerrum et al., 1961 and Bishop et al., 1969, describe field examples of liquefied flow and many other references are listed in the bibliography.

Of interest in this dissertation is the process by which granular materials, which may be set in motion by a landslide, can in certain circumstances continue their motion and flow on very shallow slopes to form a deposit far from their origin. The opportunity has been taken to review some of the work published by geologists and sedimentologists who have undertaken extensive research into the fossil remains of old sediment flows.

7.3.2   Classification of Flow Types

It will be useful first to divide the flow of granular suspensions into several groups. Middleton and Hampton, 1973, make a distinction between 'sediment gravity flow', and 'fluid gravity flow' . A 'fluid gravity flow' is maintained by the flow of a transporting liquid under gravity. This is the condition of both the suspended and bed load of sediment in a river, and of windblown sand; Bagnold, 1954, Allen, 1970. A 'sediment gravity flow', on the other hand, is propelled principally by the action of gravity on the sediment, which in turn entrains the interstitial fluid. It is this latter case that is of interest here.
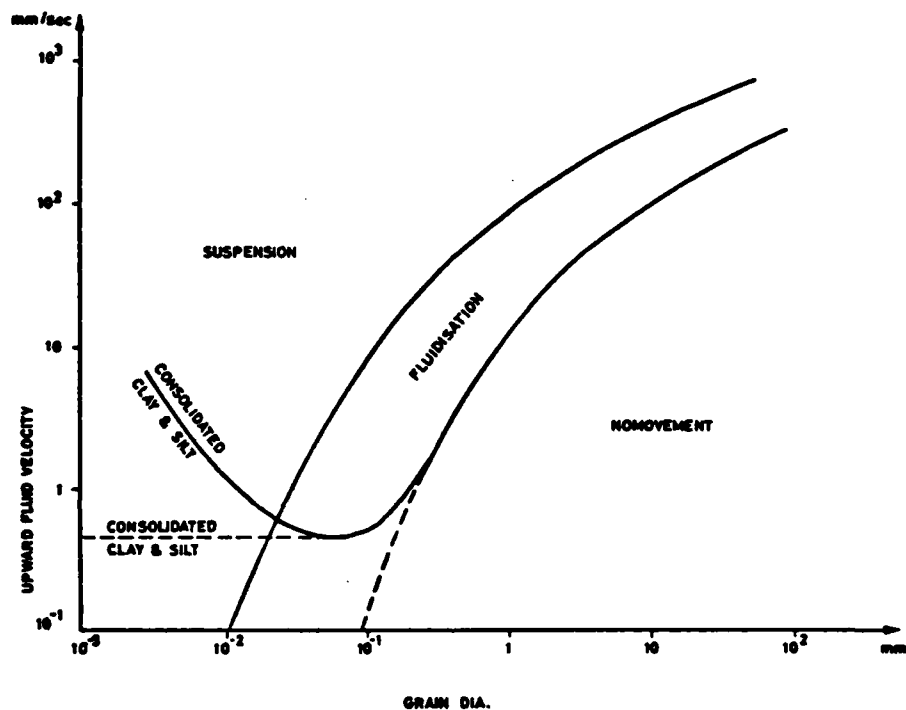
FIG. 7·6 RANGE OF FLUIDISATION AND MINIMUM FLUIDISATION
VELOCITY (Taken from Lowe 1975)

The same authors further classify subaqueous 'sediment gravity flows' into four groups, according to the mechanism of sediment support within the suspension.

Classification		Support Mechanism
7.3.3	Fluidised and liquefied flow	Relative velocity of fluid past grains
7.3.4	Grain flow	Intergrain collisions
7.3.5	Debris flow	Matrix of finer particles
7.3.6	Turbidity and density currents	Turbulence

All these four flow types will be discussed below, though only the section on Fluidised and Liquefied Flow is found to be of immediate relevance to the discussion of Mississippi flowslides.

7.3.3 Fluidised and Liquefied Flow

It is important first of all to distinguish between a fluidised and a liquefied bed. In both cases the grains are supported by their own relative motion through a fluid. The major difference is that the fluidised bed is in dynamic equilibrium and the liquefied bed has a finite lifetime.

Fluidised sediment occurs where pore fluid is pumped upwards through a granular bed and exerts a drag force on the grains equal to the force cf gravity. No resedimentation occurs and the process is in dynamic equilibrium. The bed is fluidised over a range of fluid velocities. Provided the bed is loosely packed, the grains first lose contact with one another at the minimum fluidisation velocity, Fig. 7.6, (cf. Fig. 7.3). As the fluid velocity is increased the effect on the particles is to maintain them further apart: the bed expands stably until at a certain limiting velocity the uppermost grains are carried away. In other words the fall velocity of a grain aggregate depends on the concentration of the grains; the expression derived by Richardson and Zaki, 1954, for this is:

$$\frac{W_d}{W_\infty} = (1 - C)^n \tag{7.2}$$

where W_d = fall velocity of the dispersion

W_∞ = free fall velocity of single particle

n = exponent varying from 4.65 at low R_e to 2.39 for $R_e > 500$

C = concentration = $\frac{1}{1+e}$.

Further work on the relationship between W_d and W_∞ may be found in Davidson and Harrison, 1963, and Maude and Whitmore, 1958.

Lowe, 1976.ii, has shown that it is not possible for fluid, which is escaping from the resedimentation of a liquefied stratum, to fluidise over-lying layers of the same grain size. However, it is common for beds of granular material to fine upwards and in this case superficial layers of fine sand may be fluidised by water escaping from the resedimentation of deeper coarser liquefied layers (Ambraseys and Sarma, 1969). This is assumed by Seed and Idris, 1967, to have been the mechanism responsible for the collapse of the tower blocks during the Niigata earthquake.

If the fluidised bed experiences no lateral support or indeed is sloping in the earth's gravitational field, it may be able to flow. It is likely that such flow will remove the granular material from the source of upwelling water in which case the grains will start to resediment and the layer will revert to the state of a liquefied bed.

The same relations apply for a liquefied layer as for fluidisation, although the depth of fluid supported grains is steadily decreasing since as the grains fall under gravity a surface of resedimentation moves up the suspension. In the time that the grains are suspended the entire layer may be occasioned to flow downhill; but the flow, without a continuous supply of upwelling water, has a finite lifetime.

There are three distinct routes by which a stratum of granular material may assume a liquefied state. The first, through fluidisation, has been discussed above. The second may be characterised as 'liquefaction before failure' and the third by 'liquefaction after failure' of, for example, a slope of granular material.
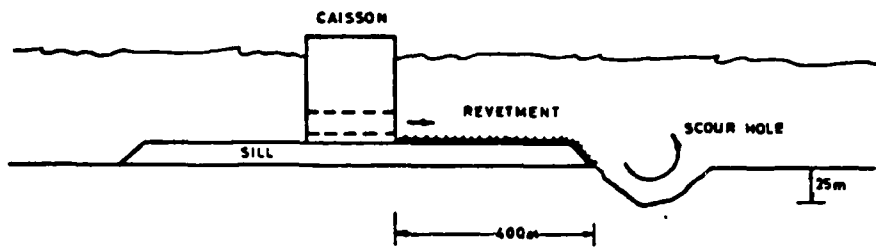
FIG 7·7 OOSTE SCHELDE CLOSURE CAISSONS
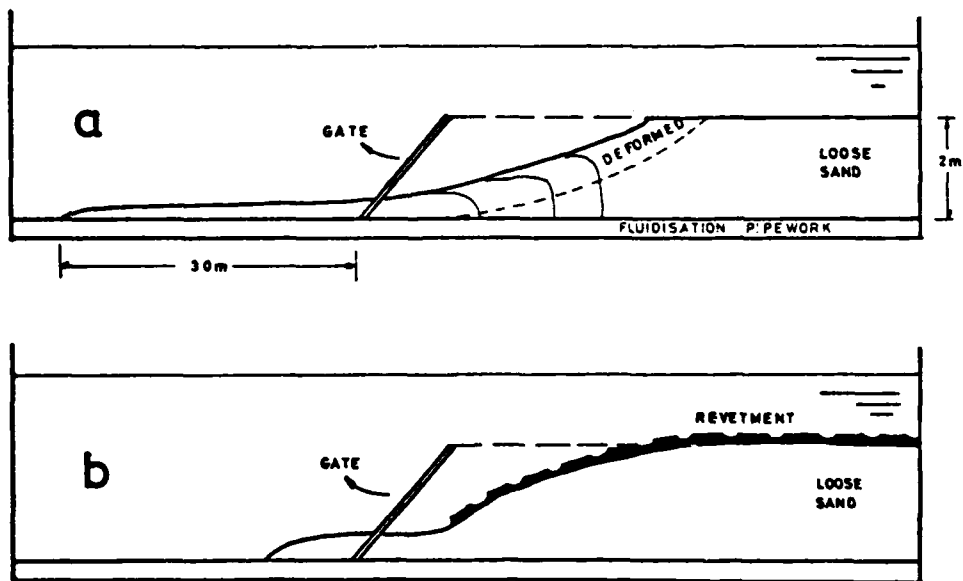
FIG 7·8 EXPERIMENTS ON THE SPONTANEOUS FLOW
OF LOOSE SAND

MICROCOPY RESOLUTION TEST CHART
NATIONAL BUREAU OF STANDARDS 1963

2.   Tests 3DM1-3 preliminary tests with fine sand at 100g.
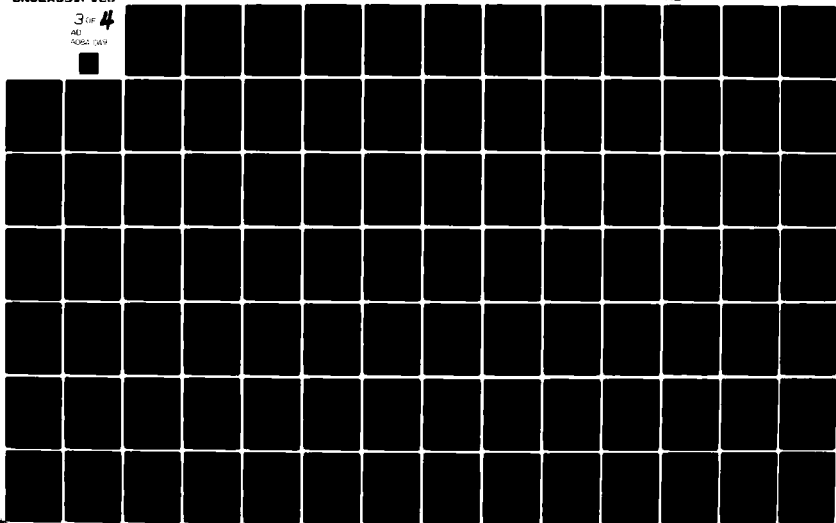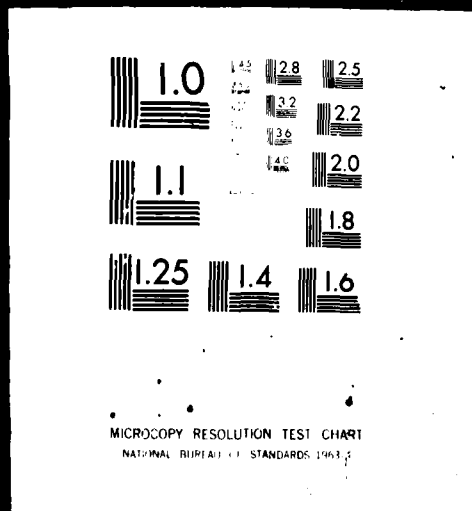
Liquefaction before failure has been extensively researched recently and is essentially the spontaneous liquefaction of Terzaghi, 1956, which requires the collapse in situ of a metastable structure of grains. If unsupported, the liquefied bed may start to flow. Generally speaking the initiation of liquefaction in such a stratum occurs progressively. A shock loading is normally required to cause spontaneous liquefaction of an entire stratum.

As an example of research into this aspect of liquefied flow, some recent experiments by Dutch engineers at the Delft Hydraulics Laboratory, 1977*, show how a 2 m thick layer of very loose sand is in certain circumstances able to generate a flow. The problem was the stability of the sills and revetment either side of the closure caissons, Fig. 7.7a, on the Ooste Schelde sea arm in Holland. The revetment is designed to resist erosion and is anchored at its end by a heavy beam. There is a danger that a scour hole will develop at the edge of the matting and that sand will start to flow into this hole from under the revetment. The aim of the experiments was to show whether the revetment inhibits the flow of sand.

A series of experiments has been carried out in a flume 3 m × 3 m × 60 m, Fig. 7.8 in which a 2 m layer of sand was brought into a loose state by fluidisation and resedimentation. The restraining gate was rapidly removed and the propagation of the resulting flow behaviour of the sand observed. Interestingly the sand only flowed at all if extremely loose (relative density < 45.5% for a 2 m layer of Haringvliet sand, D_{50} = 145µ). The profile after flow is shown in Fig. 7.8a. Also of interest here is that when the matting was present very much less sand was seen to flow, Fig. 7.8b. This latter observation has clear relevance to the interpretation of the Empirical Criterion made in this thesis. The clay overburden in the Mississippi may also inhibit sand flow. The experiments reported above are planned to be repeated for a 10 m thick sand layer in a modified canal

---

*Unpublished data communicated to the author by A. van Os, 1977.

lock.

Liquefaction after failure applies generally for a denser or partially saturated stratum. Of primary interest in this dissertation is the phenomenon of retrogressive failure in a dense sand deposit, becoming shallower as it goes. Sand falls off the face and forms a carpet of sedimenting grains at the foot of the face. This carpet is a liquefied layer with a finite lifetime which flows away from the face, but the layer from which it originates may be extremely dense. A second example is given by the flowslide at Aberfan. Bishop et al, 1969, argued that the failure along an old slip plane of part of the slope allowed large shear deformations to build up in certain saturated layers. The shear deformation was accompanied by undrained volume contraction of the soil matrix and associated positive pore pressures. The soil partially liquefied when the pore pressures had built up high enough to reduce the shear resistance throughout the saturated soil to a value below the applied shear stress. The waste tip was located on the edge of the valley slope and the liquefied debris was able to flow freely downhill.

Both of these topics, liquefaction before and after failure, will be related to the phenomenon of Mississippi river bank stability in Chapter 10. Whichever of these two initiating events is involved in a particular failure, the conditions for the development of a flowslide are more complex than is suggested by a mere study of the initiation of 'liquefaction'. A flow failure will only develop as discussed in Section 1.3, if the material is caused to start flowing, is maintained in flow, and has somewhere to flow to. The conditions for this unobstructed flow will depend on the details of the site of the failure and very likely also on the geometry of the mechanisms of deformation of overlying layers.

The rate of flow of a liquefied layer under shear has been predicted from several different viewpoints. Morgenstern, 1967, used the Chezy equation because his main interest was the high velocity turbidity

currents. Allen and Banks, 1972, treated a liquefied sand layer as a viscous fluid, and Lowe, 1976 used the equations of Keulegan, 1958, and Middleton, 1966, arguing that the flow of a liquefied sand layer is in fact a form of density current.

7.3.4   Grain Flow

The phenomenon of grain flow was postulated by Bagnold, 1954, whose early researches into the shearing of granular suspensions are still relevant. Grain flow, Bagnold, 1954 and Middleton, 1969, is a flow process which can occur with no excess fluid pressures and generally occurs on slopes steeper than the angle of repose of the grains. The dispersion of rolling grains is maintained by the transfer of momentum at interparticle collisions. If the interstitial fluid is viscous the grains may be deflected from collision by the shear resistance of the fluid.

Except where interstitial fluid pressures or suspended fines modify the flow, a grain flow is usually restricted to steep slopes and thin layers (maximum 20 cm for a fine sand), Lowe, 1976.i and as such is not directly relevant to the present study.

7.3.5   Debris Flow

The equations for grain flow show that if the interstitial fluid were mud of density $2\gamma_w$ the slope angle necessary for inertial grain flow can be as little as 5°. The term debris flow covers the flow of poorly graded material, Enos, 1977, Rodine and Johnson, 1976. The presence of colloidal particles gives the interstitial fluid a finite yield strength which can support fine sand particles. The density of the water/clay/sand mixture is sufficiently great to support coarse sand particles, and so on until a small percentage of large boulders or aggregates can be supported by a matrix of finer material. In certain parts of a flow, where the shear strain rate is low, the material 'freezes' and is rafted along as a rigid plug.

7.3.6 Turbidity Current Flow

This is a mechanism of flow which is able to carry sediment many miles over the deep ocean bed. The flow is usually intermittent and resembles a subaqueous stream.

For a history of the evidence for turbidity currents, see Menard, 1964, Middleton, 1969, Morgenstern, 1967 and Walker, 1973. Briefly there are extensive deposits of graded sand on the ocean bed beyond the continental shelf which for various reasons could not have been deposited by ordinary ocean currents. The deposits contain evidence in the form of fossil organ- isms that they have been displaced from shallower waters. It is at present accepted that these deposits are the result of turbidity currents which are able to move at extremely high speeds over the bed of lakes or the sea.

Typically, sediment from the land builds up on the continental shelf until it becomes unstable. The sediment may have been deposited rapidly and so be underconsolidated, in which case slumps may be initiated on slopes angled at only a few degrees to the horizontal, Shepard, 1963. When such a slump of loose material is channelled into one of the steep submarine canyons that descend from the continental shelf, it may become accelerated and diluted to form a liquefied flow of sediment. Eventually, when the flow down the canyon becomes sufficiently rapid it becomes turbulent and flows as a density current downslope. Leading from the mouths of these submarine canyons channels are sometimes found, Menard, 1964, with, on either side, natural levees which contain the stream and enable the turbidity current to flow for many miles out to sea.

7.3.7 Concluding Remarks

In conclusion to this Chapter it should be noted that the different types of flow described above may evolve such that, for instance, a liquefied flow may develop into a turbidity current, or a fluidised flow into a grain flow if factors such as the slope of the bed or fluid supply are changed. In the next Chapter certain aspects of liquefied flow will be considered in

detail and a new analysis is developed to account for the phenomenon
of flowsliding in the Mississippi. Other flow processes, grain flow and
turbidity current flow, may play a part in the phenomenon, but they do not
enter explicitly into the analysis. The new analysis quantifies the effect
of scale on liquefied flow behaviour and thereby an assessment can be made
of the usefulness of a centrifuge in modelling a flowslide.

CHAPTER 8

MISSISSIPPI FLOWSLIDES - EROSION TEST SERIES

8.1 Introduction

In this Chapter an account is given of the experiments which were performed to attempt to model on the centrifuge the phenomena which occur when a cohesive overburden layer is undermined on a river bank by the flow and removal of its fine grained substrate.

Before it was possible to try to model a flowslide it was necessary to make some assumptions about the material properties required and the nature of the erosion event that precipitates a flowslide in point bar material. The first major decision was whether to orient the tests towards producing the extremely loose specimens that would be required to initiate a truly spontaneous liquefaction. In seemed unlikely that extremely loose sands were a prerequesite for the development of a flowslide since much of the sand found along the Mississippi itself was relatively densely packed*.

Formidable experimental difficulties were anticipated in testing very loose subaqueous sands on the centrifuge and it was decided that a more fruitful approach would be to attempt to model the complete two layer system with a uniform sand of medium density and an homogeneous layer of clay. At a later stage tests were envisaged with prototype sands but in the first instance a uniform sand (Leighton Buzzard 70-120 μm) slightly finer than the prototype sand (Reid Bedford D_{50} = 180 μm) was chosen. The first few tests were, however, set up with the sand layer as loose as possible. It was found that the voids ratio of the sand after consolidation of the overburden was the same whether it was set up loose or compacted by hand and so the latter alternative was taken in later tests since it considerably simplified the experimental technique .

_____

*Torrey, 1976, personal communication.

The perturbation which initiates failure in the field was understood to be oversteepening of the river bank due to scour by the river. Accordingly a mechanism was sought by which the model river bank could be oversteepened. A technique was chosen that involved the removal of a portion of the front face of the model slope by a water jet. There were two possible ways of doing this. Firstly the jet could be located in front of and directed upon the slope to wash out material from the sand layer. Alternatively, the water jet could be directed outwards from within the slope to remove the material directly. The latter option was chosen on the basis that it involved less disturbance to the surrounding material, the degree of which would be unknown in any event. In hindsight the choice was justified by the arguments presented in Chapter 10: that the phenomenon of liquefaction involved may be a retrogressive propagation of failure in a dense sand and not a spontaneous collapse of the entire layer. The water jet served only to establish a vertical sand face and to remove debris that fell off that face. The jet had no further effect on the slope.

8.2   Test Objectives

The tests were initially undertaken for two objectives. Firstly, they were designed to test the hypothesis that two distinct modes of plastic collapse of the cohesive overburden would be observed depending on whether the underlying sand layer was thick or thin with respect to the clay. These two modes of behaviour were expected to affect the flow behaviour of the sand in different ways.

The second and parallel objective of the tests was to see whether at model scale, behaviour would be observed which could be interpreted as analogous to flow behaviour at full scale. At this stage in the planning the theory that is presented in Chapter 10 had not been developed and it was not obvious how flow behaviour would scale on the centrifuge. Despite this
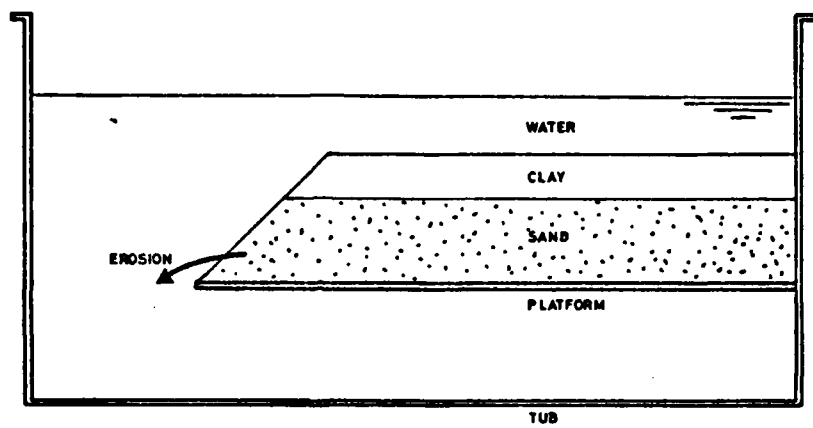
FIG. 8-1 SECTION VIEW OF MISSISSIPPI RIVERBANK
MODEL.

reservation, craters were obtained in the sand layer which undermined the overburden and mechanisms of interaction between the two layers were observed. The first objective mentioned above was achieved successfully.

The idealised model river bank consisted of two layers of material: sand and a clay overburden. These layers were placed subaqueously on a platform in a large steel tub on the centrifuge. The two layers were cut to a smooth batter along the front of the platform to model the river bank, Fig. 8.1. In this way any material that was released by a failure of the bank could be carried away by the water jet, fall off and settle underneath the platform, modelling the removal of debris by the river. The model was constructed using the apparatus described in the following sections.

8.3 Apparatus

The purpose of the apparatus in this series of tests was to contain and provide the services to the idealised model described above. The apparatus was also designed to form the nucleus of a standard range of apparatus for future research workers on the centrifuge. As was the case for the Thames Flood Embankment tests, very little ancilliary equipment was available on the centrifuge at the time these tests were planned and consequently many items were required for the complete set of apparatus. In many ways the experimental series described here represents as much a development of the facilities and operation of the Cambridge centrifuge as of the experimental techniques themselves. The sequence of photographs, Plates 8.1-8 show the equipment in use.

The steel tubs, were 850 mm in diameter and 400 mm deep, fabricated from mild steel, rolled, welded and machined to 8 mm wall thickness. The base of each tub was designed to fit on the swinging platforms of the centrifuge, Plate 8.6. The top flange of the tub bolts onto the lid which functions as a pressurised water tank, Plate 8.4 and a mounting frame for displacement transducers, Plate 8.3. The tub and lid comprise the basic strong box which
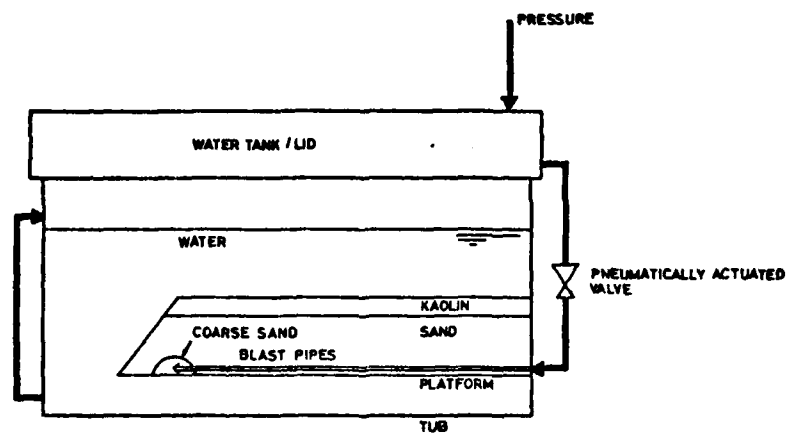
PLUMBING FOR EROSION TEST
VERTICAL SECTION
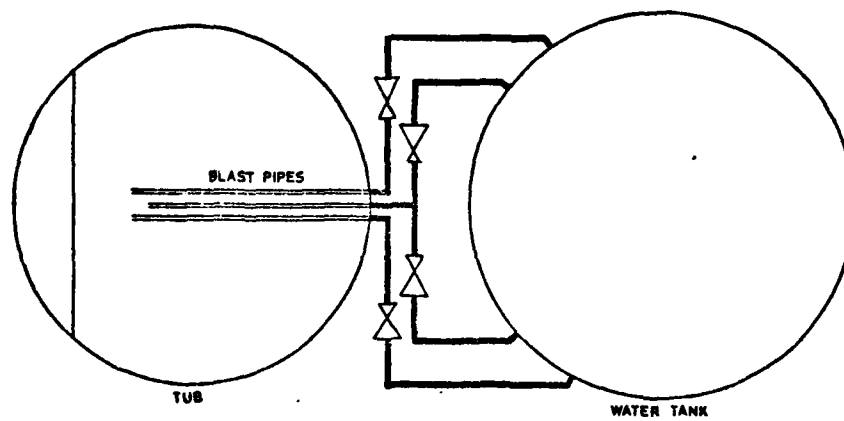
SCHEMATIC REPRESENTATION
TOP VIEW

FIG. 8·2

must contain any conceivable catastrophic events within the model. The

equipment was designed using plastic design theory, Calladine, 1964, and

proof tested full of sand and water to the maximum speed of the centrifuge.

The platform is supported 75 mm clear of the base of the tub on steel

webs welded to its underside. The platform is divided into two portions,

the smaller of which forms a 90° sector of the circle and could be removed

to leave the straight edge of the larger portion overhanging the space

between the platform and the base.

The erosion event was modelled using a water jet which issues from three

nozzles, Plate 8.1. The nozzles are directed towards the front of the model

river bank, perpendicular to the stream alignment and are situated under the

crest of the slope. The first ten tests 3DM1-10 (Table 2, discussed

below) were devoted to finding a suitable arrangement of nozzles and plumb-

ing to give an efficient blast of water. The final arrangement is shown in

Fig. 8.2 with three blast pipes all connected independently to the pressurised

water tank. This arrangement ensures the removal of a vertical slice of

sand in the front of the slope. The neighbouring sand collapses into the

crater and is removed by the water blast.

Tests 3DM19,20 were performed on the laboratory floor instead of on the

centrifuge and for these the consolidation was achieved using a large con-

solidometer designed by the author and built for the purpose, Plate 9.2.

8.4   Materials Used

The soils used were all readily available commercially. It was intended

to continue the test series by using prototype soils, but in the event

these tests were never required. The use of standard laboratory soils

reduces the number of parameters which are free to vary in the tests; they

were cheap and reliable.

Fine Sand

The sand used was fine Leighton Buzzard sand of 120/200 seive size

(fine sand, uniform grain size 70-120μ). Maximum and minimum voids ratio tests gave a variation of 0.68 < e < 0.98 for dry sand. After sedimentation through water an e value of 0.85 was achieved and after disturbance and consolidation on the centrifuge the voids ratio was regularly around 0.72 regardless of the initial density of placement.

Ground Silica Sand (Silt)

For various reasons to be discussed in Section 8.9.2, a very much finer material was used in Tests 3DM4-12. This was a commercially ground silica sand finer than 350 sieve. The grains were so angular that the material was self supporting on near-vertical subaqueous slopes for several hours. This interlocking caused the material to dilate intensely when sheared but on the other hand to flow like a very viscous fluid under cyclic stress. The ground silica did not behave like a natural river sand and it was abandoned after the twelfth test. Its voids ratio after consolidation on the centrifuge was approximately 0.70 in all tests.

Clay

The clay layer was composed of kaolin, mixed with water to form a slurry and consolidated on the sand layer in the centrifuge. The maximum surcharge loading applied during consolidation at 100g amounted to 96 kN/m^2 after which the kaolin was allowed to swell under self weight loading only. Moisture contents measured immediately after the tests revealed a voids ratio of typically e = 2.1. The clay layer was heavily over-consolidated in all tests.

8.5 The Test Series - Outline

In total twenty tests were performed with this apparatus. Each test was given a code number beginning 3DM (3 Dimensional Mississippi) to aid in centrifuge planning. The tests may be divided into six groups:

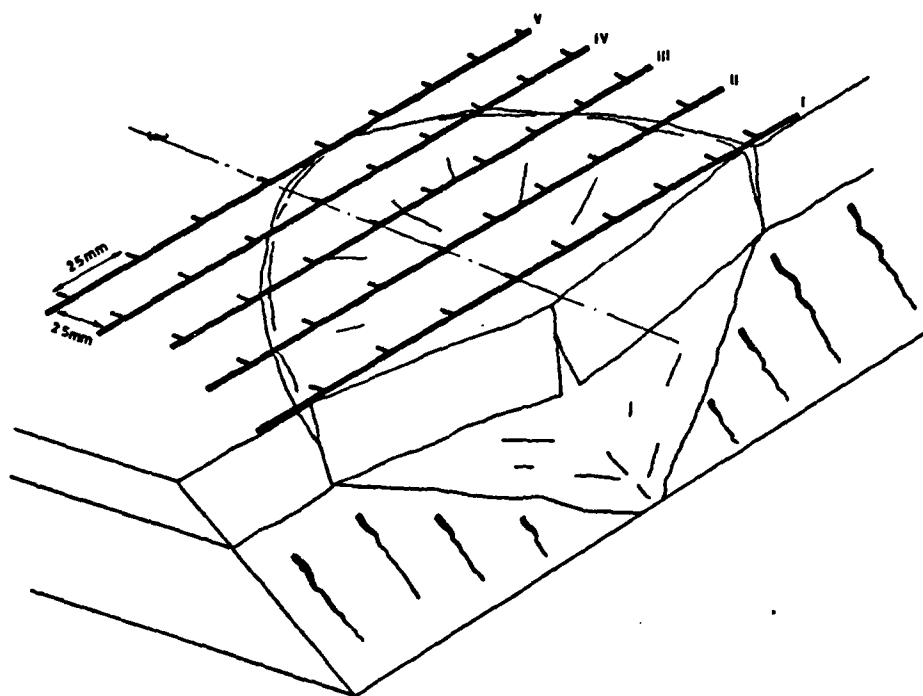1. Preliminary test in modified apparatus.

FIG. 8·3 LINES ALONG WHICH AFTER-FAILURE PROFILES
WERE TAKEN

2.   Tests 3DM1-3 preliminary tests with fine sand at 100g.

3.   Tests 3DM4-12 attempt to model flowslide with ground silica.

4.   Tests 3DM13-14 tests with fine sand at 50g.

5.   Tests 3DM15-18 tests with fine sand at 10g.

6.   Tests 3DM19-20 tests with fine sand at earth's gravity.

The most important parameters of these tests are given in Table 2, bound at the end of the dissertation. In Section 8.6 the test preparation and procedure are described. In Section 8.9 the tests are discussed individually.

Few quantitative observations were made during the tests described in this series. So many factors were involved in the development of the experimental method that the entire test series is in one sense preliminary as successive unnecessary features were eliminated and it was eventually realised that the centrifuge itself was not essential for the tests.

8.6   Model Preparation and Test Procedure

In the following description reference should be made to Plates 8.1-8. A model river bank was prepared for test in the following way. The tub was filled with water and the spaces under both portions of the platform were thoroughly de-aired. The blast tubes were purged of air and capped with small adhesive hats to prevent the ingress of sand. The sand was carefully pluviated through the water. In the first tests, which were prepared with extremely loose sand, the sand was placed damp and was later saturated. Many problems were experienced with these loose highly unstable layers. Later tests with the fine sand concentrated on the behaviour of the clay and for these the sand layer was compacted by hand vibration in layers under water which gave a more repeatable result.

In Tests 3DM4-12 where ground silica was used, it was necessary to allow the material to settle for several hours. When this sedimentation was complete a surcharge loading of 30 kN/m^2 was applied to consolidate the silica. The load was removed and a layer of kaolin slurry (160% water) was

BEFORE TEST

100 mm

32mm KAOLIN

65mm 120/200 SAND

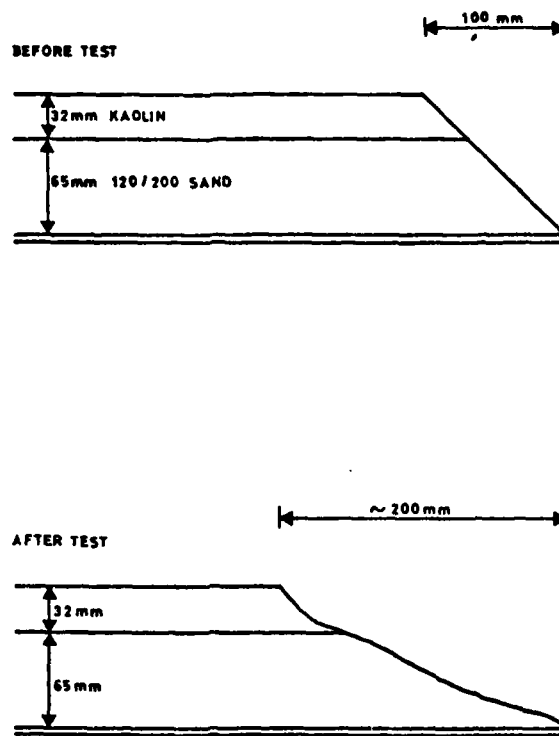AFTER TEST

~ 200 mm

32 mm

65 mm

FIG. 8·4 PRELIMINARY MODEL TEST

poured over the top. This was in turn levelled and covered with several layers of 'wet strength' filter paper and the edge sealed with tissue paper. A surcharge plate of half inch mild steel was placed on top of the filter paper and the model was ready for consolidation. This was achieved in four increments of gravitation on the centrifuge and terminated when the settlement of the plate was completed at 100g.

The machine was then stopped and the surcharge plate and filter paper removed. The excavation was performed by hand, Plate 8.5, the smaller portion of the platform removed and the final batter shaped to a slope of 30° by ruling off excess material between the front edge of the platform and a wooden template on the upper surface of the model. The tub was refilled with water, a steel weight placed in the tub to redress the inbalance caused by the excavation and the lid was bolted on and plumbed up to the blast tubes. The model was then ready for testing.

8.7 Test and Observations

Before the water blast was fired the model was accelerated to the required 'ng' value for ten minutes to allow the excess pore pressures to dissipate in the sand. A two minute jet of water was then fired through the blast tubes. The test was usually conducted blind although an attempt was made to follow the failure in several of the later tests by using displacement transducers mounted on the lid, Plate 8.3. The centrifuge was stopped, the tub was opened and the failure observed and measured.

The topography of the model failure was in all cases mapped by measuring the depth to the surface from a 'perspex' plate mounted on the top flange, Plate 8.8. The perspex plate was drilled with a square array of holes through which thin graduated perspex rods could be passed. The grid of measurements and the profiles plotted in the figures which appear in the following sections are shown in Fig. 8.3.
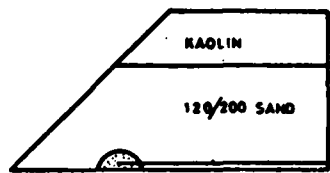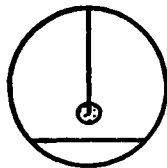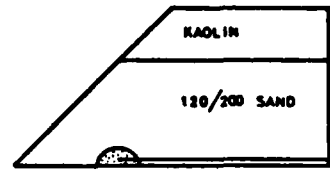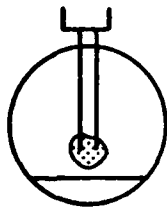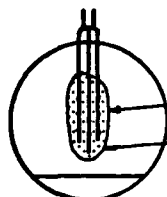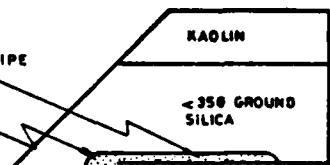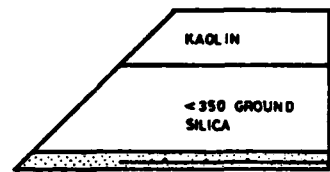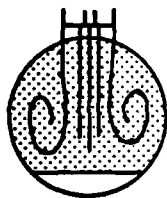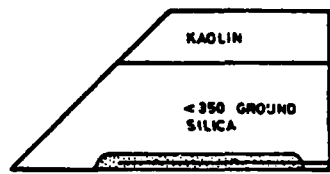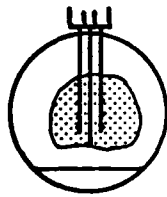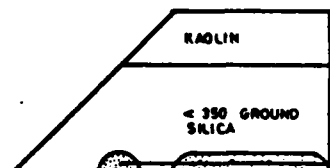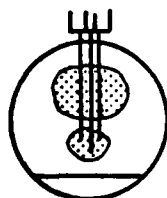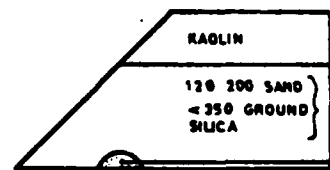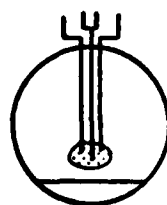
FIG 8·5 DIAGRAMS SHOWING ARRANGEMENT OF
PLUMBING AND COARSE SAND LAYER

8.8 Preliminary Test

Before the design of the main range of equipment was finalised, one preliminary test was performed in a modified cylindrical tub borrowed from the centrifuge facility at Manchester, (U.M.I.S.T.). The test was planned and prepared with the assistance of A. Mochizuki of Osaka City University who was a visitor at that time. The test procedure and equipment were essentially the same as that just described. The test failed because the single blast pipe became filled with sand and was not able to clear itself under the pressure applied. The test served to prove the basic concept of model preparation and to measure the time required for the consolidation of the layers. The initially oversteep slope, Fig. 8.4, of fine sand and clay failed over its whole length and retreated to a slope of 1:2. The blast pipe was not able to produce a crater of any sort.

8.9 The Main Test Series

For each test performed the plumbing pattern within the sand layer is shown in Fig. 8.5. Where available, a series of profiles across the failure is given with the description of each test. The relevant data for each test is given in Table 2 which folds out at the end of the dissertation. The ratio O/A relates to the relative thickness of the clay and sand layers, see Fig. 1.14a.

8.9.1 Preliminary Tests with Fine Sand at 100g

3DM1   O/A = 0.43

The sand layer was compacted with 8% moisture since this method was found to give the loosest possible packing. The sand was then slowly, though imperfectly saturated by adding water to the base of the sand layer from an external reservoir. One single plane ended blast pipe was used, connected
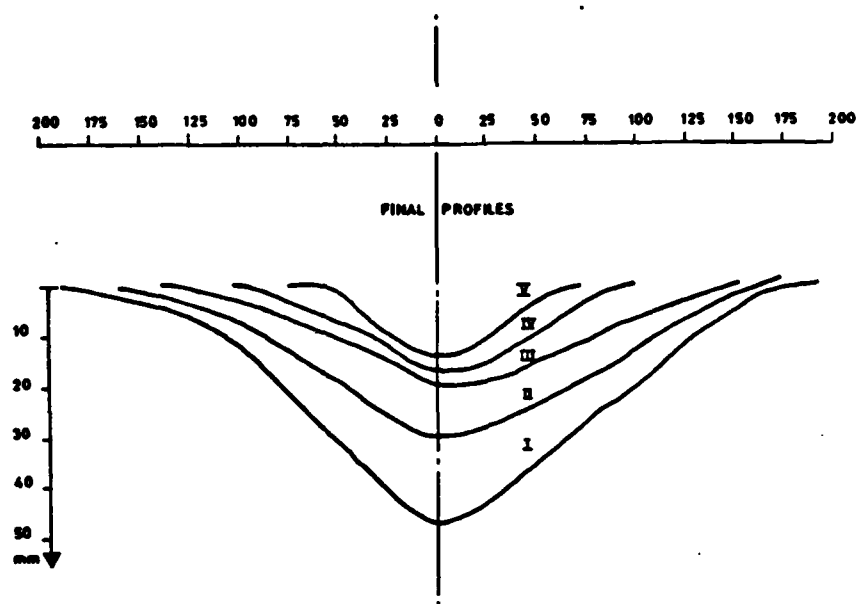
FIG. 8·6   3DM2

through a valve to the pressurised water tank. The mouth of the pipe was located in the slope 5cm back from the crest. Difficulties were encountered placing the clay layer on top of the extremely loose sand.

When the water blast was applied, no sand was removed from the front face of the slope. The only failure which occurred was one by vertical piping of sand above the end of the blast pipe. The blast (250 kN/m^2 in the water tank) was fired at 100g. The blast pipe was modified for Test 3DM2.

3DM2   O/A = 0.42

In this test the blast pipe was of larger bore than that used in 3DM1 and it was longer such that it terminated under the crest of the slope. The pipe was fed by two ¼" BSP valves from independent tappings in the tank to increase the flow rate of water in the blast. The two valves failed to operate at 100g and so the machine was slowed down.

At some stage during the deceleration of the machine, probably below 10g, the valves opened and caused sufficient erosion of the sand slope to give a very clear 'fold-down' type of failure, Fig. 8.6 and Plates 8.9 and 8.10. Erosion was imperfect however, and the crater had not developed fully in the sand layer. The folded down portion of the clay plate was still attached to the parent layer at the base of its cross section. The clay surface in this test was covered with sand, which at the low ng value at which the valves had fired, had been carried onto the clay surface by the turbulence of the water. At higher ng values the sand is centrifuged out of suspension and settles under the platform.

The crack pattern, Plates 8.9-10, was circumferential over the upper surface and radial on the underside of the failed clay plate. The mode of failure is similar to that predicted by yield line theory for the plastic collapse of a reinforced concrete slab subjected to a point load on a free edge.
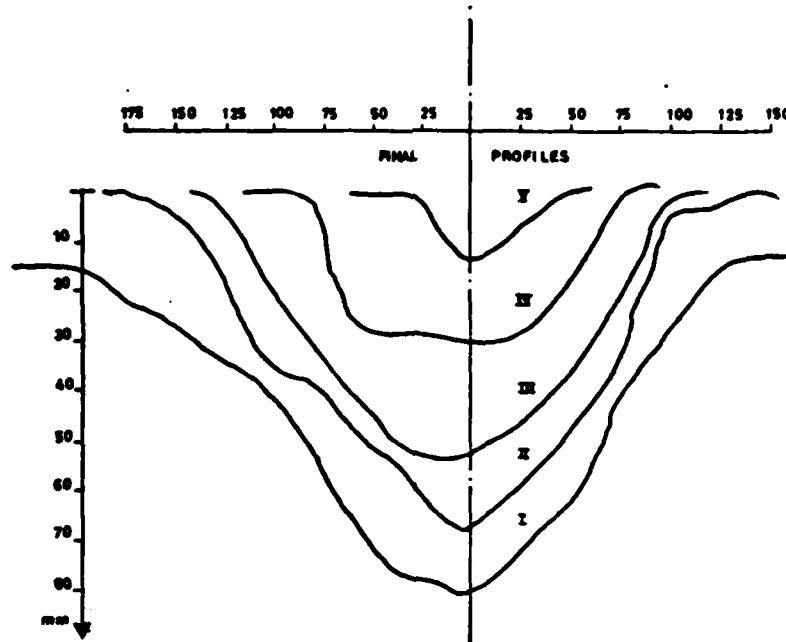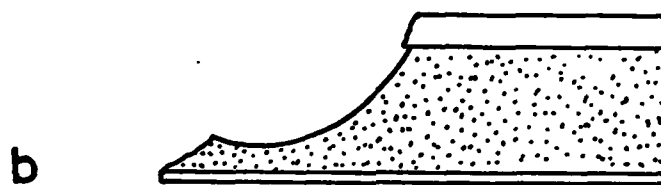
FIG. 8·7   TEST 3DM3

One longitudinal crack on the surface was initiated at an imperfection caused during model making. The profiles shown in Fig. 8.6 are equivalent to the soundings which would be made of a failure on the Mississippi river bank. The clay layer is largely intact and blanketing the surface of the crater. The resulting cross sections of the failure show gentle slopes which are equivalent to a 'shear type' failure in the field, as will be seen in Chapter 9.

At this early stage in the test series this result was seen as a success. The cracking pattern was clear. The significance of the fact that this model actually failed at a low value of ng was missed at the time and the following test was planned at 100g with a thicker sand layer to test whether a different failure mechanism would occur.

3DM3   O/A = 0.24

In Tests 3DM1 and 3DM2 it had proved extremely difficult to apply the kaolin slurry to the loose saturated sand layer without initiating a contraction and expression of water from the sand, which created inhomogeneities in both the sand and the clay layers. In this test the sand was tamped dry and the same slow and imperfect process used to saturate the sand as had been used in the two previous tests. The plumbing was changed again for this test to try to improve sand removal in the crater and comprised twin plane ended blast tubes connected independently to larger valves ($\frac{1}{4}$" BSP).

The cross sections of the resulting failure, Figs 8.7a,b and Plate 8.11 show that the blast tubes were still not entirely effective in removing the sand. In this test, the sand layer was thicker than that used in test 3DM2 and the clay layer was slightly thinner, Table 2, such that the ratio over- burden thickness/sand thickness was only 0.24. The failure was different in kind from 3DM2 and is called a 'breakaway' type failure in this disser- tation. In this case the clay plate had separated away from its parent layer and disappeared on the flowing sand. A neat bowl failure was left, Plate 8.11
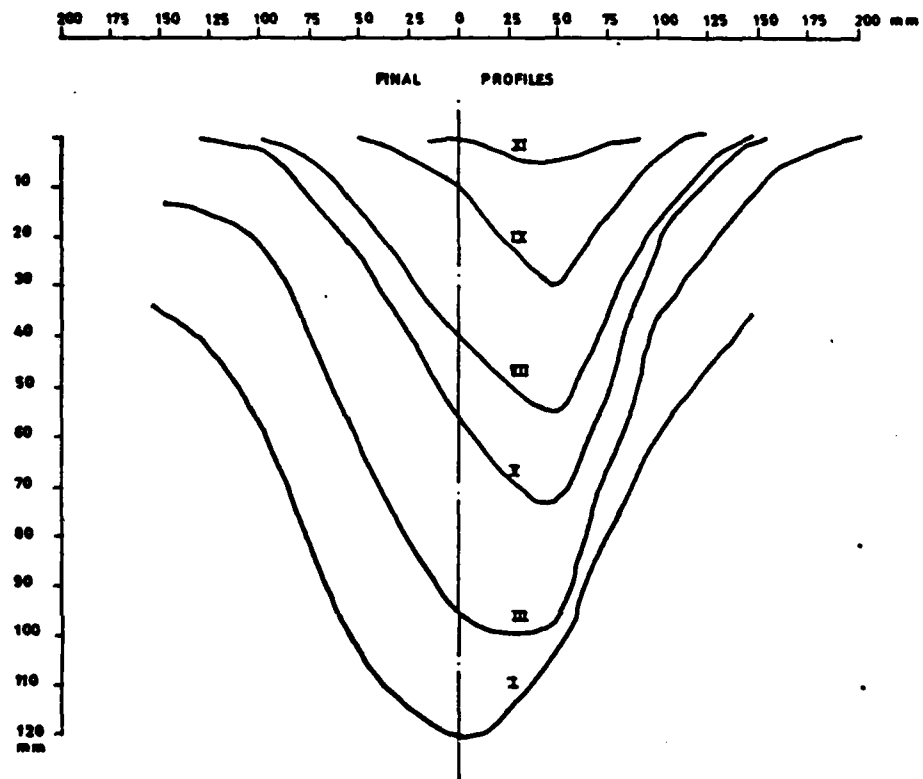
FIG. 8·8   3DM4

which had not propagated further. The profiles shown in Fig. 8.7 indicate that the failure is considerably steeper sided than that produced in Test 3DM2.

The hypothesis that two distinct failure mechanisms would be observed was validated by this test although the conditions that decided which type of failure should occur remained to be determined. The following test was planned to investigate further the possibility that a liquefaction flowslide could be modelled on the centrifuge.

8.9.2   Attempt to Model a Flowslide with Ground Silica Sand

3DM4   O/A = 0.30

In an attempt to reduce the permeability of the sand layer, a new finer material was substituted. It was hoped that the reduced permeability would allow excess pore pressures to remain long enough to enable the fine material to flow and thereby generate a flowslide on the model. This new material was a commercially ground silica sand finer than 350 mesh. The sample was prepared by pouring the silica slowly through water and allowing it to settle. The silica was preconsolidated at 30 kN/m^2 before the clay layer was applied.

Three blast pipes with nozzles were now used, interconnected; the central pipe longer than the others. Three small holes were drilled in each pipe as shown in Fig. 8.5 to supply water to the silica if it required to dilate. No excess water pressures were hereby injected into the silica since a layer of coarse sand surrounded the tiny holes and communicated with the external water.

The failure obtained was very large, Fig. 8.8 and Plate 8.12, involving three distinct terraces of retrogressive slip. The clay layer had broken away all round the edge of the rather irregular crater which was taken at the time to be a model flow failure.
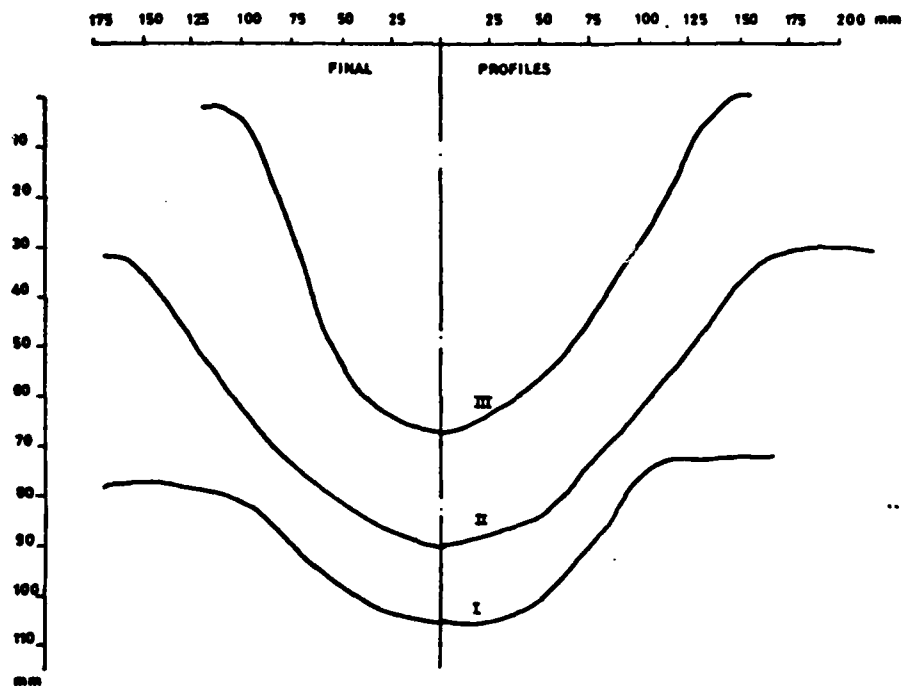
FIG. 8·9   3DM 12

This result was interesting and encouraging but turned out to be a distraction. As a result of this test, the Tests 3DM5-12 were devoted to trying to repeat this 'liquefaction', but without success. The occurrence of this extraordinary model failure remains unexplained.

3DM5-12 $0.23 < O/A < 0.5$

As shown in Fig. 8.5 the plumbing arrangements were changed several times, first to try to improve on and later to try to reproduce the failure seen in Test 3DM4, but entirely without success. In Tests 3DM5, 6 a layer of coarse sand was placed under the silica to facilitate the uptake of water from additional pipes which were provided with many small holes. The result of this was only that the pressure in the blast pipes dissipated uselessly with no removal of sand. In Tests 3DM9,10 the high water pressures which built up at the mouths of the nozzles before the top of the slope was removed, caused piping failures to develop just behind the crest of the slope. In Tests 3DM11,12 no additional layers of coarse sand or tiny holes supplying water were used and the blast pipes were able to excavate the front of the slope. The silica remained standing in near-vertical curved scarp faces, Plate 8.13, 14. On no occasion was the retrogressive failure repeated.

The blast pipe geometry developed for Tests 3DM11,12 was used for all later tests. Four lightweight ¼" BSP valves connected the pipes independently to the water tank. Two valves fed the central blast pipe.

The failure obtained in Test 3DM12 was instructive in one feature, Fig. 8.9 and Plate 8.13: the failure was bottle-neck shaped. A simple geometrical argument shows that the shape of the crater necessarily widens further up the slope of the river bank and the bottleneck shape of failure is seen to be only a result of the geometry, not in this case necessarily, of a mechanism of liquefaction.

The tests on the fine silica were abandoned after Test 3DM12 on account of the unusual dilatant properties of the material. In none of the
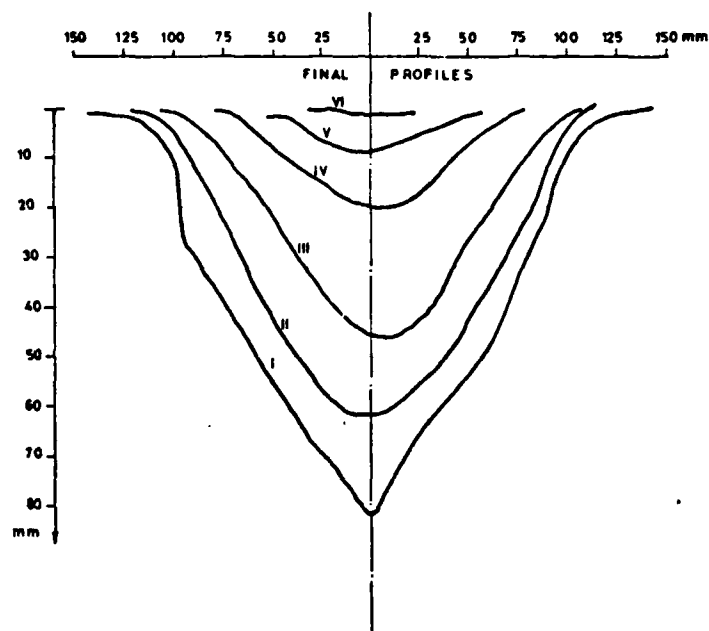
FIG 8·10   3DM 13

models tested using ground silica sand did the overburden have any effect
on the behaviour. The failures were small, only affecting the very edge
of the clay layer.   The tests do not relate to any known prototype
event.

8.9.3   Tests with Fine Sand at 50g

<u>3DM13</u>   O/A = 0.56

In this and subsequent tests lower ng values were used for the test
although the consolidation was always performed at 100g. The reason for this
change in policy concerns the anomalous result of Test 3DM2. In Test 3DM2 the
clay layer had been largely intact even after extensive deformation. In all
of the other tests at 100g, the clay layer was very broken up where it had def-
ormed. Subsequent tests were performed at 50g, 10g and 1g to assess the
influence of gravity on the behaviour. In the event, the flow behaviour of
the sand was apparently unaffected. The major difference observed was a
tendency for the clay layer to break up less at lower values of ng.

In this and the remaining tests the 120/200 sand was sedimented through
water. Test 3DM13 produced a breakaway failure but 50g was still high enough
for the clay to flow and a thin carpet of clay 5mm thick was left behind on
the sand, Fig. 8.10 and Plate 8.15. The test did not elucidate the problems
under study.

<u>3DM14</u>   O/A = 1.05

The result of this test was similar to Test 3DM13 except that a thick carpet
of clay (30mm) lined the (small) crater. It will be seen from Plate 8.16,
where the crater is shown sectioned, that the remaining clay blanket consid-
erably limited the size of crater that was able to develop in the sand
layer.
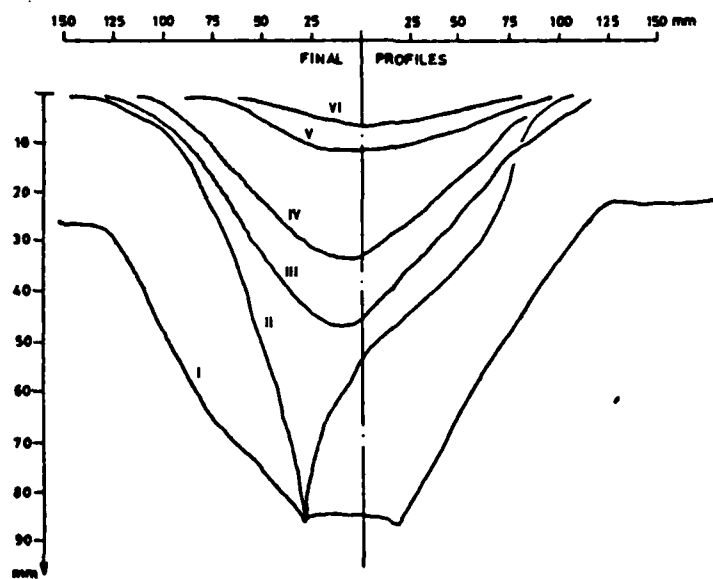
FIG. 8·11   3 DM 15
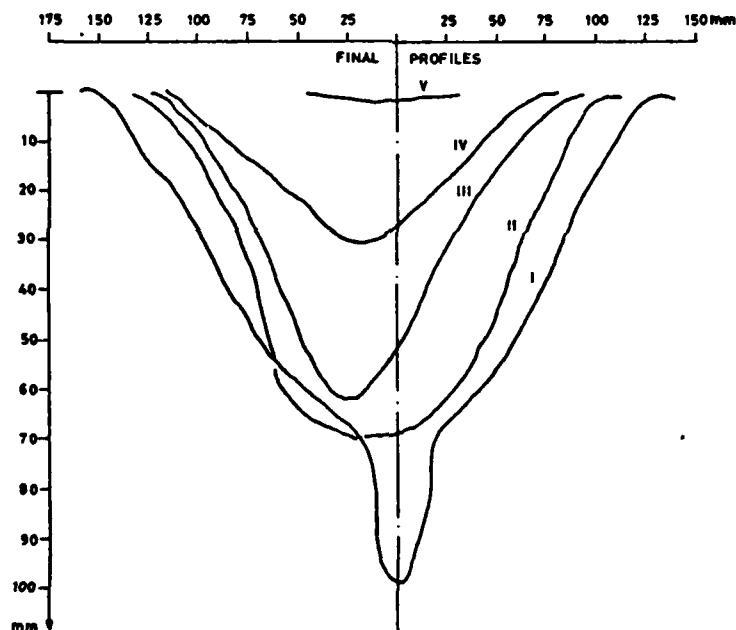
FIG. 8·12   3 DM 16
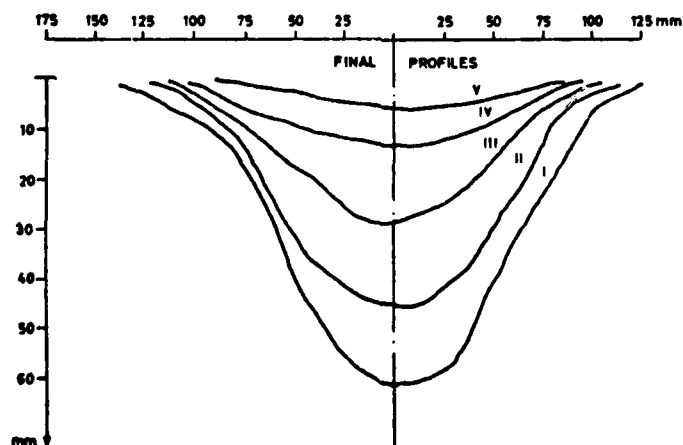
FIG. 8·13   3 DM 17

8.9.4   Tests with Fine Sand at 10g

<u>3DM15</u>   O/A = 0.51

This test was performed at 10g. The clay layer was less deformed than in the previous test and showed extensive cracking. The clay inhibited the flow of sand to some extent reducing the size of the crater, Plate 8.17. The sand slope under the restraining influence of the clay was maximally 50° whereas the free slope in the absence of a clay layer was of the order of 35°. The failure may be classified as of the 'folddown' type in which the clay, though cracked, was not removed from the crater, Fig. 8.11.

The following three tests were performed to see whether different behaviour was observed for three different clay thicknesses at 10g on a sand layer 70mm thick. Displacement transducers were used to monitor the development of the failure.

<u>3DM16</u>   O/A = 0.49

The test result was similar to Test 3DM15 except that the collapse was followed by four displacement transducers arranged in a line perpendicular to the crest of the slope. The aim was to determine how rapidly the failure developed and whether it developed retrogressively. The failure occurred within ten seconds with minor settlement continuing for a further 25 seconds, too rapidly for the data logger to properly follow the collapse. Fig. 8.12 and Plate 8.18 show that the cracking at the edge of the crater was extensive.

<u>3DM17</u>   O/A = 0.76

Again in this test displacement transducers were used but the deformation proceded to rapidly that successive scans of the data logger reveal first the profile before failure and then the final failure profile with no intermediate steps. Plate 8.19 and Fig. 8.13 show the failure to be a regularly shaped folddown failure.

FIG. 8·14   3 DM 18

a

DEVELOPMENT OF
DEFORMATION OF ε

b
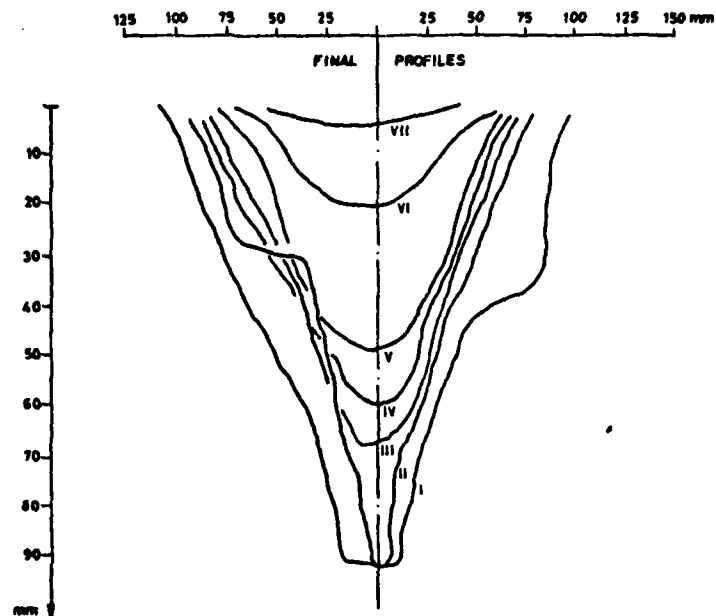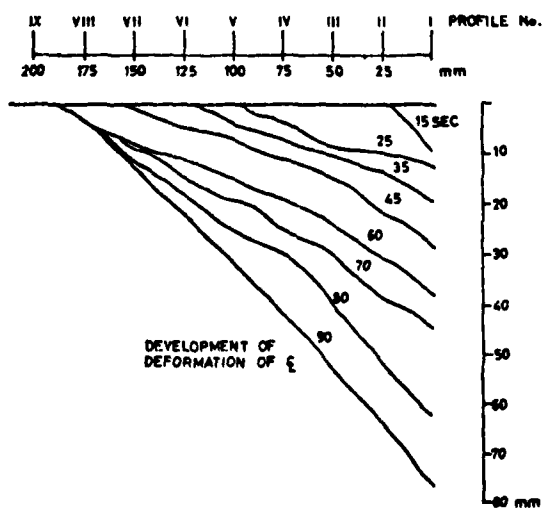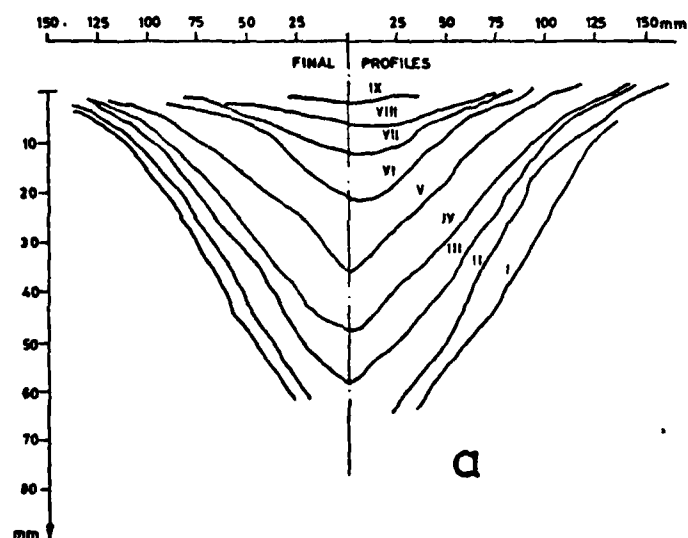
FIG. 8·15   3 DM 19

3DM18   O/A = 0.31

The same problem was experienced in using the displacement transducers. In this test the clay layer broke up into several discrete blocks, Plate 8.20 which shows the influence of the clay layer thickness. The thick layer of Test 3DM17 (O/A = 0.76) had remained intact whereas the thin layer in this test (O/A = 0.31) had broken up, Fig. 8.14.

Conclusions to Tests 3DM15-18

In all tests failure was observed to be essentially complete within 10 seconds and all movement had ceased after 30 seconds. The clay layer exerted a strong restraining influence on the sand causing slopes to remain as steep at 50°. The clay layer remained in place in each case, more or less broken up by the deformation involved in failure, depending on the clay layer thickness. The dependence of the type of behaviour on the ratio (O/A) is shown in Table 3, bound at the end of the dissertation.

8.9.5   Tests with Fine Sand at Earth's Gravity

The intention in these tests was to observe more carefully the development of the collapse.

3DM19   O/A = 0.30

The model was tested at 1g on the laboratory floor. The crater was a slightly unusual triangular shaped breakaway type failure, Plate 8.21 although the clay remained within the crater. Failure was followed by photographing light Perspex rods which were supported on the clay surface. The final profiles are shown in Fig. 8.15a where it may be seen that the failure which developed was large. Longitudinal profiles on the centre line of the crater are shown in Fig. 8.15b at time intervals of 5 and 10 seconds. It will be seen that a travelling hinge develops as the crater expands in the sand layer.

DEVELOPMENT OF PROFILE I

DEVELOPMENT OF PROFILE II

DEVELOPMENT OF PROFILE III

a

DEVELOPMENT OF
DEFORMATION OF ₵
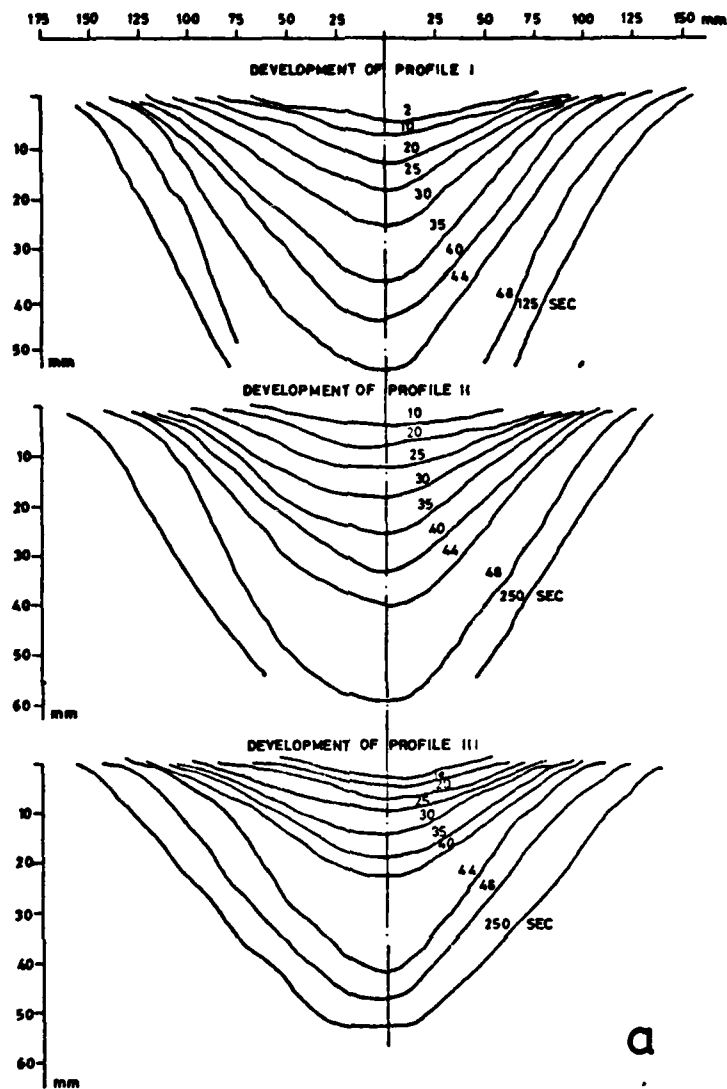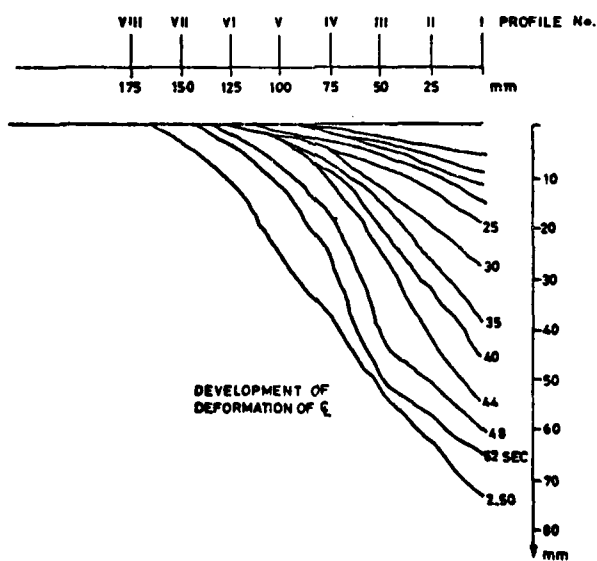
b

FIG. 8·16   3 DM 20

3DM20   O/A = 0.27

Again a typical circular failure resulted, Plate 8.22. As the crater

expanded it was possible to watch the development of a travelling plastic

hinge as the clay lost its support from the sand, Fig. 8.16a,b,c. The clay

did not collapse immediately but held itself up for a short while after the

sand support had been removed, suggesting that the clay had some tensile

strength in the short term. However, when the central deflection had

increased to the order of the plate thickness, the cracks rapidly widened

and the clay collapsed onto the surface of the sand as shown in the figures.

8.10   Concluding Remarks

Few quantitative results were obtained from the tests described in this

section. They serve mainly to show that folddown and breakaway mechanisms

of the kind hypothesised are possible. In retrospect the tests should

perhaps have been performed at say 25g and with a thick sand layer, say

120 mm thick. At that stress level the clay was able to fully separate from

the parent layer and the flowing sand layer is of such a thickness (cf. Test

3DM3) that the clay, if thin, could be transported away. Throughout the

test series this type of speculative argument had to be used: about methods

of sample preparation, layer thickness, materials, blast pipes, ng level.

The number of possible variations in the experimental method was so large

that at no stage was a standard experimental technique accepted with which

to conduct a proper parametric study.

It appears now that the attempt to model a complex phenomenon on the

centrifuge is a task which involves many technical problems and which

requires the development, modification and planning of a large body of equip-

ment and method. Perhaps most importantly, in a speculative investigation

of this kind, care should be taken in planning the tests to avoid the pro-

liferation of variables. A hypothesis should be set up and tested in such an
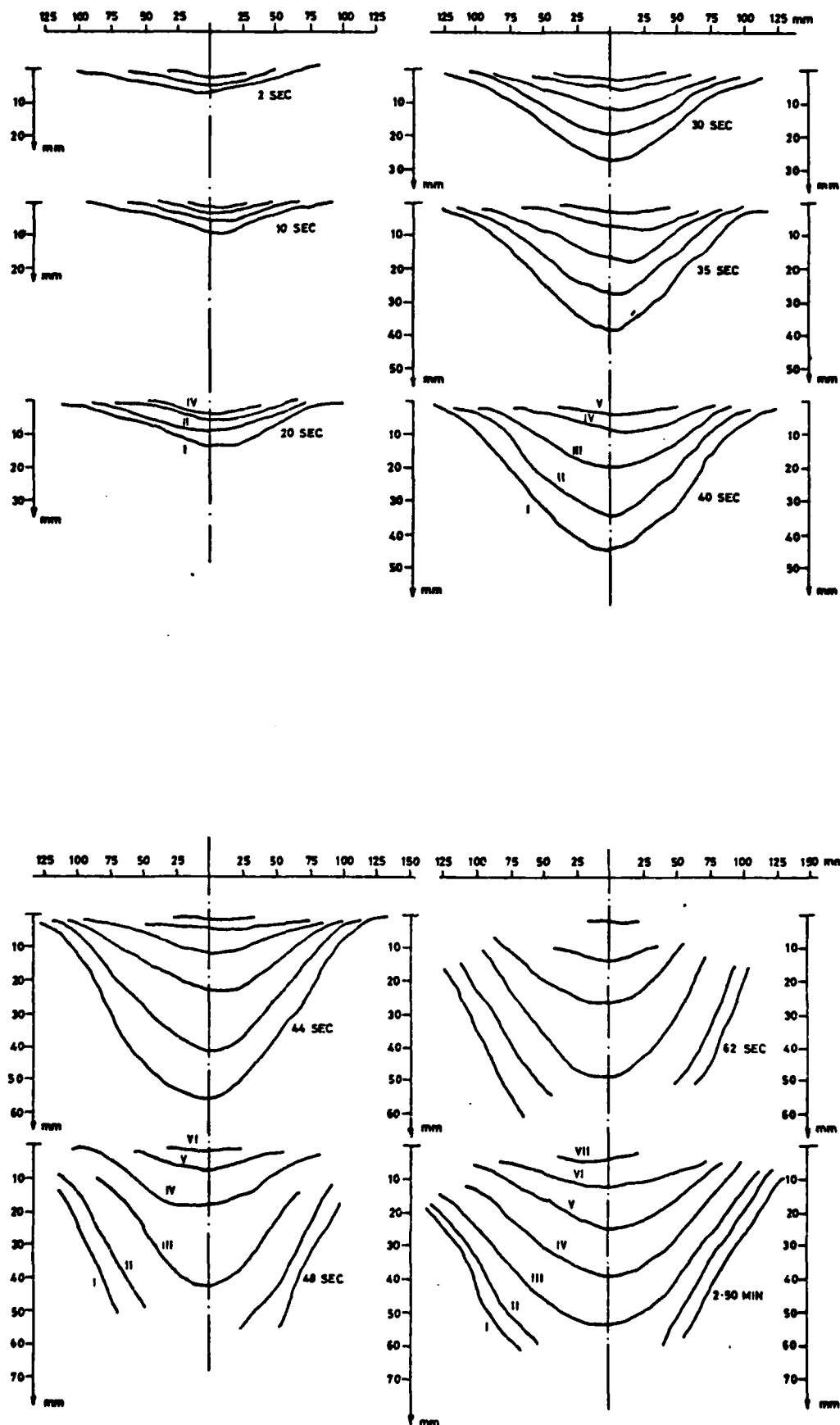
FIG. 8·16c 3 DM 20 DEVELOPMENT OF DEFORMATION OF PROFILES

idealised form that it can be rejected or verified before its relevance to a more complex problem is considered.

In the tests the two distinct mechanisms of failure which were seen, however unclearly, were somewhat different from the mechanisms of plastic collapse hypothesised at the outset. It seems that the clay has essentially no tensile strength although in the short term pore suctions may allow plastic deformation. The two distinct mechanisms have been called folddown and breakaway types of failure. The former occurs where a clay plate is sufficiently thick to retain compressive stress within its depth and deform into the crater. A breakaway failure will occur (as in Test 3DM3) when the clay layer is thin with respect to the sand and the detached overburden can be carried away on the flowing sand.

Certain variables were eliminated from consideration by these tests:

1. No features were seen at elevated ng levels which appeared to be analagous to a flowslide at full scale.

2. The cohesive overburden layer did not behave plastically - rather it cracked in tension and either spread out in a sheet or broke up depending on the ng level.

3. Injection of water into the front of the sand slope did not induce a flow failure.

4. The complexity of the failure geometry was such that it was difficult to draw conclusions about the behaviour of the overburden during deformation.

5. It would be extremely difficult to model a two-layer geometry of this type with a very loose sand in the centrifuge.

As a result of these tests it was decided to give attention to another series of experiments to be described in Chapter 9, and later to return to the Erosion Tests to experiment with different clay layer thicknesses on a thick sand layer. For this there proved to be too little time and the Erosion Tests were left at an inconclusive stage.

a KAOLIN UNDER CONSOLIDATION

b ONE TEST PERFORMED
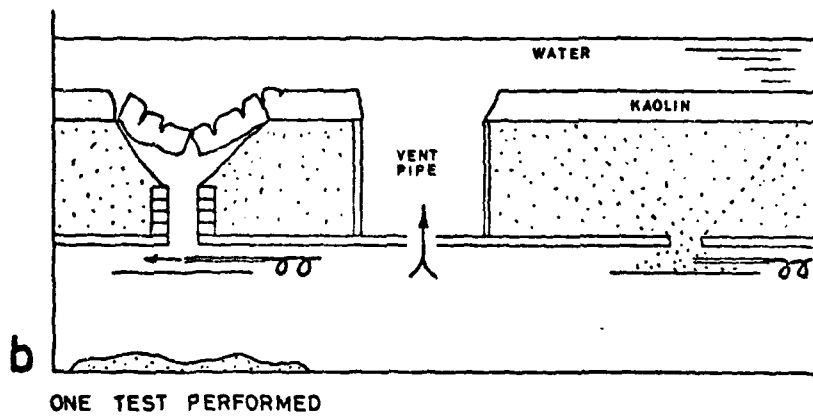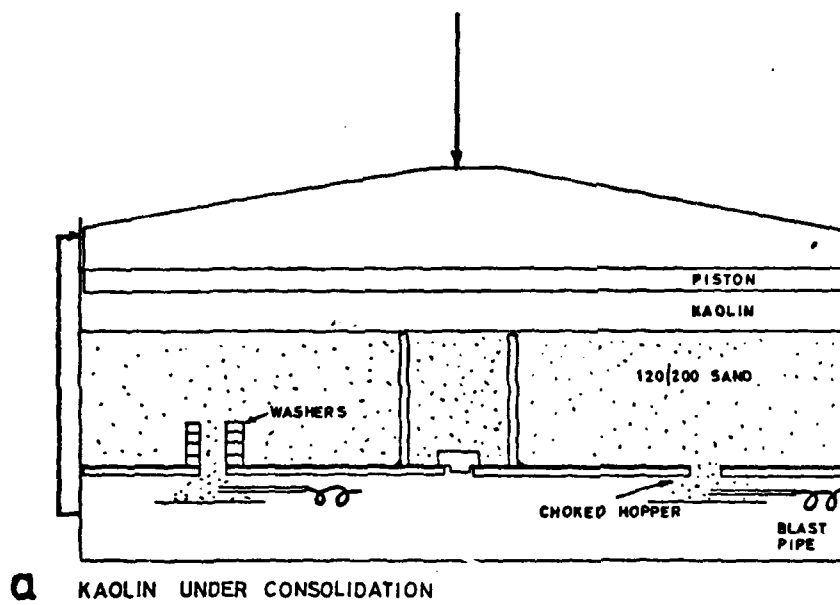
FIG. 9·1 CRATER TEST APPARATUS

CHAPTER 9

MISSISSIPPI FLOW SLIDES

THE BEHAVIOUR OF THE OVERBURDEN

9.1   The Clay Plate

The experimental results presented in Chapter 8 have added a new dimension to the elucidation of the processes behind the flowsliding phenomenon.   The experiments revealed two distinct modes of failure of the clay overburden which may account definitively for the two different types of failure which are observed to occur along the Mississippi River.   In the following sections the problem is examined from an idealised standpoint to see whether a clay plate will be able to support itself over a circular hole.   Experiments were performed, Section 9.2, to test this hypothesis and it is found that the actual clay plate is able to sustain only small spans. The results of the experiments performed suggest a mechanism of arching which is described in Section 9.4.   The mechanism of arching is seen to account for the validity of the Empirical Criterion.

9.2   Crater Tests

9.2.1   Apparatus

In these tests a layer of sand overlain by a layer of kaolin in the normal way rested on a special circular platform in a tub on the laboratory floor.   The platform, Plate 9.1 and Fig. 9.1, was designed such that any one of four 'trapdoors' could be opened under the sand layer.   Once a 'trapdoor' had been opened, the sand was free to collapse into the hole and be deposited under the platform.   The clay layer subsequently found itself undermined symmetrically and required to span across the crater formed in the sand layer.

RETROGRESSING
FACE
OVERHANGS
IN 3D

1.

2.

3.

4.

5.

6.

VERTICAL FACE RETROGRESSES
IN 2D.
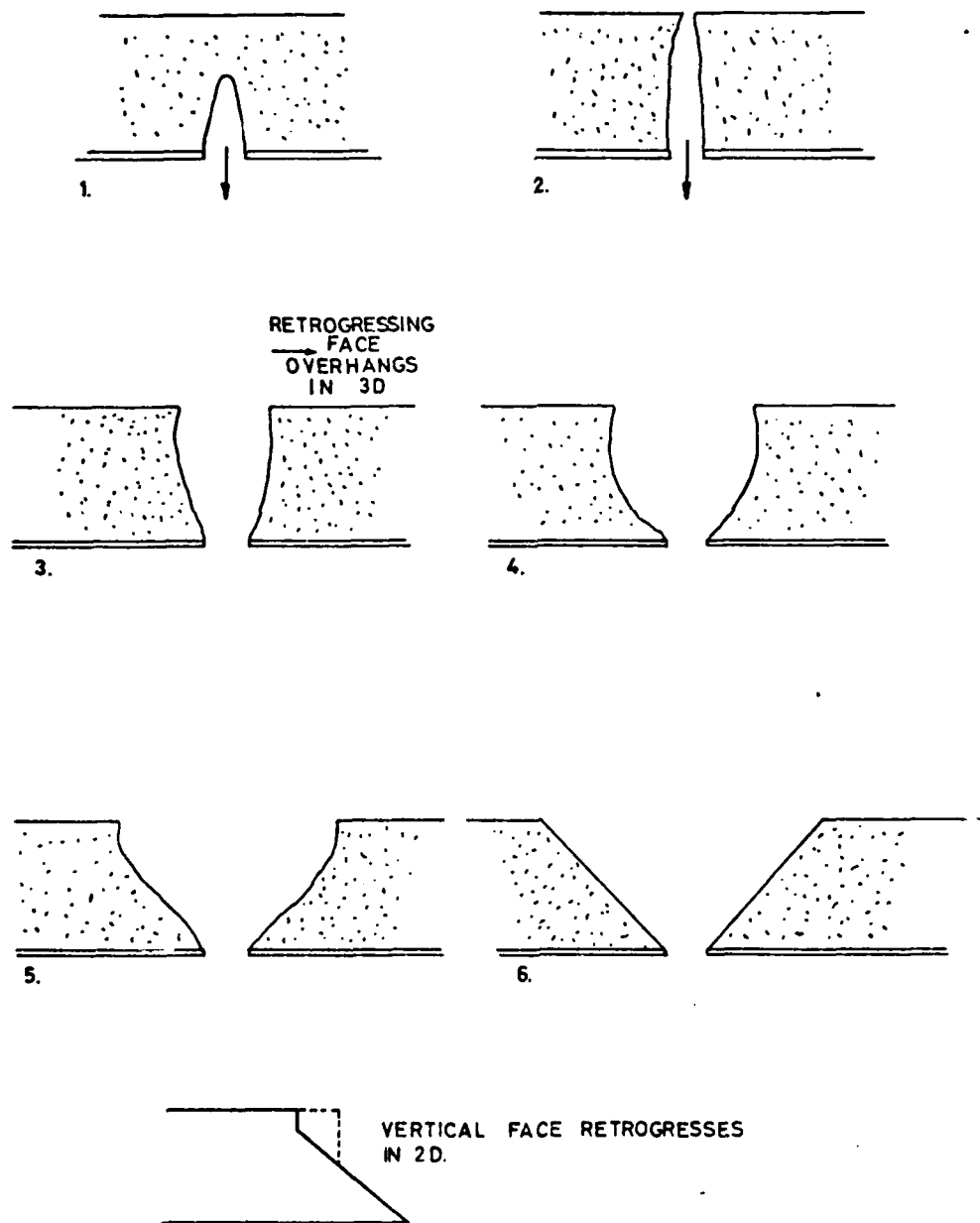
FIG. 9·2 DEVELOPMENT OF THE CRATER

The trapdoors were operated by use of the principle of the choked hopper. Plate 9.1 and Fig. 9.1 show a half cylindrical tube mounted under the hole. During model preparation and until the 'trapdoor' was opened the tube was filled with coarse sand. The coarse sand sits at its angle of repose and blocks further sand movement through the hole. When a blast pipe is operated the tube is rapidly cleared of sand and material is able to fall through the hole and be removed by the water jet into the space under the platform. The other two holes visible in Plate 9.3 are provided in order that a steel tube can be fitted through the soil layers to connect the space under the platform with that above the clay so that the water pumped in through the blast pipe can escape harmlessly. This is illustrated in Fig. 9.1b.

The manner in which the sand was removed is shown diagrammatically in Fig. 9.2. Note that a vertical face (overhanging in the early stages) works its way back through the sand to form the crater. This phenomenon is further discussed in Chapter 10.

The original intention was to relate the deflection of the clay plate to the diameter of the crater it spanned, but this proved difficult to perform. Tests conducted with no clay layer showed that after the blast pipe was fired, an indeterminate time elapsed before the crater in the sand started to form. This elapsed time varied from test to test and it was not possible from above the clay to see when the process had begin. The clay behaviour has, however, been simply related to the final diameter of the crater, measured by removing the clay after the test. This data is presented in Table 4, bound at the end of the dissertation.

The equipment was so designed that four independent craters could be made in the sand layer for each test. Thus, four different crater tests could be performed on a clay layer of a given thickness. The size of the crater was altered by varying the effective depth of the sand layer. This was accomplished, Fig. 9.1b, by piling washers on top of the trapdoor, thus reducing
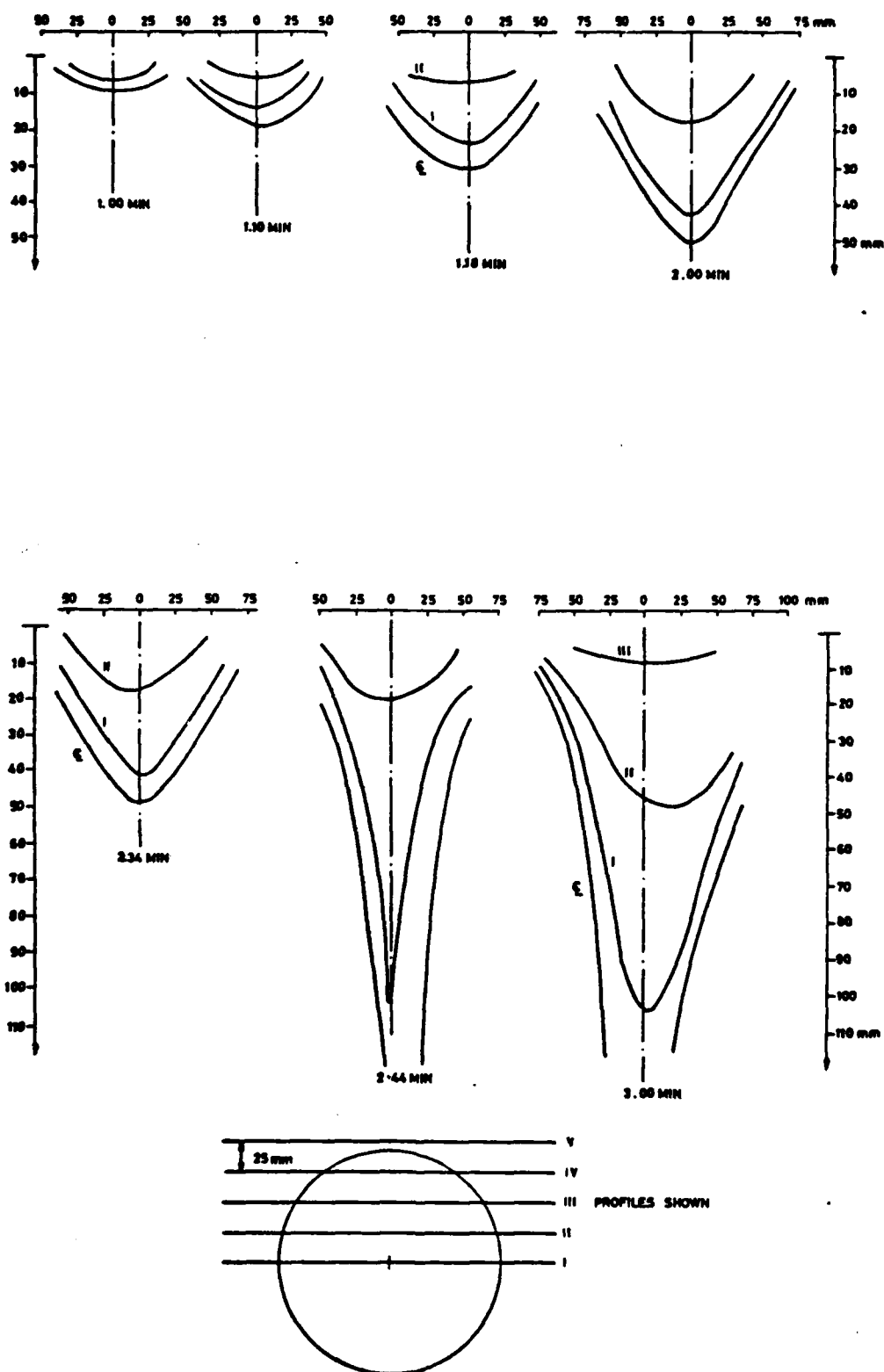
FIG. 9·3 CRATER TEST 5 FINAL Φ CRATER = 225 mm

the height and hence the diameter of the crater.

9.2.2 Test Method

Test preparation was similar to that involved for the Erosion Tests. The tub was filled with water and the blast tubes purged of air. Sand was poured to the required depth through the water such that it also filled the steel vent tubes. A clay layer was consolidated onto the sand in the consolidometer shown in Plate 9.2. After the load was removed, the sand and clay was excavated from the vent tubes and the tub was filled with water.

A test was performed by firing a blast of water into the half cylindrical tube under the 'trapdoor'. The deformation of the clay plate was followed from above by an array of graduated perspex rods that rested on the clay surface. These were photographed at suitable intervals to obtain a permanent record of deformation. Unfortunately, for the three final tests an error was made in the exposure of the photographs and the perspex rods were not clearly visible from their background. One set of displacement data is given as an example of the mode of deformation observed. The failed plate is illustrated in Fig. 9.3.

The test procedure was time consuming and since very little time was available the number of useful tests performed with this apparatus was limited to three (Tests 5-8). The test results are described in the following section.

9.2.3 The Crater Tests

Test 1 The platform was tested as designed with a layer of loose sand. Only occasionally did a crater form when the blast pipes were fired.

Test 2 As above, but with 70 mm sand and a 16 mm clay layer. The trapdoors appeared to block and no craters were produced. After this attempt the trapdoor holes were enlarged from 20 mm to 28 mm diameter.

Test 3 The apparatus was tested with and without a 30 mm clay layer. Craters formed with slope angles of 31° without a clay layer. The clay layer inhibited sand flow to a small extent and increased average crater slope to

about 45°. After experimentation with the aluminium washers it was decided to use a configuration which gave craters under the clay of approximately 180mm and 235mm diameter.

Test 4   Preliminary test with 22mm clay layer. In all cases the clay layer deformed only slightly ($\delta/h < 0.5$) until a sudden increase in deflection occurred when a crack appeared running right through the plate at midspan. This deflection was accompanied also by extensive cracking around the circumference. The span which cracked away in this fashion was 170mm (±5 mm) in diameter.

Tests 5,6,7   The results from these tests are given in the Table 4 and the displacement profiles for Test 5 with a crater of 225mm are given in Fig. 9.3.   Three clay thicknesses were used 18.5, 29 and 37 mm and craters of size 180mm and 230mm in diameter were formed. Two tests were performed with each combination, such that, for example, two 180mm craters were formed under a 29mm clay layer. The reason for the doubling of all the tests is that the pattern of behaviour was somewhat irregular and depended on the onset of cracking. It was evident from the outset that the spans did not deform plastically in the ordinary way. In the tensile region small cracks very rapidly appeared which widened slowly as the deformation of the plate, on constant span, continued to increase. There came a time when the deformation had reached a limiting value, and the cracks thereafter rapidly widened and the plate collapsed. In the case of the 29mm plate on a 180mm span and of the 37mm plate on 235mm span the cracks stabilised and deformation remained limited to $\delta/h < 0.5$. It is likely that since the clay manifested only slight long term tensile strength this stability was due to wedging or arching. In the stable cases the stress in arching was taken entirely in compression; some stress distribution had developed in the thickness of the clay which, though yielded, was in equilibrium with the self weight. A thinner plate on the same span would have continued yielding, seeking an equilibrium
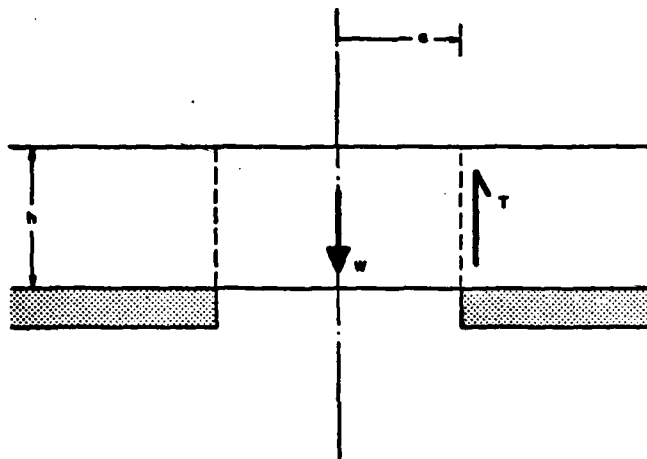
FIG. 9·4 PUNCHING SHEAR OF CLAY PLATE THROUGH
CIRCULAR ORIFICE IN SUPPORT

stress distribution, but when $\delta/h > 0.5$ the area of cross section avail-able to take compression was so small that deformation accelerated, cracks widened and the span failed. This is further discussed in Section 9.4.

From the Crater Tests 5-7 the following general picture was obtained for the behaviour of a kaolin plate over a circular hole

Plate Thickness (h)	Maximum Intact Span	δ/h
18.5 mm	< 180 mm	
29.0 mm	180 mm	~0.2
37.0 mm	> 235 mm	

where maximum intact span means the span at which the clay did not crack away although deformation was considerable.

9.3 Punching Shear

The suggestion that a clay plate is an extremely weak structure is further reinforced by considering the punching shear of the clay plate through the hole. Equating load to shear resistance from Fig. 9.4, for limiting equilibrium, the limit span is shown to be

$$a_o = \frac{2c_u}{\gamma'} \tag{9.1}$$

which is independent of plate thickness. This value of 'a_o' will be reduced if the clay plate is cracked around the edge since the area available to take shear will thereby reduced.

The voids ratio of the clay at the time of test was $e = 2.12$ and $\gamma' = 5.2$ kN/m^3. Hydrostatic stress p' at critical state for $e = 2.12$ is $p' = 12$ kN/m^2 which using critical state values predicts, as an overestimate of the undrained strength

$$\frac{c_u}{p} = \frac{1}{2} M e^{-\lambda} = 0.2275 \tag{9.2}$$

$$c_u = 2.8 \text{ kN/m}^2$$

FLAT ARCH

POINT LOAD
ONLY

POINT LOAD
AND SELF WEIGHT
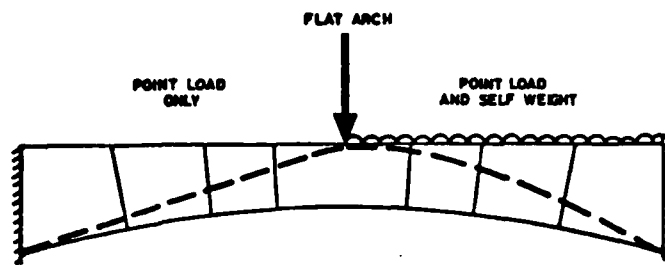
FIG. 9·5a NO COLLAPSE MECHANISMS POSSIBLE

SEMICIRCULAR ARCH
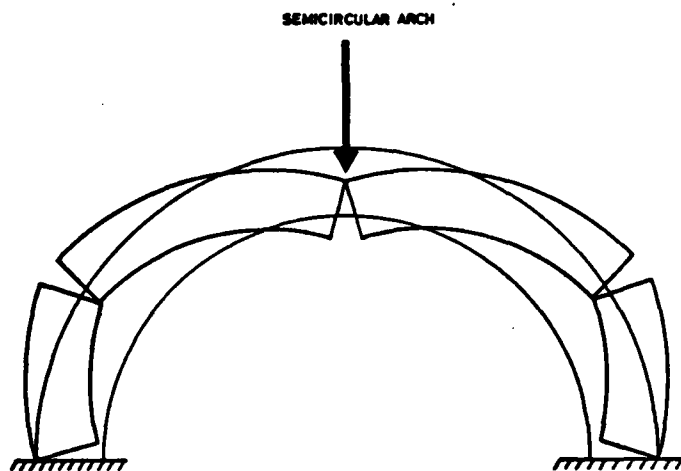
FIG. 9·5b MECHANISM OF COLLAPSE
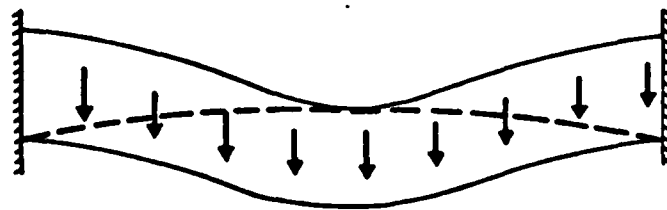
FIG. 9·5c CONCAVE MASONRY OR CLAY ARCH

which compares with a value measured with the miniature vane of $c_u = 1$ kN/m^2.
Let us take a mean value $2c_u = \sigma_y = 3$ kN/m^2.

For the material in the experiments the maximum theoretical span was
0.6 m for a self supporting uncracked plate: far larger than the exper-
imental value. Overburden soils along the Mississippi are stronger
$10 < c_u < 50$ kN/m^2 but even for these the predicted values are $1 < a < 5$ m
in the self supporting uncracked condition if the soil is assumed to be of
the same density as the kaolin.

In practice, the span which a clay plate can sustain has been shown
to depend on the thickness of the clay, which suggests that arching may be
important in the thickness of the slab. No stress distribution that
requires the development of tension in the plate is likely to be adequate
to explain the behaviour. For this reason, although they were considered
in detail, tensile tests on clay specimens were rejected as unlikely to be
helpful.

9.4 Arching

Arching is the mechanism whereby load may be taken in a structure by
compressive action alone without either bending or tension. A masonry arch
is a useful analogue, Heyman, 1966. Consider the flat arch in Fig. 9.5a.
If the material is rigid and the abutments do not spread, there is no limit
to the load which may be applied to the span since a line of thrust may
always be found which lies wholly within the masonry. This is in contrast
to the arch of Fig. 9.5b for which mechanisms of failure will develop when
the only possible line of thrust touches the external surface of the arch
ring at three or more points.

By extension of these ideas it may be seen that a concave masonry
arch of the form shown in Fig. 9.5c can remain in equilibrium provided a
line of thrust can be found within the masonry. In this latter case, the
shallow line of thrust will require high abutment reactions and large com-
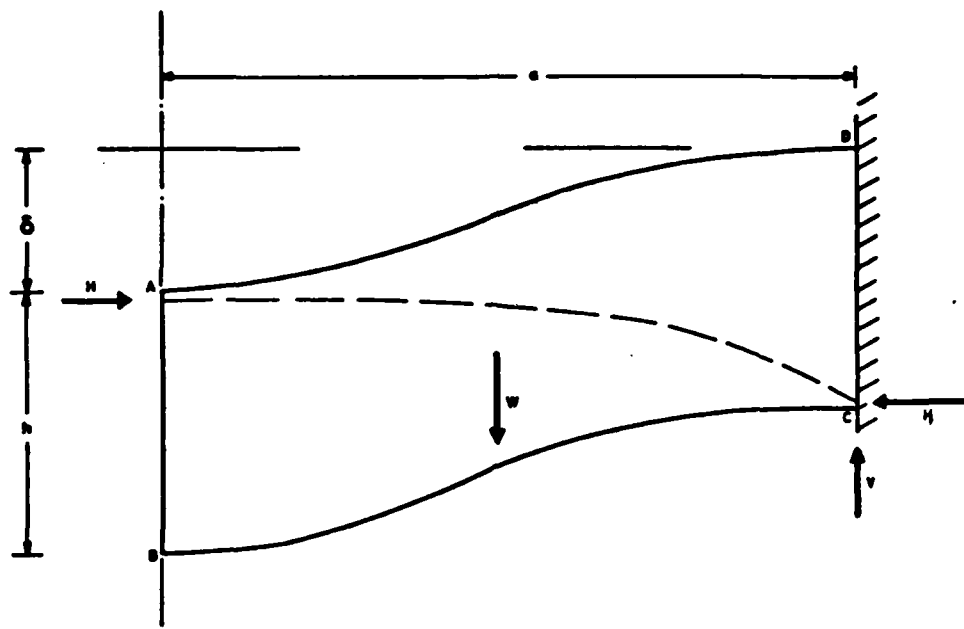
FIG. 9·6a HALF SPAN OF DEFORMED CLAY BEAM
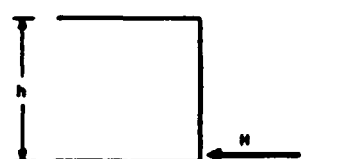
HORIZONTAL REACTION
AT CD
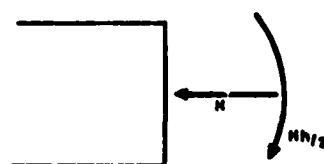
EQUIVALENT REACTIONS
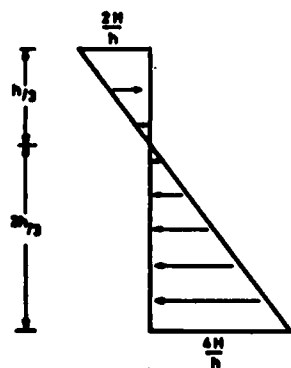
STRESS DISTRIBUTION
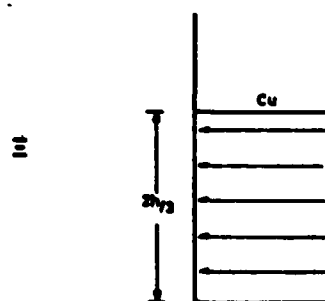
ALTERNATIVE STRESS
DISTRIBUTION FOR
PLASTIC MATERIAL

FIG. 9·6b

FIG. 9·6c

pressive stresses near the extrados in mid-span.

Consider the deformation of a two-dimensional clay beam since this is simpler than the deformation of a plate and also leads to conservative answers. Fig. 9.6a shows half a span of a clay beam deformed into a shape similar to that shown in Fig. 9.5c, in which the line of thrust reaches the surface of the clay at the springing and at midspan. Taking moments about A the horizontal reaction may be calculated:

$$H = \frac{Wa}{2(h-\delta)} \qquad\qquad (9.3)$$

which will produce a stress distribution (I) in the beam at the springing (similar at mid-span) as shown in Fig. 9.6b. If the material is regarded as elastic the neutral axis is 2/3 of the way up the depth of the beam. By way of approximation to the behaviour of the clay, the stress distribution (II), Fig. 9.6c, may be substituted which gives the same moment about the neutral axis when

$$c_u = \frac{9Wa}{8h(h-\delta)} \qquad\qquad (9.4)$$

In the Trapdoor experiments a plate of thickness 29 mm was self-supporting on a span of 180 mm. Substituting this span and an experimental value for $\delta/h = 0.2$, the Equation 9.4 yields a value of $c_u = 2kN/m^2$ required by the material, which is reasonable. Again, assuming that in the field the plate supports only one half of its own weight then for $c_u = 30$ kN/m^2, $h = 10$ m, $\gamma' = 5.2$ kN/m^3, $\delta/h = 0.7$, the equation yields a value for the limit span of a = 30 m. In this case the clay plate can stay sensibly attached at the edge since the material there remains in compression over part of the cross section.

If, as seems likely, the sand supports the majority of the weight of the clay as the sand flows away, spans of perhaps 70 m at $\delta/h = 0.7$ are able to remain in compression. When, however, deformation proceeds so far that $\delta > h$ there is no further possibility of arching and the plate will separate away at the edge of the crater.
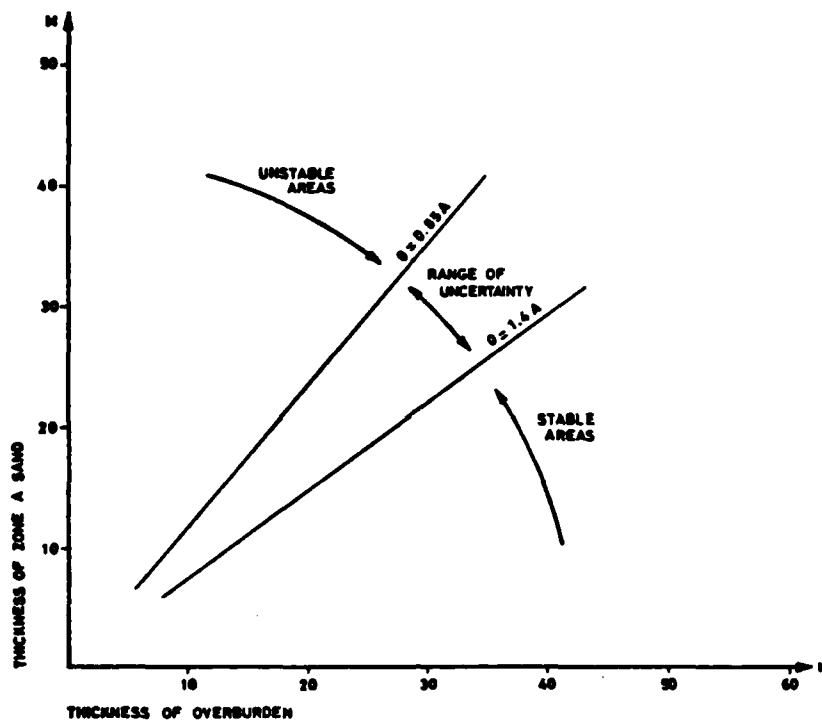
FIG. 9·7 THE EMPIRICAL CRITERION FOR RIVERBANK
STABILITY
(Taken from Potomology Report 12-2 Wes)

9.5 Interpretation of Field Events

The significance of this is as follows. Fig. 9.7 shows a correlation of behaviour which led to the empirical criterion (WES, 1956). It is readily seen that the regions which are designated fully stable have $\delta/h < 0.7$ and hence arching is possible. Regions designated unstable have $\delta/h > 1.2$ for which the clay will crack at the edge and be bourne away on the flowing sand, Fig. 9.8b. There is no possibility of arching in this range. In between these two definite extremes there is a transition region where the nature of the failure will depend on the site conditions.

It seems likely that in the stable cases the clay will indeed collapse, following and being largely supported by the sand surface but will inhibit the flow of sand, Fig. 9.8a. The clay will remain in place folded down into the crater and attached at the edges when the crater has developed to its full width. Less sand will flow away in this case than if the clay were not present. The failure will be interpreted as a shear failure.

In areas where the sand layer was so thick that the profile may be designated unstable the clay will be bourne away into the river leaving the failure scar clear for the failure to propagate a stage or more back into the bank and resulting in a very deep failure.

Very little is known from field observations concerning how an overburden layer might restrict the flow of an underlying liquefied sand layer. However, the mechanisms proposed in this section help to answer one further question concerning Mississippi flowslides. It becomes possible to understand why a flowslide, once initiated, is brought to a halt. Consider the initiation of a slide where $O/A = 0.2$. The slide will expand with blocks of overburden breaking off and flowing away on the sand. As the slide retrogresses the base of the failure climbs up the sand layer progressively reducing the depth of sand involved in the failure and thereby increasing the ratio O/A. The flowslide will stabilise when $O/A > 0.85$ at the active face.
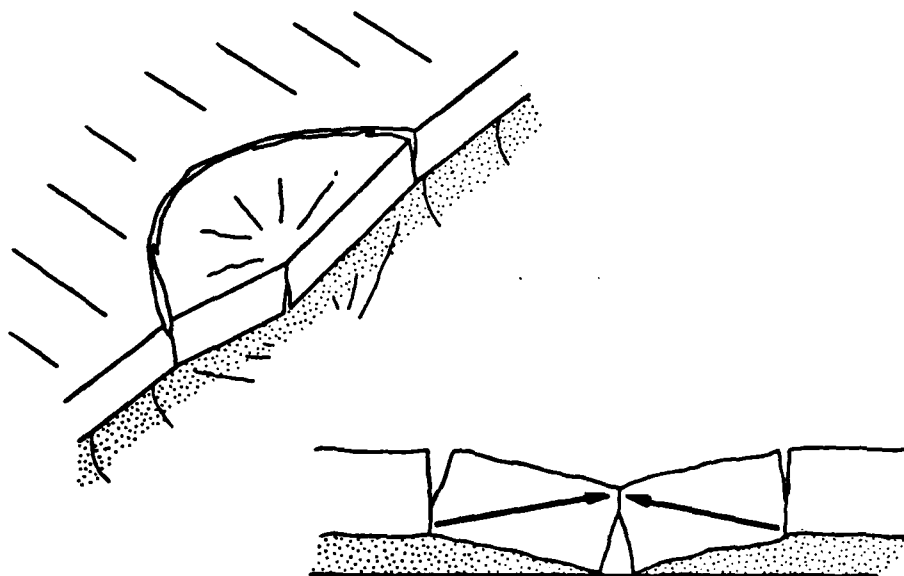
FIG. 9·8a O>A ARCHING POSSIBLE CLAY REMAINS IN PLACE 'SHEAR TYPE' FAILURE
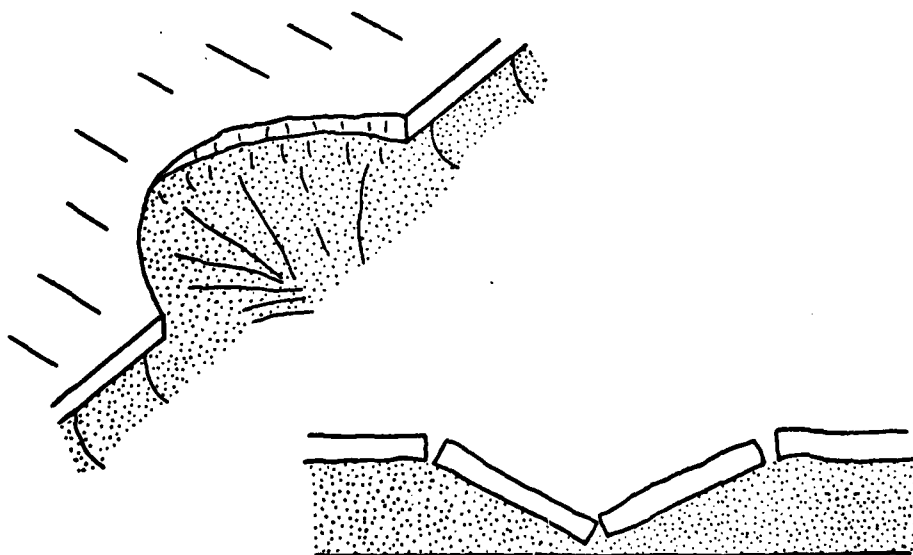
FIG. 9·8b O<A ARCHING IMPOSSIBLE CLAY CRACKS AWAY 'FLOW TYPE' FAILURE

Unfortunately, the scale effects discussed in this dissertation make experimentation difficult at small scale. The only experiments known to the author where tests on the flow of sand have been attempted at intermediate scales are those reported in Section 7.3.3, performed by the Delft Hydraulics Laboratory. However, certain references in the literature are informative. Work by Mitchell, 1974, suggests that a flowslide in Champlain Sea Clay will stop propagating when the base of the retrogressing steep face is at such a depth that the pressure due to the weight of a block is equal to the shear strength of the material. In other words, the propagation is arrested when the base of the liquefying region meets a form of crust, which may be compared with the overburden in a Mississippi flowslide. Ishihara[*] recognised the scars in the Mississippi river bank shown in the frontispiece, and remembered seeing the same features on the banks of other meandering rivers. It is to be expected that they occur on many of the world's large rivers. Ishihara further pointed out that crustal behaviour of the sort postulated in the Mississippi flowslide interaction (and which was investigated in the Crater Tests of Section 9.2) is to be seen in Romania in karst limestone countryside. The surface crust of limestone may on occasion be undermined and collapse into the subterranean crater. Meyerhof, 1965, studied the bearing capacity of sea ice sheets, the deformation of which under point loading bears strong resemblance to the mechanisms of failure observed in the Crater Tests. Much work remains to be done, however, to validate and quantify the mechanisms of interaction proposed above for the cohesive overburden and the retrogressively failing sand layer in flow-slides on Mississippi river point bar deposits.

---

[*] Ishihara, 1977. Personal communication to A.N. Schofield.

CHAPTER 10

MISSISSIPPI FLOWSLIDES

LIQUEFACTION AND FLOW OF SAND

10.1 Introduction

Two aspects of this phenomenon will be discussed: firstly, the initiation of liquefaction in a previously stable deposit, and secondly, how the flowing sand suspension maintains itself in motion. In the first part of this discussion it is argued that the sand can come into motion and leave a scar similar to the flowslide scars observed along the lower Mississippi even if it is very densely packed in the deposit. In the second part of the argument an analysis is developed which within the limitions of the assumptions made, accounts for the transportation away from the failure of any sand which starts to flow.

The discussion in this section deals in rather more detail with the process of liquefied flow and flow initiation discussed in Section 7.3.3. The moderating influence of the clay layer is not included in the analyses although the results obtained are expected to be modified if an overburden is present.

10.2 Initiation of Flow

10.2.1 Spontaneous Liquefaction

It has been mentioned above that a sand layer may be induced to liquefy as a result of the deformation involved in failure or conversely a slope may fail as a result of spontaneous propagation of liquefaction within the stratum. It should in either case be possible to achieve an understanding in terms of soil mechanics of the processes involved up to the point where the sand becomes liquefied and viscous deformations proceed.
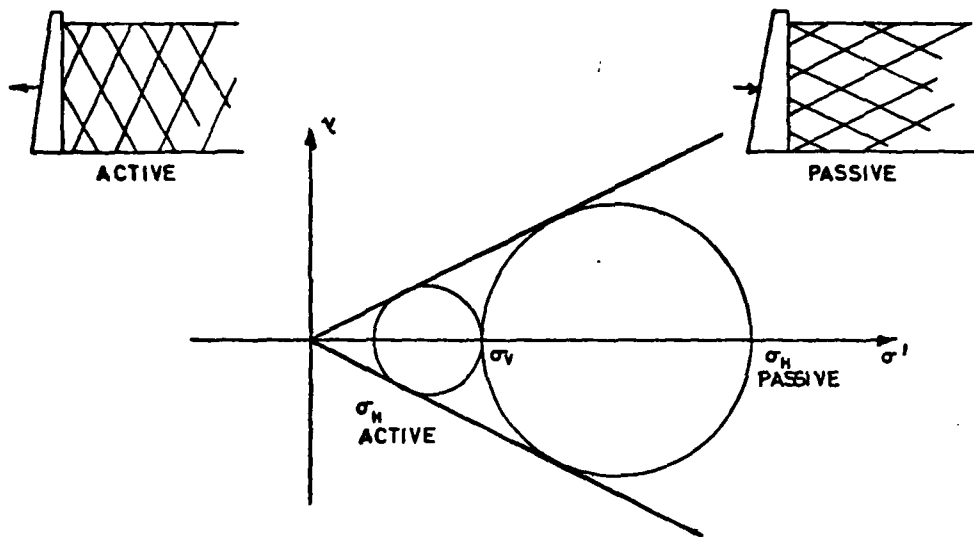
FIG. 10·1 ACTIVE AND PASSIVE EARTH PRESSURES
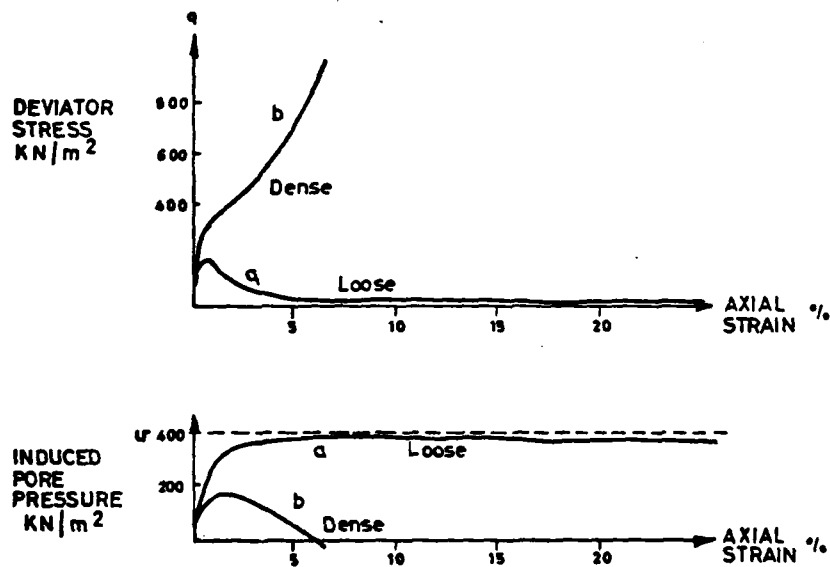
FIG. 10·2 TEST RESULTS FOR UNDRAINED STRESS CONTROLLED
TRIAXIAL TESTS ON LOOSE (a) AND DENSE (b)
SAND SPECIMENS. (Taken from Castro, 1969)

In the case of a horizontal sand layer, consider the initial per-
turbation of equilibrium to be caused by an oversteepening or removal of
support from the front of the slope. Consider a mass of soil behind a
retaining wall, as shown in Fig. 10.1. If the support to the soil from
the wall is steadily reduced the horizontal stress on an element of soil
close to the wall decreases. This change of stress state rotates the planes
of maximum shear and increases the deviator stress q. The same process
occurs when a sand layer is steepened due to the erosion of a scour hole.
The sample of soil is loaded in shear, possibly to failure.

Consider the stress strain properties of sands under this loading.
The plots shown in Fig. 10.2 are experimental results obtained by Castro,
1961, from undrained stress controlled triaxial tests on two sand specimens.
Sample (a) was loosely packed and sample (b) densely packed at the start
of the test. Sample (b) behaved stably: as axial strain increased, the
deviator stress experienced by the sample increased. Initially positive,
but with increasing axial strain, negative pore water pressures were gen-
erated. On the other hand, the loose specimens behaved unstably. The axial
load was increased in increments over 20 minutes and caused a steady build-
up of positive pore pressure. The final load increment caused a very rapid
increase in strain and a further increase in pore water pressure. The struct-
ure of the sample collapsed, a phenomenon described by Castro as lique-
faction.

By this mechanism of structural collapse loose sand layers are post-
ulated to have liquefied along the Dutch coast, Koppejan et al., 1948, and
on the continental slope, Morgenstern, 1967, but the liquefaction fail-
ures on the Mississippi are not self-evidently of this type. It is by no
means proven that the susceptible sand layers are to be found in a very
loose condition*. Very few failures have been observed during the flow

---

*Torrey, 1976, personal communication, WES Archives
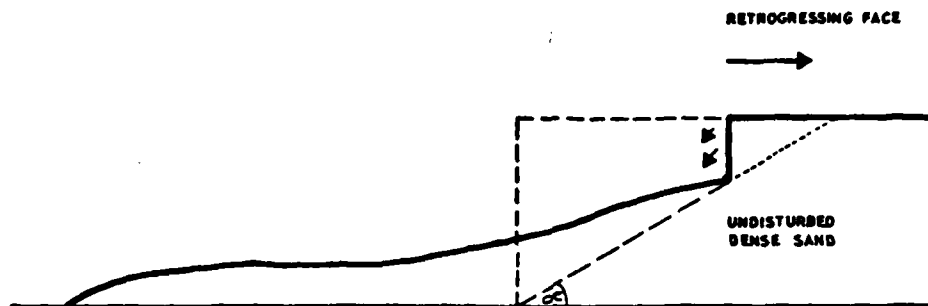
FIG. 10·3 RETROGRESSING FACE IN DENSE SAND DECREASES
IN HEIGHT.
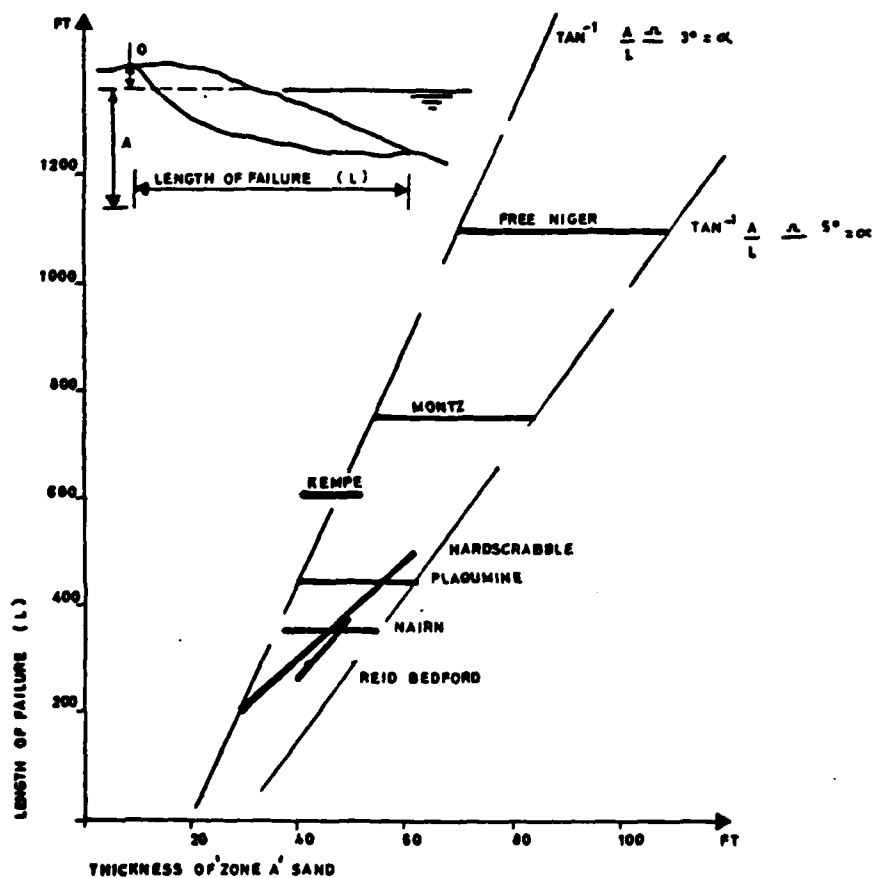
FIG. 10·4 (taken from potomology report 12–5 wes)

process, but the evidence available from the Montz and the Free Nigger

point failures, suggest a process of retrogression of the failure over

perhaps twenty hours. This relative slowness indicates that the process

may be one of failure before liquefaction which will be discussed in the

following section, and not in fact a spontaneous liquefaction at all.

10.2.2   Retrogressive Liquefaction

Recently Denner and James* performed a series of small scale tests on

the retrogression of an unsupported subaqueous face of dense fine sand.

They found that an artificially induced steep face is able to retrogress

stably in dense sand, maintaining the steepness of the face itself. In

most cases the height of the face diminished steadily, Fig. 10.3, due to the

fact that the base of the face climbed up at an angle to the horizontal and

eventually intersected the top surface. They found that the phenomenon of

retrogression did not occur at all for a loose sand deposit. The unsup-

ported face of loose sand slumps and no retrogression is produced. In the

case of the experiments reported in Section 7.3.3 the same experience is

reported but slumped material actually flows a short way.

Fig. 10.4 shows a correlation of actual bank failures along the

Mississippi, WES, 1956. It may be deduced from the figure that if the

mechanism of failure is indeed one of stable retrogression of a steep face

in a dense sand layer, then the base of the face must climb up at an angle

of approximately $\alpha = 5^o$. This would suggest a very efficient mechanism

of material removal. This topic is resumed in Sections 10.3 and 10.4.

Meijer and Van Os, 1976, report larger scale experiments and theoret-

ical work on the same topic. In this case a suction dredger, Fig. 10.5a,

moves steadily along the x' axis, removing the material which flows off a

steep subaqueous face of dense fine sand. They interest themselves in the

magnitudes of the pore suctions that are developed within the sand and

serve to sustain the face. They show that the dominant feature is the

*Denner, 1977 "The Propagation of Flowslides in Submerged Slopes", Undergrad-
uate Project Report, Cambridge University Engineering Department.
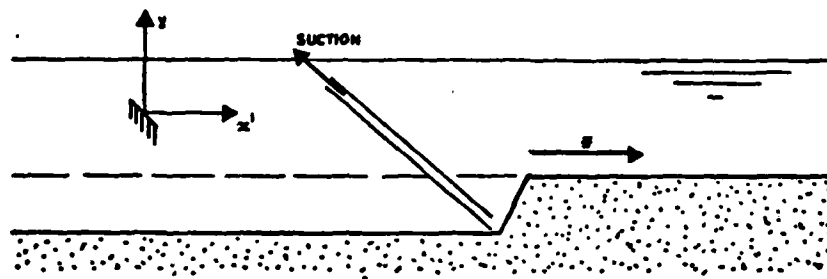
FIG. 10·5a SUCTION DREDGER MOVES AT SPEED $\bar{z}$
REMOVING SAND WHICH FALLS OFF DENSE
SAND FACE
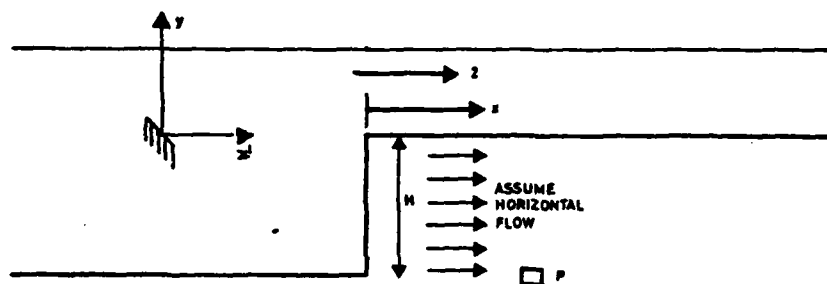
FIG. 10·5 b MOVING AND STATIONARY REFERENCE FRAME

dilation induced by shear of the dense sand. As the base of the steep slope advances on an element of soil, P, the shear stress on the element increases. The element develops pore suctions which are sufficient to hold up the slope.

The first part of the analysis that follows is derived from that presented by Meijer and Van Os, 1976. Thereafter a suggestion of Denner and James (op cit) is worked into the calculation to derive a new analysis of the retrogression of a steep unsupported face in dense sand. In Section 10.4 this analysis is combined with equations which describe the flow of the liquefied sand away from the face, to develop a comprehensive new explanation of the phenomenon of Mississippi flowsliding.

Consider the two coordinate systems of Fig. 10.5b which describe the steady state retrogression of the face at velocity Z. Diffusion of pore water into the sand body, in terms of the stationary (x', y) frame of reference, is described by

$$\frac{\partial^2 u}{\partial x'^2} = -\frac{\gamma_w m_{vc}}{k} \frac{\partial u}{\partial t} = -\frac{-\gamma_w}{(1+e_o)k} \frac{\partial e}{\partial t} = \frac{-\gamma_w}{k} \frac{\partial v'}{\partial t} \qquad (10.1)$$

where u = pore water pressure

$v' = \frac{\Delta v}{v_o}$ = volumetric strain

k = permeability ($= f(v')$ which we shall ignore)

m_{vc} = coefficient of volume compressibility

γ_w = density of water

e = voids ratio

A transformation from the stationary (x',y) frame to the moving (x,y) frame of reference requires that derivatives with respect to x' are replaced by those with respect to x; derivatives with respect to y remain unchanged and the differential quotient $\partial/\partial t$ for $(x', y = \text{constant})$ becomes

$$\frac{\partial}{\partial t} (x',y = \text{const.}) = \frac{\partial}{\partial t} (x,y = \text{constant}) - Z \frac{\partial}{\partial x} \qquad (10.2)$$

where $x = x' - Zt$ \hfill (10.3)
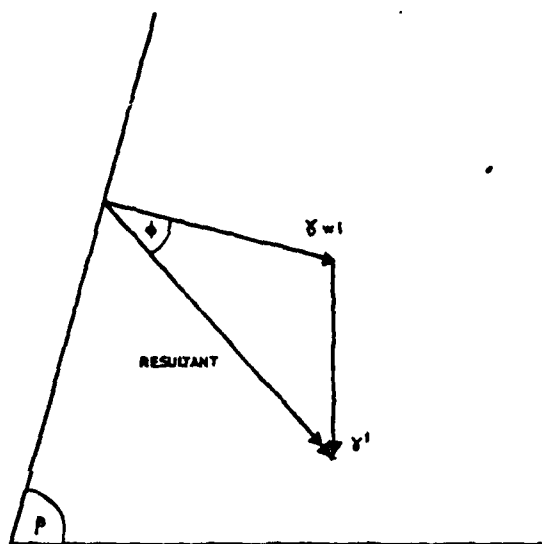
FIG. 10·6 TRIANGLE OF FORCES FOR STEEP DENSE SAND
SLOPE MAINTAINED IN LIMITING EQUILIBRIUM
BY INWARD SEEPAGE

Diffusion of pore water into the dilating sand body for any element P moving with the reference frame will now be described by:

$$\frac{\partial^2 u}{\partial x^2} = -\frac{\gamma_w}{k}\left(\frac{\partial v'}{\partial t} - \frac{Z\partial v'}{\partial x}\right) \tag{10.4}$$

Under steady state conditions when element P moves at velocity Z with the retrogressive face, $\frac{\partial v'}{\partial t} = 0$ and

$$\frac{\partial^2 u}{\partial x^2} = \frac{\gamma_w}{k}\frac{Z}{\partial x}\frac{\partial v'}{\partial x} \tag{10.5}$$

Equation 10.5 no longer describes a time dependent diffusion problem. The transformation has resulted in a steady state boundary value problem which for the purposes of the present analysis may be integrated to give:

$$\frac{\partial u}{\partial x} = \frac{\gamma_w}{k}\frac{Z}{v'} v' \tag{10.6}$$

whence $\quad Z = \frac{ki}{v'} \tag{10.7}$

where $i = \frac{du}{dx}$ = the hydraulic gradient horizontally into the face.

The analysis may be further simplified by using an equation derived by Bernatzik, 1969*, who points out that a simple triangle of forces as shown in Fig. 10.6 yields the following relation for seepage into a slope for the condition of limiting equilibrium

$$\frac{\gamma_w i}{\sin(\beta-\phi)} = \frac{\gamma'}{\sin\phi} \tag{10.8}$$

$$i = \frac{\gamma'}{\gamma_w}\frac{\sin(\beta-\phi)}{\sin\phi} \tag{10.9}$$

where ϕ = the angle of friction.

The experimental validity of this relationship has been demonstrated by Bernatzik. We can observe the stable angle β from experiments and so require only a value for v' for a determination of Z in Equation 10.7. If we estimate likely values for e in the undisturbed bed and at the free face to be 0.67 and 0.75 respectively, the volumetric strain becomes v' = 0.048 and hence the velocity of retrogression of the face may be calculated from

---

*Derived independently by D.M. Wood, 1977. Personal communication.

Equations 10.7 and 10.9 to give

$$Z = \frac{k\gamma'}{0.048\gamma_w} \frac{\sin(\beta-\phi)}{\sin\phi} \qquad (10.10)$$

where Z depends chiefly on the particle size distribution and packing, not on the height of the slope.

To check this it is possible to do a back analysis on the data given by Meijer and Van Os. Using their experimental values for $\beta = 80°$, $\gamma'/\gamma_w = 0.6$, $k = 0.15$ mm/sec and $\phi = 30°$, Equation 10.10 yields $Z = 0.29$ cm/sec. The actual value of Z in the experiments was 0.5 cm/sec. The two values are in fairly close agreement, but this agreement depends entirely on the values chosen for e and hence the value of v'.

10.3   Flow of Liquefied Sand

10.3.1   Prediction of Flow Properties

In the previous section an expression was developed which predicts the rate of regression of a steep face in dense sand. The material which falls off the face in the experiments is seen to flow for a short way before coming to rest. In this section the flow away from the face will be quantified and the two analyses will be related one to the other in Section 10.4.

Numerous studies, Bagnold, 1954, Happel and Brenner, 1965, Clarke, 1967, Davidson and Harrison, 1963, have shown that a dispersion of solid particles in water may be treated as a viscous liquid. At low rates of shear there is little evidence of viscous dilatancy, although at higher shear rates the viscosity is found to increase and eventually at high Reynolds numbers the process must be treated as a turbulent flow. A fully liquefied sand bed is a concentrated dispersion which resediments from the bottom upwards, but the portion of the bed which is mobile is able to flow for a limited time as a viscous fluid under the action of

FIG. 10·7 VISCOUS FLOW DOWNHILL OF LIQUEFIED SAND LAYER
MOVING COORDINATE AXES
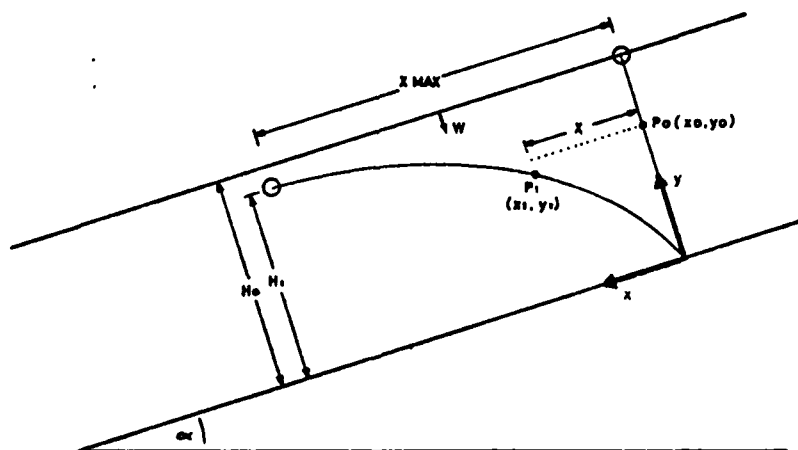
FIG. 10·8 STATIONARY COORDINATE AXES

gravity. If the bed is only partially liquefied a component of frictional resistance modifies the viscous behaviour.

An analysis presented by Allen and Banks, 1972, is used as the starting point for the study of the steady flow downslope of a layer of liquefied sand. Allen and Banks concern themselves with the shear deformations induced in liquefied layers of sand by surficial current drag. In the analysis presented in this section the loading in shear is gravitational. Several assumptions are made in the analysis. The gravitational loading has been lumped for simplicity into a concentrated load on the surface of the layer. Furthermore, the simplifying assumptions have been made that the flow is laminar and displays a linear velocity gradient with depth. The latter assumption leads to an overestimate of the distance travelled by the uppermost grains.

Fig. 10.7 shows the liquefied bed inclined at angle α to the horizontal. The total initial depth of the bed perpendicular to the slope is H_o and d is the instantaneous depth from the top surface of the bed to the upward moving surface of resedimentation. The thickness of the bed is steadily decreasing: the upper surface is moving downwards with velocity W_d , the fall velocity of the grain aggregate, taking with it the co-ordinate axes (X,Y). The particle volume concentration in the dispersion and the deposit, Fig. 10.7, are C_o and C_1 respectively where

$$C = 1/(1+e)$$

The surface resedimentation is moving upwards with respect to stationary axes (x,y), Fig. 10.8, at velocity V. The resedimentation of a fine sand dispersion obeys Equation 7.3 of Richardson and Zaki, 1954, quoted in Section 7.3.3

$$W_d = W_\infty (1-C_o)^n \tag{10.11}$$

where W_d is the fall velocity of the grain at concentration C_o, W_∞ is the fall velocity at infinite dilution and $n = 4$ for the present purposes. Relative to the co-ordinate axes (X,Y) that are descending with the uppermost grains, the surface of redeposition is moving upwards with velocity $(V+W_d)$. Therefore in one second $(V+W_d)C_o$ grains land on the surface. The velocity of accretion of the surface of redeposition is then, with respect to the fixed co-ordinate axes (x,y)

$$V = \frac{(V+W_d)C_o}{C_1} \tag{10.12}$$

and hence

$$V = \frac{C_o\, W_d}{(C_1-C_o)} = \frac{C_o\, W_d}{\Delta C} = \frac{C_o\, W_\infty (1-C_o)^n}{\Delta C} \tag{10.13}$$

The length of time taken for the layer to resediment completely is then given by Equations 10.11 and 10.13 as

$$T = \frac{H_o}{V} = \frac{\Delta C\, H_o}{W_\infty\, C_1 (1-C_o)^n} \tag{10.14}$$

Experimental values of T/H_o are given in the Table below. These values were obtained by Lowe, 1976ii, for the resedimentation of liquefied beds of uniform glass spheres in salt water for which $C_o = 0.54$ and $C_1 = 0.60$

Grain Diameter × 10^{-3} mm	$\dfrac{\text{Resedimentation Time}}{\text{Bed Thickness}} = \dfrac{T}{H}\ (\dfrac{\text{sec}}{\text{mm}})$
0.062	1.19
0.125	0.27
0.25	0.071
0.50	0.026
1.0	0.011
2.0	0.006

Use of these sedimentation equations represents a slight departure from normal soil mechanics practice which often uses the initial value diffusion equations. The sedimentation is a steady state process involving a linear pressure gradient and constant fluid velocity through the depth
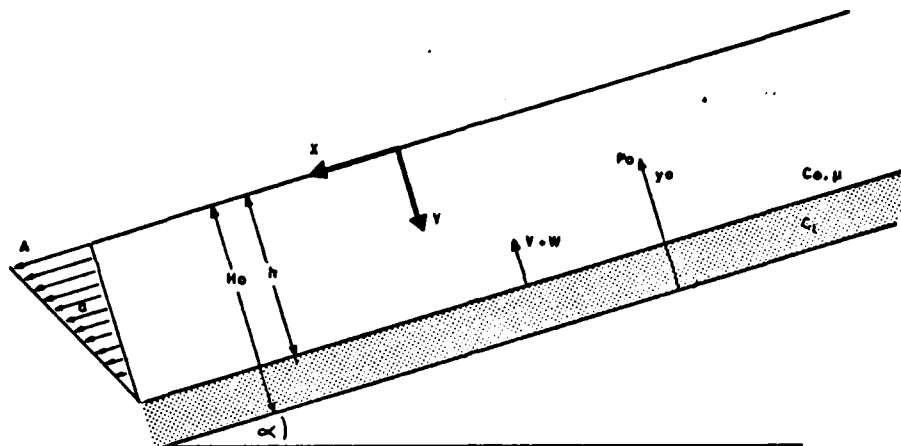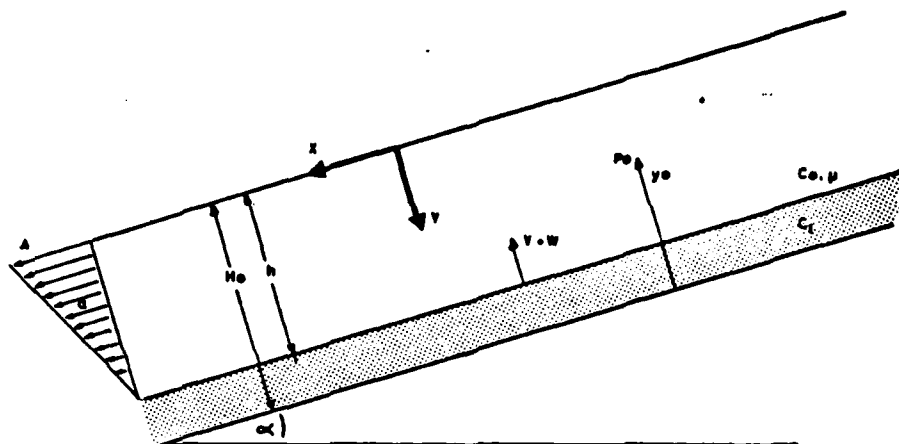
FIG. 10·7 VISCOUS FLOW DOWNHILL OF LIQUEFIED SAND LAYER
MOVING COORDINATE AXES
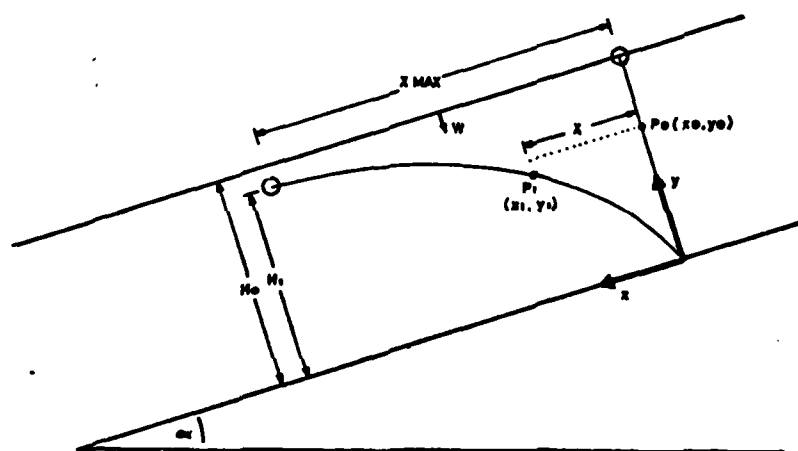
FIG. 10·8 STATIONARY COORDINATE AXES

of the suspension. The diffusion equations are not involved.

In order to calculate the distance travelled by the flowing sand layer before it resediments it is necessary to set up the equations of equilibrium and continuity for the layer. The two co-ordinate systems will again be used; the moving co-ordinate reference frame (X,Y) on the descending upper surface of the layer and (x,y) on the fixed lower boundary, Figs 10.7,8. From the assumption of linear velocity gradient, see Fig. 10.7,

$$a(\text{at depth } Y) = a(Y) = A \left(1 - \frac{Y}{h}\right) \qquad (10.15)$$

where h = the current thickness of the flowing layer.

The shear stress within the flowing layer is assumed to be constant over the full depth. This derives from the simplifying assumption discussed above that gravitational stress is lumped on the surface of the layer. The shear stress is given by

$$\tau = h\gamma'g \sin\alpha \qquad (10.16)$$

where $h = f(\text{time})$

For viscous flow of the liquefied layer

$$\tau = -\mu \frac{da}{dY} \qquad (10.17)$$

where μ = viscosity

From equations 10.15 and 10.17

$$a(Y) = \frac{\tau}{\mu}(h-Y) \qquad (10.18)$$

Referring now to Fig. 10.8, consider the motion of a particle P_o at initial height y_o above the base of the bed. After resedimentation P_o will have moved to P_1 and the y co-ordinate of P_1 will be $y_1 = y_o\, C_o/C_1$ and similarly the final depth of the deposit will be $H_1 = H_o\, C_o/C_1$.

Now Equation 10.18 may be transformed into (x,y) co-ordinates to obtain

$$a(y_o) = \frac{\tau}{\mu}(h-H_o+y_o) = \frac{h\gamma'g \sin\alpha}{\mu}(h-H_o+y_o) \qquad (10.19)$$

It is also possible to relate the value of h to time as follows:

$$h = H_o - t(V + W_d) \tag{10.20}$$

which, substituting Equation 10.13 becomes

$$h = H_o - t\, W_d\, (\frac{C_o}{\Delta C} + 1) \tag{10.21}$$

where $t = t_o$ at $H = H_o$ and hence Equation 10.19 becomes

$$a(y_o, t) = \frac{\gamma'g\, \sin\alpha}{\mu} \{y_o - t\, W_d\, (\frac{C_o}{\Delta C} + 1)\}\{H_o - t\, W_d\, (\frac{C_o}{\Delta C} + 1)\} \tag{10.22}$$

The particle P will come to rest when $d = H_o - y_o$, that is when

$$t = t_1 = \frac{y_o}{W_d(\frac{C_o}{\Delta C} + 1)} \tag{10.23}$$

from Equation 10.21. At this time $t = t_1$, $y = y_1$ and $x = x_1 = x_o + X$ where

$$X = \int_{t_o}^{t_1} a(y_o, t)\, dt \tag{10.24}$$

$$= \frac{\gamma'g\, y_o^2 \sin\alpha}{6\mu W_d(\frac{C_o}{\Delta C} + 1)} \cdot (3H_o - y_o) \tag{10.25}$$

Equation 10.25 is a general expression for distance travelled by a particle at any depth y_o. The distance travelled by the uppermost layer of grains for $y_o = H_o$ is

$$X = \frac{\gamma'g\, H_o^3\, \sin\alpha}{3\mu W_\infty(\frac{C_o}{\Delta C} + 1)(1-C_o)^n} = \frac{\gamma'g\, \sin\alpha \Delta C}{3\mu\, C_1\, W_\infty(1-C_o)^n} H_o^3 \tag{10.26}$$

and the average speed of travel of the uppermost grains is

$$\overline{A} = \frac{X}{T} = \frac{\gamma'g\, H_o^2 \sin\alpha}{3\mu} \tag{10.27}$$

The choice of values for these parameters is discussed in Section 10.4.
The values given below are quoted to a high degree of accuracy only for

the purposes of Section 10.4. They are intended to be reasonable values.

$C_1 = 0.59$ ($e_1 = 0.69$) $\Delta C = 0.0127$

$C_o = 0.5773$ ($e_o = 0.732$)

$\gamma' = 0.58\ \gamma_w$

$\alpha = 20^o$ $\sin\alpha = 0.342$

$\mu = 200$ poise (Bagnold, 1954, Lowe, 1976, Allen and Banks, 1972)

$g = 9.81$ m/s^2

$W_\infty = 4 \times 10^{-4}$ m/s for sand of grain diameter 125 μm

whence $X = 5470\ H_o^3$

and $\overline{A} = 3.24\ H_o^2$

The flow begins to become turbulent for $R_e > 500$ or $H_o > 0.16$ m and so for values of thickness less than $H_o = 0.16$ m the following flow distances and velocities are obtained:

H_o	X	$\overline{A}$
10 mm	5 mm	0.32 mm/sec
0.1 m	5.47 m	0.0324 m/sec
0.16 m	22 m	0.082 m/sec

Notice that the sand travels a long way if the layer which starts to flow is thicker than about 100 mm. Velocities of the order of several m/sec have been suggested for turbidity currents, in other words very much greater than the values derived above. The flow of a liquefied layer can evolve into a turbidity current if it is accelerated on a steep subaqueous slope, becomes turbulent and dilates.

The development of the flow from rest requires a period of acceleration. Schlichting, 1960, found that this steady state condition was developed for

all practical purposes once the dimensionless quantity

$$\frac{1}{H}\sqrt{\frac{\mu t}{\gamma}} = 1 \qquad\qquad (10.28)$$

where the symbols are defined above

or $\qquad t \simeq \dfrac{H^2\gamma}{\mu}$ $\qquad\qquad\qquad\qquad$ (10.29)

This time may be compared with the time for which the layer remains mobile, Equation 10.14. The period of acceleration is short for the purposes of this analysis if

$$\frac{H_o^2\,\gamma}{\mu} << \frac{\Delta CH_o}{W_\infty\,C_1(1-C_o)}n \qquad\qquad (10.30)$$

Consider the Inequality 10.30 to determine whether the time taken to accelerate the flow is indeed small in comparison with the lifetime of the layer:

If H_o = 10 mm

$\qquad$ 0.02 sec << 17 $\qquad$ A factor of 840

If H_o = 1 m

$\qquad$ 200 sec << 1700 $\qquad$ A factor of only 8.4

With increasing depth the inertial acceleration of the layer becomes more important.

In conclusion it must be stressed that the analysis presented above is largely speculative and requires substantiation. It would be strengthened by experimental verification of the assumptions which concern viscous deformation and the voids ratios involved in the flows. However, the phenomenon may be observed in the laboratory at small scale and the observations of Allen and Banks of flow structures in sand-stones support the physical possibility of the mechanism hypothesised.

10.3.2 Scaling of Flow Behaviour on Centrifuge

From this analysis two important points emerge. Firstly the distance travelled by a liquefied sand layer increases with the cube of the initial

layer thickness, Equation 10.26. The *flow process is heavily scale*
dependent. Thus a thick layer of Zone 'A' sand will flow further and
faster than a thinner layer. Secondly, the speed of movement of the
unsupported face during retrogressive failure in dense sand discussed in
Section 10.2.2 depends on the permeability and dilational properties of
the deposit. The mass flow rate of material falling off the face varies
linearly with the height. Only the flow of material from the base of
the face is governed by the cube rule.

It should be noted that the analyses presented above are very sens-
itive to the assumptions made about slope angle and voids ratio. In
fact, any assumption about the voids ratio is the governing assumption
since it will be seen in the following section that the slope angle may
be calculated once values have been assumed for the voids ratios.

From the equations for distance travelled by the uppermost grains in
the flowing sand layer, Equation 10.26, it may be seen that very thin sand
layers sediment so rapidly that they are only able to flow a short way.
Even if full liquefaction is achieved in a small scale model the sand
will not flow far and the effects of the liquefaction may not even be
noticed.

This point is of fundamental importance in modelling. In Equation
10.26 for X, the free fall velocity of a particle at infinite dilution,
W_∞, varies linearly with ng, ($W_\infty = \frac{1}{12}\frac{D^2 \gamma' g}{\mu}$ for a sphere falling at ter-
minal velocity under gravity in a viscous fluid, Stokes law). X is in
effect independent of g but is extremely dependent on scale. The cent-
rifuge may be of some use in modelling the flow behaviour of reduced
scale granular materials although it may only be of use in the qualitative
sense of visualisation of mechanisms of failure. However, certain aspects
of material transport may be scaled by altering the grain size distribution
of the granular material. Inspection of the equations shows that the

distance X scales linearly if both the layer thickness H_o and the particle diameter D are scaled by the same factor. X is independent of the value of gravitational acceleration, g. However, for other types of process not dominated by sedimentation, a different scaling factor may be appropriate for D. For example, where diffusion of water pressures and so permeability govern the behaviour D may have to be scaled by $1/\sqrt{n}$ if H_o is scaled by $1/n$. In short, the proper scaling factor depends on the process involved, Pokrovski and Fyoderov, 1968. The centrifuge may also, in certain circumstances, be required to initiate a flow. It has been suggested that the time scale of a small scale model may be extended by increasing the viscosity μ of the fluid phase, but Equation 10.26 shows that X is also independent of μ since W_∞ varies inversely with μ. It seems that flow phenomena can only be fully reproduced at full scale.

10.4   Prediction of Failure Geometry

Using the analyses developed above it is possible to make a prediction of the final shape of a flowslide scar. The results of the analysis depend strongly on the assumptions made, but the necessary assumptions do not seem at all unreasonable, and until experimental evidence is presented to verify or reject them, the prediction seems to describe the phenomenon rather well.

Imagine that some agency has scoured away the front face of a point bar sand deposit to leave a steep retrogressing face, Fig. 10.9. The sand layer is horizontal and uniform and the sand which flows into the scour hole is immediately removed.

In front of the moving retrogressing face a continuous process of sedimentation is taking place. The sand which falls off the face collects in a smoothly flowing viscous carpet of grains. The base of the moving layer is moving upwards at a speed

$$V = \frac{C_o W_d}{\Delta C} \qquad (10.13 \text{ bis})$$
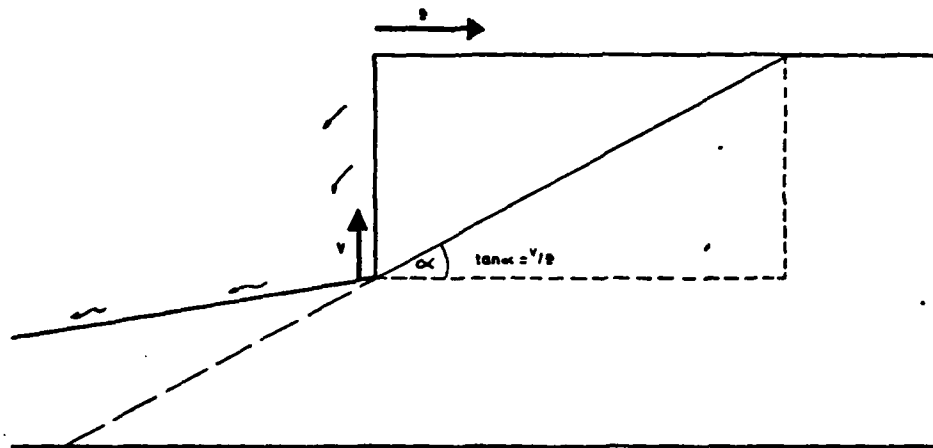
FIG. 10·9 STEEP RETROGRESSING FACE IN DENSE SAND
RATE OF DECREASE IN HEIGHT OF FACE
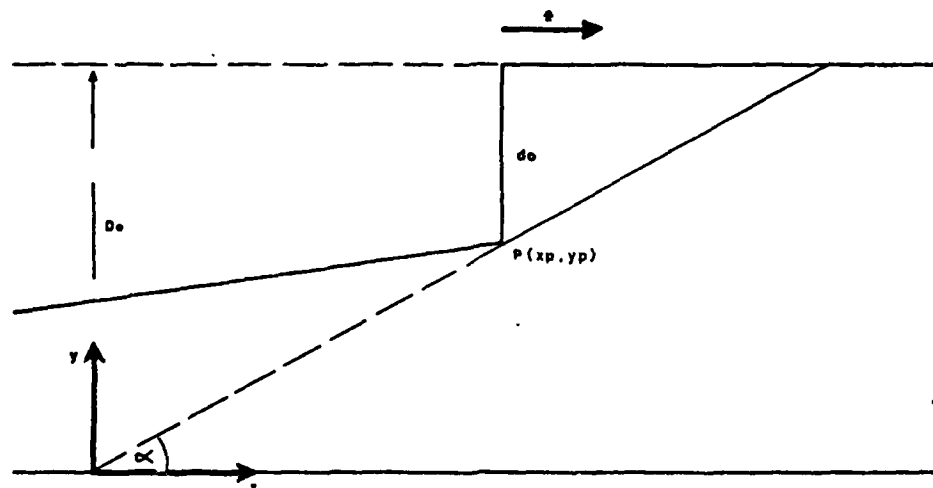
FIG. 10·10 COORDINATE AXES

This means that the foot of the retrogressing face is being continuously choked up by sedimenting grains which results in a steady decrease in the height of the face. Fig. 10.9 shows the steep face (drawn in the figure as vertical) moving through the layer and becoming progressively shorter. The angle of the wedge of disturbed material is given by the relation between V and the velocity of regression, Z of the face. Hence, using Equations 10.11 and 10.13,

$$\tan\alpha = \frac{V}{Z} \cdot \frac{C_o \, W_\infty (1-C_o)^n}{Z\Delta C} \qquad\qquad\qquad (10.31)$$

This angle depends strongly on the assumptions made for C_o and C_1. The grains which sediment out are rolled over one another and will achieve a medium dense packing, say $e = 0.7$. The density of packing of the grains in the suspension must remain a guess in the absence of experimental evidence. A value $e = 0.73$ gives a wedge angle of 6.5^o which agrees well with results of flow failures along the Mississippi, and will be used in the following analysis. The variation of α with C_o is considerable however:

For $C_1 = 0.59$, ($e_1 = 0.69$)

C_o	0.54^o	0.55^o	0.56^o	0.57^o	0.5775^o	0.58^o	0.585^o
e_o	0.85^o	0.82^o	0.79^o	0.75^o	0.73^o	0.72^o	0.71^o
α	2.21^o	2.58^o	3.20^o	4.46^o	6.5^o	8.21^o	30.3^o

In Fig. 10.10 the datum height of the face is taken to be D_o at an arbitrary origin along the x axis. Consider a point P, through which the base of the face has passed. The co-ordinates of P are $(x_p, \frac{Vx_p}{Z})$. After the face has passed, sand grains will flow over P, steadily building up a layer of newly deposited grains. The flowing layer will thin slowly, as the face moves further away, but the rate of deposition is constant until some instant T_p seconds after the scarp passed through P, when the 'last grain' will settle above P. This 'last grain' set off as the top particle

of the flowing layer when the face was displaced a distance X along the axis from P. X is given by

$$X = \frac{\gamma' g \sin\alpha}{3\mu} \frac{\Delta C}{W_\infty C_1 (1-C_o)} n \, H_o^3 = b \, H_o^3 \qquad (10.26 \text{ bis})$$

where H_o was the thickness of the flowing layer when the "last grain" set off. The time taken for the particle to get to P from the moment it set off is given by Equation 10.14

$$t_F = \frac{\Delta C \, H_o}{W_\infty C_1 (1-C_o)^n} \qquad (10.32)$$

The time taken by the vertical retrogressing face to get from P to the point where the "last grain" started its journey is

$$t_R = \frac{X}{Z} = \frac{b H_o^3}{Z} \qquad (10.33)$$

In other words between the time the face passed through P and the time the "last grain" landed the time elapsed is

$$T_p = t_F + t_R = \frac{b H_o^3}{Z} + \frac{\Delta C \, H_o}{W_\infty C_1 (1-C_o)} n \qquad (10.34)$$

At the time the last particle set off the height of the face was

$$d = D_o - \frac{xV}{Z} - \frac{b V H_o^3}{Z} \qquad (10.35)$$

and the flow velocity of the "last grain" away from the face on the top of its layer was, from Equation 10.18,

$$A = \frac{\tau H_o}{\mu} = \frac{H_o^2 \gamma' g \sin\alpha}{\mu} \qquad (10.36)$$

A value for H_o may be obtained by equating the flow rates of material leaving the face and that flowing away on the carpet of grains to give:

$$dZC_1 = \frac{A \, H_o \, C_o}{2}$$

$$\therefore \left(D_o - \frac{xV}{Z} - \frac{b V H_o^3}{Z}\right) ZC_1 = \frac{H_o^3 \gamma' g \sin\alpha}{2\mu} C_o \qquad (10.37)$$
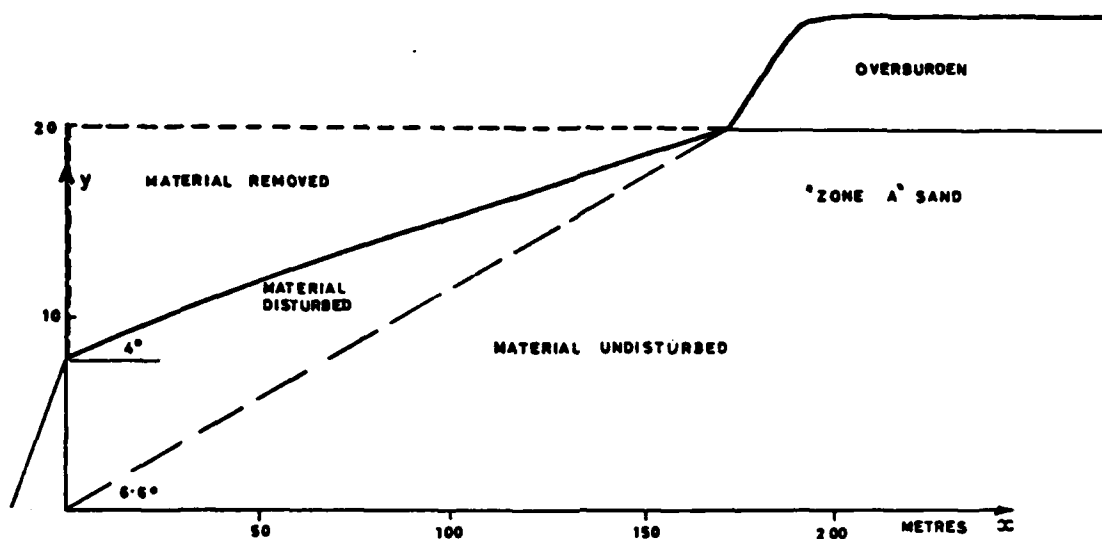
FIG. 10·11 THEORETICAL AFTER FAILURE PROFILE FOR
INITIAL SCARP OF 20m IN 'ZONE A' SAND.
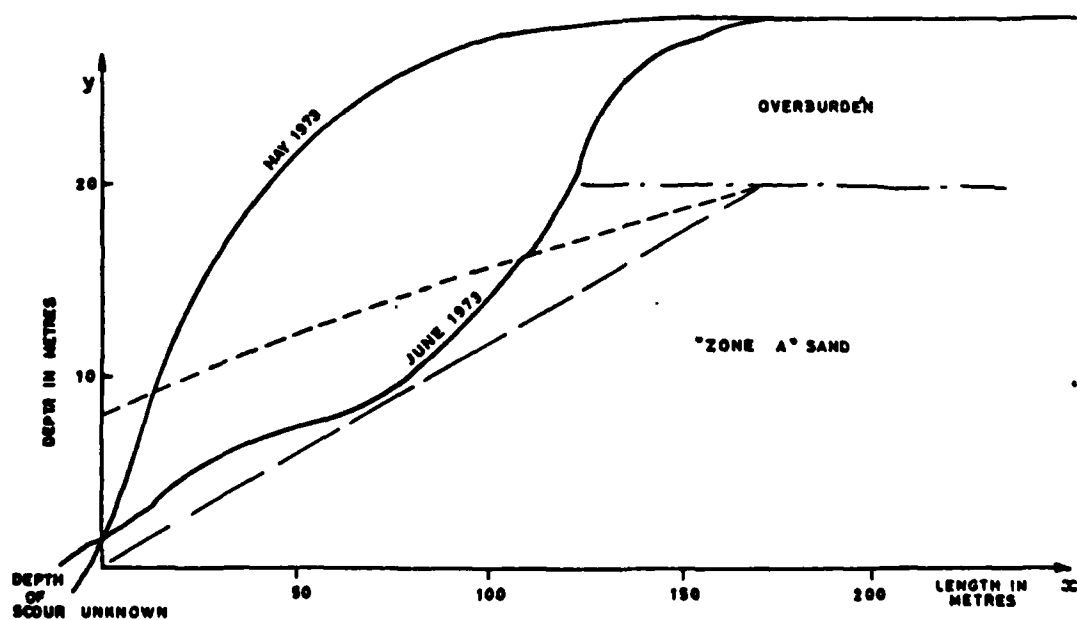
FIG. 10·12 PROFILES BEFORE AND AFTER FLOW
STANTON FLOWSLIDE 1973.

whence

$$H_o = \sqrt[3]{\frac{2\mu C_1 (ZD_o - xV)}{\gamma'g \sin\alpha\, C_o + 2\mu bVC_1}} \qquad (10.38)$$

In time T_p the sedimenting sand has built up a layer $T_p V$ thick on top of P and so the new co-ordinate of the upper surface above P, and hence the equation of the final surface after failure is

$$y = \frac{xV}{Z} + T_p V \qquad (10.39)$$

$$= \frac{xV}{Z} + V\{\frac{bH_o^3}{Z} + \frac{\Delta C\ H_o}{W_\infty C_1 (1-C_o)}n\} \qquad (10.40)$$

$$= \frac{2D_o}{5} + \frac{3W_\infty C_o (1-C_o)^n\ x}{5Z\ \Delta C} + \frac{C_o}{C_1} \sqrt{\frac{6\mu C_1 (ZD_o\ \Delta C - xW_\infty C_o (1-C_o)^n}{5\gamma'g \sin\alpha\, C_o\ \Delta C}} \qquad (10.41)$$

Substituting the values used above, viz

$W_\infty = 4.10^{-4}$ m/sec $\qquad Z = 5 \times 10^{-3}$ m/sec $\qquad \sin\alpha = 0.115$

$C_o = 0.5772$ ($e_o = 0.73$) $\quad \mu = 200$ poise $\qquad \alpha = 6.5^{\circ}$

$C_1 = 0.59$ ($e_1 = 0.69$) $\quad \gamma' = 0.58\ \gamma_w \qquad\qquad n = 4$

$\Delta C = 0.127 \qquad\qquad\qquad g = 9.81$ m/sec^2

Equation 10.41 simplifies to

$$y = 0.07x + 0.4D_o \qquad (10.42)$$

This may be further simplified by taking a typical value for D_o = Zone A thickness = 20 m to give $y = 0.07x + 8.0$ which generates the after failure profile shown in Fig. 10.11. In this diagram the vertical scale is exaggerated. A wedge of redeposited material is left behind at a slope of approximately 4°. The steep face has eaten its way 172 m into the deposit in $9\frac{1}{2}$ hours at an angle of 6.5°. The shape of the final surface is slightly curved and the material removed (1030 m^3 per m run) has been transported away by the river.

It can be seen that although this mechanism is unproven it accounts well for the observed facts (cf. Fig. 10.12, which shows the Stanton failure).

It is more likely that this stable process of retrogression is the cause of the spectacular flow failures along the Mississippi, than the more generally supposed spontaneous liquefaction. The calculation presented above is however, not a complete answer to the problem: several anomalies remain to be cleared up and further research is required to elucidate them.

Manipulation of the equations yields for the distance travelled by the uppermost grain which has fallen off a retrogressing face of height D

$$X = \frac{2DZ\Delta C}{3W_{\infty} C_{o}(1-C_{o})^{n}}$$ (10.43)

whence for the numerical values used above X = 5.74D. In this case X varies linearly with D but implicit in this equation is the liquefied flow behaviour which may not be scaled. Simple small scale tests with fine sand show that the angle α is closer to 30° than to 6°, which shows again that the small scale test is inappropriate to model flow behaviour. Very probably the assumption of pure viscous flow and the assumptions about voids ratios will not be valid for all scales. At small scale and at large scale the analysis may be inadequate, but at intermediate scale it agrees well with the phenomena observed both in experiment and in the field. It should be stressed however that this quantitative agreement depends very strongly on the numerical values chosen for all the parameters.

10.5 Relation of the Analysis to Prototype Sand Flow

The analysis has shown that:

1. The distance travelled by the uppermost grain of a liquefied layer increases with the cube of the initial thickness of the layer.

2. The distance travelled by the uppermost grain of the liquefied layer which flows away from a steep retrogressing face in a dense sand layer increases linearly with the depth of the dense layer.

If the process involved in a liquefied flowslide on the Mississippi is indeed, as is currently thought, a process of spontaneous liquefaction involving the whole depth of the layer, then the distance travelled by the debris varies with the cube of the layer thickness. The results of such a

flowslide in the deep formations of the Mississippi delta would be serious,
involving a very deep failure which would develop extremely rapidly. If,
on the other hand, the process is one of retrogression in a dense layer then
the material transport is proportional to the depth of the sand layer. The
time predicted for the development of such a failure agrees well with the
time taken in the field. The Empirical Criterion is a simple linear rel-
ation which describes the facts well. In the light of this it is extremely
unlikely that the phenomenon of flowsliding on the Mississippi is one of
spontaneous liquefaction.

The analysis presented in this Chapter was developed only after it was
realised that alternative explanations had to be sought for the phenomenon
of Mississippi flowsliding. At the outset of the project the author accepted
the datum that loose sand strata were responsible for the failures. The
first approach to the subject was an experimental investigation to model a
flowslide on the centrifuge. It was the failure of this investigation in
its attempt to demonstrate flowsliding in the small scale which led to the
analytical description of the phenomenon presented above.

CHAPTER 11

CONCLUSIONS RELATING TO MISSISSIPPI FLOWSLIDES

11.1 Conclusions

The discussions in Part II of this dissertation have served to put forward a complete alternative interpretation of the phenomenon of flow-sliding on the Mississippi. To do this the emphasis has been placed

1. on debris transport rather than on initiation of liquefaction, and

2. on the response of the overburden to lack of support due to the flow of sand, rather than the precise in-situ material conditions of the sand layer.

The following conditions have been identified for the successful propagation of a flowslide of any type:

(a) The granular material deforms, fails and becomes liquefied.

(b) The liquefied layer is able to flow away from the failure and does not remain choking up the outlet of the flowslide scar.

(c) Overlying layers do not, by their deformation, restrict the flow or block the outlet of the failure.

In regard to the specific conditions on the Mississippi four main conclusions can be drawn.

1. Flowslides along the Mississippi are often attributed to the flow of debris from the propagation of a failure into a loose sand formation (contractional response). It has been shown that it is also possible that the same type of crater may result from a retrogressive failure in a very dense sand layer (dilatant response).

2. The flow of a liquefied soil depends strongly on scale. If the flow failures are caused by the retrogression of a slide in dilatant materials the scale effect as between two prototype events may not be

serious: material transport varies linearly with the depth of the sand
layer. If, on the other hand, the phenomenon is one of spontaneous
liquefaction of a whole layer, or indeed depends on the liquefied
flow of a sand layer, the distance travelled by the flowing material
is found to vary with the cube of the layer thickness involved.

3. A study of the behaviour of the cohesive overburden layer of a point
bar deposit when the sand layer starts to flow away suggests that it
may deform in one of two ways. If the overburden layer is thicker than
the sand layer it will remain in place and inhibit sand flow. The
resulting bank depression is called a shear failure. If the
cohesive overburden layer is thinner than the sand layer then the
overburden will crack off into the crater which forms in the sand and
will be carried away into the river. The failure is able to
propagate and is called a flow-failure. This reasoning supports and
validates the empirical criterion. The criterion should apply at
any scale.

4. A section of river bank which is particularly sensitive to flow-failure
may be rendered stable by inhibiting the flow of sand into the river.
This may be done for example by providing horizontal reinforcement
and additional cohesive fill to the overburden.

11.2 Further Research

To elucidate the quantitative relevance of these conclusions requires
additional research.

1. Actual Site Conditions

Very little is known about the propagation of a flowslide in Mississippi
river point bar 'Zone A' sand. It should be possible by suction dredging
to initiate such a slide at some point along the river bank and observe the
progress of the slide with transducers within the sand layer to decide
whether the process is essentially contractive, dilatant or some other
mechanism such as the collapse of a single loose layer.

Borings may be made through old shear failures to determine whether the overburden layer is still intact and hence validate the hypothesis forwarded here.

2.   Flow Initiation

Tests may be performed at different scales with sands in a dense, intermediate and loose state to observe and measure the development of retrogressive flow initiation.

3.   Flow Processes and Resedimentation

The conditions for which turbulent or viscous flow relations are applicable may be determined by experiment with liquefied sand layers of different thickness at varying angles to the vertical. These may very simply be set up using the route to liquefaction through fluidisation.

Further experiment is required to quantify the assumptions made about voids ratios in the flowing and resedimented layers of a liquefied flow. These values may also depend on scale.

4.   Interaction of Layers

It is possible that certain other features of flowslides may be understood in terms of the interaction of layers. For example, it is possible that the characteristic bottleneck shaped scar in quick clay flowslides results from the thinning of a stiff crust away from the front face of the layer. Certain other examples were mentioned in Section 9.7, and it is likely that a wide ranging literature review will yield further examples of deformation and failure of layers of soil or rock which would be simply explained in terms of interaction.

CHAPTER 12

GENERAL CONCLUSIONS

12.1 Centrifuge Modelling

The phenomena that have been modelled in the course of this research have been complex. The modelling has necessarily simplified the loading and structure of the systems under study but has nevertheless provided relevant data. Observation of model behaviour provides food for thought such that misconceptions may be eliminated and preconceptions about behaviour of the prototype may be revised in the light of the observed model response to different boundary conditions. The subaqueous banks of a large river at flood stage provide an inclement environment for geotechnical research. Experiments may be performed on the centrifuge, which, for a fraction of the cost of full scale trials, give an indication of the relative importance of different parameters. However, the centrifuge is useful in modelling a process only when the process under study is influenced by the intensity of the gravitational field. If the process is independent of gravity then the experiment might just as well be performed on the laboratory floor. Nevertheless, a series of experiments at different values of gravity can confirm or reject the analytical hypothesis that the process is independent of gravity. In each case a series of centrifuge tests is useful, since both confirmation and rejection of a hypothesis are equally informative.

12.2 The Interaction of Layers

Two examples have been presented in this dissertation of complex natural processes, which may be clarified and explained by application of the concept of interaction. In both cases, two alternative modes of behaviour seem to be available to the natural event - one catastrophic, the other relatively controlled. The factor that decides which type of failure shall occur has

been previously unknown, but it has been shown in this dissertation that
it is the mechanisms of interaction between the two layers that are involved
in the deformation which are responsible for the bifurcation in behaviour.
Once the conditions are understood for which the different mechanisms of
deformation will occur it becomes clear that one mechanism is favoured in
certain cases and the other mechanism in others. This approach is the counter-
part of many calculations in the theory of plasticity but has not previously
been successfully used in soil mechanics.

REFERENCES

Al-Qassab, A.A.M. (1974) The stability of a compacted embankment in centrifugal model tests and in theory, Ph.D. Thesis, University of Manchester.

Allen, J.R.L. (1965) A Review of the Origin and Characteristics of Recent Alluvial Sediments, Sedimentology $\underline{5}$, 89-191.

Allen, J.R.L. (1969) Some Recent Advances in the Physics of Sedimentation, Proceedings of the Geologist's Association $\underline{80}$, 1-42.

Allen, J.R.L. (1970) The Avalanching of Granular Solids on Dune and Similar Slopes, J. Geol. $\underline{78}$, 326-351.

Allen, J.R.L. (1970) A quantitative Model of Grain Size and Sedimentary Structures in Lateral Deposits, Geol. J. $\underline{7}$, 129-146.

Allen, J.R.L. (1970) Physical Processes of Sedimentation, George Allen and Unwin, London.

Allen, J.R.L. and Banks, N.L. (1972) An Interpretation and Analysis of Recumbent Folded Deformed Cross Bedding, Sedimentology $\underline{19}$, 257-283.

Ambraseys, N. and Sarma, S. (1969) Liquefaction of Soil Induced by Earthquakes, Bull. Seis. Soc. of America $\underline{59}$, 651-664.

Andresen, A. and Bjerrum, L. (1967) Slides in Subaqueous Slopes in Loose Sand and Silt, Marine Geotechnique (Richardson, A. ed.).

Avgherinos, P.J. (1969) Centrifugal Testing of Soil Models, Ph.D. Thesis, Cambridge University.

Avgherinos, P.J. and Schofield, A.N. (1969) Drawdown Failure of Centrifuged Models, Proc. VII Int. Conf. on SM and FE $\underline{2}$, 497-504.

Bagnold, R.A. (1954) Experiments on a Gravity Free Dispersion of Large Solid Spheres in Newtonian Fluid Under Shear, Proc. Roy. Soc., London, Series 'A' $\underline{225}$, 49-63.

Bagnold, R.A. (1954) The Physics of Wind Blown Sand and Desert Dunes, London, Methuen and Co.

Bagnold, R.A. (1955) Some Flume Experiments on Large Grains but Little Denser than the Transporting Fluid, and their Implications, Proc. ICE, London $\underline{4}$, 174-205.

Bagnold, R.A. (1956) The Flow of Cohesionless Grains in Fluids, Phil. Trans. Roy. Soc., London 'A' $\underline{249}$, 235-297.

Bagnold, R.A. (1962) Autosuspension of Transported Sediment; Turbidity Currents, Roy. Soc., London Proc. 'A' $\underline{265}$, 315-319.

Bagnold, R.A. (1963) An Approach to the Sediment Transport Problem for General Physics, U.S. Geol. Survey Prof. Paper 422-I, 37pp.

Bagnold, R.A. (1968) Deposition: The Process of Hydraulic Transport, Sedimentology $\underline{10}$, 45-56.

Bassett, R.H. (1973) Centrifugal Model Tests of Embankments on Soft Alluvial Foundations, Proc. Int. Conf. on SM and FE $\underline{2.2}$, 33-38.

Beasley, D.H. (1973) Centrifugal Modelling of Soft Clay Strata Subject to Embankment Loading, Ph.D. Thesis, Cambridge University.

Begemann, H.K.S., Koning,H.Z., Lindenberg, J. (1977) Critical Density of Sand, Proc. 9th Int. Conf. on SM and FE, Tokyo.

Bernatzik, W. (1947) Baugrund and Physik.

Bishop, A.W. (1955) Use of Slip Circles in the Stability Analysis of Slopes, Geotechnique 5.1, 7-17.

Bishop, A.W., Kumapley, N.K., El-Ruwayih, A. (1975) The Influence of Pore Water Tension on the Strength of Clay, Phil. Trans. Roy. Soc. London 278, 511-554.

Bishop, A.W. and Morgenstern, N. (1960) Stability Coefficients for Earth Slopes, Geotechnique 10.4, 29-149.

Bishop, A.W. (1967) Progressive Failure - With Special Reference to the Mechanism Causing it, Proc. Geotech. Conf. Oslo, Norway 2, 142-150.

Bishop, A.W. et al (1969) Geotechnical Investigation into the Causes and Circumstances of the Disaster of 21 October 1966, in a 'Selection of Technical Reports Submitted to the Aberfan Tribunal', London HMSO (1969), 1-60.

Bjerrum, L. (1954) Theoretical and Experimental Investigations on the Shear Strength of Soils, NGI Pub. No. 5.

Bjerrum, L. Kringstad, S. and Kummeneje, O. (1961) The Shear Strength of a Fine Sand, Proc. 5th Int. Conf. on SM and FE 1, 29-37.

Bjerrum, L. (1971) Subaqueous Slope Failures in Norwegian Fjords, NGI Pub. 88, 1-8.

Bjerrum, L. (1973) Problems of Soil Mechanics and Construction of Soft Clays and Structurally Unstable Soils, Proc. 8th Int. Conf. on SM and FE, Moscow.

Bolton, M.D., English, R.J., Hird, C.C. and Schofield, A.N. (1973) "Modelling", Proc. Symp. on the Role of Plasticity in Soil Mechs, Cambridge.

Bridge, J.S. (1975) Computer Simulation of Sedimentation in Meandering Streams, Sedimentology 22, 3-43.

Brooker, E.W. and Ireland, H.O. (1965) Earth Pressures at Rest Related to Stress History, Canadian Geotech. Journal 11.

Calladine, C.R. (1968) Simple Ideas in the Large-Deflection Plastic Theory of Plates and Slabs, Engineering Plasticity, Cambridge University Press, (ed. Heyman, J. and Leckie, F.A.).

Calladine, C.R. (1969) Engineering Plasticity, Pergamon, London.

Cairncross, A.M. and James, R.G. (1977) Anisotropy in Overconsolidated Clays, Geotechnique 27, 31-36.

Casagrande, A. (1936) Characteristics of Cohesionless Soils Affecting the Stability of Slopes and Earthfalls, Journal Boston Soc. Civ. Eng. 37 405-429.

Casagrande, A. (1976) Liquefaction and Cyclic Deformation in Sands - A Critical Review, 5th Panamerican Conf. on SM and FE.

Castro, G. (1969) Liquefaction of Sands, Harvard Soil Mechs Series No. 81.

Castro, G. (1975) Liquefaction and Cyclic Mobility of Saturated Sands, Proc. ASCE 101, GS6, 551-569.

Clarke, B. (1967) Rheology of Coarse Settling Suspension, Trans. Inst. Chem. Engrs 45, 251-256.

Cooling, L.F. and Marsland, A. (1953) Soil Mechanics Studies of Failures in the Sea Defence Banks of Essex and Kent, Proc. I.C.E. Conf. N. Sea Floods, Lond., 58-73.

Cooling, L.F. (1955) Measurement of Pore Water Pressures and Application in Some Civil Engineering Problems, Rilem Symp. 18 Theme 1b, Lisbon.

Cornforth, D.H. (1964) Some Experiments on the Influence of Strain Conditions on the Strength of Sand, Geotechnique 14, 143-167.

Craig, W.H. (1974) Model Studies of the Stability of Clay Slopes, Ph.D. Thesis, University of Manchester.

Davidson, J.F. and Harrison, D. (1963) Fluidised Particles, University Press, Cambridge.

Davis, E.H. and Booker, J.R. (1973) The Effect of Increasing Strength with Depth on the Bearing Capacity of clays, Geotechnique 23, 551-563

de Koning, J. (1970) Field Observations of Gravity Flow to Suction Dredger in Sand Pits, Civ. Eng. Public Wks Review 65, 765, 903-5.

Durham, G.N. and Townsend, F.C. (1973) Effect of Relative Density on Susceptibility of a Fine Sand under Stress Controlled Loading, ASTM STP 523, 319-331.

Eden, W.F. and Mitchell, R.J. (1970) Mechanics of Landslide: Leda Clay, Canadian Geotech. Journal 7, 285-296.

Edgeton, A.E. (1970) Electronic Flash, Strobe, McGraw Hill.

Endicott, L.J. (1970) Centrifugal Testing of Soil Models, Ph.D. Thesis, Cambridge University.

Enos, P. (1777) Flow Regimes in Debris Flow, Sedimentology 24, 133-142.

Farquharson, W.I. (1953) Storm Surges on the East Coast of England, Conf. on the N. Sea Floods, Inst. Civ. Eng., London.

Fisk, H.N. (1977) Fine Grained Alluvial Deposits and their Effects on Mississippi River Activity, WES Vicksburg.

Florin, V.A. and Ivanov, P.L. (1961) Liquefaction of Saturated Sandy Soils, Proc. 5th Int. Conf. on SM and FE 1, 107-111.

Fredhund, D.G. and Krahn, J. (1976) Comparison of Slope Stability Methods of Analysis, Can. Geo. Conf. 'Slope Stability'.

Fuglsang, L.D. (1971) Preliminary Centrifugal Studies of the Deformation and Failure of Uniform Earth Slopes, M.Sc. Thesis, University of Manchester.

Geuze, E.C.W.A. (1948) Critical Density of Some Dutch Sands, Proc. 2nd Conf. on SM and FE 3, 125-130.

GLC (1969) 1st Report (1970) 2nd Report of Studies in Thames Flood Prevention.

Gretener, P.E. (1969) Fluid Pressure in Porous Media - Its Importance in Geology, a Review, Bull. Petrol. Geol. 17, 255-295.

Grieve, H. (1959) The Great Tide - The Flood of 1953, Essex C.C.

Happel, J. and Brenner, H. (1965) Low Reynolds Number Hydrodynamics, Prentice Hall, Englewood Cliffs, N.J.

Henkel, D.J. (1956) Discussion on 'Earth Movement Affecting the LTE Railway in Deep Cutting E. of Uxbridge', Proc. Inst. Civ. Eng. Pt II 5, 32-3.

Henkel, D.J. (1971) The Relevance of Laboratory Measured Parameters in Field Studies, Proc. Roscoe Mem. Symp., Cambridge.

Heyman, J. (1966) The Stone Skeleton, Int. J. Solids and Structures 2, 249-279.

Hird, C.C. (1974) Centrifugal Model Tests of Flood Embankments, Ph.D. Thesis, Manchester (UMIST).

Hird, C.C., Marsland, A., Schofield, A.N. (1978) The Stability of the Thames Flod banks, Geotechnique, 28, 85-106.

Horner, R.W. (197) 1. Historical Background to the Thames Barrier. 2. Sites and Schemes Considered. 3. The Site Chosen, Proc. Conference on Thames Barrier Design, 5 October, 1977, Institution of Civil Engineers, London.

Hutchinson, J.N. (1967) Discussion "Flowsliding", Proc. Geotech. Conf. Oslo, 214-5.

Hvorslev, M.J. (1960) Physical Components of the Shear Strength of Saturated Clays, ASCE Res. Conf. Shear Strength Cohesive Soils, Boulder, California.

James, R.G. (1972) Some Aspects of Soil Mechanics Model Testing, Proc. Roscoe Mem. Symp.,Cambridge.

Johnson, A.M. (1965) Physical Processes in Geology, Soc. Econ. Paleontologists and Minerologists Spec. Pub. 2, 14-33 (Freeman Cooper and Co., San. Fran. Cal.).

Keulegan, G.H. (1958) The Motion of Saline Fronts in Still Water, Rep. U.S. Nat. Bur. Standards, 5831.

Keunen, ph. H. (1951) Properties of Turbidity Currents of High Density, in (Turb. Currents and Transport of Coarse Sediments to Deep Water).

Keunen, ph. H. (1952) Estimated Size of the Grand Banks Turbidity Current, American Journal of Science 250, 874-884.

Keunen,ph. H. (1964) Deep Sea Sands and Ancient Turbidities, in Turbidities Bourne, A.H. and Brounever, A. eds, (Amsterdam, Elsevier).

Kolbuszewski, J. (1948) Exp. Study of Max. and Min. Porosity of Sand, Proc. 2 Int. Conf. on SM and FE 1, 158.

Koppejan, A.W., van Wamelan, B.M. and Weinberg, L.J.H. (1948) Coastal Flow-slides in the Dutch Province of Zeeland, Proc. 2 Int. Conf. on SM and FE 5, 89-96.

Lee, D.I. (1969) The Viscosity of Concentrated Suspensions, Trans. Soc. Rheol. 13, 273-288.

Leopold, L.B. and Wolman, M.G. (1957) River Channel Patterns: Braided, Meandering and Straight, U.S. Geol. Survey Profess. Papers 2828, 39-85.

Leopold, L.B., Wolman, M.G. and Miller, J.P. (1969) Fluvial Processes in Geomorphology, W.H. Freeman and Co., San Francisco.

Lowe, D.R. (1975) Water Escape Structures in Coarse Grained Sediments, Sedimentology 22, 157-204.

Lowe, D.R. (1976i) Grain Flow and Grain Flow Deposits, J. Sed. Petrol. 46, 188-199.

Lowe, D.R. (1976ii) Subaqueous Liquefied and Fluidised Sediment Flows and their Deposits, Sedimentology 23, 285-308.

Lyndon, A. (1972) Centrifugal Model Tests of a Natural Clay Slope Failure, Ph.D. Thesis, Manchester (UMIST).

Malushitsky, (1975) The Stability of Slopes and Embankments, In translation, Cambridge University Press.

Marsland, A. (1957) The Design and Construction of Earthen flood banks, Journ. I.W.E. II, 236-258.

Marsland, A. (1957) Discussion Proc. 4th Int. Conf. Soil Mechanics and FE, 3, 257.

Marsland, A. (1961) A Study of a Breach in an Earthen Embankment Caused by Uplift Pressures, Proc. 5th Int. Conf. SM and FE, Paris 2, 663-668.

Marsland, A. (1968) Report on the Preliminary Investigation to Study Stability River Banks at Thamesmead, B.R.E. Report.

Marsland (1973) Instrumentation of Flood Defence Banks Along the River Thames, In Symposium Papers, Proc. Symp. on Field Instru. 1, 287-303 (B.R.E. Cp 26/73).

Marsland, A. and Powell, J.J.M. (1977) The Behaviour of a Trial Bank Constructed to Failure on the Soft Alluvium of the River Thames, B.R.E. to be published.

Marsland, A. and Randolph, M. (1978) Modelling of Tidal Water Flow in a Gravel Aquifer at Crayford Ness, To be published in Geotechnique.

Maude, A.D. and Whitmore, R.L. (1958) A Generalised Theory of Sedimentation, Brit. for App. Physics 9, 477-482.

McTaggart, K.C. (1962) The Mobility of Nuées Ardentes, Amer. Jour. Sci. 258, 369-382.

McTaggart, K.C. (1962) Nuées Ardentes and Fluidisation - A Reply in Discussion, Amer. Jour. Sci. 260, 470-476.

Meijer, K.L. and van Os., A.G. (1976) Pore Pressures Near Moving Under-
water Slope, ASCE JGED 102, GT4 301-372.

Meijerhof, G.G. (1965) Bearing Capacity of Floating Ice Sheets, Proc. Am.
Soc. Civ. Eng., J. Eng. Mech. Div. 86, 113-145.

Menard, H.W. (1964) Marine Geology of the Pacific, McGraw Hill.

Middleton, G.V. (1966) Small Scale Models of Turbidity Currents and the
Criterion for Autosuspension, J. Sedimentary Petrology 36, 202-208.

Middleton, G.V. (1969) (i) Turbidity Currents GM-A-1 to 20, (ii) Grain
Flows and Other Mass Movements Down Slopes GM-B-1 to 14, AGI Short Course
Lecture Notes, 7 November, 1969, Philadelphia (American Geological
Institute) 'The New Concepts of Continental Margin Sedimentation'.

Middleton, G.V. and Hampton, M.A. (1973) Sediment Gravity Flows - Mechanics
of Flow and Deposition, 1-38, Turbidities and Deep Water Sedimentation,
Short Course Lecture Notes, Pacific Section SEPM, Los Angeles.

Mikasada, Takada, Yamada (1969) Centrifugal Model Test of a Rock Fill
Dam, 7th Int. Conf. on SM Mexico 2, 325-333.

Mitchell, R.J. and Markell, A.R. (1974) Flowsliding in Sensitive Soils,
Can. Geot. J. 11, 11-31.

Mooney, M. (1951) The Viscosity of a Concentrated Suspension of Spherical
Particles, J. Colloidal Science 6, 162-170.

Moore, D.G. (1961) Submarine Slumps, J. Sed. Petrol. 31, 343-357.

Morgenstern and Price (1965) The Analysis of the Stability of General Slip
Surfaces, Geo. 15, 59-63.

Morgenstern, N.R. (1967) Submarine Slumping and the Initiation of Turbidity
Currents, Marine Geotechnique (Richardson, A. ed.).

Nadarajah, V. (1973) Stress Strain Properties of Lightly Overconsolidated
Clays, Ph.D. Thesis, Cambridge.

Palmer, A.C. and Rice, J.R. The Growth of Slip Surfaces in the Progressive
Failure of Overconsolidated Clay, Proc. Roy. Soc., London, A 332, 527-548.

Parry, R.H.G. (1970) Overconsolidation in Soft Clay Deposits, Geotechnique
20, 442-446.

Parry, R.G.H. (1972) Stability Analysis for Low Embankments on Soft Clays,
Proc. Roscoe Mem. Symp., Cambridge.

Parry, R.G.H., Nadarajah, V. (1973) Volumetric Yield Locus for Lightly Over-
consolidated Clay. Geotechnique 23, 450-453.

Parry, R.H.G. and Wroth, C.P. (1976) Pore Pressures in Soft Ground under
Surface Loading: Vol. 1 - Theoretical Considerations, Vol. 2 - Inter-
pretation of Field Records, Contract Report S-76-3, WES Vicksburg.

Peck, R.B., and Kaun, W.V. (1948) Description of a Flowslide in a Loose Sand, Proc. 2 Int. Conf. on SM and FE 2, 31-33.

Peters, S.P. (1953) Some Meteorological Aspects of North Sea Floods, with Special Reference to February 1953, Conf. on the N. Sea Floods, Inst. Civ. Eng., London.

Pokrovski, G.I. and Fyoderov, I.S. (1936) Studies of Soil Pressures and Deformations by Means of a Centrifuge, Proc. 1st Int. Conf. on SM and FE, Harvard 1, 70.

Pokrovski, G.I. and Fyoderov, I.S. (1968) Centrifugal Model Testing in the Construction Industry, In translation, B.R.E.

Pokrovski, G.I. and Fyoderov, I.S. (1969) Centrifugal Modelling of Mining Works, In translation, B.R.E.

Poulos, A.G. and Davis, E.H. (1974) Elastic Solutions for Soil and Rock Mechanics, John Wiley.

Reynolds, O. (1886) Dilatancy, Nature 33, 429-430.

Richardson, J.F. and Zaki, W.N. (1954) Sedimentation and Fluidisation, Part I Trans. Inst. Chem. Engng S. 32, 35-53.

Rodine, J.D. and Johnson, A.M. (1976) The Ability of Debris, Heavily Freighted with Coarse Elastic Materials, to Flow on Gentle Slopes, Sedimentology 23, 213-234.

Roscoe, K.H. (1968) Soils and Model Tests, J. Strain Analysis 3.

Russell, R.J. (1970) River and Delta Morphology, Louisiana State University Press, Coastal Studies Series 20.

Schlichting, H. (1960) Boundary Layer Theory, McGraw Hill, N.Y. 4th Ed.

Schofield, A.N. (1976) Use of Centrifugal Model Testing to Assess Slope Stability, CUED/C Soils TR.30.

Schofield, A.N. and Wroth, C.P. (1968) Critical State Soil Mechanics, McGraw Hill.

Scott, R.F. (1975) The Centrifugal Technique in Geotechnology, California Institute of Technology.

Scott, R.F. (1977) Feasibility and Desirability of Constructing a Very Large Centrifuge for Geotechnical Studies, California Institute of Technology.

Seed, H.B. (1976) Evaluation of Soil Liquefaction Effects on Level Ground During Earthquakes, ASCE National Convention, Philadelphia.

Seed, H.B. and Idriss, I.M. (1967) Analysis of Soil Liquefaction: Niigata Earthquake, ASCE 97, SM9

Shepard, F.P. (1963) Submarine Geology, New York, Harper and Row.

Sketchley, C.J. (1973) The Behaviour of Kaolin in Plane Strain, Ph.D. Thesis, Cambridge University.

Sketchley, C.J. and Bransby, P. (1973) The Behaviour of Overconsolidated Clay in Plane Strain, Proc. 8th Int. Conf. SM and FE, Moscow 1.2, 377-384.

Smalley, I.F. (1972) Flowsliding, Trans. Inst. Min. Metall. (Series A) <u>81</u>,
    31-36, 188-193, 238.

Sokolovski, V.V. (1965) Statics of Granular Media, Pergamon, London.

Spencer, E. (1967) A Method of Analysis of the Stability of Embankments
    assuming Parallel Inter-slice Forces, Geotechnique <u>17</u>, 11-26.

Taylor, D. (1948) Fundamentals of Soils Mechanics, Wiley, New York.

Terzaghi, K. (1947) Shear Characteristics of Quicksands and Soft Clay,
    Proc. 7th Texas CSMFE, Austin.

Terzaghi, K. (1950) Mechanism of Landslides from Application of Geology to
    Eng. Practice, Berkay Volume Geol. Soc. of America, 181-194.

Terzaghi, K. (1956) Varieties of Submarine Slope Failures, 8th Texas Conf.
    on SM and FE, Spec. Pub. 29, Bur. Eng. Res., Texas University.

Torrey, V. (1976) Investigation of Liquefaction Susceptibility and
    Prevention of Flowslides on Mississippi River Banks, WES Potomology
    Investigations, unpublished research.

Tovey, N.K. (1970) Liquefaction: A Study of Sand Grains with the
    S.E.M., Cambridge University Engineering Department.

V de Knaap, W., Eijpe, R. (1969) Some Experiments on the Genesis of Tur-
    bidity Currents, Sedimentology <u>11</u>, 115-124.

Walker, R.G. (1973) Mopping up the Turbiditemess, In Evolving Concepts
    in Sedimentology, ed. Ginsburg, R.N., John Hopkins University Press,
    1-37.

Wallis, G.B. (1969) One Dimensional Two Phase Flow, McGraw Hill, New York.

Flood Problems in Deltaic Areas, Proc. 4th Regional Tec. Conf. on Water
    Res. Development.

WES (1956) A Review of the Soils Studies, WES Potomology Report 12-5.

WES (1976) Potomology Report 12-22, Verification of Empirical Criterion
    for River Bank Stability, U.S. Army Waterways Experiment Station,
    Vicksburg.

Wroth, C.P. (1971) Some Aspects of the Elastic Behaviour of Overconsol-
    idated Clay, Proc. Roscoe Memorial Symposium, Cambridge.

Zaruba, Q. and Mencl, V. (1969) Landslides and Their Control, Elsevier,
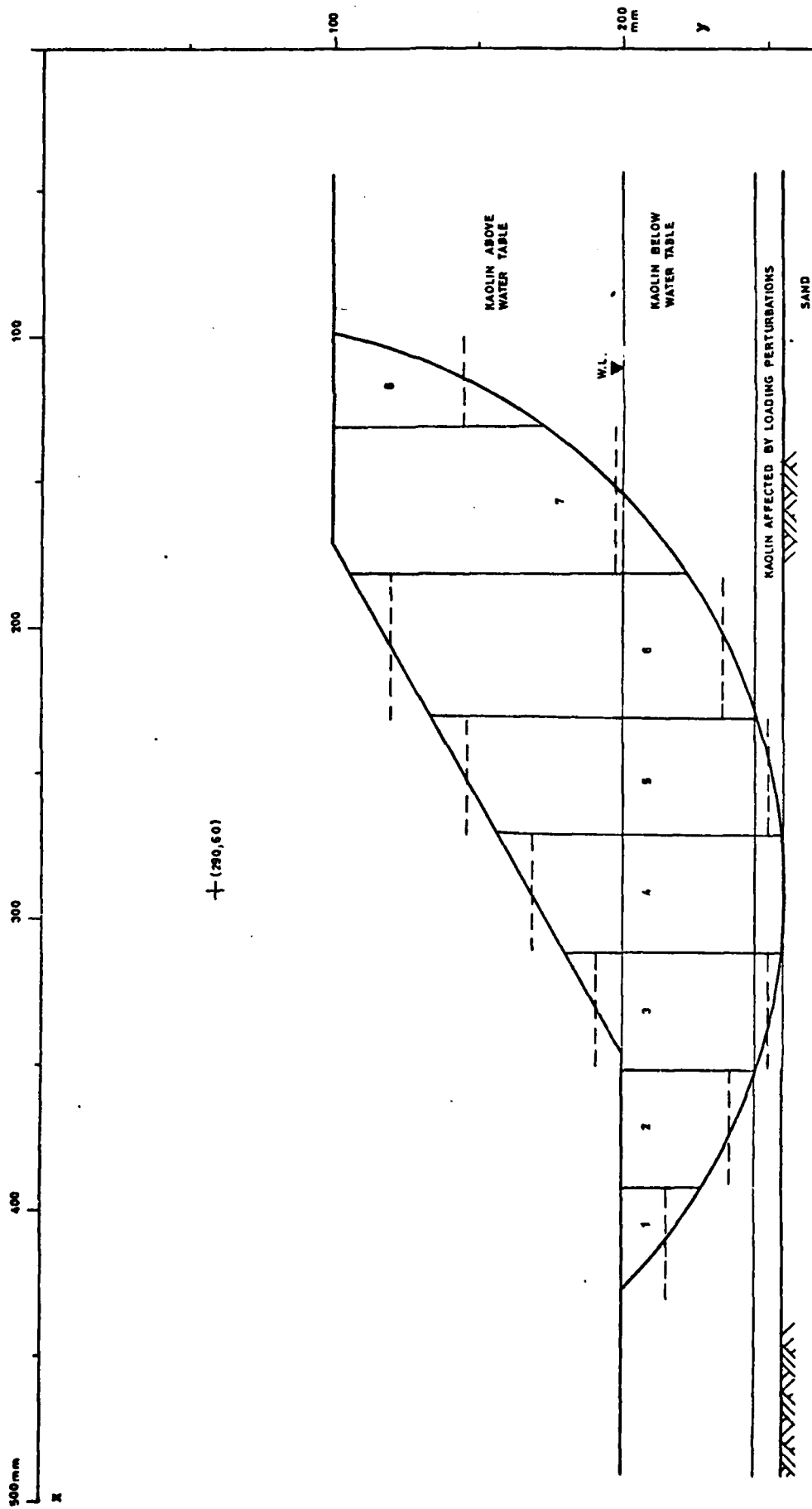   Amsterdam.

FIG A1. SLIP CIRCLE IN MODEL WITH 55 mm MARSH LAYER

APPENDIX

SLIP CIRCLE CALCULATION OF EMBANKMENT STABILITY

The calculation of embankment stability by the use of slip circles
is illustrated in this appendix by the presentation of the calculations
for a circle through the model with a marsh layer 55 mm thick, Fig. A1.
The mechanics of the slip circle calculations are illustrated in Fig. 2.21
and reproduced here as Fig. A2. The equation used for the factor of
safety was,

$$F_s = \frac{\Sigma \ b \ c \ \sec\alpha}{\Sigma \ W \ \sin\alpha} \tag{A.1}$$

where $W = bh\gamma ng$ kN/m^2 at n gravities $\qquad$ (A.2)

c = undrained shear strength of soil = $f(h,n,u) = f(p_o')$

$\quad = c_u$ if $p_o' > p_x'$ (Fig. 2.14)

$c = c_H$ if $p_o' < p_x'$ (Fig. 2.15)

$$c_u = 0.56 \ \exp. \left\{ \frac{0.8788 + 0.05 \ln p_o'}{0.26} \right\} \tag{2.23 bis}$$

$$c_H = 0.21 \ \exp. \left\{ \frac{0.8788 + 0.05 \ln p_o'}{0.26} \right\} + 0.29 \ p_o' \tag{2.22 bis}$$

u = pore water pressure in foundation

$\quad = MU\gamma_w$ $\qquad$ (2.9 bis)

$\gamma = 1.66 \ \gamma_w$ = bulk density of soil

$h = h_a + h_b$, b, α are the height, width and base inclination of an
individual slice and must be determined from the geometry of the circle,
Fig. A1 and is given in Table A1.

For a typical slice, the effective stress on the sliding interface
is given by

$$\sigma_v' = \sigma_v - u_{static} - \Delta u \tag{2.26}$$

$$= 1.66ng \ (h_a + h_b) - h_b ng - Mng \ (U-1)$$

$$= ng\{1.66h_a + 0.66h_b - M(U-1)\} \tag{A.3}$$

and $\sigma_H' = 33.9 + 0.47 \ \sigma_v'$ $\qquad$ (from equation 2.11)
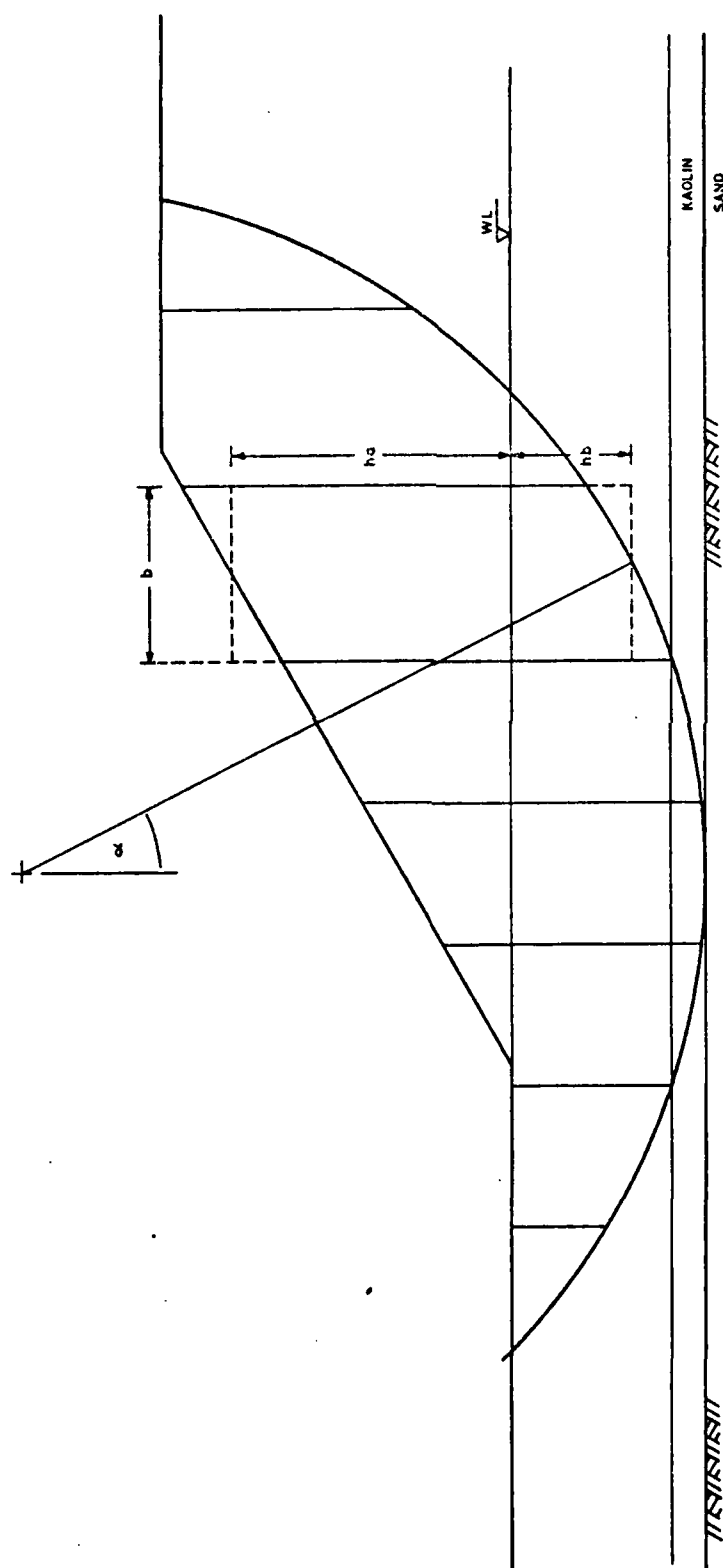
FIG. A2 GEOMETRY OF A SLIP CIRCLE

END
DATE
FILMED
6-80
DTIC

1.0

4.5
5.0
5.5
6.0

2.8
3.2
3.6
4.0

2.5

2.2

2.0

1.1

1.8

1.25   1.4   1.6
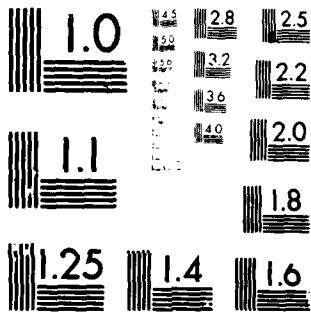
MICROCOPY RESOLUTION TEST CHART
NATIONAL BUREAU OF STANDARDS-1963-A

Hence $p_o' = \dfrac{\sigma_v' + 2\sigma_H'}{3}$ may be calculated for the base of any slice.

As explained in Section 2.4 it has been assumed that a layer 10 mm thick, Fig. A1, experiences the full swelling occasioned by uplift U and that in the rest of the material p_o' is unaffected by variations in either uplift or selfweight loading. Consequently for slices 3-5 the value of U in Equation A.3 is a variable, while in all the other slices it is constant at U = 1.

Using the above considerations it was possible to calculate for every slice and at any value of U or ng, the value of undrained shear resistance along the sliding surface. At any particular value of ng this was tabulated, Table A2, for all the slices at uplift values of U = 1 and U = 1.60. This was done in turn for ng values ranging in increments of 20g from 50g to 130g. A Texas programmable pocket calculator T158 was programmed with the data for each loading case in turn and the factor of safety F_s determined in each case, Table A3. It was then possible by interpolation between the values given for F_s in Table A3 to calculate the value of U required to bring the safety factor to unity Table A4. These results only represent a real case of loading within the range $0 \le U \le 1.66$ out of which the range of interest for this study is $1 \le U \le 1.66$. The values listed in Table A4 are plotted on the interaction diagram with the axes F(= n/50) and U in Fig. 2.23.

Table A1

DATA OF SLICE GEOMETRY

Slice	b metres	h_a metres	h_b metres	h metres	sinα
1	0.035	0	0.015	0.015	-0.598
2	0.040	0	0.037	0.037	-0.399
3	0.040	0.008	0.050	0.058	-0.208
4	0.040	0.031	0.054	0.085	0
5	0.040	0.054	0.050	0.104	0.208
6	0.050	0.080	0.034	0.114	0.442
7	0.050	0.097	0	0.097	0.701
8	0.031	0.045	0	0.045	0.910

Table A3

CALCULATED SAFETY FACTORS, F_s

F	ng	U = 1.00 F_s	U = 1.60 F_s
1.0	50g	2.07	1.99
1.4	70g	1.52	1.45
1.8	90g	1.21	1.15
2.2	110g	1.00	0.95
2.6	130g	0.86	0.82

Table A4

INTERPOLATED VALUES OF F, U FOR WHICH F_s = 1.00

F	1.0	1.4	1.8	2.2	2.6
U	9.40	5.46	3.10	1.00	-1.10

Table A2

MATERIAL STRESS STATE AND UNDRAINED SHEAR STRENGTH AT SLIDING SURFACE

Slice	50g			70g			90g			110g			130g		
	σ'_v	p'	C_u^H	σ'_v	p'	C_u^H	σ'_v	p'	C_u^H	σ'_v	p'	C_u^H	σ'_v	p'	C_u^H
1	4.4	25.4	18.9	4.4	25.4	18.9	4.4	25.4	18.9	4.4	25.4	18.9	4.4	25.4	18.9
2	10.9	29.6	20.4	10.9	29.6	20.4	10.9	29.6	20.4	10.9	29.6	20.4	10.9	29.6	20.4
3	21.0	36.2	22.8	29.4	41.6	24.7	37.8	47.0	26.6	46.2	52.4	28.4	54.6	57.9	30.2
4	40.2	48.6	27.1	56.3	59.0	30.6	72.4	69.4	33.8	88.4	79.7	34.8	115.0	96.9	36.1
5	57.1	59.6	30.8	79.9	74.2	34.3	102.8	89.0	35.5	125.6	103.2	36.6	148.5	118.5	37.5
6	72.8	69.7	33.9	72.8	69.7	33.9	72.8	69.7	33.9	72.8	69.7	33.9	72.8	69.7	33.9
7	76.1	71.8	34.1	76.1	71.8	34.1	76.1	71.8	34.1	76.1	71.8	34.1	76.1	71.8	34.1
8	35.3	45.4	26.0	35.3	45.4	26.0	35.3	45.4	26.0	35.3	45.4	26.0	35.3	45.4	26.0
3	4.9	25.7	19.0	6.8	27.0	19.5	8.7	28.2	19.9	10.7	29.5	20.4	12.6	30.7	20.8
4	24.1	38.1	24.5	33.7	44.4	25.7	43.3	50.6	27.8	52.9	56.8	29.9	73.0	69.8	33.9
5	50.0	49.1	27.3	57.1	59.7	30.8	73.7	70.2	33.9	90.1	80.8	34.9	106.5	91.4	35.7

All in kN/m^2

1.00

1.60

TABLE 1

TWO DIMENSIONAL FLOOD EMBANKMENT MODELS: TEST PARAMETERS

TEST CODE		BANK HEIGHT mm	MARSH DEPTH mm	MAX CONSOL^n PRESSURE σ'_v kN/m²	SWELLING PRESSURE σ'_v kN/m²	TEST BY INCREASE IN	U AT FAILURE	PS AT FAILURE	SOKOLOVSKY SLOPE x	y	SUPERFICIAL FAILURE R	
2DF1	R	102	48	128	50	PS		50	288	66	201	PRELIMINARY TESTS
	B	102	48	128	50	PS		50	305	48	204	
2DF2	R	102	48	128	50							SOFT MODELS
	B	102	48	128	50							SHEDDED UPLIFT INTERACTION
2DF3	R	100	75	200	50	PS	1.577	117				DRAWDOWN / EXPLORATORY TEST
	B	100	75	200	50	PS	0.83	122				
2DF4	R	100	55	200	-	PS	1.0 No failure	110	-	52	203	
	B	100	55	200	-	r_u	2.03	50				
							1.91	100				
2DF5	R	100	55	200	-	PS	1.0	106	315	50	204	
	B	100	55	200	-	PS	1.76	113	300	50	205	
2DF6	R	100	55	200	-	PS	1.74	90	329	26	248	
	B	100	55	200	-	PS	1.79	110	296	46	217	
							0.75	130				
2DF7	R	100	75	200	-	r_u	1.0	121	360	24	262	
	B	100	75	200	-	PS	1.83	110	348	-20	313	
2DF8	R	100	95	200	-	r_u	1.53-1.56	100	350	43	251	
	B	100	95	200	-	r_u	1.44	115	359	44	251	MAIN SERIES OF TESTS
							1.48-1.54	115				
2DF9	R	100	75	200	-	r_u	1.46-1.58	97	340	36	255	
	B	100	75	200	-	r_u	1.48-1.54	115	338	36	239	
2DF10	R	100	75	200	-	PS	1.0	119	323	25	247	
	B	100	75	200	-	PS	1.41	118	338	28	247	
2DF11	R	100	75	200	-	PS	1.38	122	331	33	247	
	B	100	75	200	-	PS	1.26	119	347	40	234	
2DF12	R	100	55	200	-	PS	1.13	114	316	30	205	
	B	100	55	200	-	PS	1.38	117	304	49	204	
2DF13	R	100	55	200	-	PS	1.13	126	304	48	203	
	B	100	55	200	-	PS	1.38	118	320	61	190	

SLIP CIRCLE CENTRE/RADIUS (For axes see Figs 4.12, 4.14 etc)

PRESSUREHEAD IN SAND / MARSH THICKNESS

TABLE 2

Test No.	Sand Type	Method of Prep[a]	Overburden Thickness	Sand Thickness	R = %A	'mg' Value at Test	Failure Type	Length mm	Width mm
1	120/200	Tamped damp	30mm	70mm	0.43	100	Foldown	100	320
2	120/200	Tamped damp	25	60	0.42	>10	Breakaway	90	240
3	120/200	Tamped dry	22	90	0.24	100	Retrogressive slump	300	260
4	>350	Pluviated thro water	32	108	0.30	100	-	-	-
5	"	"	45	104	0.43	100	-	-	-
6	"	"	25	110	0.23	100	-	-	-
7	"	"	32	64	0.50	100	-	-	-
8	"	"	23	114	0.20	100	-	-	-
9	"	"	28	113	0.25	100	-	-	-
10	"	"	29	108	0.27	100	-	-	-
11	"	Slurry consolidated in situ	29	111	0.26	100	Settlement	100	200
12	>350	Slurry consolidated in situ	29	121	0.25	50	Settlement	75	200
13	120/200	Pluviated thro water	32	57	0.56	50	Breakaway	80	240
14	"	"	61	58	1.05	50	Carpet	60	220
15	"	"	29	57	0.51	10	Foldown	105	210
16	"	"	33	67	0.49	10	Breakaway	135	225
17	"	"	51	67	0.76	10	Foldown	100	200
18	"	"	22	70	0.31	10	Breakaway	170	240
19	"	"	21	70	0.30	1	Breakaway	120	215
20	120/200	Pluviated thro water	20	74	0.27	1	Breakaway	145	165

TABLE 3

APPROXIMATE CORRELATION OF 3DM MODEL BEHAVIOUR

G FACTOR	100	50	10	1
R value				
0.2	Breakaway			
0.3			Breakaway	Breakaway
0.4			Breakaway	
0.5			Folddown	
		Carpet		
0.6				
0.7				
			Folddown	
0.8				
0.9				
1.0				
1.1		Carpet		

TABLE 4

TRAPDOOR TESTS 5 - 7

CLAY THICKNESS	CRATER SIZE	CLAY CRACKED AWAY ON:	
m		m dia.	
0.085	0.23	0.18	Collapse of the plate was signalled by the appearance of a star-shaped crack running right through the plate at mid-span. The plate collapsed on ϕ = 180. After two minutes the outer ring cracked away on ϕ = 200.
	0.18	0.18	Deforms, crack runs right through in centre and then plate cracks away on edge.
0.029	0.23	0.2	Development of deformation shown in Fig. Slight hair cracks on ϕ = 175mm which move out to 200mm. Central crack runs right through when circumferential cracks at ϕ = 185. Plate fails on ϕ = 200.
	0.18	Intact	No hint of central crack or failure. Plate self supporting with hair cracks on ϕ = 175mm.
0.037	0.23	Intact	Plate drooped approx. 12mm with hair cracks on ϕ = 224.
	0.18	Intact	Hardly any deformation $\delta/h \simeq 0.1$ and small hair cracks on ϕ = 185mm.

- 176 -

Plate 3.1 Liner and Consolidometer
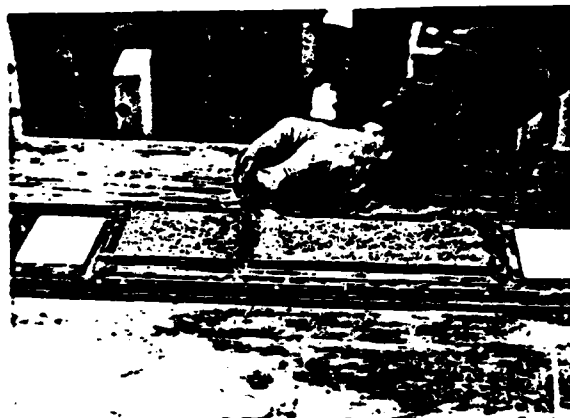
Plate 3.2 Foundation Sand layer

Plate 3.3 Liner in Consolidometer

Plate 3.4 Model Cut to Shape
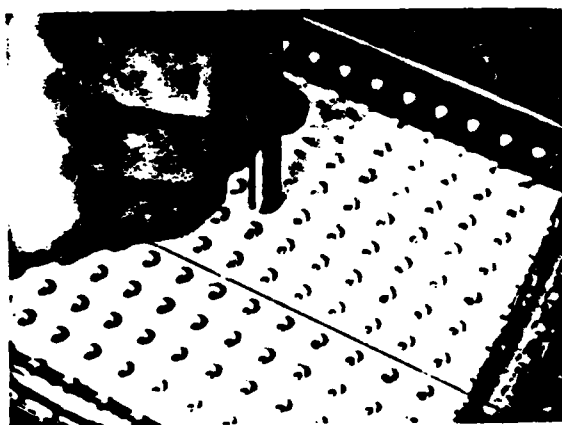
Plate 3.5 Array of Silvered Balls
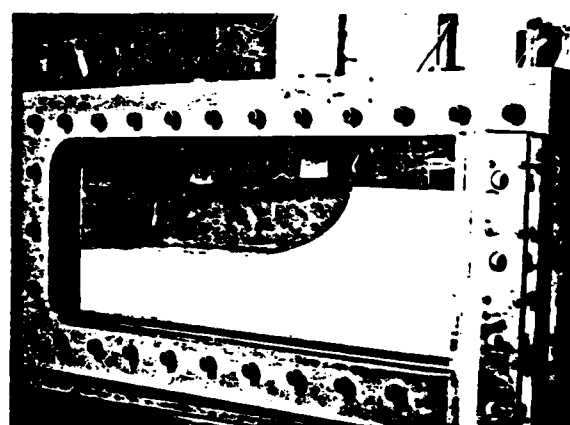
Plate 3.6 Strong Box Front
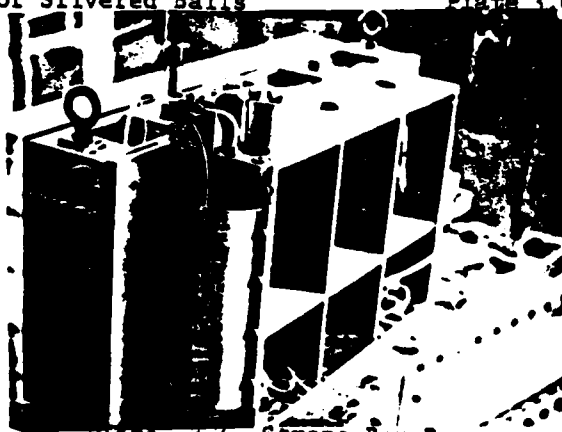
Plate 3.7 Strong Box Rear

Plate 4.1 Model 2DF1 Blue

Plate 4.2 Model 2DF4 Blue

Plate 4.3 Model 2DF11 Red

Plate 4.4 Model 2DF12 Red
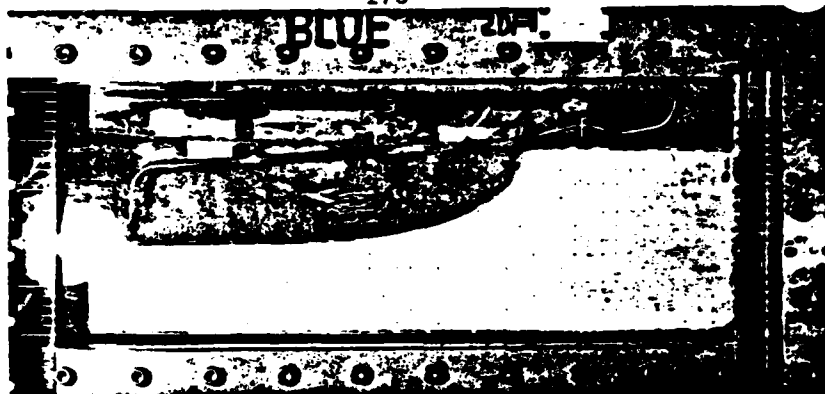
Plate 4.5a Model 2DF3 25g Achieved
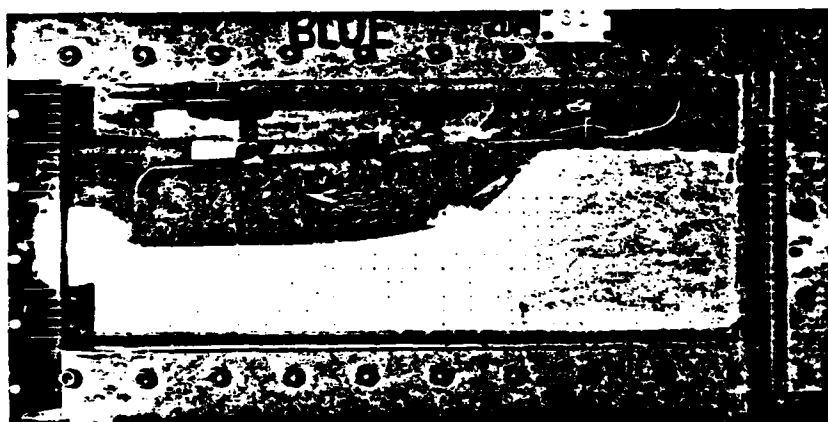
Plate 4.5b Model 2DF3 After 20 Mins at 25g
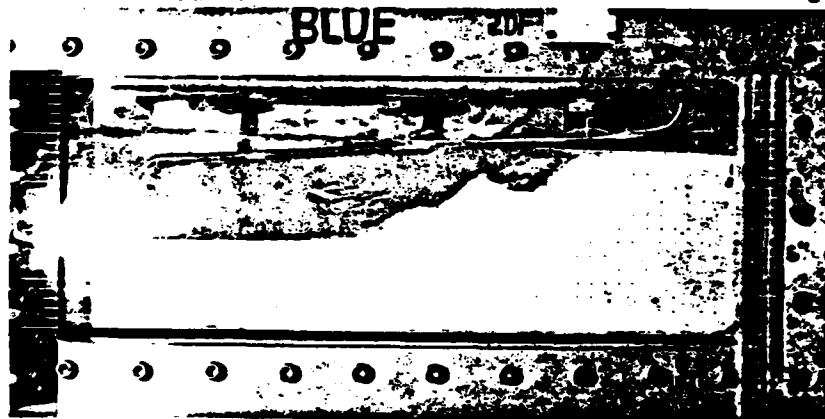
Plate 4.5c Model 2DF3 50g Achieved
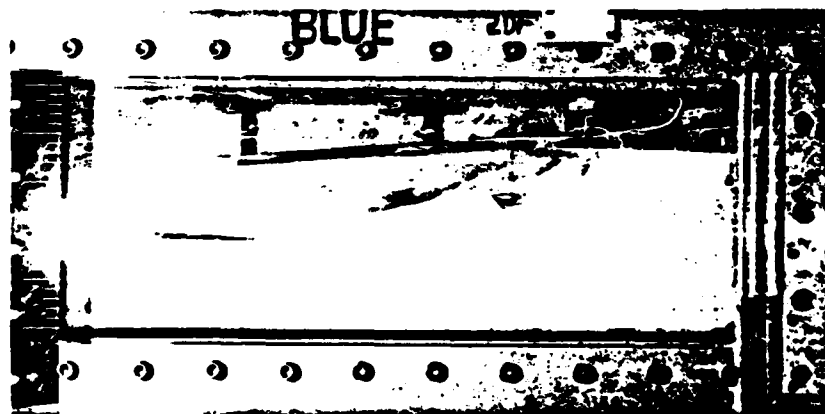
Plate 4.5d Model 2DF3 Drawdown at 50g

- 179 -

Plate 4.7   Model 2DF6 Red

Plate 4.9   Model 2DF7 Red and Blue

Plate 4.6   Model 2DF3 Red

Plate 4.8 Model 2DF6 Blue
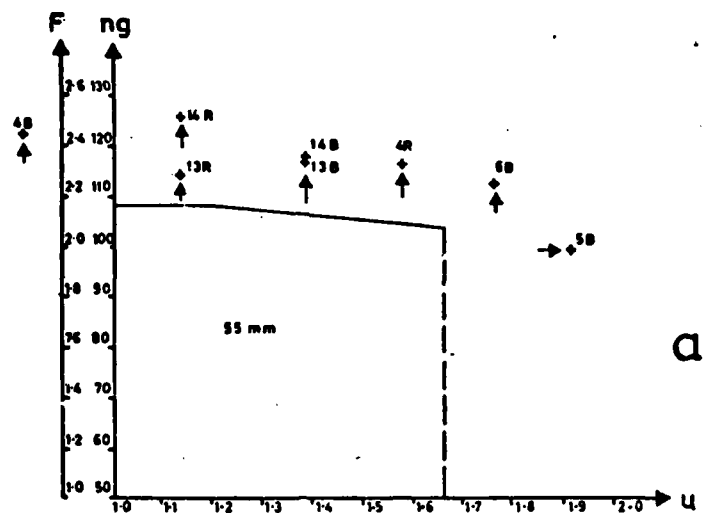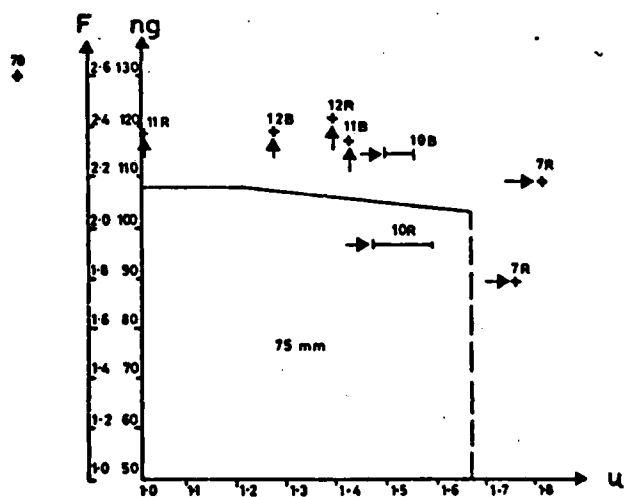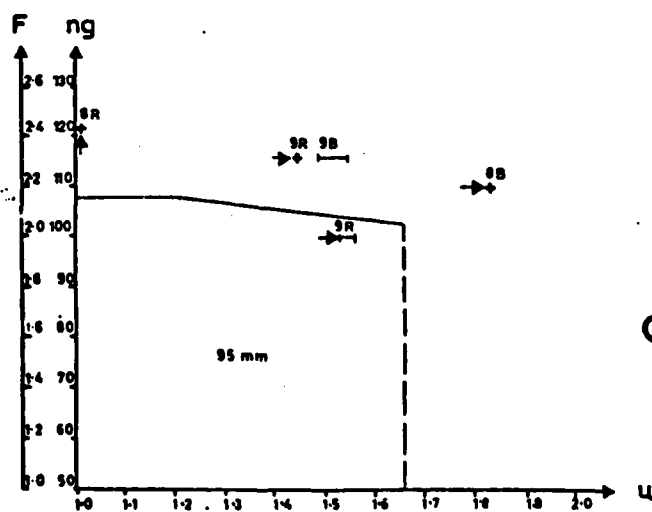
PLATE 4·10 INTERACTION DIAGRAM REPRESENTATION
FOR FAILURE STATES OF MODEL
EMBANKMENTS

Plate 8.1 Blast Pipes

Plate 8.2 Surcharge Plate in Tub
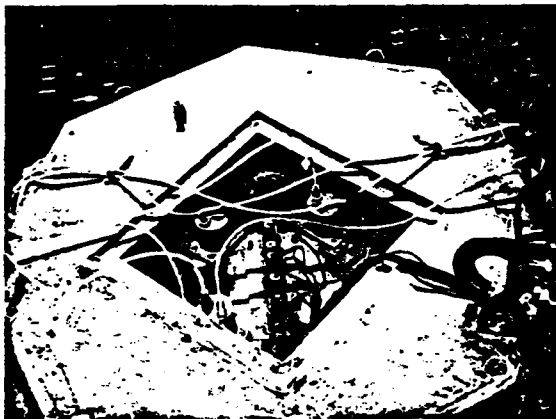
Plate 8.3 Lid with Transducers
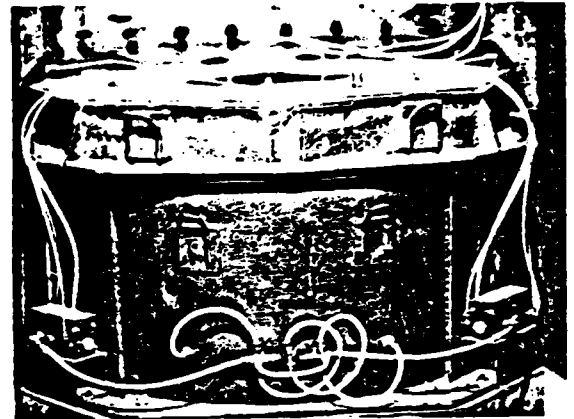
Plate 8.4 Tub and Lid on Centrifuge

Plate 8.5 Cutting Slope
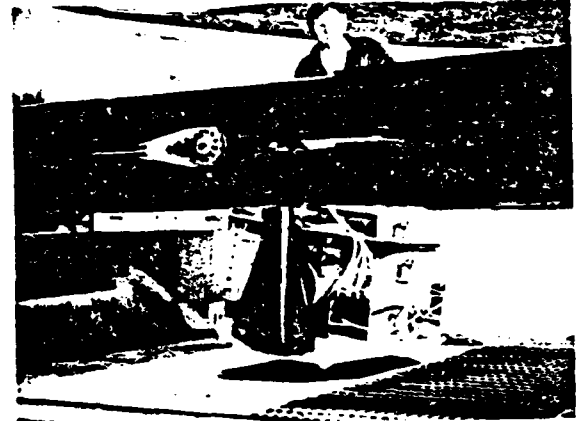
Plate 8.6 Swinging Platform

Plate 8.7 Model After Failure
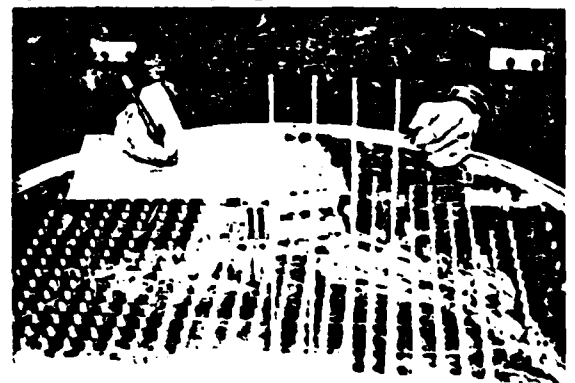
Plate 8.8 Surface Profile Measurement

Plate 8.9 Failure 3DM2
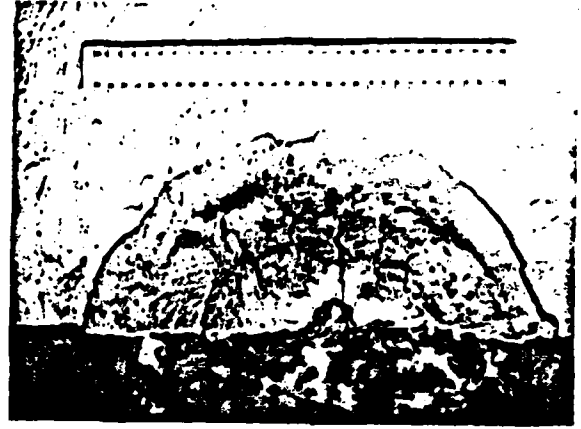
Plate 8.10 Underside 3DM2

Plate 8.11 Test Failure 3DM3

Plate 8.12 Test Failure 3DM4

Plate 8.13   Test 3DM12
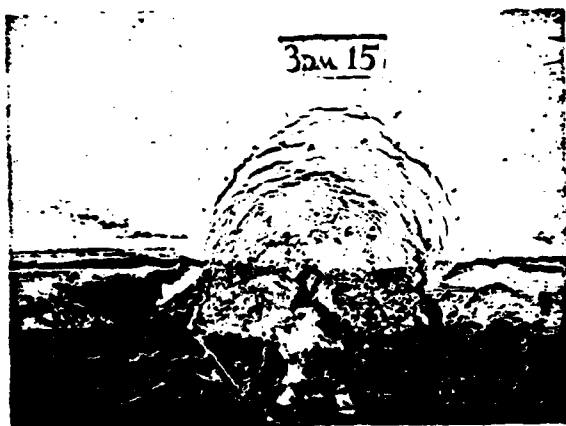

Plate 8.14   Closeup 3DM12

Plate 8.15   Test 3DM13

Plate 8.16   Test 3 DM14

Plate 8.17   Test 3DM15
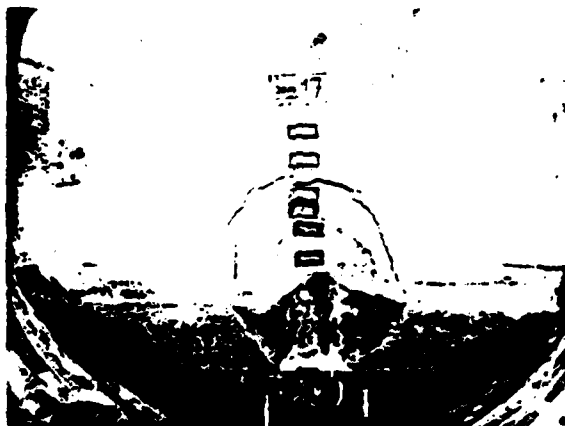

Plate 8.18   Test 3DM16

Plate 8.19   Test 3DM17

Plate   8.20   Test 3DM18

Plate 8.21 Test 3DM19
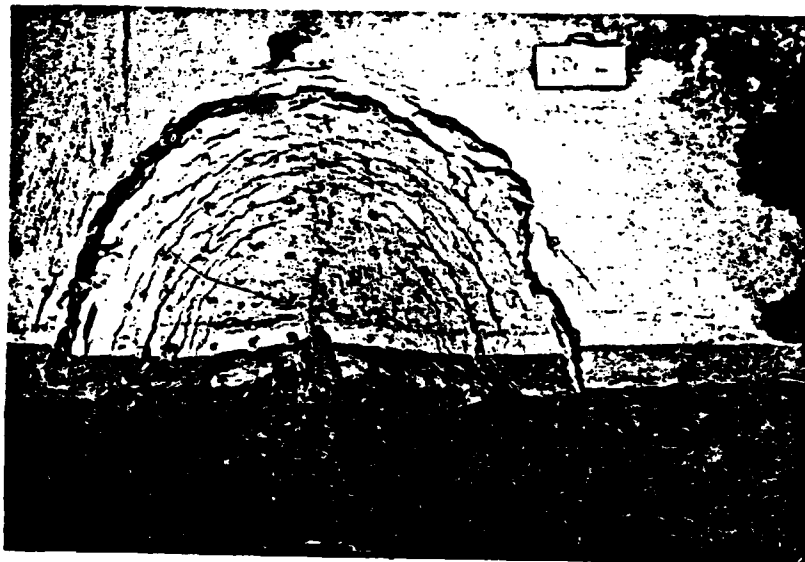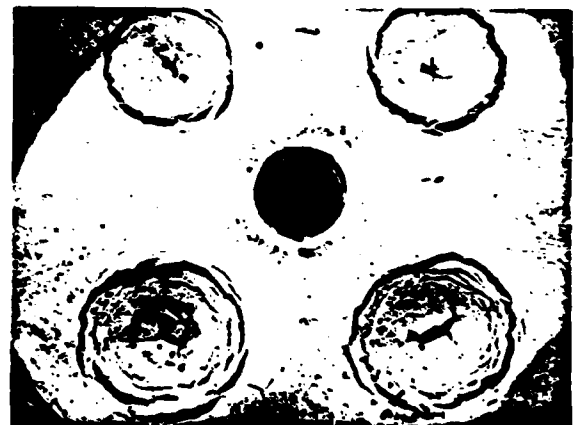

Plate 9.1 Blast Pipes

Plate 8.22 Test 3DM20

Plate 9.2 Consolidometer

Plate 9.3 Failed Clay Plate in Crater
Experiments